212
Topics in Current Chemistry

Springer

Berlin
Heidelberg
New York
Barcelona
Hong Kong
London
Milan
Paris
Singapore
Tokyo

Dendrimers III

Design, Dimension, Function

Volume Editor: Fritz Vögtle

With contributions by
M. Ballauff, R. M. Crooks, B. I. Lemon III,
M. Möller, K. Müllen, D. Muscat, S. S. Sheiko,
R. A. T. M. van Benthem, T. Weil, U.-M. Wiesler,
L. K. Yeung, M. Zhao

Springer

The series *Topics in Current Chemistry* presents critical reviews of the present and future trends in modern chemical research. The scope of coverage includes all areas of chemical science including the interfaces with related disciplines such as biology, medicine and materials science. The goal of eaxch thematic volume is to give the non-specialist reader, whether at the university or in industry, a comprehensive overview of an area where new insights are emerging that are of interest to a larger scientific audience.

As a rule, contributions are specially commissioned. The editors and publishers will, however, always be pleased to receive suggestions and supplementary information. Papers are accepted for *Topics in Current Chemistry* in English.

In references *Topics in Current Chemistry* is abbreviated Top. Curr. Chem. and is cited as a journal.

Springer WWW home page: http://www.springer.de
Visit the TCC home page at http:/link.springer.de/series/tcc/
or http://link.springer-ny.com/series/tcc/

ISSN 0340-1022
ISBN 3-540-67828-X
Springer-Verlag Berlin Heidelberg New York

Library of Congress Catalog Card Number 74-644622

Springer-Verlag Berlin Heidelberg New York
a member of BertelsmannSpringer Science+Business Media GmbH

Printed in Germany

Cover design: Friedhelm Steinen-Broo, Barcelona; MEDIO, Berlin
Typesetting: Fotosatz-Service Köhler GmbH, 97084 Würzburg

SPIN: 10719376 02/3020 ra – 5 4 3 2 1 0 – Printed on acid-free paper

Volume Editor

Prof. Dr. Fritz Vögtle
Kekulé-Institut für Organische Chemie
und Biochemie der Universität Bonn
Gerhard-Domagk-Straße 1
53121 Bonn, Germany
E-mail: voegtle@uni-bonn.de

Editorial Board

Topics in Current Chemistry
Now Also Available Electronically

For all customers with a standing order for Topics in Current Chemistry we offer the electronic form via LINK free of charge. Please contact your librarian who can receive a password for free access to the full articles by registration at:

http://link.springer.de/series/tcc/reg_form.htm

If you do not have a standing order you can nevertheless browse through the table of contents of the volumes and the abstracts of each article at:

http://link.springer.de/series/tcc

There you will also find information about the

- Editorial Board
- Aims and Scope
- Instructions for Authors

Preface

As a start to a "tetralogy" on dendrimers, the volumes "Dendrimers" and "Dendrimers II" have already appeared in print. This mini-series continues now with the latest volume "Dendrimers III" and will be completed by the fourth volume "Dendrimers IV" within the next few months. Volume III offers dendrimers based on novel design concepts leading to highly stiffened and shape persistent dendritic structures as well as to new families of rather soft and floppy dendrimers and focuses on new functional properties and materials aspects. As an example, the question of host-guest interactions with dendrimers, whose existence has been under intense debate for a long time, finds its final – and positive – answer in this volume. As a consequence, dendrimers clearly represent a subset of supramolecular chemistry.

The present volume not only contains an up-to-date collection of reviews by distinguished pioneers in the field of dendritic molecules, but also gives profound insight into interdisciplinary fields. Dendritic macromolecules are included as well as the analysis of the dendrimers' shapes and densities by small angle scattering techniques. Applications in nanotechnology range from the inclusion of finely dispersed metals to nano clusters and semi-conducting materials. The advantages of dendritic architectures – the control of solubility, their nanometer dimensions, their ability to bind guests in "dendritic boxes", the "additivity" of physical properties, the protection of sensitive core units by the dendrimer shell – have been used in many respects. Dendrimers as catalyst support, sensing agents, diagnostic tools, or as promoters for gene transfection are under study or have already been realized.

"Dendrimers III" is also intended to organize the impressive variety of scientific results from the field of dendrimers. This offers a basis for further development and helps to promote future applications. The reviews presented here should also prove useful in view of upcoming events such as the dendrimer workshop in Kiel/Germany (January 2001) and the second International Dendrimer Symposium in Tokyo/Japan (October 2001).

Bonn, June 2000 Christoph A. Schalley, Fritz Vögtle

Contents

Contents of Volume 197

Dendrimers I

Volume Editor: Fritz Vögtle

ISBN 3-540-64412-1

Contents of Volume 210

Dendrimers II
Architecture, Nanostructure and Supramolecular Chemistry

Volume Editor: Fritz Vögtle

ISBN 3-540-67097-1

Nanosized Polyphenylene Dendrimers

Uwe-Martin Wiesler, Tanja Weil, Klaus Müllen*

Max-Planck-Institut für Polymerforschung, Ackermannweg 10, 55128 Mainz, Germany
E-mail: muellen@mpip-mainz.mpg.de

This chapter describes the state of the art of the synthesis, characterization, functionalization, and possible applications of all-phenylene dendrimers. Due to their high number of benzene rings, this type of dendrimer distinguishes itself by high stiffness, shape persistence, and nanometer dimensions. This allows their use especially as chemically and thermally inert nanosupports for, e.g., chromophores, catalysts, but also as hosts for guest molecules due to large stable cavities. In addition, the surface and bulk self-organization properties of these polyphenylene dendrimers are presented.

Keywords. Polyphenylene dendrimers, Dendrimer, Shape persistence, Self-assembly, Nanosupport

* corresponding author

Topics in Current Chemistry, Vol. 212

1 Introduction

Since the first reported synthesis by Vögtle et al. [1] in 1978, dendrimers have received increasing interest, well documented by an exponential growth of published articles [2]. This interest is connected with properties like globular shape and defined size resulting from low dispersities of these macromolecules with regular and highly branched three-dimensional architectures.

Dendrimers are synthesized by the repetition of a sequence of reaction steps leading after each repetition to a dendrimer one generation larger. Two different synthetic approaches are known depending on the starting point: a divergent one, building the dendrimer layer-by-layer from a central core to the periphery and a convergent one, where the dendrimer grows from the periphery toward the central core. The divergent approach has been used by Vögtle et al. [1], and later Wörner and Mülhaupt [3] and de Brabander et al. [4] to synthesize poly(propylene imine) or by Tomalia et al. [5, 6] to synthesize the starburst-polyamidoamine (*PAMAM*) dendrimers. The construction process is by the addition of dendrimer building units to a core molecule possessing one or more reactive sites, representing the zeroth generation. After addition of the branching units, each newly created branch is a starting point to which several further sub-branches may be connected. The number of branches that grow from a branching point depends on the branching unit. For example, in the case of an A_2B branching unit the number is two, in the case of an A_4B branching unit, four. By repeating this addition process, dendrimers of successive generations are synthesized. To obtain dendrimers with functional groups on the surface in defined positions, monomer units carrying the corresponding groups must be added to the growing dendrimer in the final step. The number of reactive sites, necessary for the addition of a further layer of branching units, increases exponentially with the number of generations. Therefore, the synthesis of macromolecules with molecular masses higher than 10,000 g/mol is possible by using only a few reaction steps. It is important, however, that all reactive groups react completely, because separation of product mixtures is in most cases impossible due to the small differences in properties, like molecular mass, size, or polarity.

In the case of the convergent approach, introduced in 1990 by Fréchet and coworkers [7–9] and followed shortly thereafter by Miller and Neenan [10], synthesis of dendrimers starts from the periphery of the dendrimer and ends by attaching the branches to the core. The first step is the addition of one branching unit to the terminal units. By repetition of the addition step, successive genera-

tions of dendrons (dendrimer branches with reactive groups at the focal point) can be synthesized. In the last step these dendrons are added to a polyfunctional core to yield dendrimers. In contrast to the divergent approach, only a constant and low number of reactive sites have to be converted during the formation of a new generation. Therefore, every new generation can be purified and the convergently-produced dendrimers are relatively defect free [11]. Another advantage of the convergent approach is the possibility of obtaining dendrimers with multiple types of functionalities at the periphery by the selective addition of variously functionalized dendrons to a core [12–15]. Nevertheless, due to the steric hindrance around the reactive site in the focus of the dendron, reactivity decreases with increasing generations and therefore only lower generations of dendrimers can be synthesized by the convergent approach. In summary the two approaches may be regarded as complementary, with respect to product size, purity, and functionalizability.

In addition to monodispersity at high molecular masses and high regularity, the 3-dimensional structures of dendrimers have attracted the interest of chemists. The first theoretical work was presented by de Gennes and Hervet, who developed the concept of dense [16]. Their self-consistent field model indicates that dendrimers can freely grow up to a certain limiting generation. Due to the fact that the number of branches increases exponentially with the number of generations, whereas the radius of the dendrimer increases only linearly, the outer shells have progressively higher densities leading to a globular architecture. De Gennes and Hervet concluded that dendrimers must have lower densities in the center than on the surface and that terminal reactive groups should be on the surface. Recent empirical studies (especially on the position of functional groups within dendrimers) cannot confirm the ideal structure which has been postulated by de Gennes and Hervet. Viscosimetry [17], NMR [18], and fluorescence depolarization [19] measurements have shown for Fréchet-type polyaryl-ether dendrimers that, due to the flexible nature of these dendrimers, end groups are found throughout the dendrimer volume. Furthermore, the shape and size of the dendrimer are also solvent dependent. Small-Angle-Neutron-Scattering confirms the flexible character of poly(propylene imine) dendrimers, showing that this type has a homogenous density distribution [20]. Indirect evidence for the high mobility is the self organization of alkyl or perfluoroalkyl substituted polyaryl ether dendrons, as shown by Percec et al., which requires flexible dendrimers that can organize into spheres or columns [21–23]. Therefore, flexible dendrimers tend to be neither shape persistent nor are their terminal functional groups located on the surface of the dendrimer. This is also characteristic for linear functional polymers. Their use as, e.g., support for dyes or catalysts is limited and thus there is a need for inherently more rigid dendrimers.

Given the high mobility of dendrimers based on alkyl chains, other efforts have been aimed at "stiffening" three-dimensional, nanometer sized dendrimers. One approach is to connect benzene branching points by two σ-bonds, as in the polyaromatic dendrimers. Hart synthesized dendrimers based on extended triptycenenes, and these dendrimers show high stiffness and shape-persistence [24]. Another approach is to connect the branching points of the dendrimer with inherently stiff chains, e.g., poly-*p*-polyphenylenethynylenes and poly-*p*-phenyl-

enes. They allow rotation only around the chain axis and therefore conformational isomerism is impossible. Examples of this kind are the dendrimers synthesized by Moore and Xu [25, 26] and the polyphenylene dendrimers by Miller and coworkers [10, 27, 28] and by us [15, 29–35], which will be presented in detail in this chapter. The dendrimers by Moore and Xu and by Miller and coworkers are based on 1,3,5-substituted benzenes **1** as branching points which, due to the angles in the chains, exhibit conformational isomers and therefore mobility around the chain. Our dendrimers are based on 1,3,4-substituted branching points **2.** Due to the 1,4-substitution, like in linear polyphenylenes, we have linear radiating backbones in our dendrimers that dictate size and shape (Scheme 1).

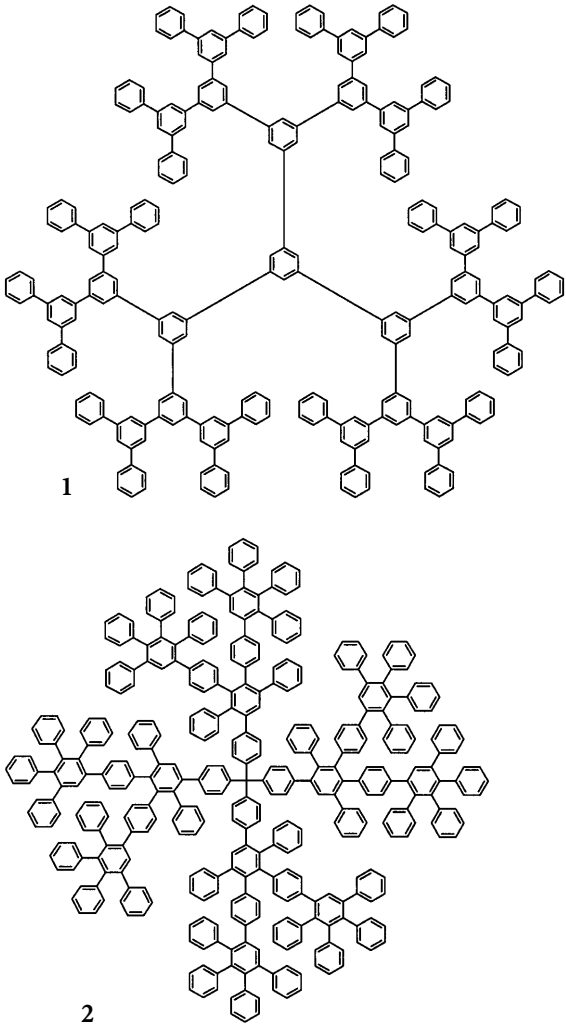

Scheme 1. Second generation of polyphenylene dendrimers based on palladium catalyzed coupling (**1**) and Diels-Alder cycloaddition (**2**)

To the best of our knowledge, apart from the above-mentioned systems of Miller and Neenan and the dendrimers presented by our group, no further work on large, highly branched polyphenylene dendrimers has been reported. This chapter will start therefore with the different ways of synthesizing these dendrimers, followed by their functionalization, characterization, and some applications. Finally, we present an outlook describing future work.

2
Synthesis of Polyphenylene-Dendrimers

2.1
Divergent Procedures

As a result of our effort to develop routes to extended polyaromatic hydrocarbons (PAH), we reported in 1997 the divergent synthesis of a new type of all-polyphenylene dendrimer. The synthesis is based on two reactions with nearly no side-reactions and yields above 99% – the Diels -Alder cycloaddition of tetraphenylcyclopentadienones to ethynes, the "growing step" and the desilylation of triisopropylsubstituted alkynes, the "deprotection step." The [2+4] Diels-Alder-type cycloaddition of tetraphenylcyclopentadienones to ethynyl compounds yields, on elimination of carbon monoxide, phenyl substituted benzenes. In order to use this reaction for dendrimer synthesis, we introduced the A_2B building unit 3,4-bis[4-(tri-*iso*-propylsilylethynyl)-phenyl]-2,5-diphenylcyclopentadienone (**3,** Scheme 2). This molecule contains a diene subunit for the Diels-Alder cycloaddition, the tetraphenylcyclopentadienone, and two protected dienophile functions, the ethynes. The bulky tri*iso*propylsilyl (TiPS) substituents serve to protect **3** from self-cycloaddition. After isolation of the TiPS-ethynyl substituted dendrimer, the protecting groups can easily be removed by fluoride salts, such as tetrabutylammonium fluoride, to give the ethynyl-substituted dendrimers. The starting material for this route, **3,** can be synthesized via

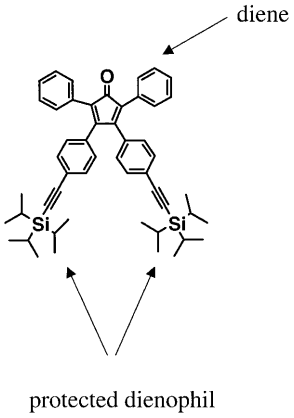

Scheme 2. The A_2B building unit **3** **3**

the double Knoevenagel condensation of 4,4′-bis(tri-*iso*-propylsilylethynyl) benzil [29] and 1,3-diphenyl-2-propanone on a large scale with yields up to 85%.

The synthesis of dendrimers via the divergent method starts with the addition of the building unit to a polyfunctional dendrimer "core." In Scheme 3 the synthesis of the dendrimers based on the core tetra-(4-ethinylphen-1-yl)-methane (**4**) is shown. The synthesis of these dendrimers starts with the "growing step," in this case the addition of the building unit **3**, to core **4**. Thus **5**, the first-generation dendrimer with TiPS-substituted ethynes, is obtained. Deprotection with tetrabutylammonium fluoride yields the corresponding ethynyl substituted first-generation dendrimer **6**. Now the free ethynes of **6** allow the build up of the next generation by repeating the cycloaddition and the deprotection. In this way, we could synthesize ethynyl-substituted monodisperse polyphenylene dendrimers up to the third generation. These dendrimers, in the case of the third generation containing 144 phenylene rings, are obtained completely monodisperse and with yields of approx. 80% over all reaction steps (Scheme 3). By Diels-Alder addition of tetraphenylcyclopentadienone to this third-generation, ethyne-substituted dendrimer, a monodisperse dendrimer containing 304 phenylene rings, can be obtained. By comparison, attempts to construct the ethynyl-substituted fourth generation by addition of our A_2B building unit **3** results in incomplete reaction. Success with the sterically less demanding tetraphenylcyclopentadienone indicates that density is sufficiently high in the third generation to prohibit higher generations.

The "growth step" procedures for the cycloaddition reaction are very simple. Combination of an ethynyl-substituted dendrimer and an excess of the cyclopentadienone in a refluxing solvent such as *o*-xylene, diphenylether, or methylnaphthalene (with b. p. higher than 130 °C) typically results in quantitative conversion within 24 h. The refluxing of the solvent is necessary to accelerate the elimination of the carbon monoxide in the cycloaddition. The purity of the resulting compounds was checked by MALDI-TOF mass spectrometry which showed quantitative reaction, facilitating work-up. By repeated precipitation in methanol, the pure product can be isolated as white amorphous powders in yields higher than 90%.

The "deprotection step" and subsequent purification are equally facile. Exposure of a TiPS-ethynyl-protected dendrimer to tetrabutylammonium fluoride in THF results in a quantitative reaction within 2 h. The tetrabutylammonium salts can be removed by silica plug filtration rendering pure product, and the obtained yields are higher than 95%. If deprotection is effected instead with ammonium fluoride and catalytic amounts of tetrabutylammonium fluoride, even silica plug filtration is unnecessary.

Due to the inherent stiffness of 1,4-phenylene based polymers and based on molecular modeling calculations (see below), the question arises whether the shape of the dendrimer can be predetermined by choosing an appropriate core. This should be important for the use of dendrimers in single molecule applications, as carriers for dyes for single molecule optical spectroscopy or as building blocks for two- and three-dimensional assemblies. There are two possibilities: variation of the core and variation of the building unit. Therefore, we synthesized dendrimers based on cores with different symmetries presented in Scheme 4.

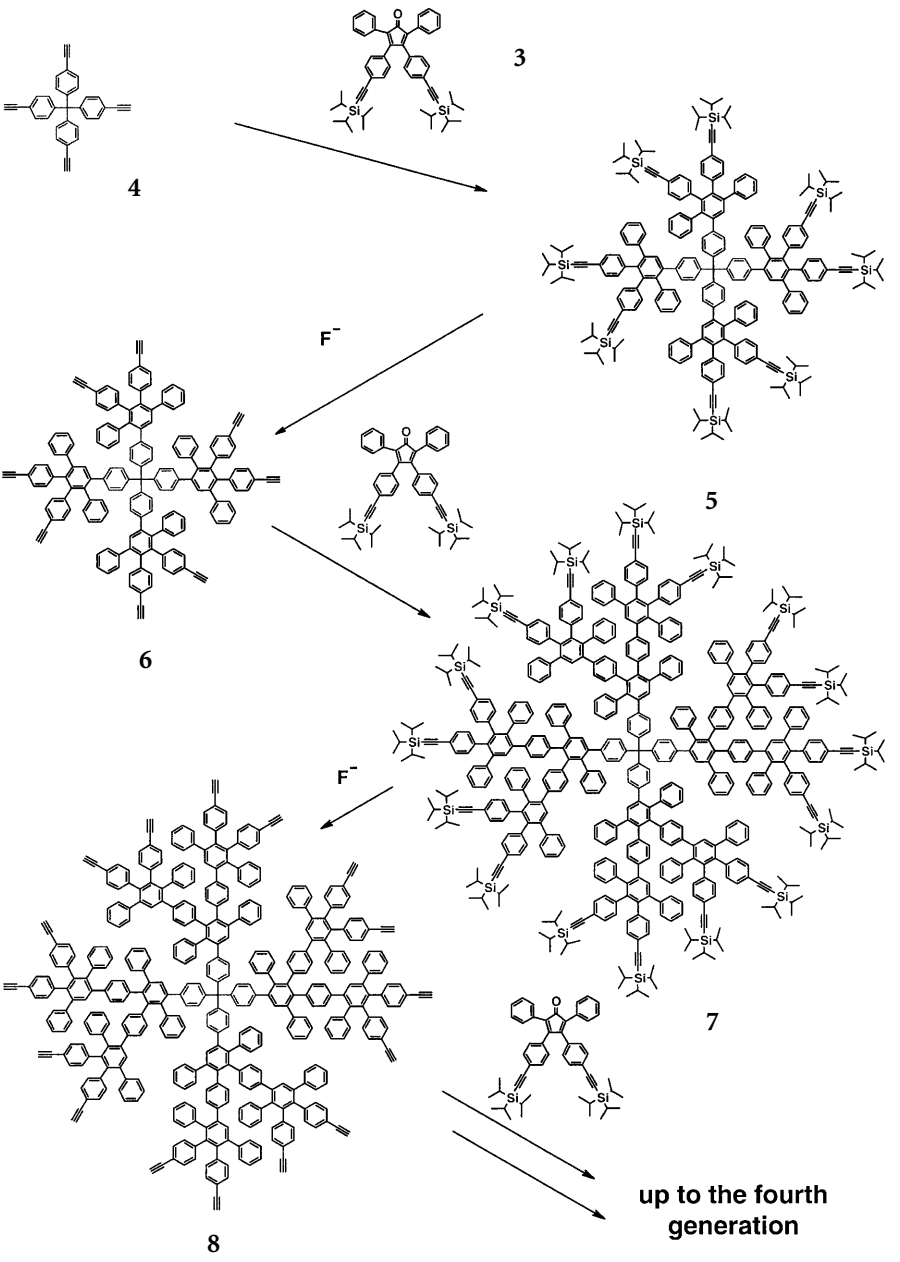

Scheme 3. Divergent synthesis of the polyphenylene dendrimers based on the Diels-Alder cycloaddition

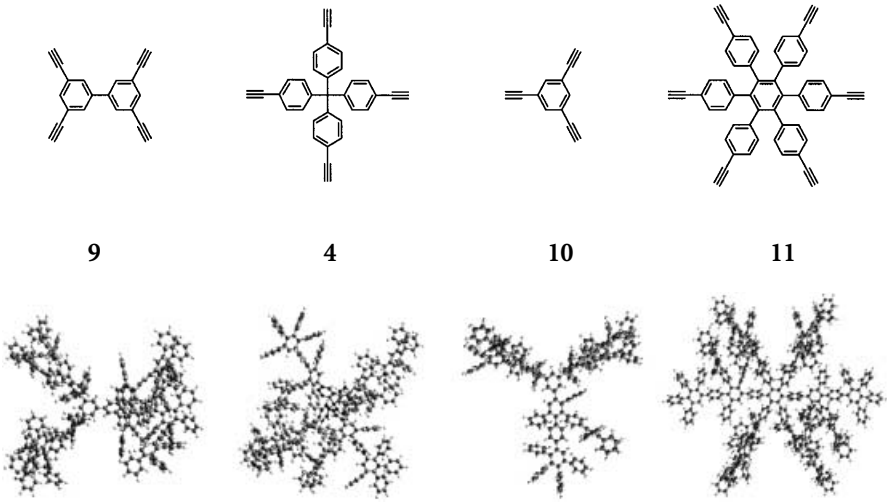

Scheme 4. Variation of the shape of polyphenylene dendrimers by using different cores

The biphenyl core **9** promotes the growth of the dendrimer from the 3,3′,5,5′ positions. The aforementioned tetraphenylmethane core **4** allows a tetrahedral growth of the dendrimer, whereas the 1,3,5-triethynylbenzene core **10** and the hexa-(4-ethynylphenyl)benzene core **11** promote an anisotropic extension along the plane of the central phenylene ring, so that propeller and pancake-shaped dendrimers should be obtained (Scheme 4). From all these cores it is possible to synthesize dendrimers up to the fourth generation, the properties of which will be presented later.

Variation is not only limited to the core. By using building units with different degrees of branching, the density of the dendrimers and therefore their shape can also be influenced. We introduced, apart from the A_2B building unit **3**, the A_4B building unit **12** (Scheme 5). This building unit contains four dienophiles instead of two, which allow the growth of four branches from each functional group. Using this building unit we are able to synthesize the first-generation dendrimers from the tetraphenylmethane core **4** and the biphenyl core **9** substituted with 16 TiPS-ethynyl functional groups. After deprotection of the ethyne groups addition of tetraphenylcyclopentadienone yields the second-generation dendrimers with 104 and 102 phenylene rings, respectively, with a calculated dendrimer diameter of 4 nm. Due to this high density, the addition of a second layer of A_4B building unit to the first-generation ethynyl-substituted dendrimer leads only to polydisperse products, indicating that structurally perfect higher generations are not possible.

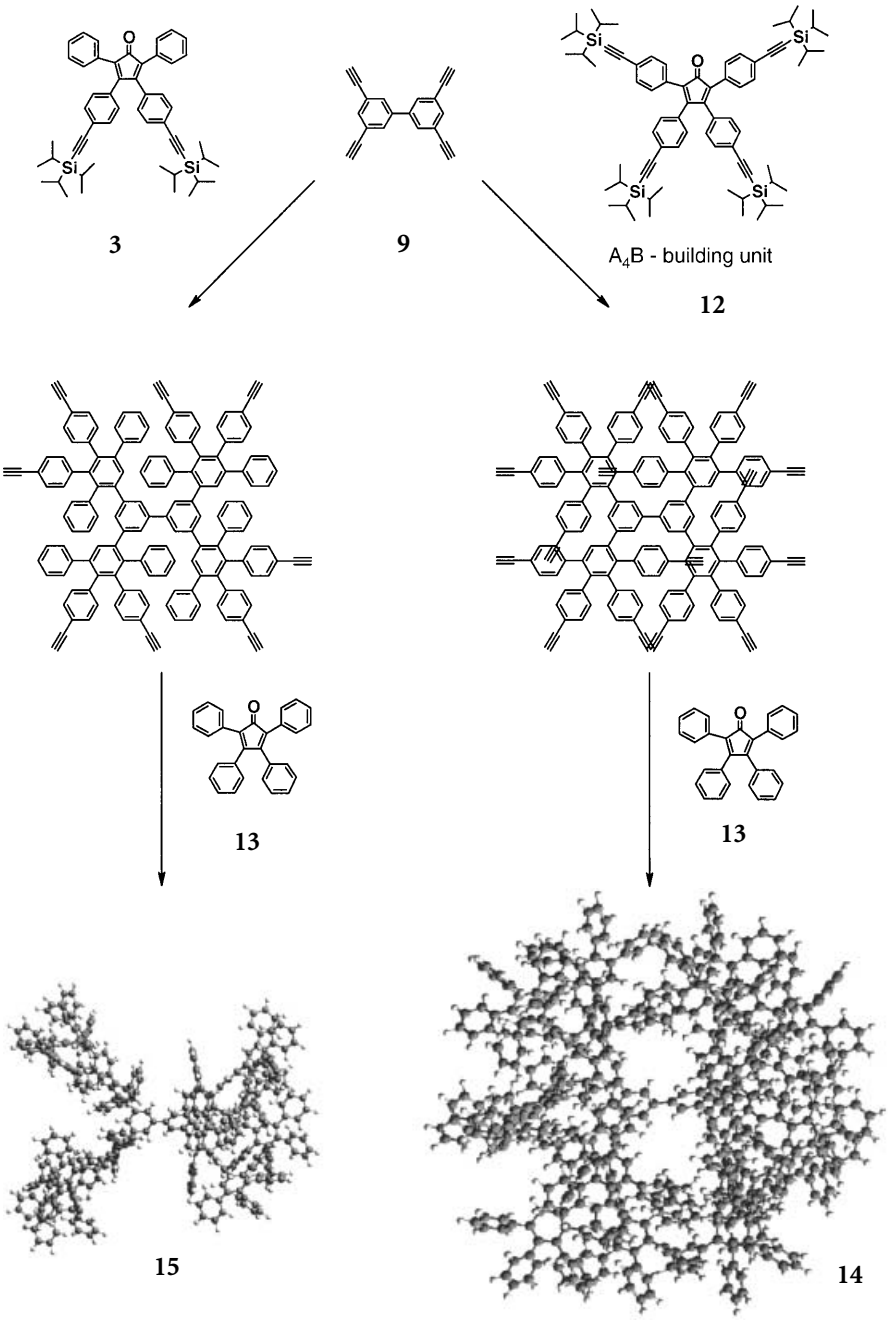

Scheme 5. Variation of the density of the dendrimer by variation of the multiplicity of the building unit

2.2
Convergent Procedures

2.2.1
Via Pd-Catalyzed Coupling

The first report of all-phenylene dendrimers was presented in 1990 by Miller and Neenan [10]. Via a convergent approach, they coupled arylboronic acids to arylbromides under Suzuki-type conditions to synthesize the first two generations of polyphenylene dendrimers based on 1,3,5-triphenylene building units (Scheme 1).

The synthesis begins with the coupling of 3,5-dibromo-1-(trimethylsilyl) benzene to phenylboronic acid, yielding the first-generation dendron **16** (Scheme 6). The trimethylsilyl function is converted to the coupling-active boronic acid by the action of boron tribromide followed by hydrolysis, yielding the first-generation boronic acid substituted dendron **17**. By repetition of the reaction sequence, the second-generation dendrons **18** and **19** are obtained. To synthesize, for example, the dendrimer **21** from the corresponding dendron, the boronic acid **17** is coupled to 1,3,5-tribromobenzene (**20**) (Scheme 6). The overall yield, with 31 %, is limited by the incomplete reactions in each step, as well as side reactions in the Suzuki coupling and the subsequent boronic acid synthesis.

In 1992 Miller and coworkers presented the synthesis of the third-generation-1,3,5-benzene-based polyphenylene dendrimer **23** (Scheme 6) [27]. Whereas the Suzuki-coupling of **19** with **16** to the trimethylsilyl-substituted second-generation dendron occurs with 67 % yield, the subsequent boronation with boron tribromide yields only the protonated product. Therefore the authors turned to a convergent/divergent approach where **19** is coupled to **22**, a core having 4 phenyl rings and 6 bromines. The yield of the coupling step is 58 % and the overall yield based on **16** and **22** is 26 % after purification by column chromatography and recrystallization. TLC-analysis of the progress of the Suzuki coupling reaction indicates that the first three bromines are replaced rapidly, whereas the replacement of the remaining bromines is slower. This result, typical for convergent dendrimer synthesis, is caused by the reduction of the rate of bond formation by nonproductive collisions of the large reactant [8, 27].

2.2.2
Via Diels-Alder Cycloaddition

In 1999 Wiesler and Müllen developed a convergent method for the synthesis of polyphenylene dendrimers based on a pentaphenylbenzene repeating unit [15]. This synthesis is based on two alternating orthogonal reactions: (i) the Diels-Alder cycloaddition of tetraphenylcyclopentadienones to phenylene-substituted ethynyls and (ii) the Knoevenagel-condensation of benzils with 1,3-diphenylacetones to cyclopentadienones. The starting point of the synthesis is 4,4′-diethynylbenzil (**24**) which contains two ethynylic dienophile units and one ethanedione function which can react in a Knoevenagel condensation

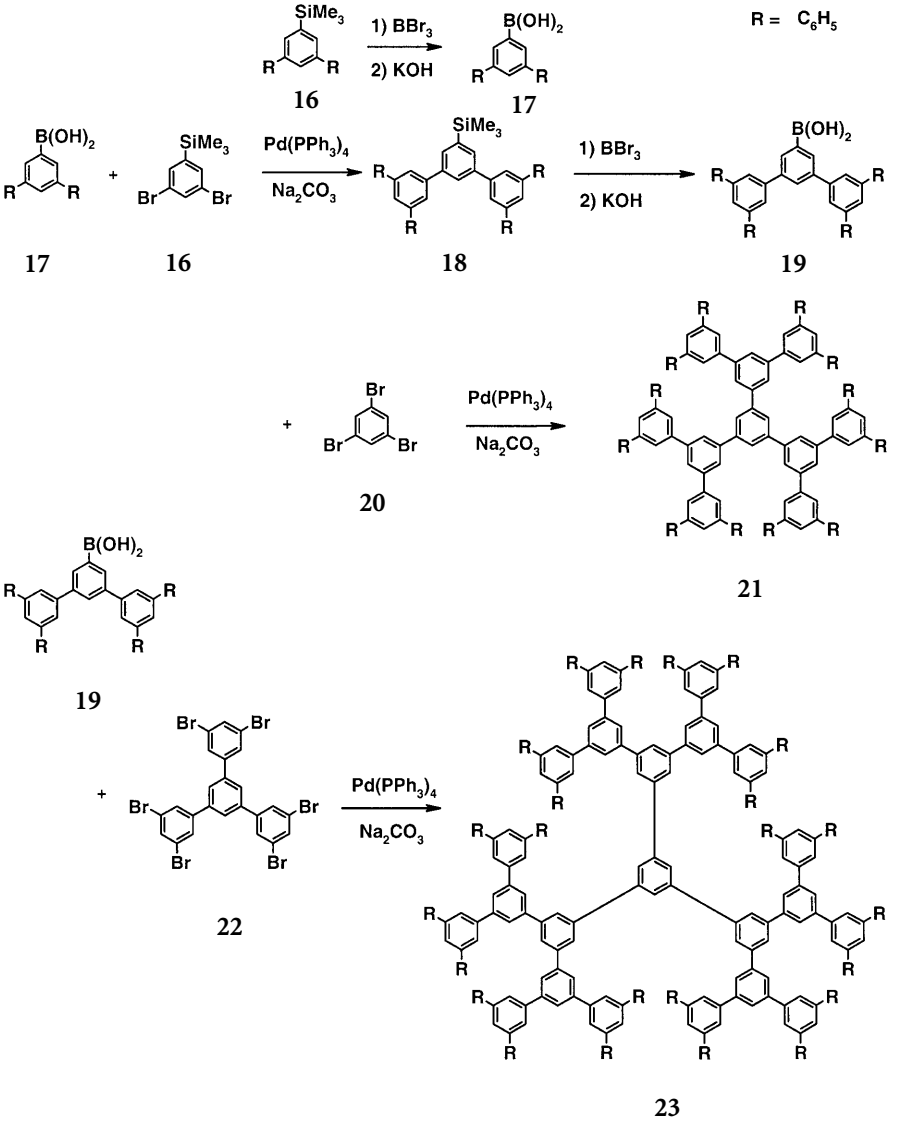

Scheme 6. Palladium catalyzed synthesis of polyphenylene dendrimers

(Scheme 7). The two-fold Diels-Alder cycloaddition of an excess of tetraphenylcyclopentadienone (**13**), which is regarded as a first-generation dendron, to **24** in refluxing *o*-xylene leads to the second-generation benzilic dendron **25**. The dendron is isolated as a pale yellow amorphous powder in 91% isolated yield. The Knoevenagel condensation of **25** with 1,3-diphenylacetone (**26**) to the corresponding cyclopentadienone dendron **27** is achieved in dioxane and in the presence of tetrabutylammonium hydroxide as a base. Like **25**, the cyclopentadi-

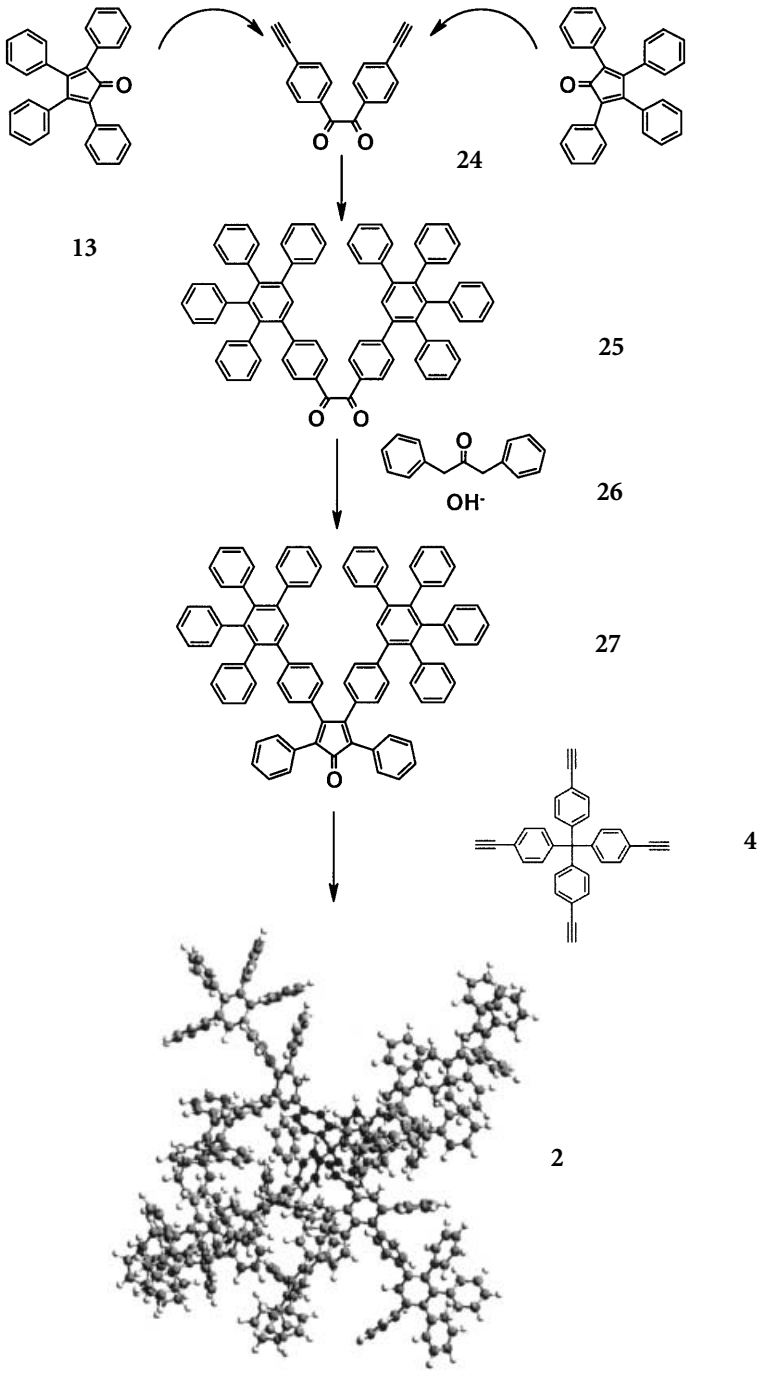

Scheme 7. Convergent synthesis of the polyphenylene dendrimers based on the Diels-Alder cycloaddition

enone dendron **27** can be easily precipitated in ethanol, in this case as a pale red solid in 85% yield. The synthesis of the next generation of the cyclopentadienone dendron, via the Diels-Alder cycloadditon of **27** to **24** and followed by the base-catalyzed Knoevenagel condensation of 1,3-diphenylacetone (**26**) to the resulting benzil dendron, fails due to the incomplete Knoevenagel condensation.

The fourfold cycloaddition of an excess of cyclopentadienone dendron **27** to the tetraethynyltetraphenylmethane **4** in diphenylether at 200 °C affords dendrimer **2** in 85% isolated yield, respectively (see Scheme 7). Dendrimer **2** corresponds to the second-generation polyphenylene dendrimer made by the divergent method [30]. It should be mentioned that while the addition of dendron **27** to the biphenyl core **9** takes two days the addition to the tetraphenylcore **4** takes one week. This can be explained by the higher mobility of the biphenylic core compared to the stiff tetrahedral core, which allows the proper orientation of the ethynyl functions for reactions with the bulky dendrons.

Compared to the divergent approach, the convergent method at first glance yields the same monodisperse products with similarly high yields. However, though the convergent method can be used to synthesize dendrimers only up to the second generation, this method opens the way to dendritic polymers carrying substituents of more than just one kind. In contrast, the divergent approach may be successfully used up to the fourth generation, but it only allows the ordered attachment of one kind of functional group. Both methods have in common that they yield monodiperse polyphenylene dendrimers in high yield.

3 Characterization

To characterize dendrimers, analytical methods used in synthetic organic chemistry as well as in macromolecular chemistry can be applied. Mass spectrometry and NMR spectroscopy are especially useful tools to estimate purity and structural perfection. To get an idea of the size of dendrimers, direct visualization methods such as atomic force microscopy (AFM) and transmission electron microscopy (TEM), or indirect methods such as size exclusion chromatography (SEC) or viscosimetry, are valuable. Computer aided simulation also became a very useful tool not only for the simulation of the geometry of a distinct molecule, but also for the estimation of the dynamics in a dendritic system, especially concerning mobility, shape-persistence, and end-group disposition.

Good solubility (see below) of the polyphenylene dendrimers enables characterization by mass spectrometry, which is an excellent tool for determining their molecular mass and purity. Usually characterization is performed using fast-atom-bombardment (FAB), matrix-assisted-laser-desorption-ionization-time-of-flight mass spectrometry (MALDI-TOF) or field-desorption mass spectrometry (FD). Miller et al. characterize their dendrimers using FAB mass spectrometry for compounds with masses up to 3500 g/mol [27]. Concerning the purity, they reported that, according to their mass spectra, clean parent ions for each dendrimer are detected [10]. We are able to characterize our polyphenylene dendrimers up to the fourth generation using MALDI-TOF mass spectrometry [36]. An example mass spectrum of one of several perfect dendrimers, in this

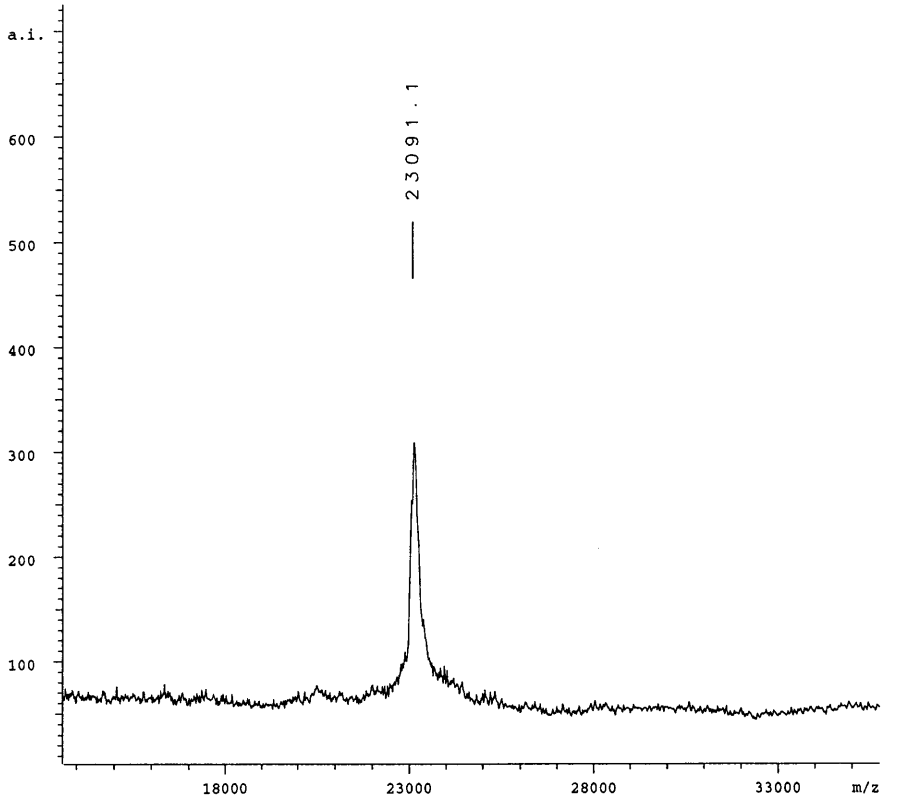

Scheme 8. MALDI-TOF mass spectrum of **30**. The calculated molecular weight of $[C_{1812}H_{1210}, Ag]^+$ **30** is 23091 g/mol

case the fourth-generation dendrimer **30**, is given in Scheme 8, showing only one single peak corresponding to the molecular mass. The perfect agreement between the calculated and experimentally determined m/z ratios for different generations of dendrimers confirms their monodispersity not only for these unfunctionalized polyphenylene dendrimers, but also for those bearing functional groups.

The characterization of our polyphenylene dendrimers via mass spectrometry is particularly valuable because it allows the detection of potential growth imperfections during the [2+4] cycloaddition, even at the higher generations with molecular masses above 20,000 g/mol. In this way, incompletely reacted products give signals at lower molecular masses with characteristic mass differences in comparison to a perfectly reacted dendrimer.

Beside mass spectrometry, NMR spectroscopy is a useful and widely applied tool to characterize the structure of dendrimers and estimate their purity [37]. In the case of polyphenylene dendrimers NMR spectroscopy is of only limited value for determining structure and purity. This is due to the large number of

aromatic protons and carbons within each new dendrimer generation, leading to an increasing number of overlapping signals in the spectra. Nevertheless, for the smaller dendrimers (up to the second generation) structural characterization is possible. Characterization of higher generations is also feasible if the dendrimers possess symmetry, such as D_{3h} symmetry for the polyphenylene dendrimers developed by Miller and coworkers, which diminishes the number of NMR signals and makes them more easily distinguishable and assignable [10, 28]. In our case, the appearance of characteristic signals, such as a singlet for the proton of the central benzene of the pentaphenylbenzene subunits, allows the identification of different layers of the dendrimer.

To obtain some insight into the dynamics of our polyphenylene dendrimers based on a biphenyl and tetrahedral core, we subjected them to solid-state NMR experiments. These experiments should provide information on the mobility of different parts of the dendrimers. For the detection of slow dynamics within the dendrimer, (typical frequencies between 10^{-1} and 10^{3} Hz), static ^{13}C exchange and CODEX (centerband-only-detection of exchange) experiments have been applied in cooperation with Spiess et al. [38, 39]. They show that our polyphenylene dendrimers are surprisingly rigid dendrimers and that slow dynamic processes are limited to local flip motions of single phenyl rings with flip frequencies of 10 Hz. Spiess et al. [39, 40] also demonstrated that the mobility of the dendrimer increases with each further generation. This can be an explanation for the observed better solubility of higher generation dendrimers. These experiments also reveal that dendrimers based on the tetrahedral core, like **2**, are less mobile than those based on the biphenyl core, like **15**, which shows mobility along the inner biphenyl bond of the core. Fast motional processes with correlation times on the μs scale were characterized by ^{13}C-^{1}H-Multiple-Quantum Spectroscopy. These motional processes can be attributed to 60° vibration of phenyl groups around their linking bond.

SEC (size exclusion chromatography) can be a useful tool in the analysis of the molecular mass, but is more reliable for the dispersity of the resulting dendrimers. However the molecular weights obtained for polyphenylene dendrimers are at best approximately correct and may in some instances be seriously in error, as is typical when dealing with molecules differing from the polystyrene standard. Size-exclusion chromatograms of Miller and Neenan dendrimers support the assertion that they are single compounds [10, 27]. Their chromatograms show monomodal single peaks whose retention times decrease with increasing molecular weight. The narrow monodispersity of these dendrimers compares quite favorably with those of polystyrene molecular weight standards. As is typical, the higher the molecular masses of our dendrimers, the shorter are the retention times on the SEC column. The measured molecular masses calculated from the SEC traces of our dendrimers based on polystyrene standards are lower than the nominal masses and the differences increase with increasing molecular mass [41]. One can interpret this phenomenon by noting the adoption of a more globular shape for the dendrimers compared to polystyrene random coils. The M_w/M_n-ratio obtained by SEC is found to be between 1.03 and 1.05 which is characteristic for monodisperse dendrimers [7]. Compared to MALDI-TOF mass spectrometry, results obtained from SEC give only qualitative

answers about the dimension and the purity because the resolution of SEC is not high enough to detect small defects on the dendrimers. Very good agreement between nominal molecular masses and measured ones is given by vapor pressure osmometry. Whereas for the second-generation dendrimer **2** the measured mass corresponds very well to the nominal ones, for higher generations the measured masses are lower due to the experimental limitations of this method for high molecular masses [42].

Polyphenylene dendrimers are thermally extremely stable, as expected for molecules consisting of benzene units. The unsubstituted polyphenylene dendrimers based upon 1,3,5-trisubstituted benzene synthesized by Miller and coworkers as well as our unsubstituted dendrimers start to decompose at temperatures above 450 °C as revealed from TGA under air and nitrogen [27]. The decomposition temperature for substituted dendrimers strongly depends on the introduced functionality. DSC experiments have been performed to study the thermal behavior and possible phase transitions of polyphenylene dendrimers. Miller and coworkers observed glass-transitions due to higher conformational mobility for their dendrimers. The glass-transition temperatures increase with molecular weight from 126 °C for the first generation to 220 °C in the third generation (**23**). Our unfunctionalized dendrimers show neither glass transitions nor other phase changes below the decomposition temperature due to the higher stiffness as well as the larger molecular weight.

It is difficult to evaluate the shape of such dendritic particles experimentally. However, some insight can be gained by atomic force microscopy (AFM) and transmission electron microscopy experiments (TEM). AFM experiments can give information about the overall size of the dendrimers, as shown by De Schryver [43], by spincoating very dilute solutions of dendrimers like **30** on mica, then visualizing single dendrimers. Their height measured in this manner corresponds very well to the diameters calculated by molecular mechanics simulations. First results from TEM measurements also confirm the expected dimensions [44]. Unfortunately, due to resolution limits, up to now direct visual information could not be obtained about the shape of the dendrimers.

In recent years, computer simulation has become a widely used tool giving the chemist a good indication of the three-dimensional structure and the dynamic behavior of a molecule. Molecular calculations therefore seems to be suitable for the consideration of structural aspects.

Molecular mechanics optimization gives information about the theoretical extension of a molecule which can be compared with experimentally obtained data, e. g., AFM to get a better idea about the size and shape of these molecules. We estimated the diameters of the first- to the fourth-generation dendrimers based on the biphenyl core by using the Cerius^2 molecular modeling package (Scheme 9) [31, 45, 46]. Table 1 gives an overview of the number of phenylene rings, molecular masses, and calculated sizes of different generations of unfunctionalized polyphenylene dendrimers from us and those synthesized by Miller et al. [27]. It is obvious, that our dendrimers grow much faster and have a higher packing density of phenylene rings in comparison to those of Miller et al.

Molecular mechanics calculations on dendrimer **28** and **15** reveal the existence of several local minima. To obtain the global energy minimum, one-half of

the molecule was optimized in the first step by energy minimization using 144 and 1024 different conformers. Following this method, one conformer for half of **28** and **15** with a lower energy than any other has been found (Scheme 10) [47]. This conformer has been used to build the complete dendrimer. Thus the proposed three-dimensional structure of **15** finally consists of a twisted central biphenyl unit carrying four branches which are nearly orthogonal to the central biphenyl unit.

Molecular dynamics calculations on a second-generation dendrimer, like **15**, based on a biphenyl core have shown that this molecule does not significantly change size and shape when allowing rotations about the inter-ring bonds. The observation of the intermolecular distances shows that all distances changed by only 5–10% throughout the whole simulation time, which indicates that the overall shape of the molecule is persistent. This behavior can be due to the very large number of benzene rings in a defined space (high packing density) causing strongly correlated rotations within the molecule as well as the rigidity of the poly-*p*-phenylene chain in each branch [45]. In fact they can thus be regarded as shape-persistent nanoparticles. This is in strong contrast to conventional dendrimers, which are built up from aliphatic bonds, where the conformational mobility allows backfolding of the branches.

This stiffness also has an influence on the shape of the dendrimers, when different core building units are employed. The biphenyl core **9** leads to the dumbbell shaped molecule whose most stable conformers show a twist between 20° and 60° around the central biphenyl unit. **2**, based on the tetrahedral core **4**, with a diabolo-like molecular shape which resembles the shape of the core very well. Due to the large number of benzene rings around the central methane unit, the branches are hindered in their rotation (Scheme 4), lowering the internal mobility of the molecule compared to **15**.

According to these simulations, the dendrimers based on core **10** adopt a false-propeller structure, while the dendrimers based on the hexaphenylbenzene core **11** adopt a true-propeller type structure. The difference lies in

Table 1. Overview of the number of phenylene rings, molecular masses, and calculated sizes of different generations of unfunctionalized polyphenylene dendrimers from us and those synthesized by Miller et al. [27]

	Number of phenyl rings	Molecular mass g/mol	Size (nm)
Dendrimers based on Pd-catalyzed coupling			
(G1)	10	760	2.0
(G2)	22	1670	2.8
(G3)	46	3500	3.5
Dendrimers based on Diels-Alder cycloaddition			
Biphenyl core (G1)	22	1670	2.5
Biphenyl core (G2)	62	4720	3.8
Biph A4B (G2)	102	7760	3.6
Biphenyl core (G3)	142	10810	5.1
Biphenyl core (G4)	302	22980	6.4

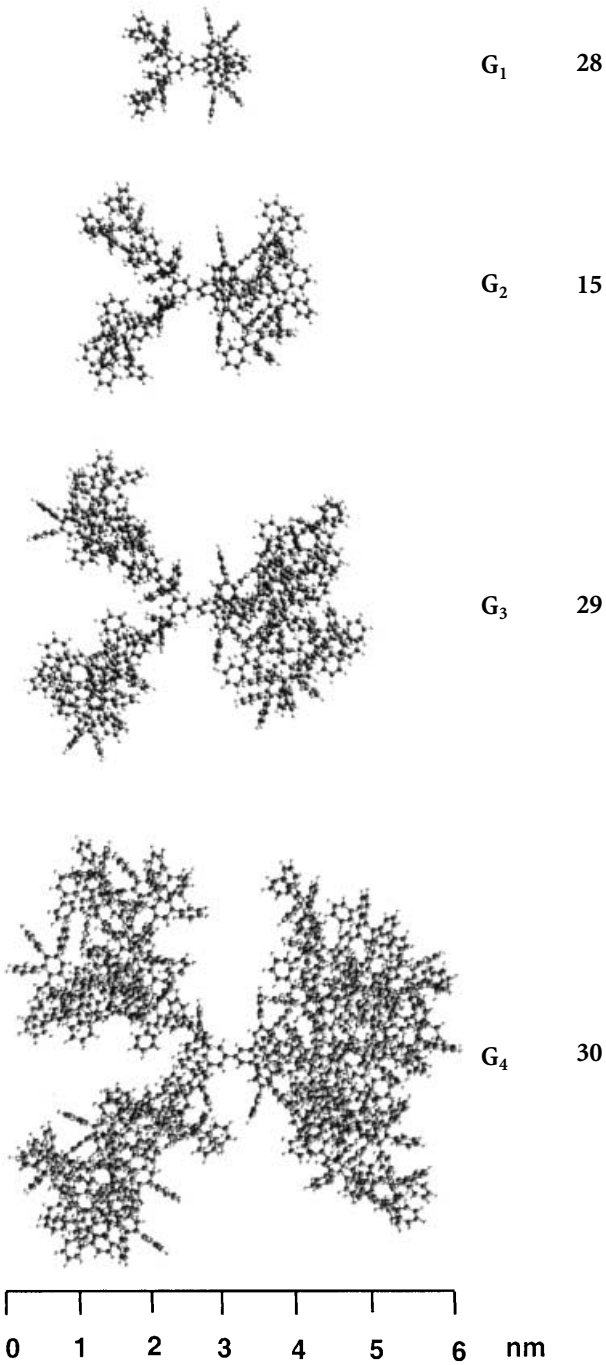

Scheme 9. Three-dimensional stick-and-ball model of the first four generations of a polyphenylene dendrimer built from the biphenyl core and the A_2B building blocks

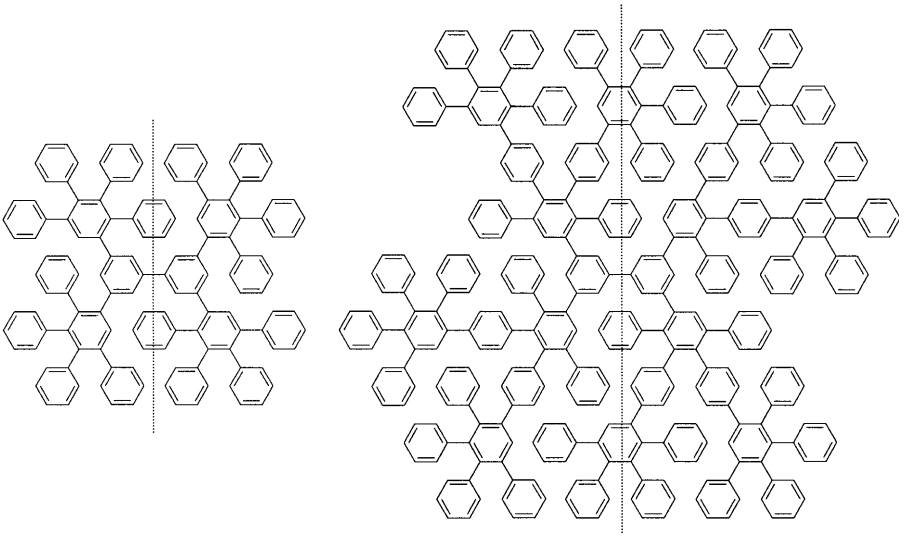

28 **15**

Scheme 10. Chemical structure and procedure for the calculation of the polyphenylene dendrimer generations G_1 and G_2. The *dotted lines* mark "half-G_1" and "half G_2," respectively

the orientation of the branches around the center of the molecule. In the case of the false propeller, there is no rotational symmetry around the center [34, 45].

The shape of the entire polyphenylene dendrimer is also determined by the building block used. Dendrimers based on the A_4B-branching unit **12** tend to adopt a spherical shape, even at lower generations, regardless of the type of the core. This is not only due to the extremely high density of phenyl rings (40 phenyl rings more in comparison to a **15** dendrimer) within the dendrimers **14**, but also to the fact that the A_4B-branching unit **12** allows a more even growth in all directions than unit **3** [33].

4 Functionalization

In contrast to dendrimers built up from aliphatic chains, polyphenylene dendrimers exist as shape persistent nanoparticles as we have demonstrated above. The preparation of functionalized dendrimers is the key step towards various applications.

Functional groups can be introduced at different locations in the dendrimer. Placement in the core of the dendrimer results in a topological isolation and protection of the functional group from the environment [48, 49]. Furthermore, single shells of the dendrimer corresponding to different generations can be endowed with functionalities [50]. Thus particles with functions having a defined depth under the surface can be realized. The decoration of the dendrimer sur-

face with functionalities yields a multiplication of the functional groups placed strictly at the outer perimeter [51].

It has been shown that the variation of the dendrimer core strongly influences the structure of polyphenylene dendrimers (Scheme 4). However, the introduction of functional groups at the periphery does not influence the shape of the polyphenylene dendrimers, because of their rigid structure where a backfolding of the branches is barely possible [31]. In this way, functionalization of the stiff dendrimer leads to a shell consisting of the functional groups shielding the aromatic interior. This constitutes a strong contrast to dendrimers built up from aliphatic chains where the functional groups of the outer generation are distributed evenly throughout the molecular volume [11]. Therefore, polyphenylene dendrimers are attractive targets as they allow tailor-made modulation of their physical and chemical properties, e.g., volatility, polarity, solubility and adsorption by introduction of functional groups into the last generation. They also allow selective group insertion into the "microsphere" inside of the macromolecule.

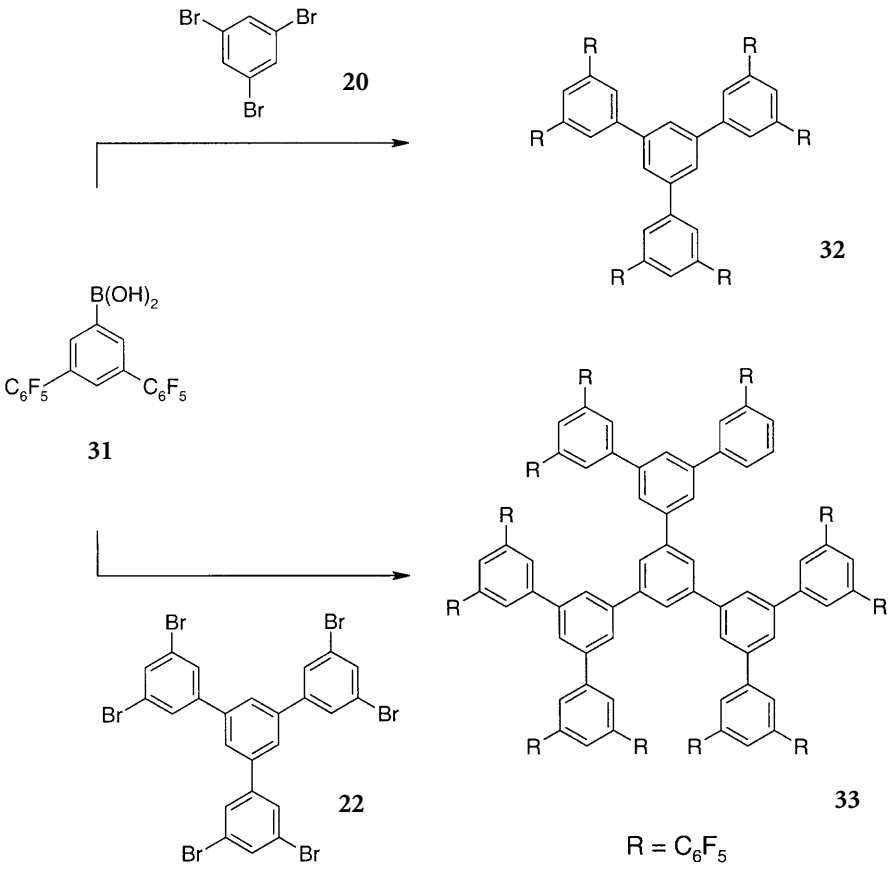

Scheme 11. Palladium catalyzed synthesis of fluorinated polyphenylene dendrimers

Miller et al. reported the convergent synthesis of different generations of polyphenylene dendrimers bearing perfluorinated phenyl rings in the outer sphere [27]. These fluorinated materials are of interest due to their more hydrophobic behavior and their increased volatility [27]. The synthesis of these fluorinated dendrimers is achieved via Suzuki-coupling of a 3,5-bispentafluorophenylboronic acid (**31**) with 1,3,5-tribromobenzene (**20**) for the first-generation or with 1,3,5-tris(3,5-dibromophenyl)benzene (**22**) for the second-generation dendrimer (Scheme 11). In this way Miller et al. were able to synthesize polyphenylene dendrimers decorated with 30 (second-generation **32**) and 60 (third-generation **33**) fluorine substituents at the periphery.

We are able to functionalize our polyphenylene dendrimers via three different methods: the use of functionalized cyclopentadienones, polymer-analogous reactions (group conversions), and electrophilic aromatic substitution.

4.1
A Priori Group Introduction

The introduction of the functional group in the course of the synthesis (a priori) presents an elegant way to place the functionalities in topologically well defined locations in the dendrimer.

4.1.1
Cyclopentadienone-Route

By means of this synthetic approach, we are able to place a defined number of groups in any shell (i.e., generation) of the dendrimer. This can be achieved by

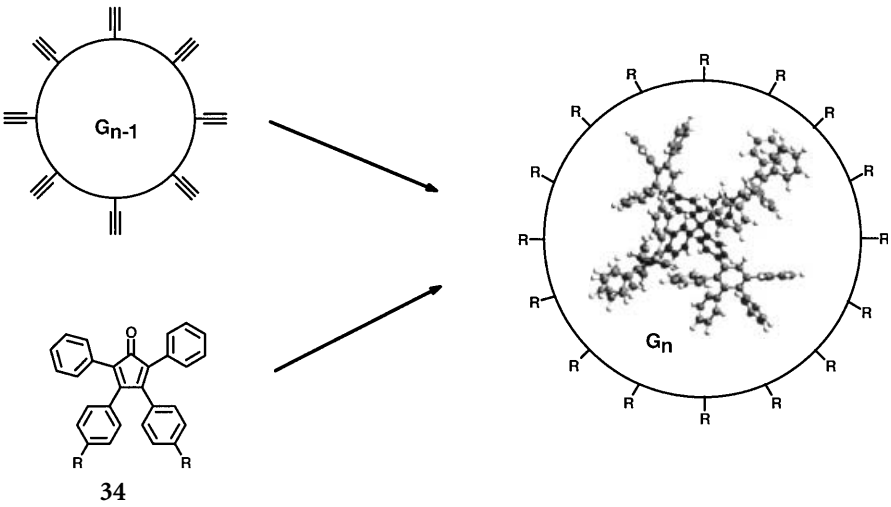

Scheme 12. Functionalization of polyphenylene dendrimers via the cyclopentadienone route

using cyclopentadienone building units carrying the functional groups **34** (Scheme 12) [29, 34, 35, 47].

We thus obtain defined, monodisperse, defect-free functionalized dendrimers, which are easily purified due to the high mass differences between the cyclopentadienone and the final dendrimer. However, for each new functionality, an appropriate cyclopentadienone building unit has to be synthesized. This can be achieved via a double *Knoevenagel* reaction of an already functionalized benzil **35** and diphenylacetone **24.** For example, 4,4′-dibromobenzil (**35 a**) as well as 4,4′-dimethoxybenzil (**35 b**) are commercially available and give the cyclopentadienone building unit with two bromo- or methoxy substituents in high yields [30, 34]. Furthermore the bromo substituent of the dibromocyclopentadienone can be quantitatively converted into a cyano (**37**) or amino (**38**) function (Scheme 13) [52].

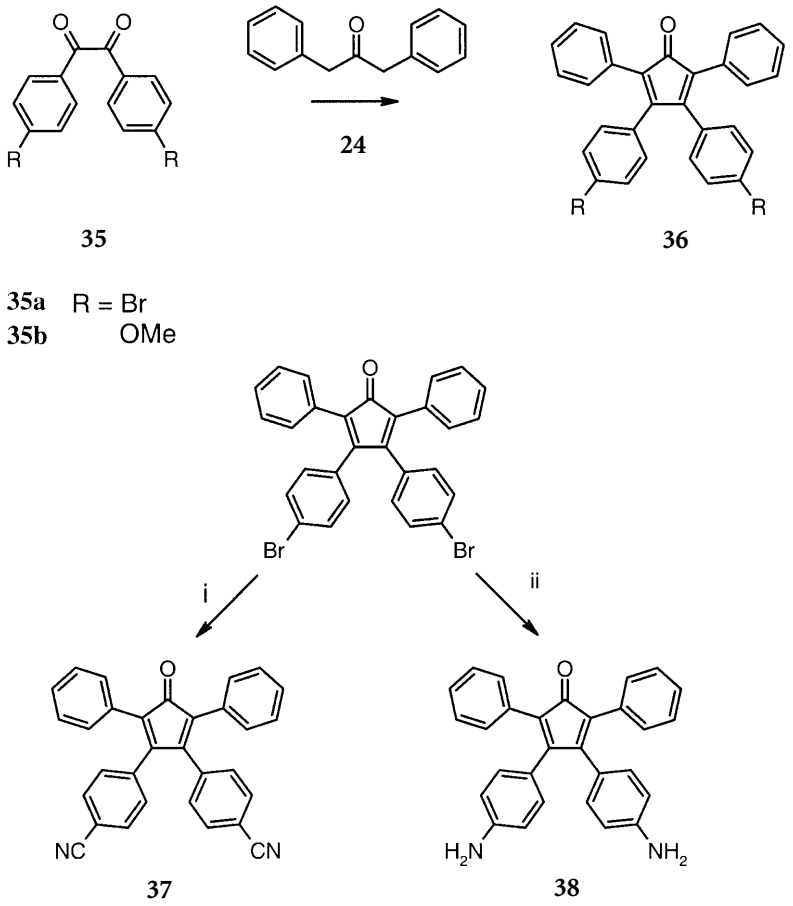

Scheme 13. Synthetic ways to functionalized cyclopentadienones (i, CuCN, DMF; ii, $(C_6H_5)_2NH$, tris(dibenzylideneacetone)dipalladium (0), 2,2′-bis(diphenylphosphinol)-1,1′-binaphthyl (rac.), $CsCO_3$, toluene)

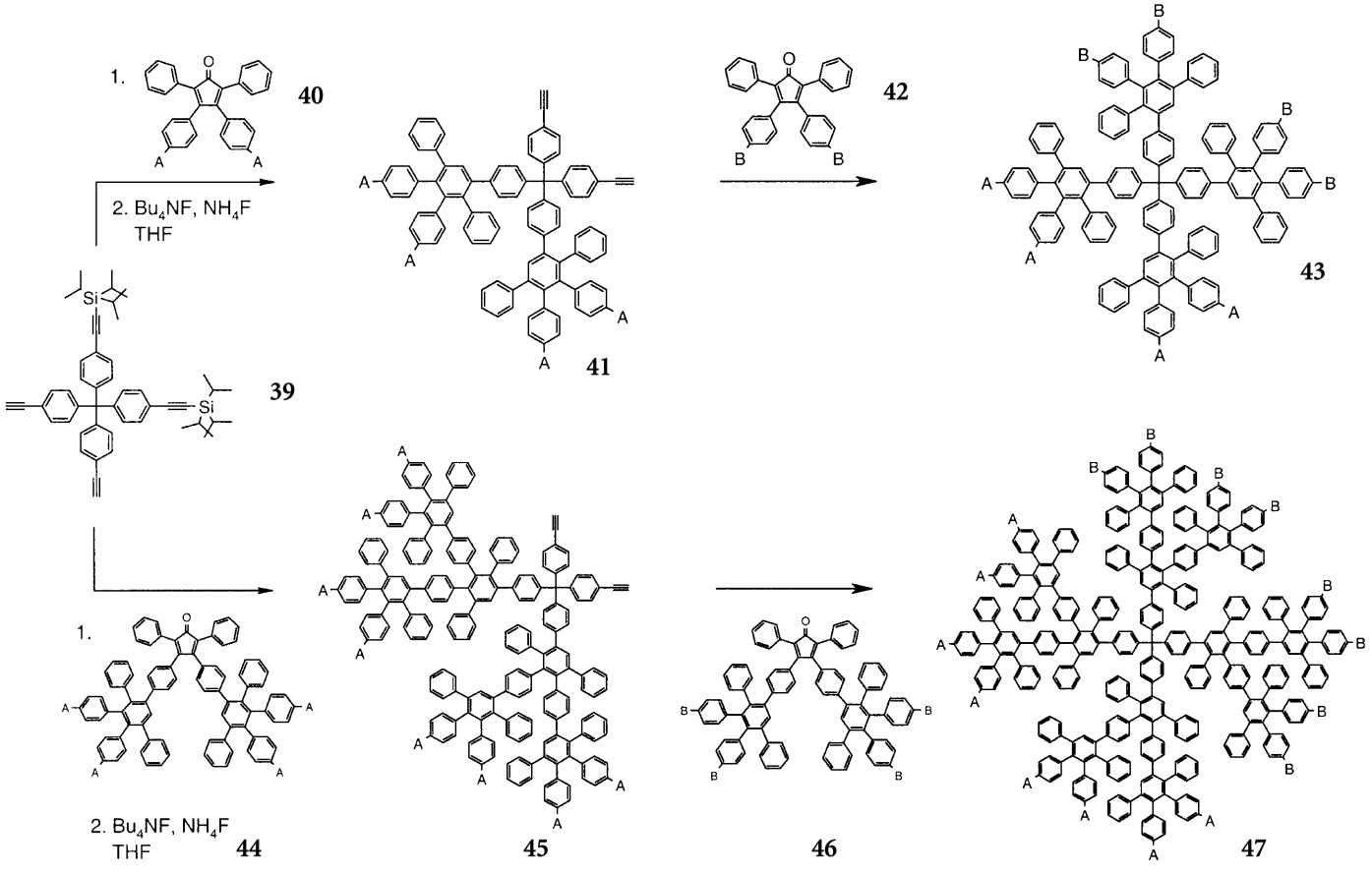

Scheme 14. Synthesis of dendrimers bearing two different types of functionalities at the periphery

Since the Diels-Alder reaction takes place at high temperatures only, an important requirement of the functional groups is their thermal stability, which in some cases necessitates protection. So far we were able to decorate our polyphenylene dendrimers via this method with various functional groups including methoxy-, amino-, cyano-, halogen-, thiomethyl-, perylenemonoimidyl-, and thiophenyl.

The cyclopentadienone chemistry also represents a powerful method for the synthesis of dendrimers bearing two different types of functional groups at the surface of a single dendrimer [52]. We started from a partially protected tetrahedral core (**39**, Scheme 14) and used a Diels-Alder reaction with the free acetylene unit of the core and a cyclopentadienone building block containing a functional group of type "A" **40**. Deprotection of the protected acetylene units of the core and Diels-Alder reaction with a cyclopentadienone coated with a functionality of type "B" **42** leads to a first-generation dendrimer **43** with two kinds of functionalities (type A and type B) in a well defined spatial arrangement at the rim. We also achieved the synthesis of a second-generation *bifunctional* dendrimer **47** using the convergent synthetic approach as presented in Scheme 7 with functionalized dendrons [52].

In contrast to aliphatic dendrimers coated with cyano and benzyl ether moieties or amphiphilic groups reported by Fréchet et al. [14, 53–56], our bifunctional dendrimers have the advantage that the distance of the two functionalities is predetermined.

4.2
A Posteriori Group Introduction

The generation of functional groups after the completed synthesis of the dendrimer (a posteriori) constitutes a quick and variable way to get access to a large number of functionalized dendrimers.

4.2.1
Polymer-Analogous Reactions

The conversion of an already existing group A on the dendrimer into a substituent B by subsequent addition of an electrophile is presented in Scheme 15. In the ideal case, this reaction should be quantitative, but the possibility of incomplete conversions or byproducts is always a danger [57]. We are able to functionalize our dendrimers via this method with carboxy-, hydroxy-, amide-, and lithium groups at the periphery (Scheme 15) [52]. Except for the conversion of an amino group to an amide, all the other groups given in the scheme are obtained quantitatively. The hydrolysis of a cyano group on a second-generation polyphenylene dendrimer with a tetrahedral core for example leads to a dendritic molecule **48** bearing 16 carboxylic acid functions at the periphery (Scheme 17).

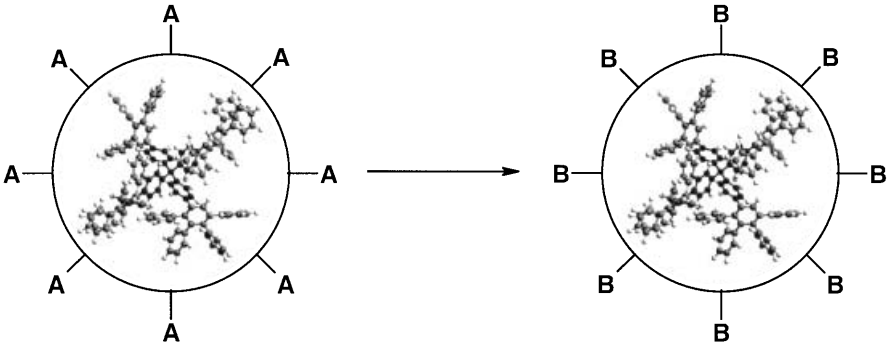

Group Conversion		
A		B
CN	$\xrightarrow{i}$	COOH
OMe	$\xrightarrow{ii}$	OH
NH_2	$\xrightarrow{iii}$	NHCOR
Br	$\xrightarrow{iv}$	Li

i KOH/TEG;
ii BBr_3/DCM, 1d;
iii RCOOH/DCC/DMAP, DCM 1:3, 3d
iv n-BuLi/THF

Scheme 15. Polymer-analogous reactions on polyphenylene dendrimers

4.2.2
Electrophilic Aromatic Substitution

Furthermore, we applied electrophilic aromatic substitution on the final dendrimer as a quick method for functionalization, because no further building units have to be synthesized (Scheme 16) [58]. However, this approach leads to a statistical distribution of the functionalities over the surface of the dendrimer. It is nevertheless possible to adjust the approximate number of groups via the electrophile/dendrimer ratio. So far, chloromethyl, aminomethyl, and sulfonic acid groups have been attached. A second-generation dendrimer with a tetrahedral core has been substituted, for example, with 3–4 sulfonic acid groups by using a small electrophile/dendrimer ratio. By applying a high electrophile concentration, up to 40 sulfonic acid functions can be attached.

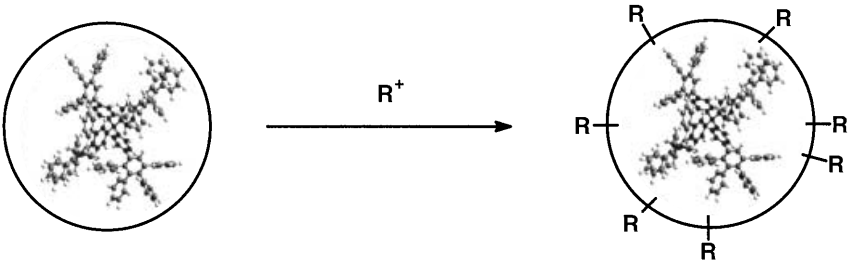

Scheme 16. Functionalization via electrophilic aromatic substitution of unsubstituted polyphenylene dendrimers

5
Functional Dendrimers – Applications

In recent years, nanochemistry – and in this context, the preparation and characterization of nanoparticles and nanostructured materials – has opened up exciting new possibilities for applications in a number of areas including automotive, sensors, color imaging, printing, computer chips, and medicine [59]. The relatively new dendrimers provide fascinating access to discrete molecules of molecular masses in the kDa scale. The polymers used until now for "nanoapplications" were limited in certain respects by not having a distinct size and chemical nanoenvironment. It can be anticipated that these limitations might be overcome by dendrimers and polyphenylene dendrimers are particularly attractive due to their shape persistence. Functionalities at the periphery of polyphenylene dendrimers can modulate their polarity and open the way to water-soluble systems, which are of interest as hosts for hydrophobic molecules. They can also serve as linkers for further modifications, e.g., the attachment of catalysts and fluorescent dyes is quite feasible [60, 61]. It is noteworthy that the invariant shape of polyphenylene dendrimers gives access to the study of interactions of neighboring groups, e.g., interactions of dyes in a close but defined vicinity, and can be used for spatial isolation of a functionality in the interior. This is a distinct advantage over more flexible aliphatic dendrimers. The application of some of our polyphenylene dendrimers as precursors for the synthesis of large graphite subunits, which goes along with a reduction in dimensionality of the dendrimer, will be discussed at the end of this chapter.

5.1
Water Soluble Polyphenylene Dendrimers as Nanocarriers

Recently, several articles have been published dealing with water soluble dendrimers, due to their outstanding structure and properties which are similar to natural micellar systems, e.g., liposomes. Scheme 17 shows such an example of a dendritic micelle containing a hydrophobic inner core surrounded by a hydrophilic layer of carboxylate groups. The most important difference to natural micelles is that dendritic micelles are covalently bound structures and not dyn-

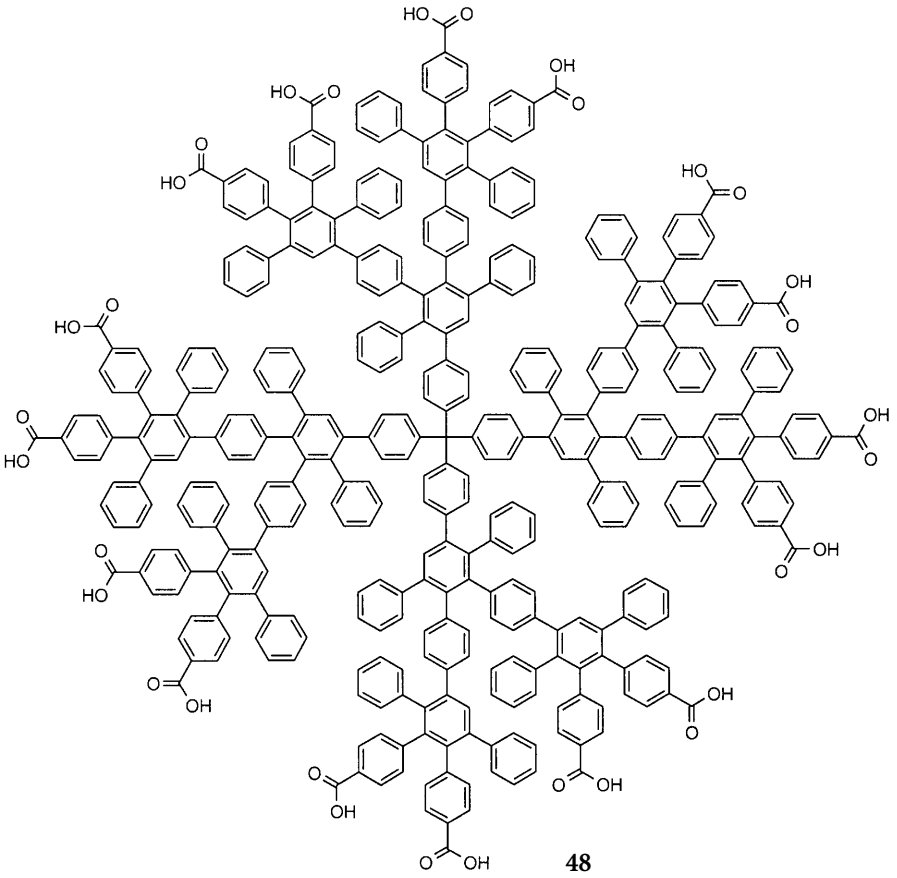

48

Scheme 17. Water soluble second-generation polyphenylene dendrimer decorated with 16 carboxy-functions

amic associations of individual molecules [62]. This property has been used to design recyclable solubilization and extraction systems which might be applied in the recovery of organic materials from aqueous solutions [55, 63]. Dendritic micelles do not display a critical micelle concentration and therefore they also show solvation ability at low concentration.

In contrast to dendrimers built up from aliphatic chains, polyphenylene dendrimer micelles possess shape and size persistent cavities due to their rigid scaffold which strongly depends on the type of dendrimer. In this case a selective incorporation of guest molecules, e.g., fluorescent dyes, should be possible, dependent on the size of the guest molecule and the cavity of the host. The non-covalent uptake of dyes with an appropriate size thus allows the investigation of their interactions within the dendritic micelle. In our case we made the second-generation polyphenylene dendrimer **48,** which bears 16 carboxy-functions at the periphery, by starting from a tetrahedral core and an appropriately

functionalized cyclopentadienone [58]. The sodium salt of this dendrimer is water-soluble. The solvatation properties of dendrimer **48** have been investigated by using the amphiphilic dye pinacyanol chloride as a solvatochromic probe.

To estimate how many dye molecules fit into the dendritic micelles, UV-titration experiments have been employed. In comparison with the spectra of a pure pinacyanol chloride solution in water, the peaks of the absorption maxima of the dye in the presence of the dendrimer are shifted bathochromically due to solvatochromic effects, which indicates the incorporation of the dye within the branches of the dendrimer. At dye-to-dendrimer molar ratios higher than 4:1, in addition to the bathochromic shifts, hypsochromically shifted peaks start to appear, indicating that the dendrimer is not incorporating further dyes. We interpret this as an incorporation of up to four dyes within the branches of the dendrimer. This observation correlates with the calculated available space within the dendrimer, obtained from the molecular simulations. Further studies of the interactions of the dyes within the dendritic micelle are in progress.

5.2 Polyphenylene Dendrimers as Nano-Supports

As previously mentioned, functionalized polyphenylene dendrimers can also be used as supports with the already existing functional groups at the periphery, serving as linkers for further modifications. The attachment of several functional centers on the surface of polyphenylene dendrimers leads to a multiplication of the properties of a single functionality, such as an increase in fluorescence intensity via the decoration of polyphenylene dendrimers with a distinct number of fluorescent dyes. Furthermore, the fact that the functional groups have a predetermined and defined distance from each other allows the study of the dependence of their interactions on the distance between them. Such investigations could give a deeper insight into the differences of single molecule behavior in comparison to the ensemble behavior. A perfect example of this context will be discussed in this chapter for the substitution of polyphenylene dendrimers with fluorescent dyes.

5.2.1 *Support for Catalysts*

For a long time, there has been a great interest in the development of new catalysts as well as the optimization of already existing catalytic systems, including the investigation of the mechanisms involved. For this purpose, polyphenylene dendrimers can be used as supports for the attachment of catalytically active groups. Such a system combines both advantages of homogeneous and heterogeneous catalysis, e.g., placement of the catalyst at the periphery of the support, good solubility of the dendrimer-catalyst, and recovery of the catalyst. In particular the good solubility is a key feature of this system which allows the study in solution and opens the way to analytical methods such as NMR spectrometry. However, shape persistent dendrimers are valuable as model compounds for ca-

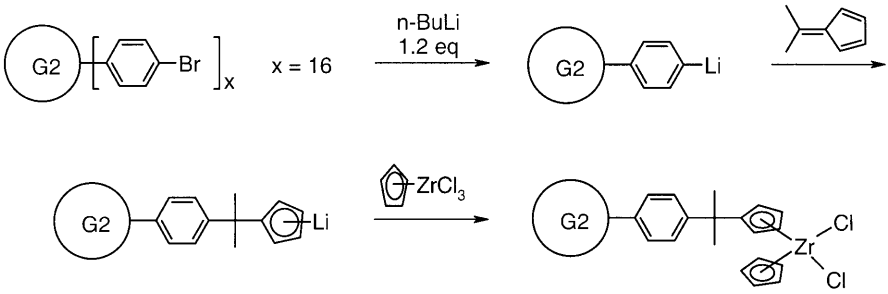

Scheme 18. Introduction of a catalytically active group on the dendrimer surface

talysis studies because the catalytically active groups are located at the periphery of the dendrimer and not in the interior.

We previously synthesized and characterized a polyphenylene dendrimer carrying zirconocene functions at the surface (Scheme 18) [65]. This target molecule has been achieved by starting from a second-generation dendrimer with a tetrahedral core bearing 16 bromine functions at the rim. After lithium exchange, subsequent addition of dimethylfulvene, and further reaction with cyclopentadienylzirconium chloride, we obtained a polyphenylene dendrimer functionalized with about eight zirconocene groups.

After activation with MAO (molar ratios [Al]:[Zr] = 1000) the polymerization of ethylene has been successfully carried out using the zirconocene functionalized dendrimer at 40 bar ethylene pressure and 70 °C. We obtained high activity and productivity values for the ethylene polymerization and polymers with very high molecular masses in the range of 2×10^6 g/mol. The polydispersity of the polymer is quite low (3.0) indicating the single site character of the catalytically active species. Optimization of this system and study of the mechanism are still under investigation. Nevertheless, these preliminary results reveal the suitability of polyphenylene dendrimers as supports for zirconocene catalysts.

5.2.2
Support for Fluorophores

The attachment of a distinct number of fluorescent dyes at the periphery of a stiff three-dimensional nanoparticle is of fundamental interest to study interactions between single chromophores in close vicinity to each other. We chose as a dye one of the rylene series, perylenemonoimide, for the decoration of our polyphenylene dendrimers due to their outstanding properties. Rylene dyes show an exceptional chemical and photochemical stability and therefore are well suited for single molecule spectroscopy (SMS) [66].

We have decorated different generations of polyphenylene dendrimers based on a biphenyl core with up to 16 perylenemonoimide chromophores at the periphery [67]. This has been achieved via the Diels-Alder reaction of a perylenemonoimide functionalized cyclopentadienone as a terminating reagent with the ethynyl precursor dendrimers. A strongly emitting nanoparticle is thus obtained.

The energy dissipation in the dendrimer bearing a certain number of perylenemonoimide chromophores can be followed by applying time resolved fluorescence techniques. These measurements indicate excimer-like interactions among neighboring perylenemonoimide dyes. Furthermore, two types of motion are detected: a rotation of the whole molecule and a fractional motion maybe of the dendrimer branch [68].

With the use of single molecule spectroscopy (SMS) it is possible to observe the occurrence of sudden changes in fluorescence intensity. This is often called on-off behavior or "blinking." The investigation of differences between single molecule spectroscopy of a single chromophore and of multichromophoric systems allows the exploration of parameters determining the transition from typical on-off single molecule behavior to ensemble behavior.

Confocal fluorescence microscopy images in a polymer film of a second-generation polyphenylene dendrimer with eight perylenemonoimide functions at the periphery **49** and a model compound bearing one single perylenemonoimide **50** reveal that the dendrimer exhibits a three- to fourfold intensity and an obvious blinking in comparison to the model compound which shows only uniform spots with less dynamics (Scheme 19) [69].

5.3
Polyphenylene Dendrimers Bearing a Functional Group in the Interior

As well as localizing chromophores at the periphery of a dendrimer it is also possible to incorporate a chromophore in the center of a shape persistent dendrimer. Such a spatial isolation of a photostable chromophore in a discrete and inert nanoenvironment is highly interesting for a variety of applications such for light emitting diodes (LEDs) or single molecule spectroscopy (SMS). The outstanding chemical and photochemical properties of rylene chromophors again make them attractive for this purpose. Therefore, a perylenediimide chromophore has been functionalized with four ethynyl groups in the imide structure from which the polyphenylene dendrons are grown **53**. Scheme 20 shows perylenediimide encapsulated by four second-generation dendrons [70].

In general, perylene dyes show a strong aggregation tendency. However, by means of the covalent encapsulation of such a chromophore in a polyphenylene dendritic shell this aggregation can be avoided. Furthermore, the dendrons also serve as solubilizing groups shielding the chromophore from atmospheric degradation. They further show good filmforming properties and hindered migration in a polymer film. These properties implicate these materials as highly interesting candidates for luminescent layers in LEDs.

Moreover, a chromophore surrounded by a perfectly defined environment might be regarded as a potential candidate for SMS, allowing study of the interactions of a fluorophore with the surrounding matrix with a very high spatial resolution, which is currently under investigation.

Recently, Kimura et al. have reported the encapsulation of electrochemically and photochemically active groups such as a porphyrin unit (**51**) or a ruthenium(II) bis(terpyridyl) (**52**) unit in the interior of a 1,3,5-polyphenylene-based dendritic structure (Scheme 21). The dendritic porphyrins have been synthesiz-

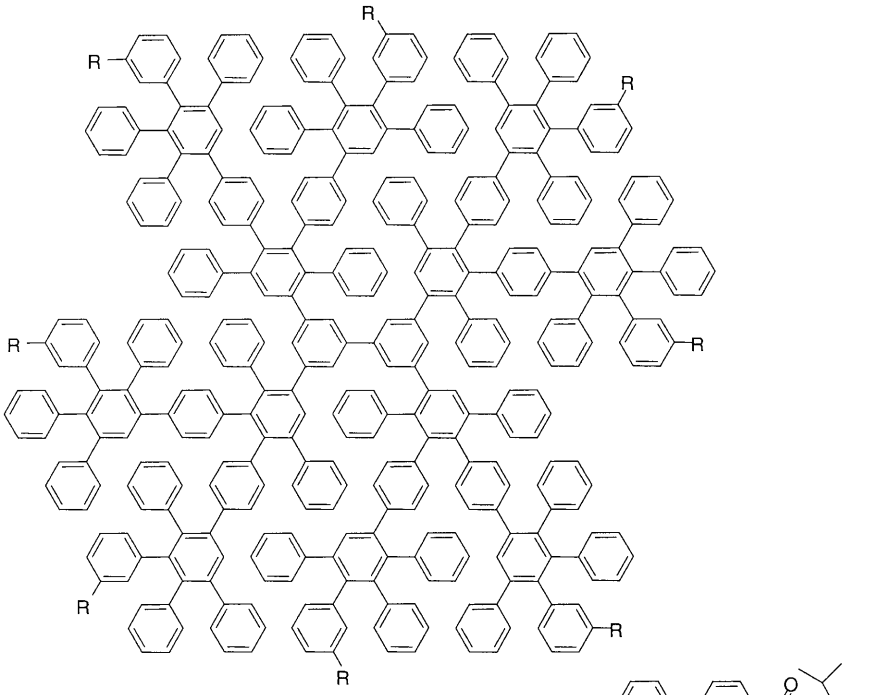

49

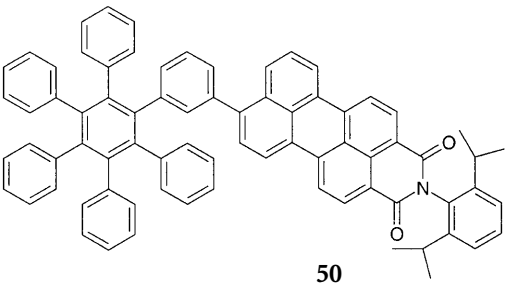

50

Scheme 19. Second generation polyphenylene dendrimer based on a biphenyl core decorated with 8 perylenemonoimide dyes

ed up to the second generation in high purities characterized by NMR, SEC, and UV-vis spectroscopy and MALDI-TOF mass spectrometry [49]. They further observe an efficient energy transfer from the phenylene-based dendron units to the porphyrin core within the dendrimer and a high efficiency of energy transfer for the first as well as the second generation is obtained.

Kimura et al. also presented the synthesis and characterization of a second-generation ruthenium(II) bis(terphenyl)polyphenylene dendrimer **52**, an attractive molecule with regard to its electrochemical and photochemical pro-

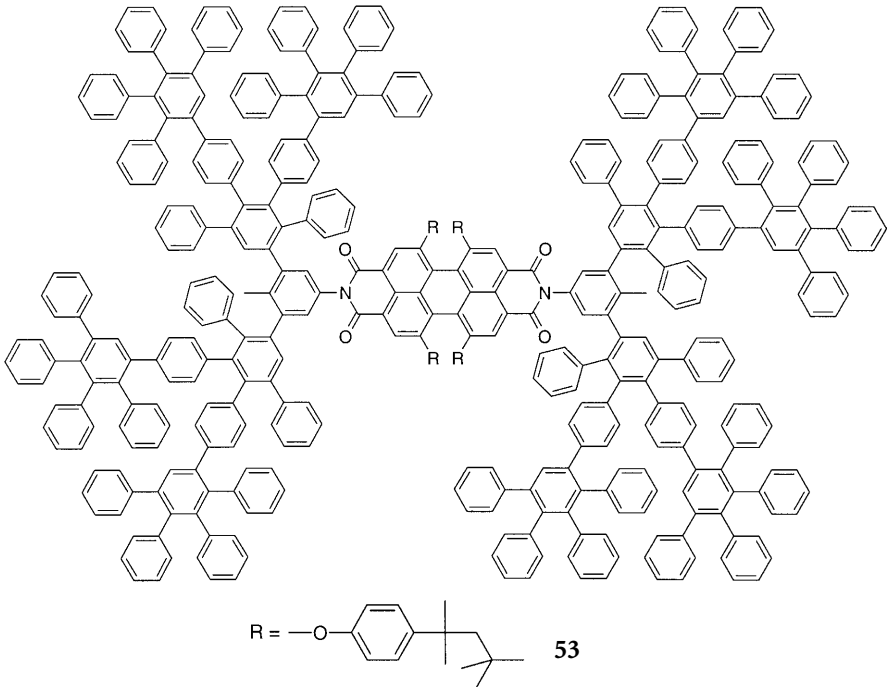

Scheme 20. Isolation of a perylenediimide chromophore in a dendritic environment

perties [71]. Cyclic voltammetry experiments reveal that the metallodendrimer exhibits one oxidation and two reduction processes where the maxima of the reduction and return oxidation wave have a large voltage difference from each other. This is explained by a slower electron transfer of the dendritic metallodendrimer in comparison to a non-dendritic complex.

5.4
Core-Shell Dendrimers

By covalent linkage of different types of molecules it is possible to obtain materials with novel properties that are different from those of the parent compounds. Examples of such materials are block-copolymers, soaps, or lipids which can self-assemble into periodic geometries with long-range order. Due to their amphiphilic character, these molecules tend to micellize and to phase-separate on the nanometer scale. By this self-assembly process the fabrication of new nanoscopic devices is possible, such as the micellization of diblock-co-polymers for the organization of nanometer-sized particles of metals or semiconductors [72–74]. The micelle formation is a dynamic process, which depends on a number of factors like solvent, temperature, and concentration. Synthesis of micelles which are independent of all of these factors via appropriately functionalized dendrimers which form unimolecular micelles is a straightforward strategy. In

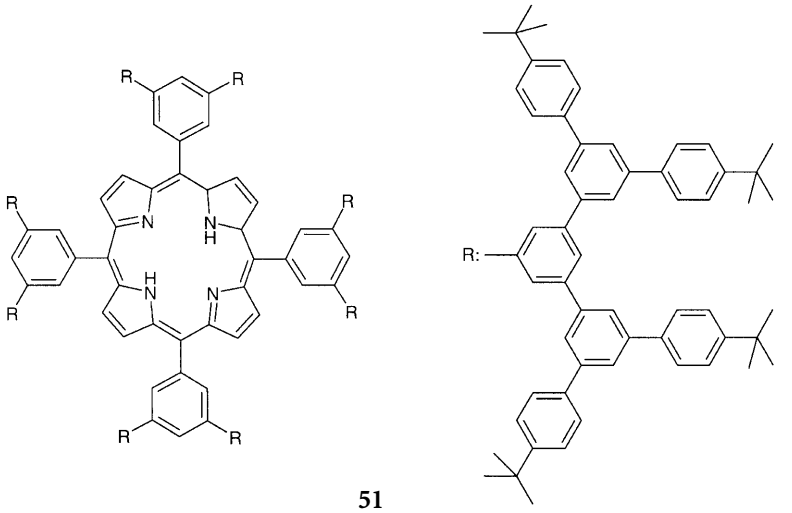

51

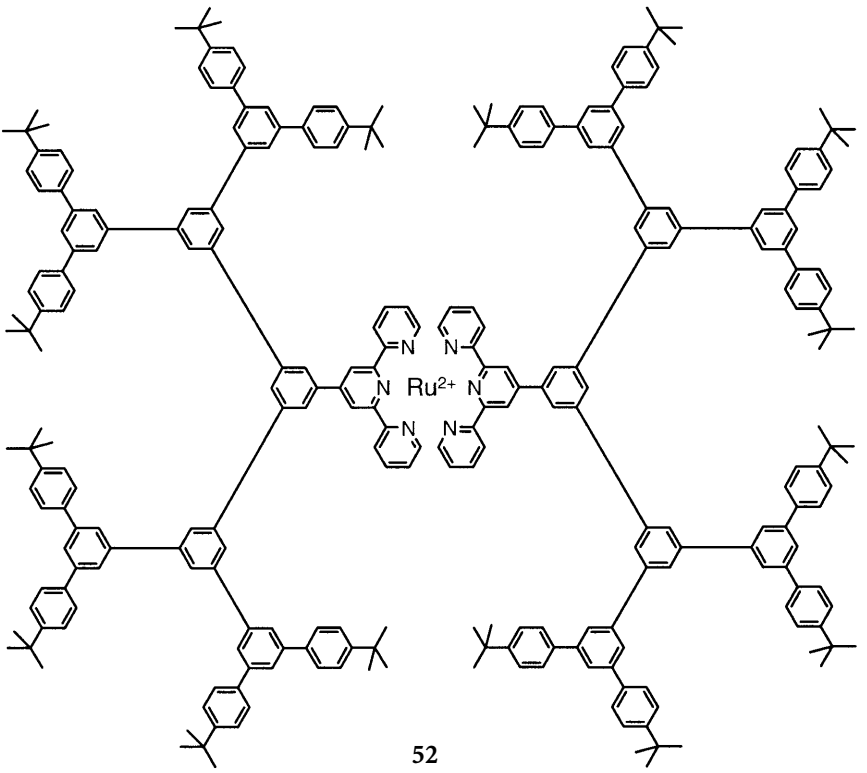

52

Scheme 21. Second generation polyphenylene dendrimers bearing a porphyrin **51** and a ruthenium(II) bis(terpyridyl) **52** core

this case, the dendrimer can be seen as the inner core and the functions, e.g., alkyl chains, linear polymers may be considered as the outer shell.

Up to now only amphiphilic dendrimers with soft cores and soft shells were used. Unfortunately the shape and the size of this type of dendrimer also show a dependence on the factors mentioned above [75–77]. By using dendrimers with a hard inner core it would be possible to study the self-organization of amphiphilic dendrimers as related to shape and size of the core.

Therefore we synthesized polyphenylene dendrimers substituted with dodecyl chains **54**, like those presented in Scheme 22. Depending on the number of alkyl substituents and the size and shape of the core, these alkyl substituted dendrimers show different properties including melting points, mesophase formation, organization on surfaces or three-dimensional organization. In this context the role of the shape of the core has to be emphasized. In the case of the trigonal-shaped dendrimers, based on core **55**, melting occurs at temperatures higher than 200 °C and birefringence is observable. However tetragonal shaped dendrimers, like **54**, show no phase transitions below 450 °C, the decomposition temperature. Small and wide angle X-ray scattering also reveals for **55,** as for **54**, reflections characteristic for nematic mesophases with columnar packing which laterally form a two-dimensional hexagonal lattice. From the diffraction patterns the intermolecular distance can be calculated as 5.48 nm for dendrimer **54**, and 3.8 nm for dendrimer **55**, which fits very well with our molecular mechanics calculation. AFM-measurements of the spin-coated alkyl-substituted dendrimers on HOPG also show the hexagonal arrangement of the dendrimers and confirm the dimensions obtained by X-ray diffraction.

Core-shell dendrimers can also be synthesized by using a dendrimer as an initiator for polymerization, as core, and the polymers as shell [78, 79]. These polymers, often called star polymers, should have a broad range of applications, like stiffeners for polymeric materials [80] or high performance additives for adhesives, lube oils, and lubricants. Therefore we synthesized such a system using a hydroxymethyl-substituted dendrimer as an initiator for the ring-opening polymerization of ε-caprolactone. The size of these dendrimers can be varied by using different generations of dendrimers or different monomer to initiator ratios. To study the properties of these core-shell dendrimers the analysis of the structure, the thermal behavior, and the viscoelasticity is under investigation.

5.5
Planarization of Polyphenylene Dendrimers – from 3-D to 2-D

A key feature of our polyphenylene dendrimers is that they can be planarized and thus reduced in dimensionality by intramolecular dehydrogenation [29, 35]. This results in large, fused polycyclic aromatic hydrocarbons (PAHs). PAHs serve as structurally distinct, two-dimensional subunits of graphite and show attractive properties such as high charge carrier mobility, liquid crystallinity, and a high thermal stability, which qualifies these materials as vectorial charge transport layers [81].

We planarized the appropriate oligophenylene derivative via oxidative intramolecular cyclodehydrogenation, which has been introduced by Kovacic and

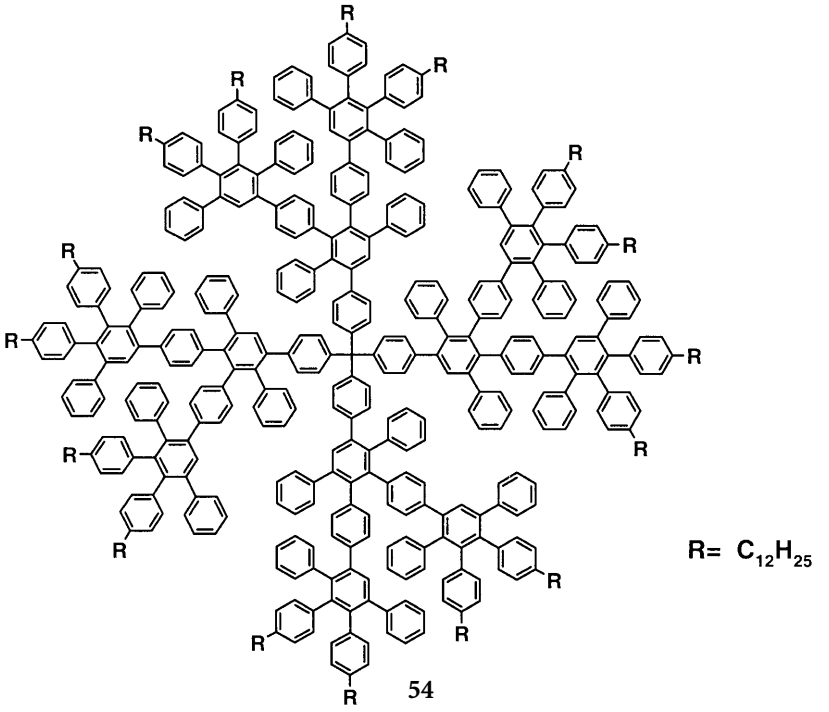

54

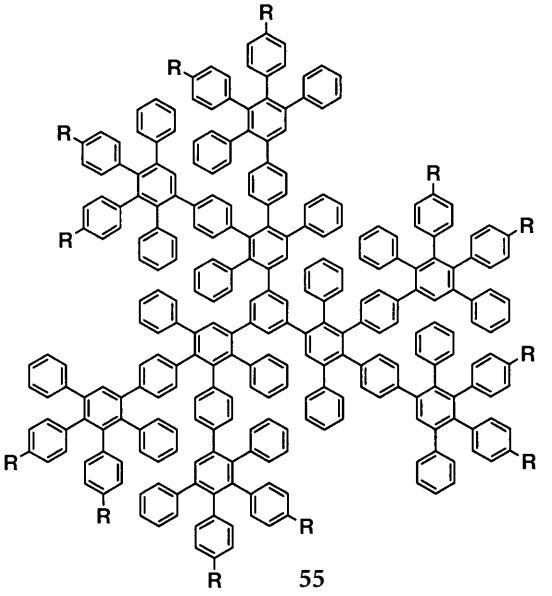

55

Scheme 22. Second generation polyphenylene dendrimer surrounded by 16 dodecyl chains used as a hard-core-soft-shell system

Koch [82] and optimized further by us. The polyphenylene **28**, which represents a first-generation dendrimer, forms 28 new bonds yielding the planar polycyclic aromatic hydrocarbon **56** (Scheme 23). Owing to its extreme insolubility in all common solvents, PAH **56** is characterized by laser desorption mass spectrometry based on its M^+ peak at $m/z = 1621$.

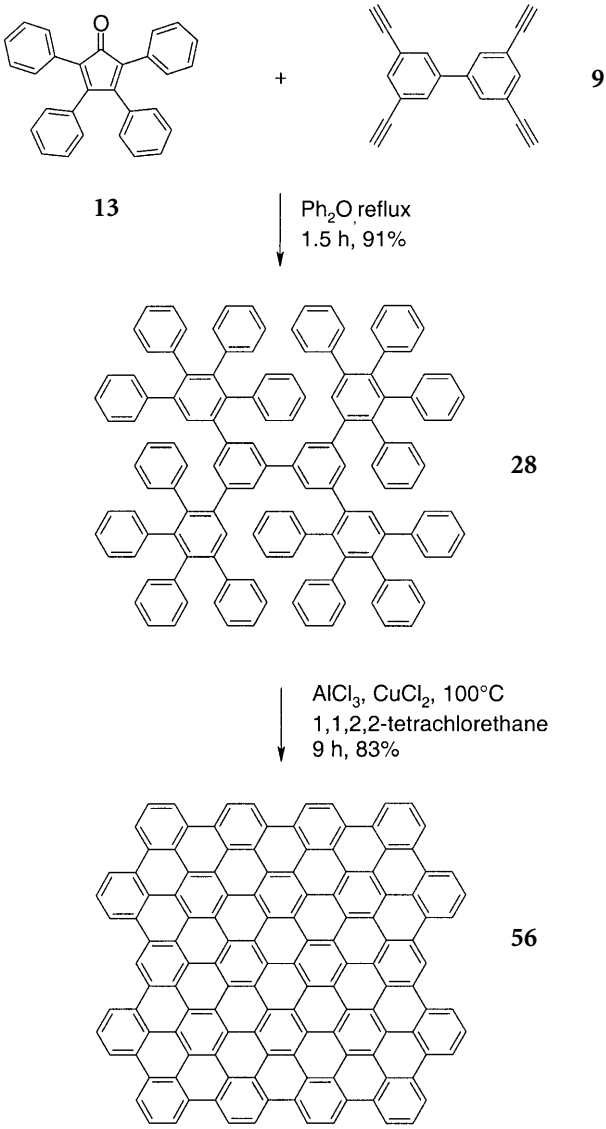

Scheme 23. Planarization of polyphenylene dendrimers yielding two-dimensional polycyclic aromatic hydrocarbons (PAHs)

PAH chemistry is of practical as well as theoretical interest. PAHs can be regarded as well defined subunits of graphite, an important industrial material, which is so far not totally understood at the macroscopic level. In this context, it is our aim to delineate the molecular size at which the electronic properties of PAHs converge to those of graphite. Furthermore, alkyl substituted derivatives of hexabenzocoronene (HBC) form discotic mesophases and, therefore, provide opportunities for materials which allow one-dimensional transport processes along their columnar axis [83, 84]. Their application for photovoltaics and Xerox processes is also of current interest.

6
Conclusion and Outlook

Polyphenylene dendrimers show a variety of unique characteristics and can be fenced off from their aliphatic analogues. Their synthesis is very straightforward so that monodisperse dendritic molecules are obtained in high yields. Noteworthy is also their availability in a variety of molecular mass ranges, their appearance in different geometries, and their shape persistence. Due to the invariant shape of polyphenylene dendrimers, functional groups can be topologically predetermined within the molecule. In this context we have emphasized a functionalization strategy via cyclopentadienones carrying different functionalities. This approach facilitates the introduction of functional groups whether in the core, in the dendritic scaffold, or at the periphery of dendrimers. Furthermore, we pointed out some applications of polyphenylene dendrimers which are taking advantage of these special features, such as the multiplication of functionalities at the periphery by using them as nano-supports for, e. g., catalysts or chromophores or the isolation of a functionality by its surrounding with polyphenylene dendrons. Until now polyphenylene chemistry still keeps its attraction not only for the organic chemist by building up tailor-made macromolecules but also due to possible applications of these nanoparticales in the recent and expanding field of nanotechnology.

A current example of the value of shape persistent dendrimers in fundamental research is their use in the study of electron transfer processes between different redox centers. If one redox center is situated in the core and another redox center is located in the shell at a distinct distance from the other center, the distances which are necessary for an electron transfer to take place can be studied. This currently presents an objective of our research. Furthermore, dendrimers coated with two types of functionalities at the periphery are currently under intense investigation. The attachment of two different types of dyes at the periphery is of interest in the study of the energy transfer between these dyes (light harvesting antenna).

In the field of molecular biology, the substitution of a polyphenylene dendrimer with fluorescent dyes and receptor units can be used for fluorescence labeling of biologically active compounds. The multiplicative effect of the number of dyes or receptor units can result in an increase in fluorescence sensitivity and an augmentation of the binding constant in the substrate receptor complex. Since we have shown that perylenemonoimide dyes at the periphery of our den-

drimers behave as single nanoemitters, a polyphenylene dendrimer bearing several dyes at the periphery can be regarded as a *superchromophor* which is of high interest for diagnostic applications in vivo and in vitro.

Acknowledgements. We gratefully acknowledge the contribution of all our colleagues, who have completed the experimental work, especially R. Bauer, A.J. Berresheim, F. Dötz, V.-M. Graubner, D. Grebel-Köhler, C. Hampel, A. Herrmann, Dr. M. Klapper, K. Martin, F. Morgenroth, Dr. J. Räder, A. Rouhanipour, V. Sinigersky, S. Spang, and Dr. M. Wagner. First, we would like to give our sincere thanks to all our external partners in a variety of cooperations. Among them are Prof. J. Bargon, Prof. M. Ballauff, Prof. T. Basché, Prof. P. Bäuerle, Prof. J. L. Brédas, Prof. H.-J. Butt, Prof. F. C. De Schryver, Dr. V. Enkelmann, Prof. G. Fytas, Prof. N. Karl, Prof. W. Knoll, Dr. G. Lieser, Dr. T. Pakula, Prof. J. P. Rabe, Dr. P. Samori, Prof. M. Schmidt, Prof. H.W. Spiess, Prof. A. Vértes, Prof. D. Vogt, Prof. J. Warman, Prof. G. Wegner, and Prof. C. Wöll. We know that without them the research would not have been possible. Second, we wish to record our thanks for internal efforts of all our colleagues within our group at the Max-Planck-Institute for Polymer Research.

Furthermore, financial support by the Bundesministerium für Bildung and Forschung (03C0299 7) and the Volkswagen Stiftung are gratefully acknowledged. U.-M. W. also thanks the Fonds der Chemischen Industrie and the Bundesministerium für Bildung und Forschung for a Ph. D. grant.

Last, but not least, we thank all the people who aided us in the preparation of this review. We would like to commend Dr. M. Watson who has kindly read the manuscript and made many valuable comments. Also we would like to thank A. J. Berresheim, M. A. Harbison, A. Herrmann, D. Stiep, S. Spang, and M. Stork for their valuable insight towards the preparation of this paper.

7 References

1. Buhleier EW, Wehner W, Vögtle F (1978) Synthesis 155
2. Fischer M, Vögtle F (1999) Angew Chem Int Ed 38:884; Angew Chem 111:934
3. Wörner C, Mülhaupt R (1993) Angew Chem Int Ed 32:1306; Angew Chem 105:1367
4. de Brabander van den Berg EMM, Meijer EW (1993) Angew Chem Int Ed 32:1308; Angew Chem 105:1370
5. Tomalia DA, Baker H, Dewald JR, Hall M, Kallos G, Martin S, Roeck J, Ryder J, Smith P (1985) Polym J (Tokyo) 17:117
6. Tomalia DA, Baker H, Dewald JR, Hall M, Kallos G, Martin S, Roeck J, Ryder J, Smith P (1986) Macromolecules 19:2466
7. Hawker CJ, Fréchet JMJ (1990) J Am Chem Soc 112:7638
8. Hawker CJ, Fréchet JMJ (1990) J Chem Soc, Chem Commun 1010
9. Fréchet JMJ, Hawker CJ, Phillippides AE (1991) US Pat. 5,041,516
10. Miller TM, Neenan TX (1990) Chem Mater 2:346
11. Bosman AW, Janssen HM, Meijer EW (1999) Chem Rev 99:1665
12. Hawker CJ, Fréchet JMJ (1990) Macromolecules 23:4726
13. Wooley KL, Hawker CJ, Fréchet JMJ (1991) J Chem Soc Perkin Trans 1:1059
14. Wooley KL, Hawker CJ, Fréchet JMJ (1993) J Am Chem Soc 115:11,496
15. Wiesler U-M, Müllen K (1999) J Chem Soc, Chem Commun 2293
16. de Gennes PG, Hervet H (1983) J Phys Lett 44:L
17. Moorey TH, Turner SR, Rubinstein M, Fréchet JMJ, Hawker CJ, Wooley KL (1992) Macromolecules 25:2401
18. Wooley KL, Klug CA, Tasaki K, Schaefer J (1997) J Am Chem Soc 119:53
19. de Baecker S, Prinzie Y, Verheijen W, Smet M, Desmedt K, Dehaen W, De Schryver FC (1998) J Phys Chem A 102:5451
20. Scherrenberg R, Coussens B, van Vliet P, Edouard G, Brackman J, de Brabander E, Mortensen K (1998) Macromolecules 31:456

21. Percec V, Johansson G, Ungar G, Zhou J (1996) J Am Chem Soc 118:9855
22. Balagurusamy VSK, Ungar G, Percec V, Johansson G (1997) J Am Chem Soc 119:1539
23. Hudson SD, Jung H-T, Percec V, Cho W-D, Johansson G, Ungar G, Balagurusamy JVSK (1997) Science 278:449
24. Newkome GR, Moorefield CN, Vögtle F (1996) Dendritic molecules. VCH, Weinheim
25. Xu Z, Moore JS (1993) Angew Chem Int Ed Engl 32:1354; Angew Chem 105:1394
26. Xu Z, Moore JS (1994) Acta Polymer 45:83
27. Miller TM, Neenan TX, Zayas R, Bair HE (1992) J Am Chem Soc 114:1018
28. Miller TM, Neenan TX, Bair HE (1991) Polym Preprints 32:627
29. Morgenroth F, Reuther E, Müllen K (1997) Angew Chem Int Ed Engl 36:631; Angew Chem 109:647
30. Morgenroth F, Müllen K (1997) Tetrahedron 53:15,349
31. Morgenroth F, Kübel C, Müllen K (1997) J Mater Chem 7:1207
32. Morgenroth F, Kübel C, Müller M, Wiesler U-M, Berresheim AJ, Wagner M, Müllen K (1998) Carbon 36:833
33. Morgenroth F, Berresheim AJ, Wagner M, Müllen K (1998) J Chem Soc, Chem Commun 1139
34. Berresheim AJ, Morgenroth F, Wiesler U-M, Müllen K (1998) Polym Preprints 39:721
35. Berresheim AJ, Müller M, Müllen K (1999) Chem Rev 99:1747
36. Wiesler U-M, Berresheim AJ, Morgenroth F, Müllen K Macromolecules (submitted)
37. Tomalia DA, Naylor AM, Goddard WA III (1990) Angew Chem Int Ed Engl 29:138; Angew Chem 102:119
38. de Azevedo ER, Hu W-G, Bonaganba TJ, Schmidt-Rohr K (1999) J Am Chem Soc 121:8411
39. Saalwächter K, Wind M, Spiess HW (personal communication)
40. Saalwächter K, Graf R, Spiess HW (1999) J Magn Reson 140:471
41. Fréchet JMJ, Hawker CJ (1996) Comprehensive polymer science. Pergamon Press, p 98
42. Kamide K (1996) Comprehensive polymer science, vol 1. Pergamon Press, p 94
43. De Schryver FC (personal communication)
44. Lieser G (personal communication)
45. Brocorens P, Zojer E, Cornil J, Shuai Z, Leising G, Müllen K, Brédas JL (1999) Synth Met 100:141
46. CERIUS2, Molecular Simulations, Waltham, MA, USA
47. Morgenroth F (1998) PhD thesis, University of Mainz
48. Dandliker PJ, Diederich F, Gisselbrecht J, Louati A, Gross M (1995) Angew Chem Int Ed Engl 34:2725; Angew Chem 107:2906
49. Kimura M, Shiba T, Muto T, Hanabusa K, Shirai H (1999) Macromolecules 32:8237
50. Newkome GR, Cardullo F, Constable EC, Moorefield CN, Thompson AMWC (1993) Chem Commun:925
51. Launay N, Caminade AM, Majoral JP (1995) J Am Chem Soc 117:3282
52. Wiesler U-M, Weil T, Dötz F, Müllen K (unpublished results)
53. Hawker CJ, Wooley KL, Fréchet JMJ (1991) Polym Preprints 32:623
54. Sanford EM, Fréchet JMJ, Wooley KL, Hawker CJ (1993) Polym Preprints 34:654
55. Hawker CJ, Wooley KL, Fréchet JMJ (1993) J Chem Soc, Perkin Trans 1:1287
56. Hawker CJ, Wooley KL, Fréchet JMJ (1993) Polym Preprints 34:54
57. Stevens MP (1999) Polymer chemistry. Oxford University Press
58. Wiesler U-M (unpublished results)
59. Nalwa HS (1999) Handbook of nanostructured materials and nanotechnology. Academic Press
60. Knapen JWJ, Vandermade AW, Dewilde JC, Vankoten G (1994) Nature 372:659
61. van Koten G, Jastrzebski JTBH (1999) J Mol Catal. A – Chem 146:317
62. Hawker CJ (1999) Advances in Polymer Science 147:113
63. Baars MWPL, Froehling PE, Meijer EW (1997) J Chem Soc, Chem Comm 1959
64. Vögtle F, Gestermann S, Kauffmann C, Ceroni P, Vicinelli V, de Cola L, Balzani V (1999) J Am Chem Soc 121:12,161
65. Stork M (2000) PhD thesis, University of Mainz

66. Lee SK, Zu YB, Herrmann A, Geerts Y, Müllen K, Bard AJ (1998) J Am Chem Soc 141:3513
67. Hofkens J, Latterini L, de Belder G, Gensch T, Maus M, Vosch T, Karni Y, Schweitzer G, De Schryver FC, Herrmann A, Müllen K (1999) Chem Phys Lett 304:1
68. Karni Y, Jordens S, de Belder G, Hofkens J, Schweitzer G, De Schryver FC, Herrmann A, Müllen K (1999) J Phys Chem B 103:9378
69. Gensch T, Hofkens J, Herrmann A, Tsuda K, Verheijen W, Vosch T, Christ T, Basche T, Mullen K, De Schryver FC, Müllen K (1999) Angew Chem Int Ed Engl 38:3752; Angew Chem 111:3970
70. Herrmann A (2000) Ph. D. thesis, University of Mainz (in preparation)
71. Kimura M, Shiba T, Muto T, Hanabusa K, Shirai H (2000) Chem Commun 11
72. Spatz JP, Roescher A, Sheiko S, Krausch G, Möller M (1995) Adv Mat 7:731
73. Roescher A, Möller M (1995) Adv Mater 7:151
74. Carrot G, Hilborn JG (1997) Polymer 38:6401
75. Schenning APHJ, Elissen-Román C, Weener J-W, Baars MWPL, van der Gast SJ, Meijer EW (1998) J Am Chem Soc 120:8199
76. Percec V, Chu P, Ungar G, Zhou J (1995) J Am Chem Soc 117:11,441
77. Stark B, Stühn B, Frey H, Lach C, Lorenz K, Frick B (1998) Macromolecules 31:5415
78. Hedrick JL, Trollsas M, Hawker CJ, Atthoff B, Claesson H, Heise A, Miller RD, Mercerreyes D, Jeraume R, Dubois P (1998) Macromolecules 31:8691
79. Liu M, Petro M, Fréchet JMJ, Haque SA, Wang H-C (1999) Polymer Bull. 43:51
80. Schartel B, Stümpflen V, Wending J, Wendorff JH, Heitz W, Neuhaus R (1996) Colloid. Polym Sci 274:911
81. Müllen K, Rabe JP (1998) Molecular electronics: science and technology, vol 852. New York Acad Science, New York, p 205
82. Kovacic P, Koch FW (1965) J Org Chem 30:3176
83. Fechtenkötter A, Saalwächter K, Harbison MA, Müllen K, Spiess HW (1999) Angew Chem Int Ed Engl 38:3039; Angew Chem 111:3224
84. van de Craats AM, Warman JM, Fechtenkötter A, Brand J, Harbison MA, Müllen K (1999) Adv Mater 11:1469

Hyperbranched Polyesteramides – New Dendritic Polymers

Dirk Muscat[1], Rolf A. T. M. van Benthem[2]

DSM Research, P. O. Box 18, 6160 MD Geleen, The Netherlands
[1] *E-mail: dirk.muscat@dsm-group.com,*
[2] *E-mail: rolf.benthem-van@dsm-group.com*

Hyperbranched polyesteramides based on commercially attractive monomers have been successfully developed, affording polymers with a high number of end groups and especially multifunctionality on the same molecule. Beside hydroxyl and carboxylic acid groups, hyperbranched polyesteramides can be modified with a broad variety of other functionalities such as unsaturated groups, tertiary amines, or long alkyl chains. Thus the concept of the synthesis allows a broad variety of structures and the resulting properties like polarity or viscosity can be adjusted and fine-tuned for a broad number of applications. This enables the hyperbranched polyesteramides to be used in a variety of (potential) applications, such as crosslinkers in coatings, as toner resin, for dyeing polyolefins, as surfactants, or in cosmetics. Especially impressive is the disperse dyeing of polypropylene fibers, which has been a problem for decades. Hyperbranched polyesteramides based on phthalic anhydride and diisopropanolamine, partially functionalized with stearic acid represent amphiphilic molecules, which are able to fix the dyes via their polar core and at the same time are compatible with the polypropylene matrix through their long alkyl chains.

Keywords. Hyperbranched polyesteramides, Polymers, Powder coatings, Air drying coatings, Dyeing polyolefins

Topics in Current Chemistry, Vol. 212

List of Abbreviations

DIPA	diisopropanolamine
GA	glutaric anhydride
HHPA	*cis*-1,2-cyclohexane-dicarboxylic anhydride
OSA	1-oct-2-ene-succinic anhydride
PA	phthalic anhydride
SA	succinic anhydride
THPA	*cis*-1,2-cyclohex-4-ene-dicarboxylic anhydride

1 Introduction

The attractiveness of dendritic molecules follows from their unique structure like the large number of end groups, enabling multi-functionality on the same molecule, special rheological behavior and cavities due to the spherical structure. Such materials appeal to the industrial user and their potential use lies in many fields, e. g., as molecular container [1], contrast agent [2], dye booster [3], etc. Interestingly, the first commercialized dendritic products were dendrimers, namely Astramol (polypropyleneimine) and Starburst (polyamidoamine). The synthesis of dendrimers requires a costly stepwise buildup with intermediate purification steps, limiting their use to high added value products. However, the advantage of dendrimers is their mono-dispersity which makes them valuable for use in medical applications such as MRI contrast agent [2] in which one of

the requirements is a defined size of the molecules. Polydisperse hyperbranched polymers could not be used without fractionation for such applications.

For most purposes, polydispersity is not an obstacle, and currently the potentially cheaper hyperbranched polymers are successfully entering industrial research and application. Nevertheless, their success is based on the know-how built up in research on dendrimers.

In this chapter we describe the synthesis of new hyperbranched polyesteramides carried out with standard melt condensation technology as well as the properties of these new structures.

2 General Concept

The theoretical concepts of the syntheses of hyperbranched polycondensates were first developed by Flory [4]. The first report of the synthesis of hyperbranched structures from commodity chemicals, albeit unintentionally, is even older, from 1929, when Kienle et al. [5] reacted glycerol with phthalic anhydride and realized only ten years later that this synthesis afforded a resinous product with a "three-dimensional complexity." Since then, many hyperbranched structures have been described from more elaborate building blocks. Most of the hyperbranched polymers reported are synthesized from AB_2 monomers, molecules equipped with two functional groups B and a functional group A. Examples are the work of Fréchet et al. [6], who used 3,5-bis(trimethylsiloxy)-benzoyl chloride, Kim and Webster [7] (3,5-dibromophenyl)boronic acid (Suzuki conditions), Malmström and Hult [8] 2,2-bis(methylol)propionic acid, Kricheldorf and Stöber [9] silylated 5-acetoxyisophthalic acid and recently trimethylsilyl 3,5-diacetoxybenzoate [9], and Feast et al. [10] who described diethylhydroxyglutarate. Our own approach deviates significantly, although appearing to look like an AB_2 system at first glance. In fact we use an Aa B_2b system, which bears a strong resemblance to an A_2/B_3 approach (Fig. 1). In contrast to this classic approach, the a of the Aa-compound and the b-group of the B_2b component are preferentially reactive towards each other. In this way, by virtue of a prereaction A-[a-b]-B_2-units are formed. In order to enable control of molecular weight, an excess of B_2b-units is used in the system. Simultaneously, however on a longer time scale, the polycondensation reaction of the AB_2-units starts to form hyperbranched polymeric materials. The excess of B-groups in the system limits molecular weight build-up and results in a predictable and stable viscosity, without the risk of gel formation with higher molecular weights as in the classic A_2/B_3 approach. According to Flory [4], at least 35 % excess of one of the two components (A_2 or B_3) are needed to prevent gelation, assuming 100 % conversion.

A different approach, presently applied by the Perstorp company in the production of hyperbranched aliphatic polyesters from 2,2-bis(methylol)propionic acid [8], utilizes a B_x starter molecule with AB_x-groups condensed in consecutive steps; see Fig. 1 in the middle of the diagram. In principle, the function of the B_x component can also be regarded as a chain stopper when all building blocks are polycondensed in one step. This also leads to a predictable and stable molecular weight at total conversion due to the excess of B-groups in the system.

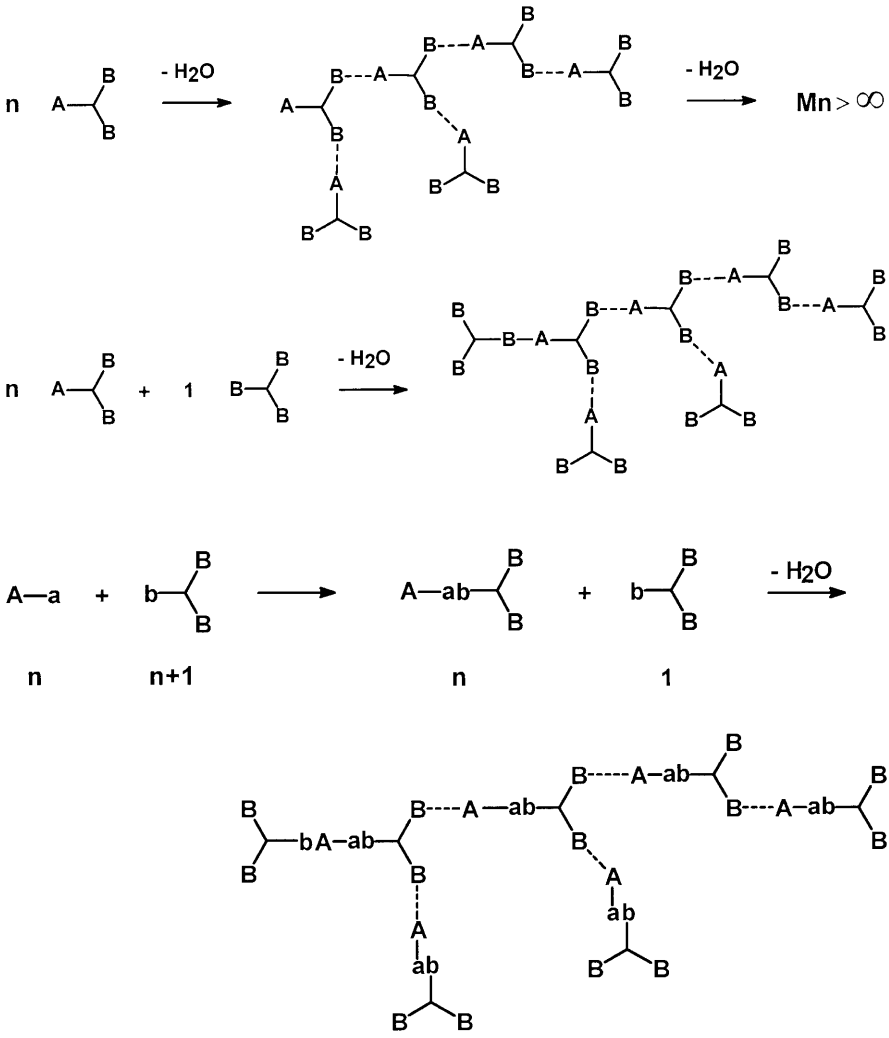

Fig. 1. *Top:* general approach to hyperbranched polycondensates: from "AB_2" monomers; *Middle:* modified approach using B_x starters/chain stoppers; *Bottom:* new approach to hyperbranched polycondensates by reacting Aa monomers with a molar excess of bB_2 monomers

2.1
Hydroxyl Functional Hyperbranched Polyesteramides

2.1.1
Molecular Weight Build-Up

In the first step of the synthesis of the hyperbranched polyesteramides, a cyclic carboxylic anhydride is reacted with diisopropanolamine, ideally forming a

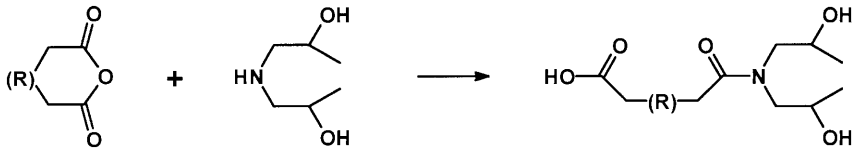

Fig. 2. Reaction of cyclic carboxylic anhydride with diisopropanolamine

molecule with one carboxylic acid and two 2-hydroxy-propylamide groups (Fig. 2).

Although both the alcohol groups and the secondary amine group of diisopropanolamine are capable of reacting with the anhydride, the amine group will react preferentially. The enhanced reactivity of the two hydroxylalkylamide groups towards carboxylic acids plays a crucial role in the further polycondensation reaction as well as in the functionalization reactions. The esterification reaction occurs much faster than with normal alcohols. Moreover, it does not proceed in accordance with the normal addition-elimination mechanism, since the reaction cannot be catalyzed with Lewis or Brönsted acids or bases [11]. It was established in 1993 [12] that this reaction proceeds via an oxazolinium-carboxylate ion pair intermediate (Fig. 3). Ring opening of the oxazolinium species via nucleophilic attack of the associated carboxylate group affords the formation of the ester linkage.

This picture is, however, incomplete because the dynamic nature of the amide bond is not taken into account. We have established through real-time IR spectroscopy that a rapid rearrangement of the hydroxyl-amide to the corresponding ester-amine (see Fig. 4) and vice versa allows a dynamic equilibrium between these two species which is strongly temperature dependent. Such a dynamic equilibrium has also been reported, albeit on a longer time-scale, for 4-hydroxyalkylamides [13].

As an illustrative example, the IR spectrum of tetrakis(2-hydroxy-propyl)adipamide (Fig. 4) was measured as a function of temperature. It appeared that ester absorptions (C=O, 1720 – 1740 cm^{-1}) appeared rapidly after melting and increased to a certain constant value with respect to the amide absorptions (C=O,

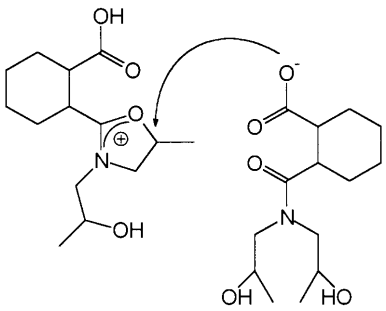

Fig. 3. Reaction mechanism of esterification of 2-hydroxyalkylamides via an oxazolinium intermediate

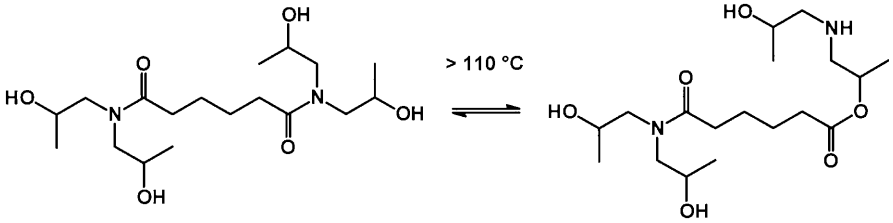

Fig. 4. Tetrakis(2-hydroxypropyl)adipamide and its thermal rearrangement product

1680 – 1700 cm^{-1}) at a given temperature. This value increased with temperature and decreased upon cooling to the original respective values.

The same rearrangement can be observed for the AB_2 building block, as shown in Fig. 5.

The occurrence of secondary amine groups as a result of this equilibrium in the reaction mixture of the hyperbranched polyesteramides can influence the molecular weight build-up. Since amines are known to react with oxazolines as well, the reaction of two 2-hydroxyalkylamides between each other (Fig. 6, pathway C) represents the unwanted reactivity among B-groups in the AB_2-type polycondensation. With this side reaction, there is a risk of uncontrolled molecular weight increase and finally gelation. Indeed, this was the case when we started our experiments in 1995 with diethanolamine instead of diisopropanolamine. Chemical and physical analyses confirmed that macromolecules were formed in which diethanolamine moieties were directly coupled (Fig. 6, product from pathway C). A change to diisopropanolamine circumvented most of these problems. However, it is probable that the extra methyl group suppresses pathway C in Fig. 6 to a considerable extent both by shifting the ester-amine/hydroxy-amide equilibrium in favor of the latter, and by sterically hindering the attack by the secondary amine on the methyl substituted oxazolinium species.

The use of diisopropanolamine in the synthesis of the hyperbranched polyesteramide resins has led to defined molecules according to the predicted structures (Fig. 7) as confirmed by MALDI-TOF (Matrix Assisted Laser Desorption Ionization – Time Of Flight) and ESI (Electro Spray Ionization) mass spectra

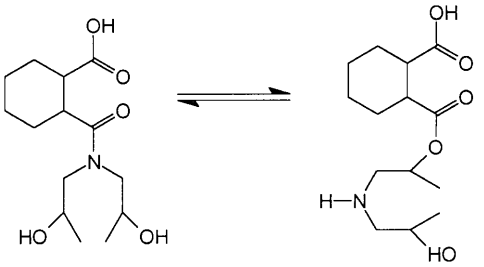

Fig. 5. Addition reaction products from hexahydrophthalic anhydride and diisopropanolamine; rearrangement from AB_2 to ABB′ monomer

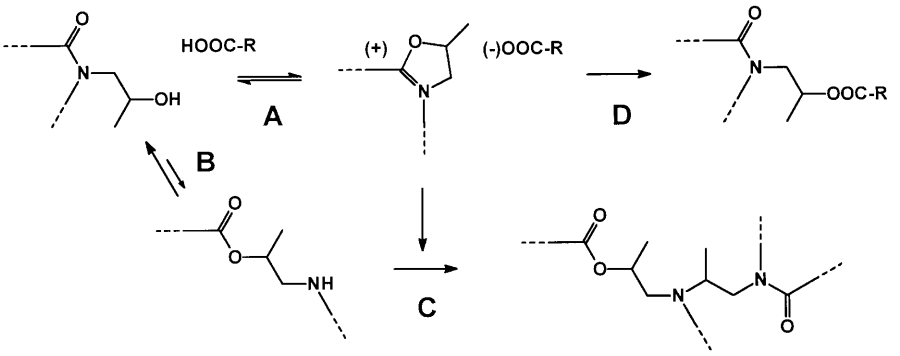

Fig. 6. Possible side-reactions in the esterification of 2-hydroxyalkylamides

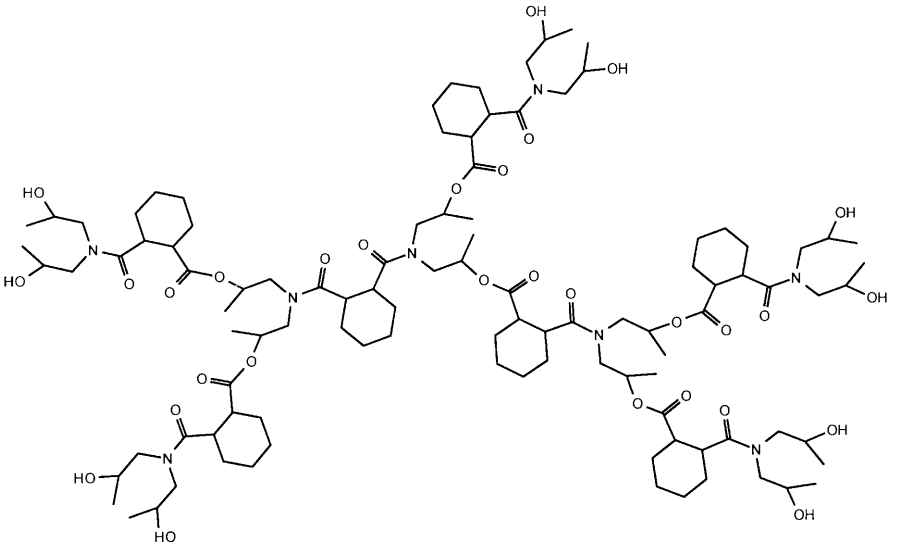

Fig. 7. Idealized structure of hyperbranched polyesteramide resin based on HHPA and diisopropanolamine (molar ratio 7:8, respectively, molecular weight 2016 g/mol)

(Fig. 8). Signals from molecules with ratios of anhydride (A)/diisopropanolamine (D) of n:n and n:(n+1) were predominantly observed. Other signals, for example composed of n:(n+2), n:(n+3), etc., indicative of the reaction proceeding via pathway C in Fig. 6 (observed abundantly in resins made of diethanolamine) appeared only in minor amounts. The signals with n:n ratios of anhydride/diisopropanolamine, also present in minor amounts (usually between 5% and 20%) compared to the n:(n+1), can be ascribed to cycle formation [14]. The relative abundance of these perspective peak series varied considerably with the monomer ratios, i.e., molecular weights and the type of cyclic anhy-

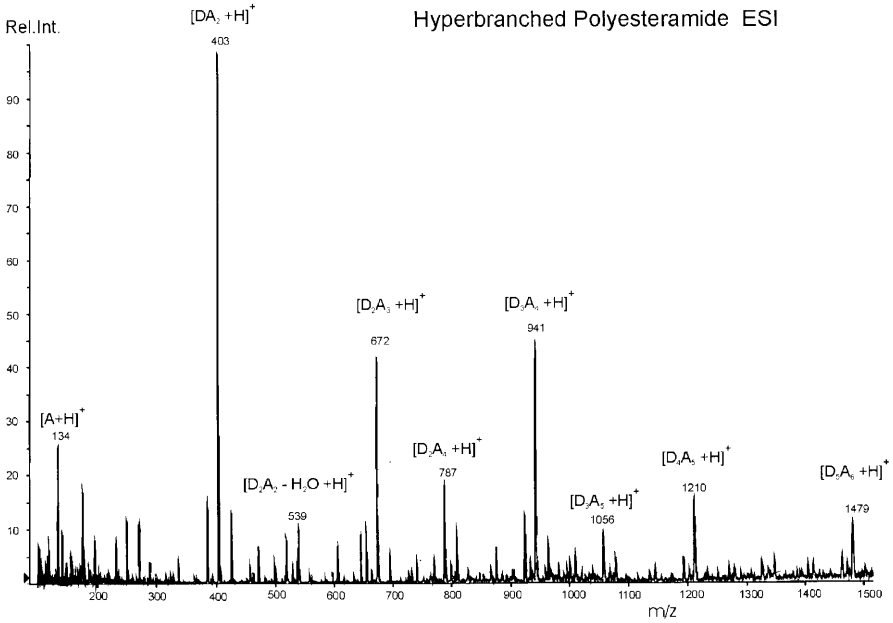

Fig. 8. Part of an ESI mass spectrum of hyperbranched polyesteramides based on HHPA and diisopropanolamine; A = DIPA, D = HHPA

dride used. In a detailed study it was observed that the faulty n:(n+2) structures are formed predominantly in the initial reaction phase, when unreacted diisopropanolamine is still present. It is therefore assumed that the n:(n+2) structures are formed by oligomer/monomer reactions rather than by oligomer/oligomer reactions.

The key to a controlled molecular weight build-up, which leads to the control of product properties such as glass transition temperature and melt viscosity, is the use of a molar excess of diisopropanolamine as a chain stopper. Thus, as a first step in the synthesis process, the cyclic anhydride is dosed slowly to an excess of amine to accommodate the exothermic reaction and prevent unwanted side reactions such as double acylation of diisopropanolamine. HPLC analysis has shown that the reaction mixture after the exothermic reaction is quite complex. Although the main component is the expected acid-diol, unreacted amine and amine salts are still present and small oligomers already formed. In the absence of any catalyst, a further increase of reaction temperature to 140–180 °C leads to a rapid polycondensation. The expected amount of water is distilled (under vacuum, if required) from the hot polymer melt in approximately 2–6 h depending on the anhydride used. At the end of the synthesis the concentration of carboxylic acid groups value reaches the desired low level.

Suitable cyclic carboxylic anhydrides for this process are for example *cis*-1,2-cyclohexane-dicarboxylic anhydride (HHPA), *cis*-1,2-cyclohex-4-ene-dicarboxylic anhydride (THPA), phthalic anhydride (PA), succinic anhydride (SA), 1-oct-2-ene-succinic anhydride (OSA), and glutaric anhydride (GA) – see Fig. 9.

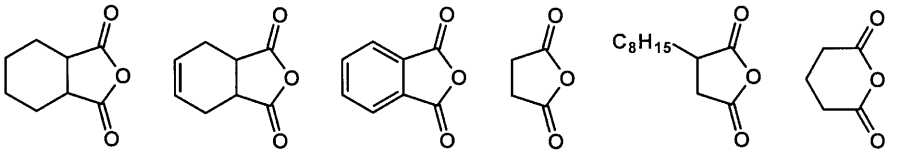

Fig. 9. Suitable cyclic carboxylic anhydrides for hyperbranched resin synthesis

2.1.2 *Analysis*

An analytical comparison of hyperbranched polyesteramide resins with different ratios of diisopropanolamine and HHPA demonstrates the control of molecular weight. GPC analysis in THF (based on linear polystyrene standards) of resins synthesized with molar ratios of diisopropanolamine to anhydride varying from 1.50 to 1.10, in Δ 0.05 steps, leading to theoretical molar masses of 670 – 2700 g/mol, showed that the measured number average molar masses (M_ns) are higher than those expected based on theoretical calculations [15] (Table 1). This would seem to contradict a branched structure, but is probably a result of higher interactions between these polymers and the solvent compared to the more apolar polystyrene used as standard. This leads to an apparent higher hydrodynamic volume. The trend of a decrease of the difference between M_n measured and calculated with decreasing excess of diisopropanolamine can be clearly seen in Table 1. At ratios of 1.15 – 1.10 the measured M_ns are even lower than calculated. This is in accordance with what would be expected for an average increasingly branched structure.

The universal calibration, derived from GPC viscosimetry online coupling, has further confirmed the predicted molecular weights. Absolute verification of this calibration principle, which neglects differences in viscosity of molecules of equal molecular weight but with different architectures, is still underway [16].

A Mark-Houwink plot results in $\alpha = 0.3 \pm 0.1$ in the range of approximately 1000 – 40,000 g/mole, clearly indicating a high degree of branching. The deter-

Table 1. Molecular weights of HHPA-based polyesteramides as determined by GPC

Molar ratio DIPA/HHPA	M_n calculated (g/mol)	M_n measured (PS standard)
1.50	670	1000
1.45	735	1060
1.40	800	1070
1.35	900	1160
1.30	1040	1350
1.25	1200	1540
1.20	1500	1720
1.15	1950	1810
1.10	2700	2070

mination of the exact degree of branching is also currently under investigation. Computer simulations resulted in a degree of branching of 0.3 – 0.45, according to Hölters definition [17] of the degree of branching and varying with the excess of diisopropanolamine, i. e., the molar mass.

The glass transition temperatures determined with these polyesteramide resins appeared to be strongly dependent on the type of anhydride used and of their molecular weight. Figure 10 shows the dependence of glass transition temperature on molecular weight for hyperbranched polyesteramides based on hexahydrophthalic anhydride. In general, the T_g for HHPA- and THPA-based resins were about 45 – 90 °C, PA based resins about 70 – 100 °C, and SA and GA about 20 – 40 °C.

The glass transition temperature is further strongly dependent on the water content of the polymer. In general, polyesters or polyesteramides of comparable molecular weight absorb 5 – 8 % water in a humid environment. In the case of the hyperbranched polyesteramides based on HHPA and diisopropanolamine, the water absorption can rise up to 25 % in a 100 % humidity environment. This results in a strong decrease of the glass transition temperature as the intermolecular forces, namely hydrogen bonds, are weakened by the water molecules. For a hyperbranched polyesteramide resin, based on HHPA and diisopropanolamine with a theoretical average molecular weight of 1500 g/mol, this drop can be as high as 50 °C. The water absorption is strongly dependent on the nature of the building blocks and functional groups and can, for example, be controlled through partial modification of the hydroxyl groups by esterification with, for

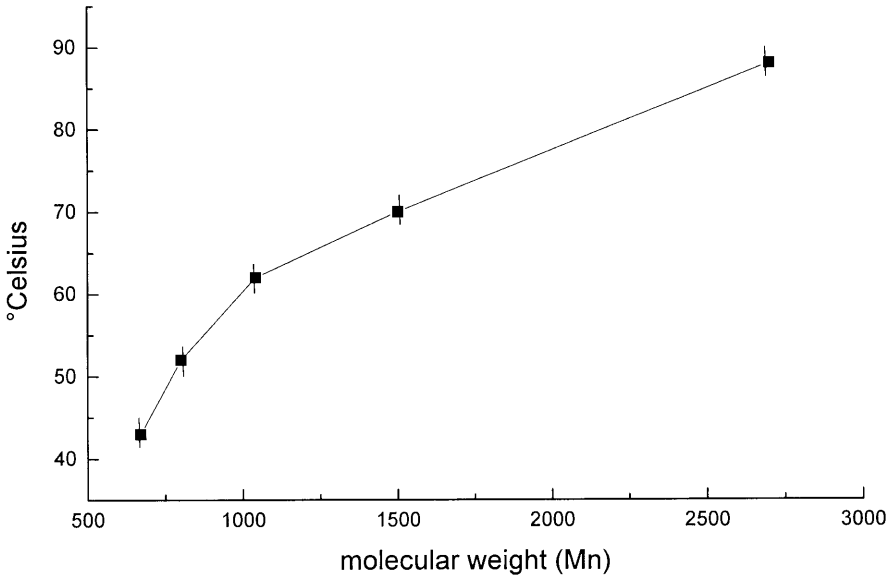

Fig. 10. Dependence of the glass transition temperature on molecular weight of hyperbranched polyesteramides based on HHPA and diisopropanolamine, measured for different samples and intrapolated

example, stearic acid. A hyperbranched polyesteramide based on phthalic anhydride and diisopropanolamine, from which 4 of the 8 hydroxyls are esterified with stearic acid, takes up only 3.7% of water, also under the conditions of a 100% humidity environment.

Besides the water absorption, the unexpected high hydrophilic character of the hydroxyl functional hyperbranched polyesteramides is also reflected in its solubility behavior. A resin, based on hexahydrophthalic anhydride and diisopropanolamine (see Fig. 7), is soluble in water/ethanol mixtures with up to 50% water! By means of GPC we followed the hydrolytic stability of this resin in 50:50 water/ethanol mixtures at different pH values (4, 7, and 10) at room temperature. Even after 28 days no degradation was observed. Only under drastic conditions, such as reflux in 50:50 ethanol/water mixture at pH 14 for 16 h was the resin completely destroyed. At other pH values such as 1 or 12, but under the same conditions, the hyperbranched polyesteramide was partly degraded.

2.2
Modifications Based on Hydroxyl Functional Hyperbranched Polyesteramides

2.2.1
Esterification with Mono Acids

The hyperbranched polyesteramides described above can also easily be functionalized by esterification with various mono carboxylic acids like acetic acid, benzoic acid, 2-ethylhexanoic acid, stearic acid, (un)saturated fatty acids, or (meth)acrylic acid. With the exception of the latter mentioned acids, which give highly temperature sensitive products, the synthesis of these functionalized hyperbranched polyesteramides can be performed in two different ways:

1. A one-pot three-step reaction, starting first with the exothermic addition reaction of the cyclic anhydride and diisopropanolamine, followed by polycondensation, and finally the esterification with the mono acid.
2. A one-pot *two*-step reaction, again first the exothermic addition reaction of the cyclic anhydride and diisopropanolamine, then concomitant polycondensation and esterification. Both procedures result in very similar products.

More detailed information on the reaction course of the three-step functionalization of an HHPA polyesteramide resin was obtained by functionalization with benzoic acid, after the polycondensation step. The reaction proceedings were monitored by multiple detector GPC (UV/RI) and titration. In the UV detector of the GPC the absorption of the aromatic acid is very dominant over the aliphatic resin itself, so that differentiation between free benzoic acid and benzoate-functionalized resin is feasible. It was observed that the titrated total acid concentration decreased much slower than the amount of free benzoic acid (Fig. 11).

During the end-group esterification the average molecular mass of the hyperbranched polyesteramides decreases at the beginning of the reaction (as

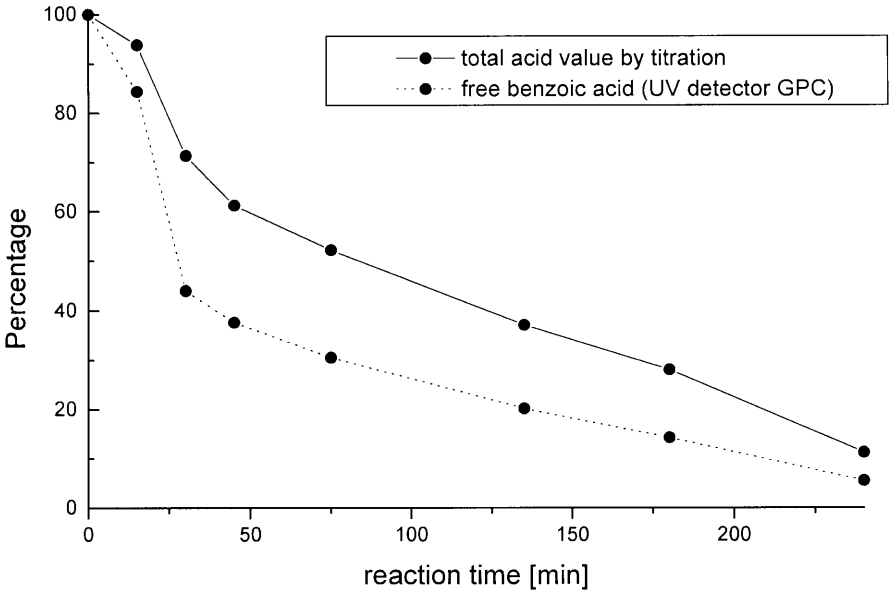

Fig. 11. Esterification of hyperbranched polyesteramide resin, based on HHPA and diisopropanolamine, with benzoic acid, as followed by titration and GPC analysis

determined with the RI detector of the GPC) and increases again to the expected values as the acid value approaches zero. Thus transesterification plays an important role in the esterification reactions of both polycondensation and functionalization. Important molecular characteristics such as molecular weight distribution and degree of branching are directly related to the average ratio of "linear" (esterified once) to "branched" (esterified twice) and "end" (unesterified) diisopropanolamide units in the polymer backbone [17]. Since this average ratio is apparently thermodynamically determined as a result of the relatively fast transesterification process, it is relatively difficult to control polydispersity and degree of branching of these resin types. When transesterification via the a – b bond (see Figs. 1 and 4) should also be taken into account, the system starts to bear properties of an A_2/B_3 system and gelation is risked at certain monomer ratios and very long reaction times or very high temperatures.

2.2.2
Properties

As is also known from dendrimers [18], the properties of highly branched structures depend strongly on the nature of the end groups. Typically a resin, based on HHPA and diisopropanolamine, was functionalized with different mono acids, demonstrating the expected drastic change of the glass transition temperature (Fig. 12).

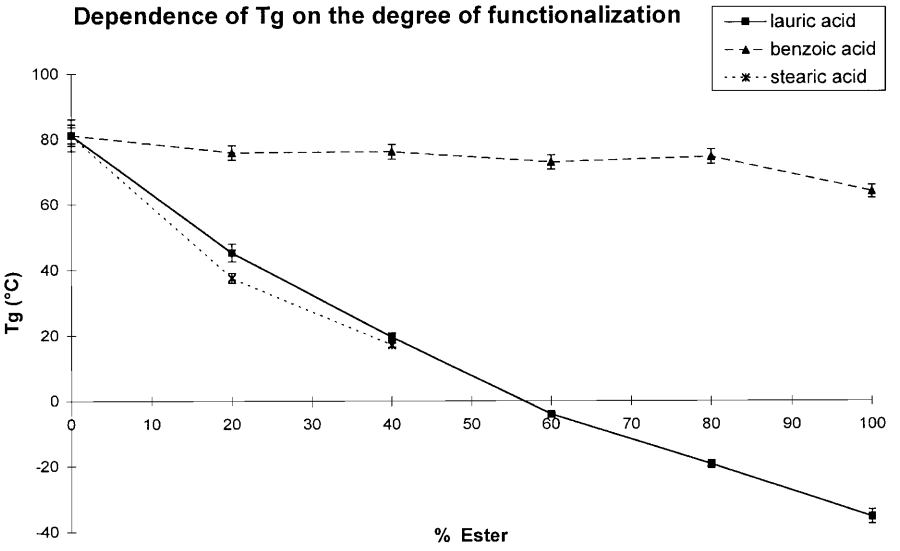

Fig. 12. Dependence of the glass transition temperature of hyperbranched polyesteramides, based on HHPA and diisopropanolamine, on amount of functionalization and type of mono acid

Unexpectedly, modification with benzoic acid does not influence the T_g. In this case the number of functional groups can be varied independently from the molecular weight of the hyperbranched core.

Esterification of at least 45% of the hydroxyl groups with long chain fatty acids, e.g., stearic or behenic acid, results in a semi crystalline material (side chain crystallization). The obtained materials are characterized by melting point ranges which are approximately 10 °C lower than the comparable methyl esters.

The esterification with methacrylic acid is performed at substantially lower temperatures than the above-mentioned procedures. An aerobic polymerization inhibitor is needed and an azeotropic removal of water with suitable solvents is also necessary.

3
Carboxylic Acid Functional Hyperbranched Polyesteramides

To the best of our knowledge, only one other example of a carboxylic acid functionalized hyperbranched structure is known in the literature, and this concerns a polyamide [19]. The synthesis reported starts from A_2 (aminofunctional) and B_3 (carboxylic acid functional) units and leads to low molecular weight products due to low conversion in dilute solution. These conditions were mandatory to prevent gelation [20]. Two different approaches to the synthesis of carboxylic acid functional hyperbranched polyesteramides are presented below [21].

3.1
Carboxylic Acid Functional Hyperbranched Polyesteramides: Two-Step Synthesis

The most simple way to introduce carboxylic acid functionalities onto hyperbranched polyesteramides is to modify the hydroxyl functions with suitable diacid derivatives. The modification can either be done in melt or in solution.

A possibility to functionalize in melt is the use of cyclic anhydrides to react with the hydroxyl groups. In the exothermic ring opening reaction the hydroxyl groups become esterified and carboxylic acid groups form the end groups. In order to ensure a good mixing of the components and a good temperature control, low viscous hyperbranched polyesteramides are more suitable to be modified in that way. The temperature control is quite crucial for the balance of the reactivity of the hydroxyl end groups with the cyclic anhydride and possible side reactions such as condensation of acid groups with residual hydroxy groups. Therefore a number of precautions have to be taken in order to prevent undesired molecular weight increase or other side reactions like the hydrolysis of the cyclic anhydrides, as residual water might not have been completely removed from the original polycondensation reaction. Figure 13 shows the idealized structure of a typical example which is characterized by a relatively low viscosity at modification temperatures, based on adipic acid and diisopropanolamine (A_2/B_3) and partially functionalized with stearic acid. The functionalization in that example is done with octenylsuccinic anhydride, also for viscosity reasons. In general, carboxylic acid functional resins obtained via the above-mentioned way indeed possess a somewhat higher molecular weight than theoretically expected due to condensation reactions.

Functionalization can, of course, also be carried out in solution, e.g., in tetrahydrofuran. In this case, temperature control is much easier and the problem of undesired condensation in the functionalization step is reduced. The viscosity increase due to the stronger hydrogen bondings of the formed carboxylic acid end groups is not of importance in the modification step in solution as viscosity can be adjusted through the amount of solvent. Nevertheless, complete solvent removal afterwards sometimes turns out to be laborious.

3.2
Carboxylic Acid Functional Hyperbranched Polyesteramides: Direct Synthesis

Another way to synthesize carboxylic acid functional hyperbranched polyesteramides is to invert the monomer ratio by using an excess of cyclic anhydride with respect to diisopropanolamine. In this case the theoretical A_2B building block consisting of 2 carboxylic acid and 1 hydroxyl function can be envisioned (Fig. 14).

At first glance this inversion of the monomer ratio seems to be logical and simple, but it is not. In the first reaction step, as described in Fig. 1, the advantage of the chemoselectivity of the anhydride reacting with the secondary amine is used to obtain AB_2 monomers. If an excess of anhydride is used, this selectivity is lost and not only amides but also esters are formed. From the synthesis of

Fig. 13. Idealized structure of the product of hydroxyl/stearic ester functionalized hyperbranched polyesteramides based on adipic acid and diisopropanolamine functionalized with octenyl succinic anhydride

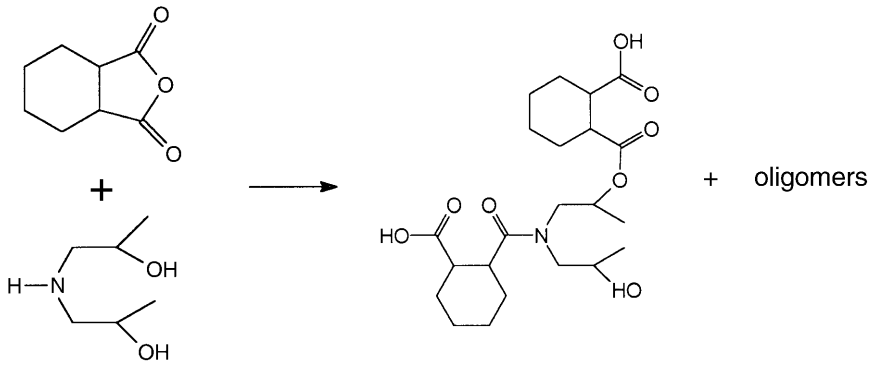

Fig. 14. Primary reaction step in the synthesis of carboxylic acid functional hyperbranched polyesteramides to obtain A_2B-type monomers from HHPA and diisopropanolamine

hydroxyl functionalized hyperbranched polyesteramides we have found that acidolysis of the esters formed plays an important role in the reaction proceedings. Hence the polycondensation of A_2B monomers leads to the formation of substantial amounts of free diacid together with the desired condensation products (Fig. 15).

At a certain conversion, esterification and acidolysis are in an equilibrium, if only the above-mentioned reactions occur. In a pure stochastic approach the ratios depicted in Scheme 1 are expected.

These theoretical results are confirmed experimentally. In attempts to prepare a resin with a ratio of the starting materials of HHPA : diisopropanolamine 2.3 : 1 the mixture gelated. This is reflected in Scheme 1, example 1 (n = 2). If a ratio of HHPA:diisopropanolamine 3.2 : 1 is chosen (Scheme 1, example 2, n = 5/6), the system does not gelate. By GPC analysis it was verified that the theoretical assumptions made in Scheme 1 are valid for this system. Besides the hyperbranched material, the presence of hexahydrophthalic acid is demonstrated. The quantity of the acid is in close agreement (29 %) with the calculated value (28 %).

Remarkable here is the fact that this special system enables one to create a relatively high molecular weight hyperbranched polymer beside starting material, as a result of the thermodynamic nature of the polymerization process. If this system were kinetic, one would have always obtained low molecular weight oligomers with ratios similar to example 2 in Scheme 1. In the case of a kinetic process, molecular weight is limited as it can be regarded as a conventional A_2/B_3 system. The limit has been predicted by Flory [4]. He calculated that one needs at least 35 % excess of one of the two components, assuming 100 % conversion. In our case, we obtain the same average molecular weight for the total system, but, as mentioned above, our products consist of monomers beside high molecular weight hyperbranched material. Upon removal of the monomers by extraction or crystallization the pure hyperbranched material can be isolated. Thus, theoretically any average molecular weight of the hyperbranched polyesteramides can be obtained. Figure 16 shows idealized molecular weight distributions as

Starting situation: A_2 = cyclic anhydride 2n + 1 mol
B_3 = diisopropanolamine n mol

assuming a complete conversion (p) of all B groups

$$p_B = 1$$

this means for the total conversion (p) of A groups

$$p_A = \frac{3n}{4n+2}$$

split into the probabilities of:

$$A_2 \text{ two twice reacted} = \left(\frac{3n}{4n+2}\right)^2$$

$$A_2 \text{ once reacted} = 2\left(\frac{n+2}{4n+2}\right)\left(\frac{3n}{4n+2}\right)$$

$$A_2 \text{ unreacted} = \left(\frac{n+2}{4n+2}\right)^2$$

two illustrative examples:

1)	2)
n = 2	n = 5/6
A_2 twice reacted = 36%	A_2 twice reacted = 22%
A_2 once reacted = 8%	A_2 once reacted = 50%
A_2 unreacted = 16%	A_2 unreacted = 28%

For the A_2B monomer the value for the critical branching coefficient is:

$$a_c = 0{,}5$$

the branching coefficient for this system is:

$$a = r\,p_B = \frac{3n}{4n+2}\,p_B^2$$

p_B is replaced by the critical conversion and a by the a_c

$$p_{B,\text{critical}} = \sqrt{0{,}5\,\frac{4n+2}{3n}}$$

This means for the first example, n = 2, that $p_{B,\text{critical}} = 0{,}913$, thus *gelation* is predicted.
For the second example, n = 5/6, $p_{B,\text{critical}} > 1$, *no* gelation is predicted.

Scheme 1. Stochastic approach of different monomer ratios

they would be obtained from GPC for the kinetic (a) and the thermodynamic product (b).

The above-mentioned concept of the synthesis of carboxylic acid functional hyperbranched polyesteramides is not limited to cyclic anhydrides as building blocks. It can be carried out with diisopropanolamine and any dicarboxylic acid as well. The same ratios as written above and calculated in Scheme 1 have been applied in the synthesis of carboxylic acid functional hyperbranched polyesteramides starting from adipic acid and diisopropanolamine. The first one (ratio 2.3:1) gelates as expected, the second one (ratio adipic acid:diisopropanolamine 3.2:1) affords the expected product. Again, with GPC the amount of free adipic acid detected is in good agreement with theory (Fig. 17).

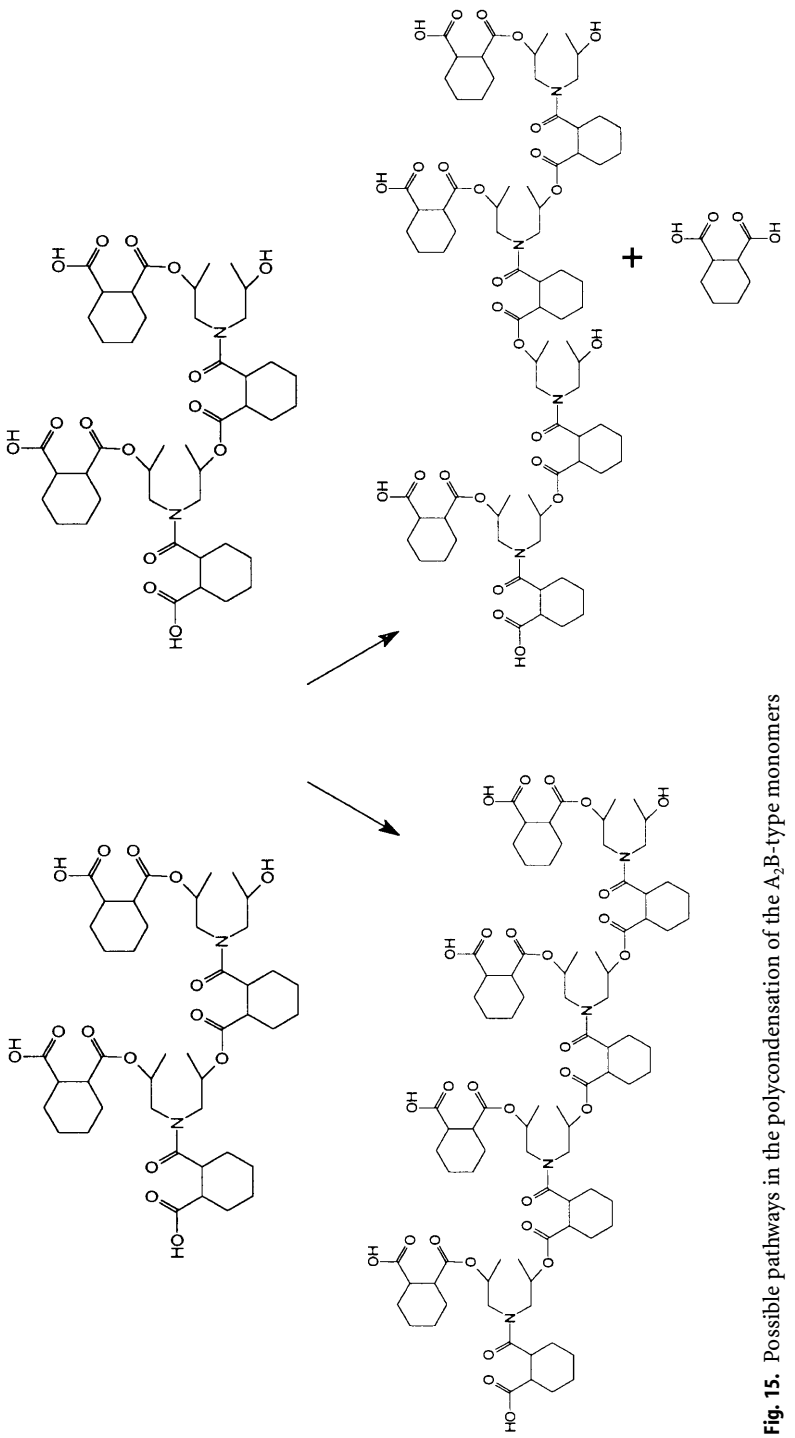

Fig. 15. Possible pathways in the polycondensation of the A_2B-type monomers

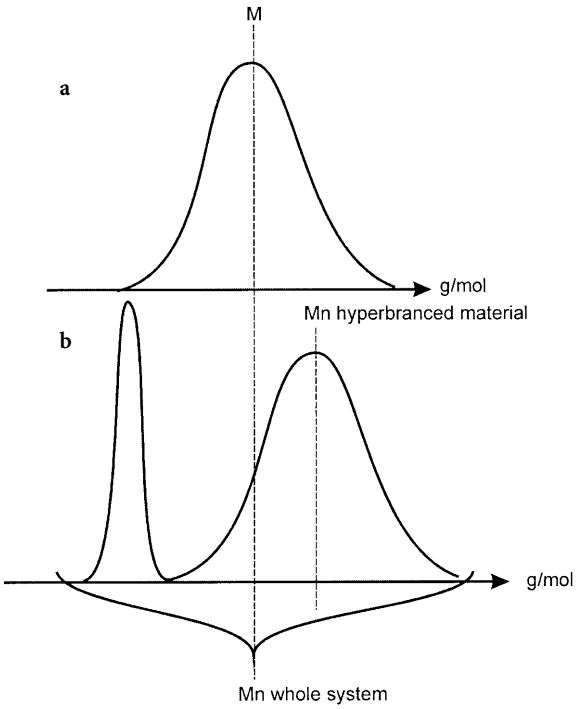

Fig. 16. Theoretical molecular weight distributions: **a** kinetic reaction product; **b** thermodynamic product (*left side* represents the "monomer signal")

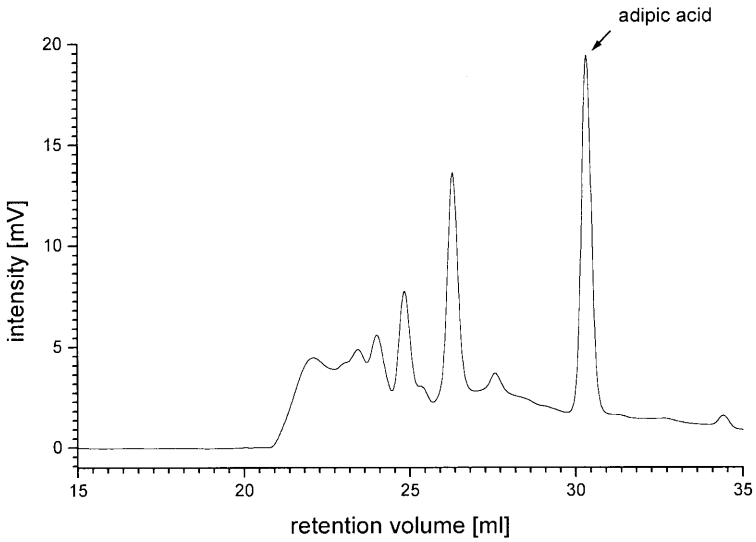

Fig. 17. GPC trace of carboxylic acid functional hyperbranched polyesteramide based on adipic acid and diisopropanolamine

End group analysis of the product via titration results in 6.3 mmol acid groups/g which is in good agreement with the theoretical expected amount of end groups, namely 6.4 mmol acid groups/g.

4
Alternatives for Diisopropanolamine in Hyperbranched Polyesteramides

The general concept of the synthesis of hyperbranched polyesteramides allows the use of any secondary amine with at least two β-hydroxyalkyl groups such as diisobutanolamine or di-β-cyclohexanolamine for the build-up of the highly branched structure. In the case of secondary mono β-hydroxyalkyl amines, e. g., methyl isopropanolamine, one obtains linear polymers. Primary amines cannot be used as they form imides in the polycondensation step.

In contrast to β-hydroxyalkylamines, other secondary amines work in our concept of our hyperbranched system as chain stoppers. As a precondition, however, they should not interfere with the oxazolinium-carboxylic acid ion pair polycondensation mechanism or react with carboxylic acid or hydroxyl groups at processing temperatures. Diisopropanolamine and secondary amines can be used simultaneously, the former for molecular weight build-up, the latter for obtaining (unreactive) end groups. Thus the amount of secondary amines is limited to at most the number of peripheral units of diisopropanolamine used in the concept of the original hydroxy functional hyperbranched polyesteramide synthesis. This maximum can be calculated according to the general formula giving the ratios of anhydride to diisopropanolamine to secondary amine as $2n+1:n:n+2$. These secondary amines, for example, dioctylamine, di(cyanoethyl)amine, diallylamine, morpholine, or 3,3′-iminobis(*N,N*-dimethylpropylamine), allow the introduction of various functional end groups. As the esterification via oxazolinium-carboxylic acid ion pairs is strongly pH-dependent, some amines might lead to incomplete conversion through their impact on the pH. Of course, mixed end group functionalities are of special interest, e. g., with hydroxyl groups and tertiary amines in polyurethane chemistry. Dialkylamines especially represent an interesting alternative for the introduction of long alkyl chains at the periphery in hyperbranched polyesteramides compared to the esterification of hydroxyl functional hyperbranched polyesteramides with fatty acids. An idealized structure of such a resin is presented in Fig. 18.

4.1
Tertiary Amine Functionalized Hyperbranched Polyesteramides

A special example, in which tertiary amine groups are introduced via 3,3′-iminobis(*N,N*-dimethylpropylamine) [22] is illustrated in Fig. 19.

Molecular weights of the products as measured with vapor pressure osmometry were in good agreement with the calculated ones. Interestingly, resins based on hexahydrophthalic anhydride and diisopropanolamine with tertiary amines as functional groups are soluble in water without quaternization of the

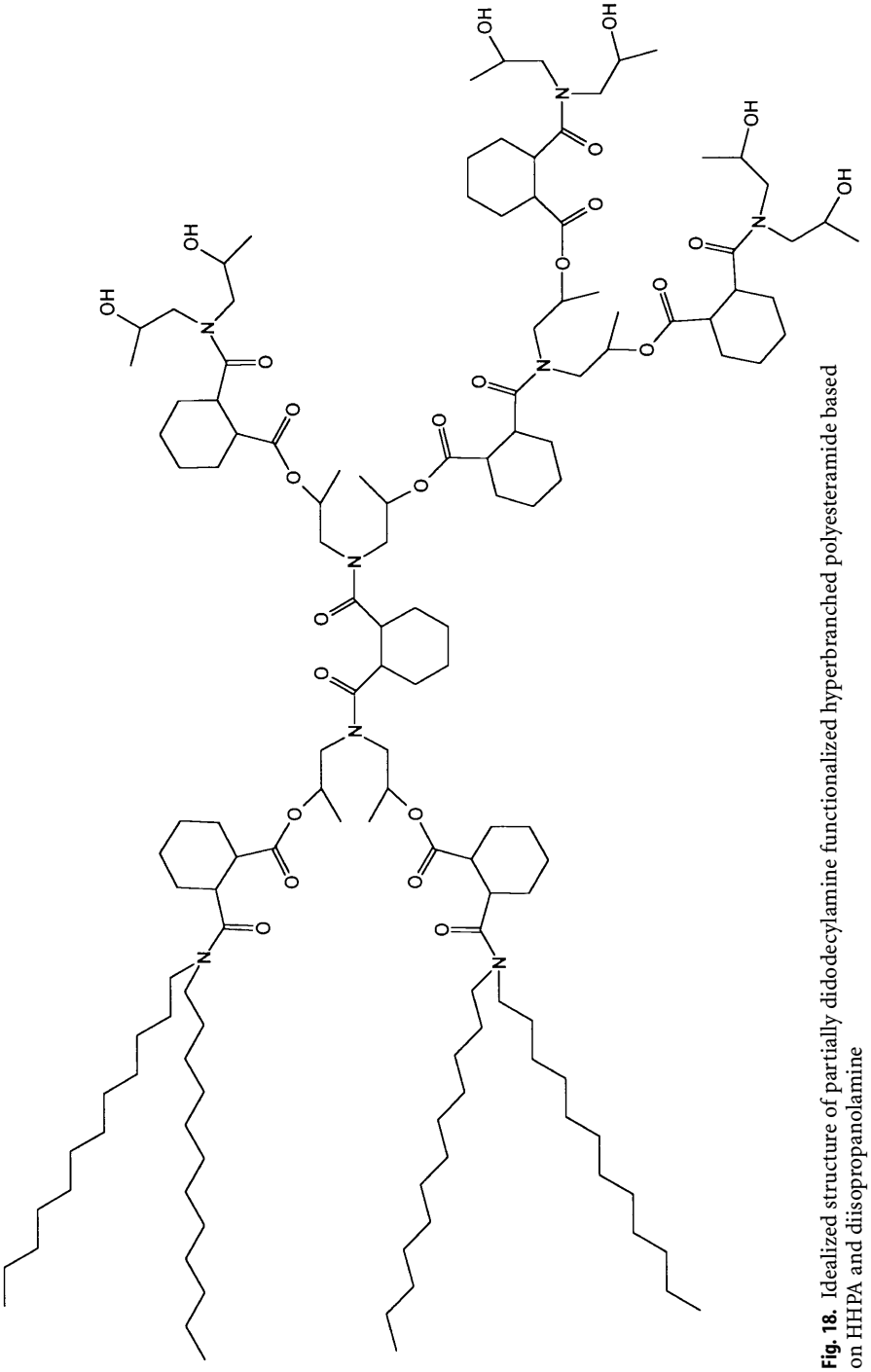

Fig. 18. Idealized structure of partially didodecylamine functionalized hyperbranched polyesteramide based on HHPA and diisopropanolamine

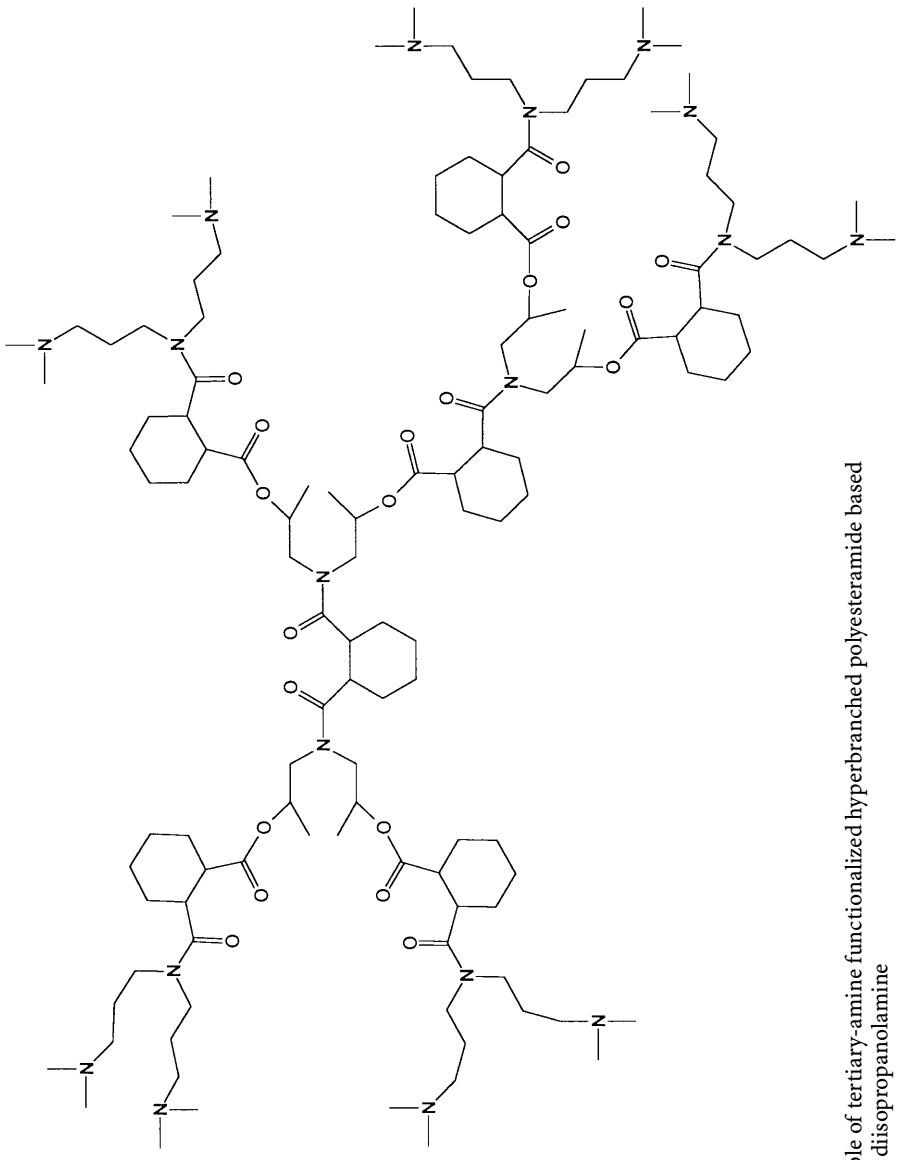

Fig. 19. Example of tertiary-amine functionalized hyperbranched polyesteramide based on HHPA and diisopropanolamine

tertiary-amines despite its relatively hydrophobic core illustrating the influence of the end groups on the resin's properties. Resins with tertiary-amine functionalities, based on other cyclic anhydrides like phthalic anhydride, succinic anhydride, etc., are also assumed to be water soluble.

5
Applications for Hyperbranched Polyesteramides

The successful application development for hyperbranched polyesteramides is primarily based on the many research programs started several years ago for dendrimers. For most of the potential and existing applications the high number of end groups and the multifunctionality are the predominant advantages. These characteristics are shared by dendrimers and hyperbranched materials alike. Only in some special cases, such as medical applications [23], is monodispersity the main issue and thus dendrimers are preferred in this particular case.

5.1
Coating Applications

With coatings being a broad field, the possibilities for highly branched materials are manifold. In the following some of the developed applications in this field are presented. In all cases the special shape and the large number of end-groups of highly branched structures are the predominant advantages for the introduction of hyperbranched materials.

5.1.1
Hydroxyl Functional Polyesteramides as Crosslinkers for Powder Coatings

A powder coating is the result of the application of a powder binder system, which generally consists of a resin, a crosslinker, flow additives, degassing agents, pigments or dyes, charge control agents, etc. Such a binder system is applied to the substrate as a fine, extruded powder (Fig. 20, step A), then melted at

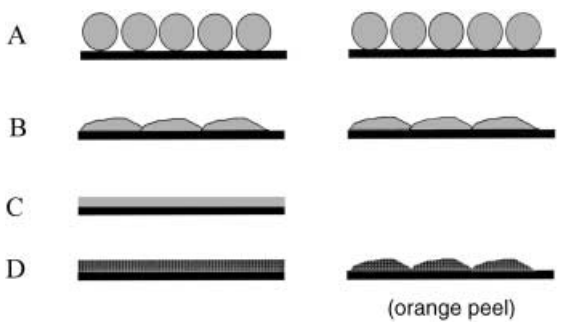

Fig. 20 a–d. Schematic representation of the different phases of the application of a powder binder system: *left* – the ideal case; *right* – the unbalanced flow/cure of a system, resulting in an "orange peel" surface of the coating

temperatures generally between 170 °C and 200 °C (Fig. 20, step B). When the temperature is raised not only does melting occur, but crosslinking also starts. These two processes have to be balanced very carefully to obtain a flat surface of the coating (Fig. 20, step C, left) before the binder is totally crosslinked (Fig. 20, step D). If crosslinking occurs too early, the flow is not ideal and the coating shows a pattern, known in the powder coating world as "orange peel" as the pattern resembles the skin of an orange (Fig. 20, step D, right).

Unfunctionalized, i. e., 2-hydroxypropylamide functional, hyperbranched polyesteramides have been tested in powder coating formulations together with stoichiometric (OH/COOH) amounts of acidic polyesters (Uralac). It was anticipated that the reaction of the hydroxyl end groups of the polyesteramide with the carboxylic acid end groups of the polyester would provide a well-crosslinked film with good mechanical properties by polymer/polymer cure.

We realized, however, that if the polyesteramides merely acted as multi 2-hydroxypropyl-amide functional polymers, they could never provide good flow and optical appearance of the coatings. From the mathematical theory of network formation [24] it is known that a binder formulation with a 2-functional resin and a crosslinker bearing many (> 5) functional groups reaches its gel-point at low chemical conversion, as shown in Fig. 21.

This means that the time for flow-out of the powder becomes shorter with increasing functionality of the crosslinker, with respect to the total cycle time required for reaching satisfactory film properties (mechanical, chemical, Fig. 20, step D). The reduced flow-phase time results in a poorer film surface quality. Moreover, when volatiles are set free as a result of the crosslinking reaction, in this case water, they will cause blister formation after the gel-point. Blister for-

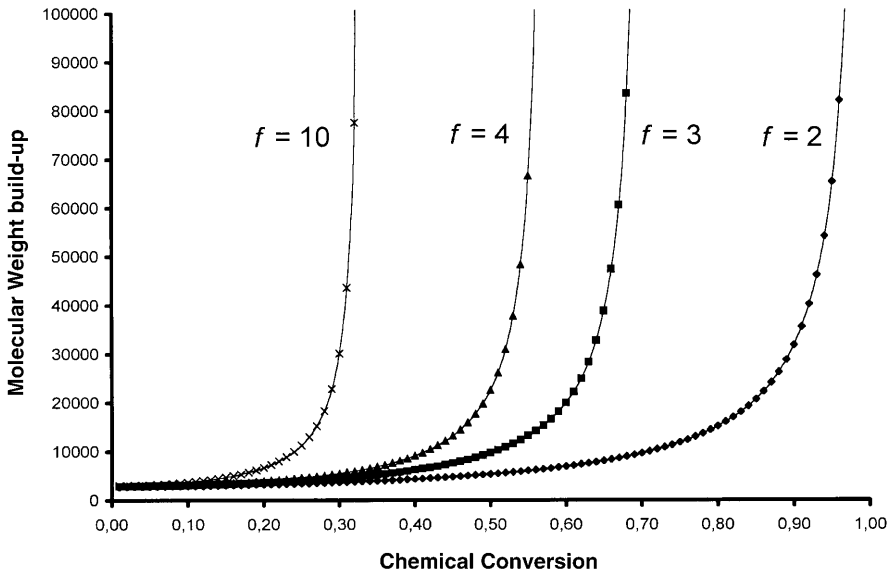

Fig. 21. Calculations for the gelation of a two functional resin (M_n of 3000 g/mol) with multifunctional crosslinkers

mation in thick layers (>100 µm) is a known phenomenon in powder coatings formulated with water or alcohol releasing crosslinkers [25]. From this point of view, extremely poor flow and optical appearance could be expected along with a very low blister formation threshold.

The compositions, according to Table 2, were prepared by mixing and extruding (Prism extruder, 120 °C). The polyesters (Uralac P 5040 and Uralac P 5261 from DSM Resins) comprise units of terephthalic acid, adipic acid, neopentylglycol, and trimellitic anhydride, and are regarded as four-functional. The former had an acid number of 55 mg KOH/g resin, and the latter 47 mg KOH/g resin. The hyperbranched polyesteramides (shown in Table 2) **1a** and **1b** were synthesized from diisopropanolamine and phthalic anhydride (PA), **2a**, **2b**, and **2c** from 1,2-*cis*-cyclohexanedicarboxylic anhydride (HHPA), **1a** and **2a** having a number average molecular weight of approximately 1500 (molar ratio 1.20) and a number average functionality of 8, **1b** and **2b** having a number average molecular weight of approximately 900 (molar ratio 1.33) and a number average functionality of 6, and **2c** having a number average molecular weight of approximately 2000 (molar ratio 1.14) and a number average functionality of 10. Gel times of these compositions were determined at 200 °C. The compositions were milled and sieved (< 90 µm) and electrostatically sprayed (Corona) on aluminum panels. After the cure cycle, carried out in a circulation oven, the panels were tested

Table 2. Powder paint formulations and coating properties

Composition	A	B	C	D	E	F	G
Polyester resin (g)							
P 5261	155			159		164	152
P 5040		156	162		160		
HB-Crosslinker (g)							
1a (PA, f = 6)	45	44					
1b (PA, f = 8)			38				
2a (HHPA, f = 6)				43	42		
2b (HHPA, f = 8)						36	
2c (HHPA, f = 10)							47
Additives (g)							
TiO_2 2160	100	100	100	100	100	100	100
Benzoin	3.0	3.0	3.0	3.0	3.0	3.0	3.0
BYK 361	1.5	1.5	1.5	1.5	1.5	1.5	1.5
Cure cycle							
Minutes	10	10	10	15	15	15	15
Temperature (°C)	200	200	200	180	180	180	180
Properties							
Gel time (s)		151	80	116	85	100	80
Hardness (s)	235	225	215	215	210	195	240
Impact (inch.pound)	>160	>160	>160	>160	>160	>160	>160
Erichsen (mm)	>8	>8	>8	>8	>8	>8	>8
Adhesion	Gt O	Gt O	Gt O	Gt O	Gt O	Gt O	Gt O
Flow	OK	OK	OK	OK	OK	OK	OK
Blister threshold (µ)	120	120	130	140	140	140	120

for their optical appearance (visually, OK stands for generally accepted high quality), flexibility (mm Erichsen), reverse impact resistance, chemical resistance (acetone double rubs), adhesion (cross hatch adhesion test), and hardness (König). The threshold indicates the highest average layer thickness on a plate (plates varying between 80 μm and 150 μm average layer thickness) that did not show blisters.

It was therefore found, surprisingly, that powder paint formulations (Table 2) of even four-functional acidic polyesters (so called "TMA-resins") with the hyperbranched polyesteramides gave smooth films of high quality and with a surprisingly high blister formation threshold. In addition, the measured gel times of the formulation were in agreement with that normally found with crosslinkers of ordinary functionality, i. e., two to four. Interestingly, these findings were irrespective of the molecular weight and the functionality of the hyperbranched polyesteramides, e. g., compare rows D, F, and G.

It is apparent that the mode of reaction of the hyperbranched polyesteramides must be distinctively different from those of the known commercial crosslinkers. In order to explain these results, the hyperbranched polyesteramides should in our view not be regarded as simply multifunctional polymeric crosslinkers but rather as precondensed forms of two-functional crosslinkers (the addition product of diisopropanolamine and the cyclic anhydride), as depicted in Fig. 22, left. Bearing in mind the chemical fate of benzoic acid (2.2.1, Fig. 11) which was condensed with a polyesteramide resin and which appeared to transesterify at least as fast as it esterified, the mode of reaction of polyesters comprising aromatic acid end groups must be in accordance and comprised of both transesterification and esterification.

When we consider transesterification to be by far the dominant process, the acidic polyester will break down the hyperbranched structure entirely and find itself esterified on all end groups with one hydroxyl group of the amine/cyclic anhydride adduct. In other words the polyester originally bearing aromatic acid groups then bears an equal number of aliphatic acid end groups and also an equal number of 2-hydroxyalkyl end groups. When these new end groups start to esterify among each other, a network is formed. As a result of this two-phase reaction mode, the overall viscosity of the binder system is lowered and the gel formation is postponed with respect to the total chemical conversion (Fig. 20, step D, left).

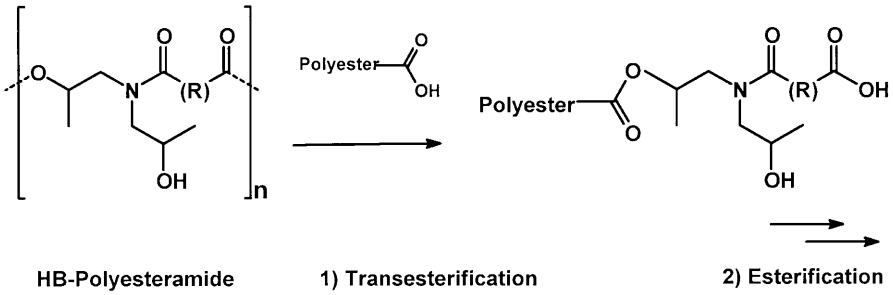

Fig. 22. Proposed mode of reaction of polyesteramide crosslinker with acidic polyesters

It is known from the literature [12] that aliphatic acids are less reactive towards 2-hydroxyalkylamide groups than aromatic ones. Since the final network formation with the polyesteramides involves predominantly aliphatic acid groups, this could explain (in part) why the gel times found were longer than the commercial 2-hydroxyalkylamide crosslinkers, which react directly by esterification alone with the aromatic acid end groups of the polyester.

5.1.2 *Air Drying Coatings*

Solvent emissions from alkyd paints have received increasing attention in the last few years, not only in the light of global warming and ozone creation but also because of increasing number of government directives associated with the risks to human health. For this reason there is a strong demand from paint formulators [26] for new air drying "high solid" resin types. This again favors dendritic architectures, since the classic alkyd resins are at the end of their formulating latitude. The combination of reduced viscosity and solvent content without compromising film hardness is particularly desired. While increasing the oil length (percentage of fatty acid in the total system) with normal alkyds reduces viscosity and speeds up the chemical drying process, the hardness of the obtained films becomes unacceptably low.

The alkyd resins can be roughly described as normal branched polyester polyols which are esterified with unsaturated fatty acids. The advantage of using a core polymer with a more dendritic architecture lies in further reduction of chain entanglements and more globular molecular shape, resulting in lower intrinsic viscosities. Furthermore, when higher molecular weights can be obtained, the drying process is accelerated by the higher functionality per molecule. This principle has already been demonstrated by Petterson et al. [27] with air drying resins made from hyperbranched poly-(bismethylolpropionic acid) esterified with tall oil fatty acids. The authors reported markedly lowered viscosities and shortened drying times in comparison with a classic high-solid alkyd resin. However, the low film hardness typically associated with high oil length alkyds (thus high amount of fatty acids) was reported here as well.

An air drying hyperbranched polyesteramide resin was compared to a normal alkyd purposely designed for high solid application (XP 3782, DSM Resins). A solution in white spirits of this resin was found to have a much lower viscosity than the normal alkyds including the high-solid resin, despite the relatively low oil length. This resulted in a much higher solids content (87%) in a paint formulation on application viscosity. Even more remarkable was the high film hardness after drying which by far outperformed the normal alkyd paints. Weatherometer tests did not show any significant differences in gloss retention at 20°C between these three resins, nor did Erichsen penetration tests show any differences in flexibility. However, a distinct disadvantage of the polyesteramide resin was its slow initial drying (tack free only after more than 12 h). This was attributed [28] to free secondary amine groups naturally occurring in the base resin (see introduction) interacting with the cobalt catalyst in the first hours.

The high hardnesses found in the high-solid and high-gloss white paints, which are in sharp contrast to reports on hyperbranched polyesters [27], have in our opinion their origin in the much higher T_g of the polyesteramide backbones (ca. 70 °C for HHPA and ca 100 °C for PA-based resins; hyperbranched polyesters based on bismethylolpropionic acid have a T_g close to room temperature). While the alkyl end groups determine overall resin properties such as T_g, viscosity [29], and the crosslinking density in the coating, the high rigidity of the polymer backbone, especially when nanoscale domains are formed, could still contribute to film stiffness after crosslinking.

5.2 Dyeable Polypropylene Fibers

Contrary to other synthetic fiber materials, polypropylene fibers cannot be colored by contacting them with an aqueous solution or dispersion of organic dyes. Due to its highly apolar nature, polypropylene is not able to interact with conventional dye molecules, so that it cannot take up any dye from the dye bath.

In the past, several approaches to circumvent this shortcoming of the otherwise very attractive polypropylene fiber have been investigated. Modification of polypropylene by the addition of polar (co)polymers can result in a material which is dyeable in acid, basic, or disperse dye processes. However, this requires a relatively large quantity of additive, which unfortunately may have a negative effect on the processing behavior of the polymer and the properties of the final fiber. Another approach is the addition to the polypropylene matrix of organonickel compounds, which can form colored complexes with special chelating dyes that are added to the dye bath. The use of nickel, however, has caused objections due to its negative environmental and health aspects.

For, e. g., the coloration of carpet fibers, the industry currently uses pigments which are added to the polypropylene before the spinning process (also known as "solution dyeing"). The use of pigments strongly limits the end producers in the selection of colors, as only a limited variety of colored base fibers can be kept in stock. Moreover, many pigments have a negative influence on the mechanical behavior of the fibers.

Earlier we found that the addition of alkyl-modified poly(propylene imine) dendrimers to polypropylene leads to fibers which can be dyed in conventional acid or disperse dyeing processes [3]. The alkyl chains make the additive compatible with the polypropylene matrix, while the polar core of the dendrimer can act as a receptor for the dye molecules. This host-guest behavior is analogous to the principle of the "dendritic box" as described by Meijer et al. [30] and elaborated by Baars et al. for dye extraction processes [31].

Based on our dendrimer know-how, we have investigated a partially stearate-modified hyperbranched polyesteramide (Fig. 23) as a dyeability improver for polypropylene. Using normal extrusion blending conditions, compounds of fiber-grade polypropylene with up to 4% of additive have been prepared without problems. The stearate carbon chains ensure a compatibility with the polypropylene matrix, so that the resulting blends are homogeneous. Using standard industrial spinning operations, these compounds were melt spun into

Fig. 23. Hyperbranched polyesteramides consisting of phthalic anhydride, diisopropanolamine, and stearic acid used as an additive making polypropylene fibers dyeable

fibers at temperatures up to 260 °C (a normal condition for polypropylene processing). The spinning and drawing behavior of the fibers, and also the final mechanical properties, were indistinguishable from unmodified polypropylene fiber.

Under conventional dyeing conditions we have succeeded in producing deeply colored fiber. This has been achieved with aqueous disperse dye systems, which are normally used for the dyeing of, e. g., polyester fibers. The coloration of the resulting materials has an excellent wash and rub resistance. Obviously, the polar amide and ester groups as well as the hydroxyl groups in the hyperbranched molecule's core enable it to give a sufficiently strong interaction with the dye molecules.

We are currently developing this concept towards a commercially viable product for application to, e. g., carpets and textiles.

6
Water Solubility and Future Developments

6.1
Water Soluble Resins

There are two ways to make hyperbranched polyesteramides water soluble. One is to functionalize the periphery of the molecule with hydrophilic groups, the other the use of suitable anhydrides to obtain water solubility via the core. These approaches are shown in Fig. 24.

The hydrophilicity can be easily controlled from being totally soluble in water, such as the two examples in Fig. 24, via dispersible in water (partly modified with stearic acid) (Fig. 25), to completely water insoluble hyperbranched polyesteramides, such as in Fig. 22.

Especially interesting are water soluble and non-toxic resins which can be used in a broad range of potential applications. Toxicity tests are currently under review.

6.2
Poly(ethyleneoxide) Functional Hyperbranched Polyesteramides

One of our future research targets is to develop poly(ethyleneoxide) functionalized hyperbranched polyesteramides, as these might, for example, be very interesting as water soluble extraction agents or carriers. An envisaged example is shown in Fig. 26. The idealized structure depicted in Fig. 26 can be considered as a unimolecular micelle [32] with a hydrophilic periphery and a hydrophobic polar core. Both can be varied: the core can be made more hydrophilic by, e. g., partially replacing hexahydrophthalic anhydride with succinic anhydride or the polarity can be changed by, e. g., partially replacing hexahydrophthalic anhydride with octenyl succinic anhydride.

The hydrophilicity of the periphery can be adjusted by chain length of the polyethyleneglycol. If this system proves to be non-toxic it might be useful for pharmacologically active compounds, e. g., as carrier.

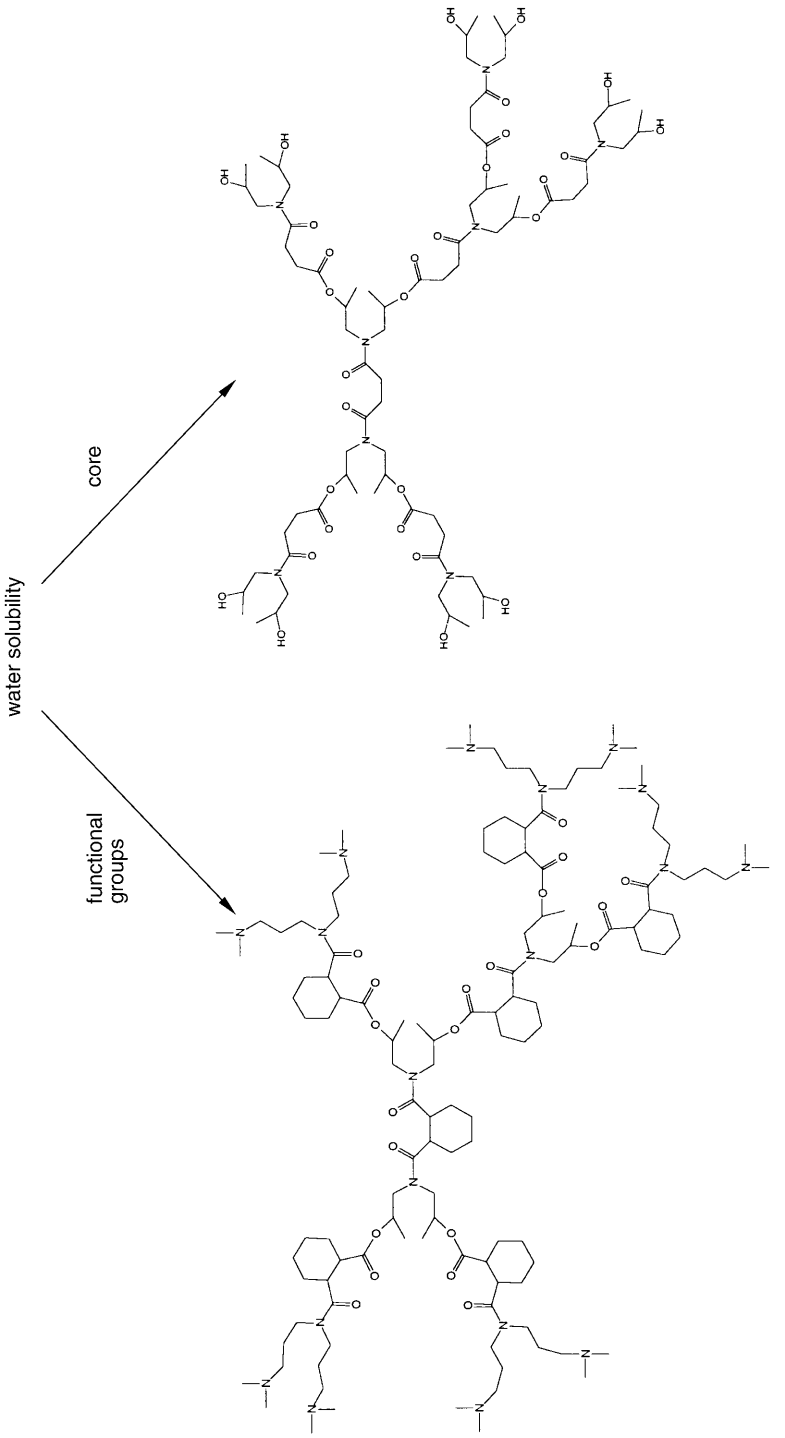

Fig. 24. Principles of making hyperbranched polyesteramides water soluble via the core or by modification of the end groups

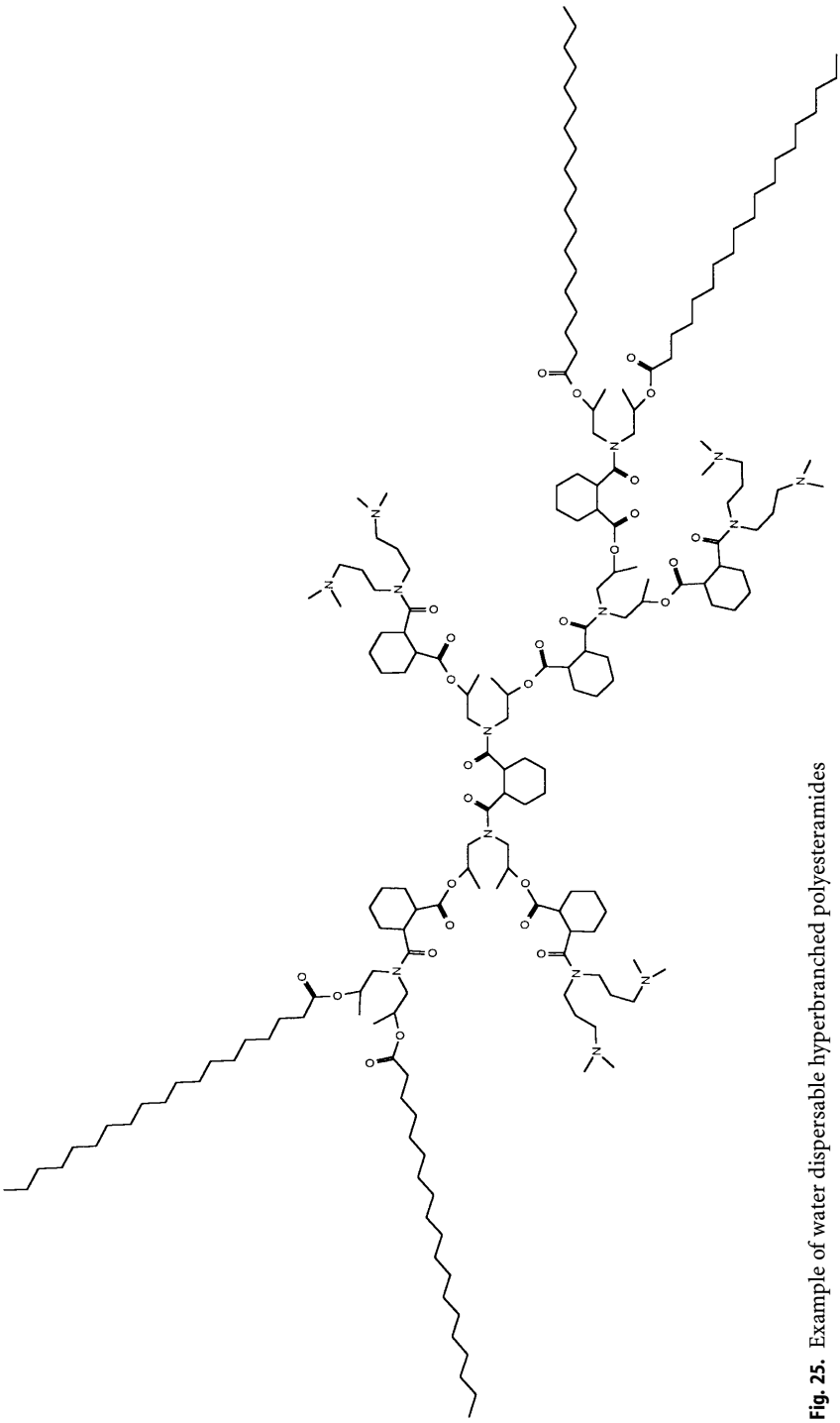

Fig. 25. Example of water dispersable hyperbranched polyesteramides

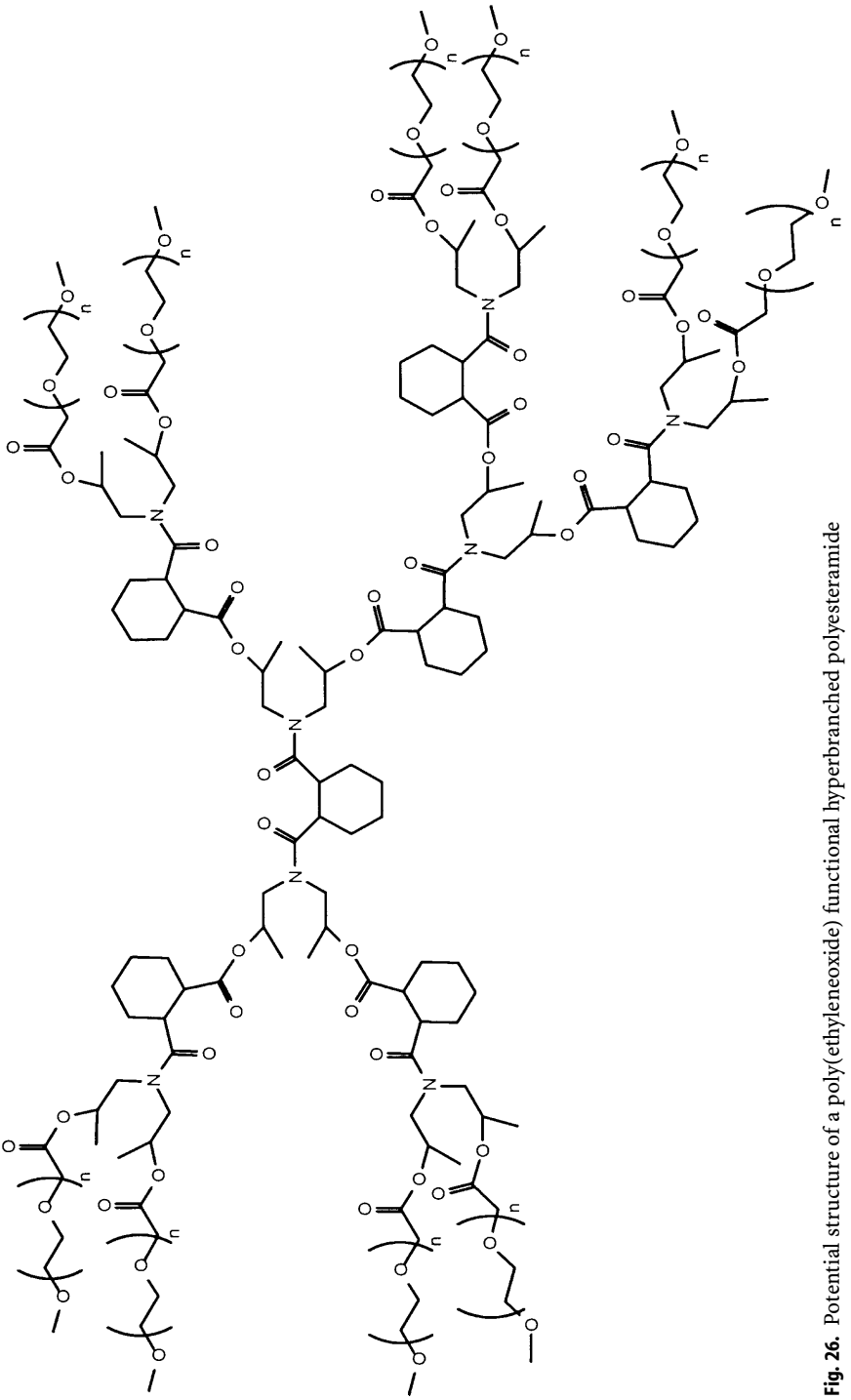

Fig. 26. Potential structure of a poly(ethyleneoxide) functional hyperbranched polyesteramide

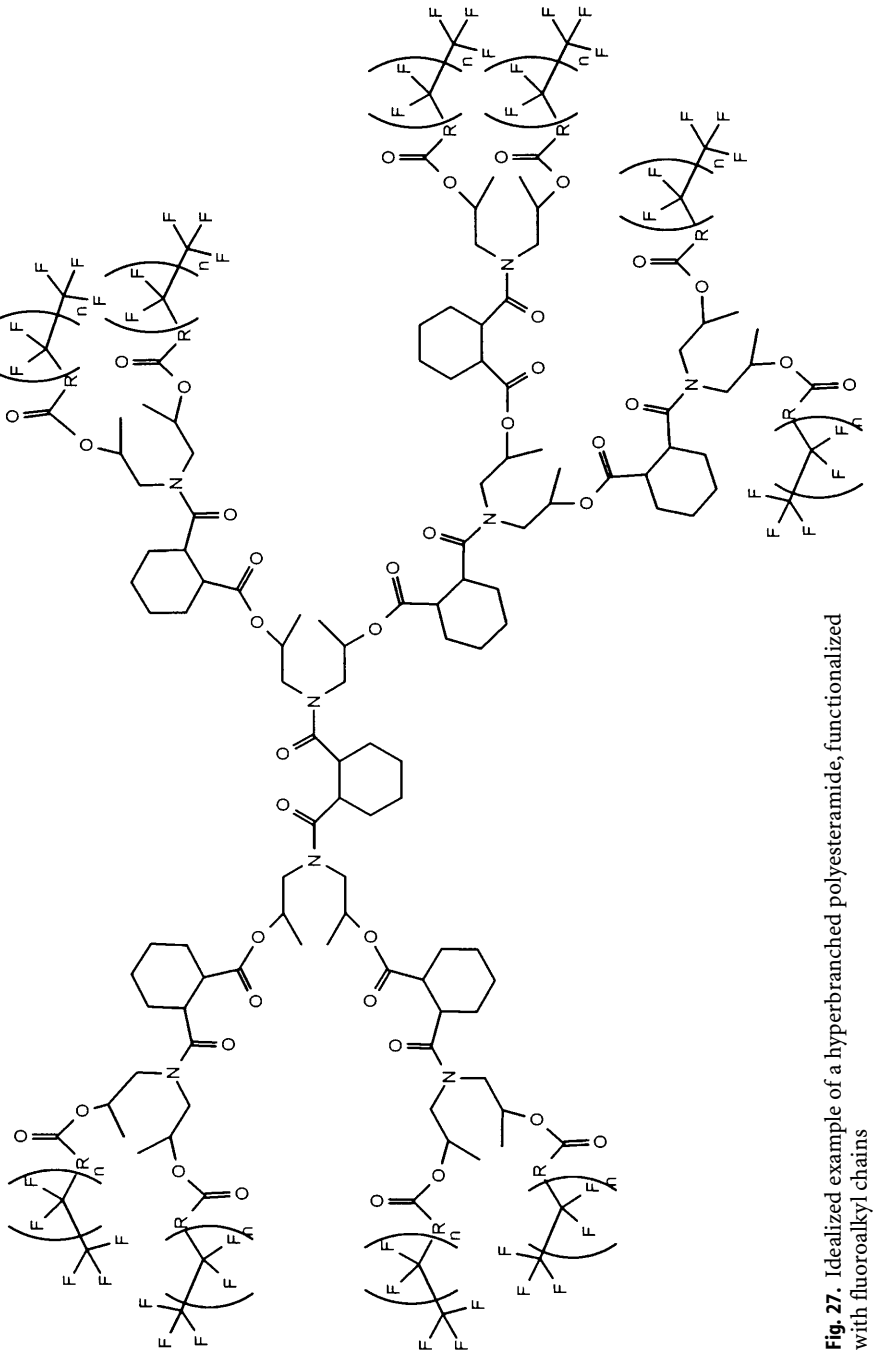

Fig. 27. Idealized example of a hyperbranched polyesteramide, functionalized with fluoroalkyl chains

6.3
Fluoroalkyl Functional Hyperbranched Polyesteramides

Hyperbranched polyesteramides, partially or fully functionalized with fluoroalkyl chains, are expected to be valuable additives for numerous applications. A fully functionalized derivative could be considered to be a unimolecular micelle (like the polyethyleneoxide functionalized analogue) suitable for, e.g., extractions in organic media. An idealized example is shown in Fig. 27.

A 50% functionalization evokes the interesting question, bearing in mind facile transesterification, of how the fluoroalkyl chains will be distributed over the molecules and how they will be distributed on one particular molecule? This question has been examined in detail for dendrimers of the poly(propyleneimine) type functionalized with stearic acid [33]. It was proven that the compositional heterogeneity (distribution of degree of substitution) is random, but the positional heterogeneity (spatial distribution of the substituents over the dendrimer molecule) is not random. However, due to flexibility, no particular effect of the spatial distribution can be observed. Unlike the dendrimers, we expect the hyperbranched polyesteramides to be stiffer, so that spatial distribution could lead to interesting effects if the molecule were composed of a functionalized side and a non-functionalized side (Fig. 28), as shown possible for dendrimers via a convergent synthesis [34].

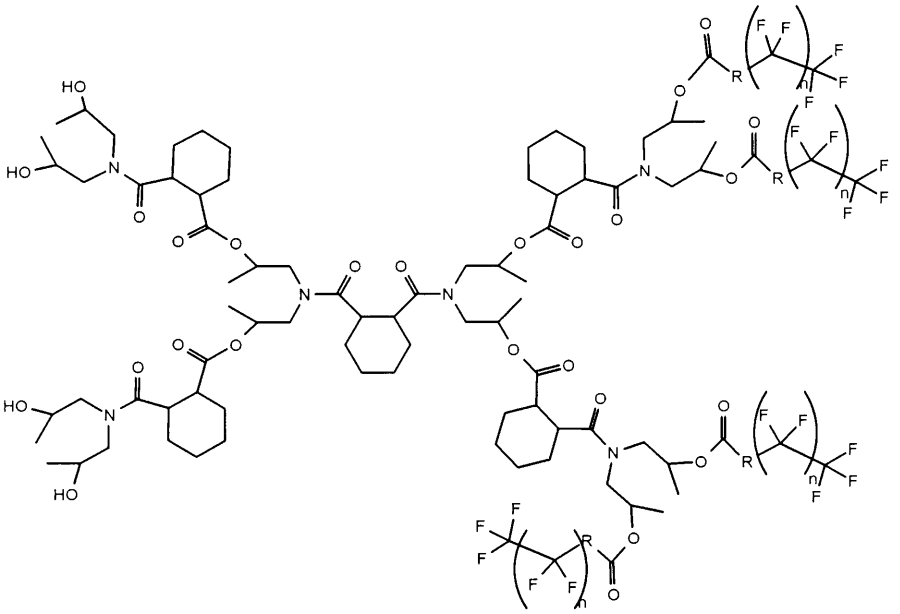

Fig. 28. Potential schematic structure of a 50% fluoralkylchain functionalized hyperbranched polyesteramides

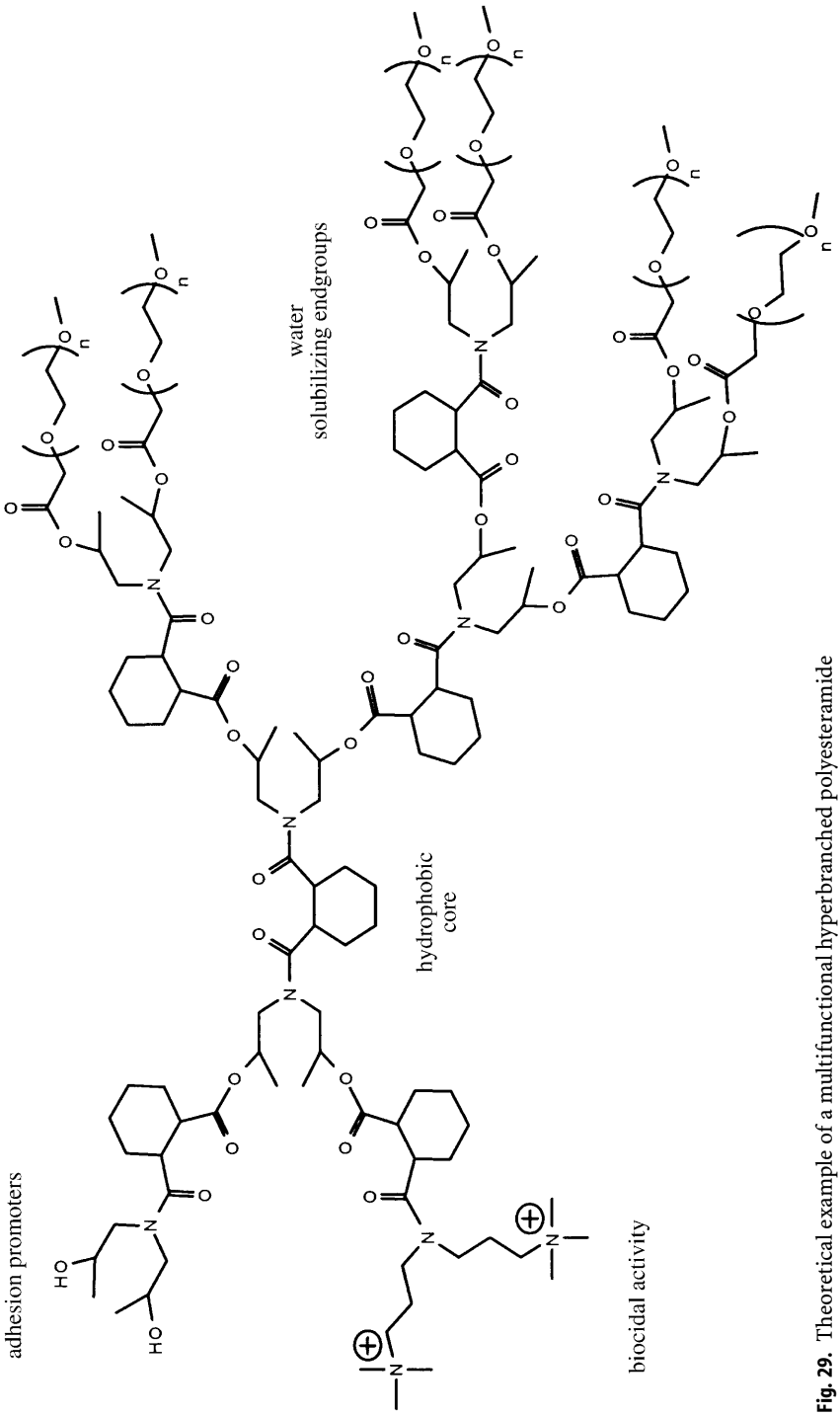

Fig. 29. Theoretical example of a multifunctional hyperbranched polyesteramide

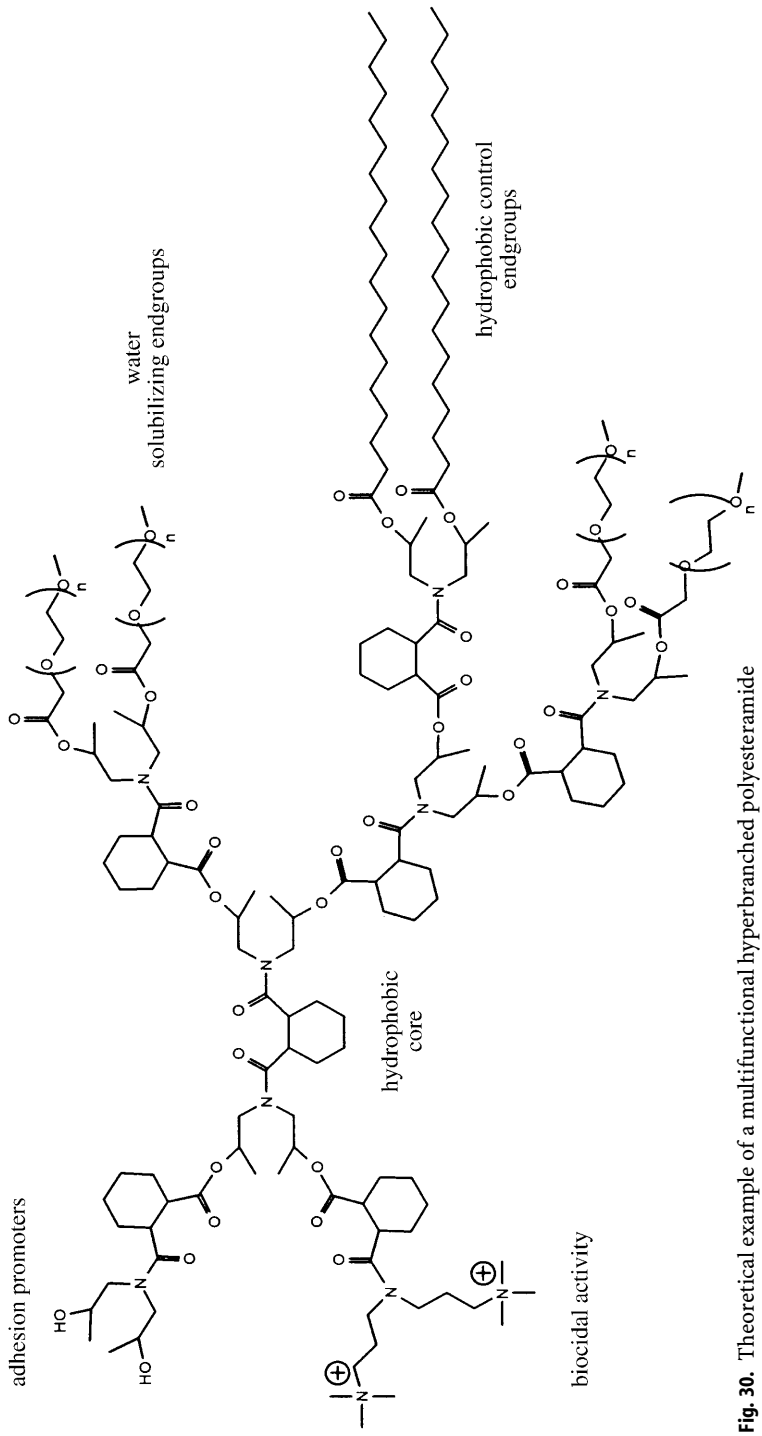

Fig. 30. Theoretical example of a multifunctional hyperbranched polyesteramide

6.4
Multifunctional Hyperbranched Polyesteramides

The easy modification of the hyperbranched polyesteramides can be used to introduce different functionalities on the same molecule. The term multifunctionality refers to different kinds of functional groups rather than a high number of end-groups of one kind. Figures 29 and 30, give some ideas of idealized hyperbranched polyesteramides which could in future carry more than two types of functional groups on the one molecule.

We are currently investigating the synthesis and characterization of such molecules for numerous different applications such as surfactants, cosmetics, and toner resins. A point of interest in the preparation and characterization of multifunctional hyperbranched molecules is the compositional heterogeneity (how many and what type of functional groups are on a particular hyperbranched polyesteramide molecule) and the positional heterogeneity (spatial distribution of the functional groups on a particular hyperbranched polyesteramide molecule).

As the hyperbranched polyesteramide resins are characterized by high polydispersity the distribution of the functional groups might vary greatly from one hyperbranched molecule to the other, even in that one particular molecule carries only one type of functional groups.

7
Conclusions

Hyperbranched polyesteramides constitute a new and promising class of resins. They can be made following a very straightforward melt polycondensation procedure which allows the use of a broad range of raw materials for optimal versatility. The synthesis does not require any catalyst, which would afterwards have to be removed, as the esterification occurs via oxazolinium/carboxylate ion pairs. Due to the easy modification, numerous different functional groups can be attached, e. g., esters, carboxylic acids, and tertiary amines. Characteristics of these resins such as molecular weight, glass transition temperature, number and type of end groups, solubility, and polarity are adjustable and thus hyperbranched polyesteramides can be tailor-made.

In powder coating formulations, the unfunctionalized base resins have proven to be valuable components, curable with acid polyesters, offering excellent mechanical, chemical, and optical properties, and a high blister threshold. It is postulated that, during the curing process of these coatings, the hyperbranched structure is at first degraded by transesterification and, concomitantly, fully integrated in the network formation by esterification.

In solvent-borne formulations such as air drying paints, the hyperbranched polyesteramide resins partly or wholly functionalized with various alkyl substituents offer important advantages in comparison with conventional resins as a result of their dendritic structure, i. e., lacking chain entanglements and the high rigidity of the polyesteramide backbone. These structural characteristics result in properties such as low viscosity/high solids content, efficient and fast network formation/good drying properties, and, most of all, exceptionally high film

hardness. This hardness allowed for formulation of relatively low molecular weight resins without compromising film properties, and also allowed the use of entirely aliphatic monomers, which in turn resulted in excellent weatherability.

The dyeing of polypropylene fibers, being an item of research for decades, is successfully accomplished with partially stearate-modified hyperbranched polyesteramides. The long alkyl chains ensure compatibility with the polypropylene matrix. The mixing-in of hyperbranched polyesteramides via extrusion affected neither the melt spinning process nor the final polypropylene fiber properties. The modified fibers are dyeable under standard conditions as are, e. g., polyesters or cotton. They can even be used for printing: for example a picture pattern on a polypropylene carpet.

Our future research will lead to new types of hyperbranched polyesteramides. The ideas presented will enable properties such as water solubility (poly(ethyleneoxide) functional groups) or reduction of surface tension (fluoroalkyl functionalized resins) to be precisely controlled. Last, but not least, mixed functional highly branched molecules with their (expected) unique set of combined properties have a huge potential to enter numerous technical fields.

Acknowledgements. The authors thank the following co-workers and colleagues for their contributions, fruitful cooperation and discussions: Manon Mak, Patrick Hendriks, Carlo Vermeulen, Paul van Mameren, Wim Grisnich, John Rietberg, Bianca Spoolder, Leendert Molhoek, Nico Meijerink, Erik Geladé, Chris de Koster, Gerard Kwakkenbos, Theo Zwartkruis, Dirk Stanssens, Engelien Kleuskens, and Richard Green.

Special thanks to Peter Froehling for his help in revising the manuscript and contributing the section on dyeable polypropylene fibers.

8 References

1. Maciejewski M (1982) J Macromol Sci – Chem 17A:689; Pistolis G, Malliaris A, Tsiourvas D, Paleos CM (1999), Chem Eur J, 5:1440; Zhao M, Crooks RM (1999) Angew Chem Int Ed 38:364
2. Fischer M, Vögtle F (1999) Angew Chem Int Ed 38:885
3. DSM Pat, WO PCT 98/12376
4. Flory PJ (1953) Principles of polymer chemistry. Cornell University Press
5. Kienle RH, Hovey AG (1929. J Am Chem Soc 51:509
6. Hawker CJ, Lee R, Fréchet JMJ (1991) J Am Chem Soc 113:4583
7. Kim YH, Webster OW (1990) J Am Chem Soc 112:4592
8. Malmström E, Hult A (1996) Macromolecules 29:1222; Malmström E, Hult A (1997) J M S Rev Macromol Chem Phys C37:555
9. Kricheldorf HR, Stöber O (1994) Macromol Rapid Commun 15:87; Kricheldorf HR, Stöber O, Lübbers D (1995) Macromolecules 28:2118
10. Feast WJ, Hamilton LM, Rannard S (1997) Polymer Bulletin 39:347
11. Wicks ZW Jr, Chiang NC (1982) J Coat Technol 54:27
12. Stanssens D, Hermanns R, Wories H (1993) Progr Org Coatings 22:379
13. Wicks ZW, Chiang NC (1979) J Org Chem 44:1244; Jones FN, Lin IC (1984) J Appl Polym Chem 29:3213; see also Cope AC, Hancock EM (1944) J Am Chem Soc 66:1738; Immediata T, Day AR (1940) J Org Chem 5:512
14. Cameron C, Fawcett AH, Hetherington CR, Mee RA, McBride FC (1997) ACS Polym Preprints 38(1):56

15. Misev TA, van Benthem RATM, Zwartkruis TJG (1998) Bull Chem Techn Macedonia 17:77; Misev TA (1989) J Coat Techn 61:772; Misev TA (1992) J Coat Techn 21:79
16. Gelade E, Goderis B, DeKoster C, Meijerink N, Scherrenberg R, VanBenthem R, Zwartkruis T, Muscat D, Fokkens R, Nibbering N, Mortensen K (2000) Macromolecules (in preparation). Previous results were reported in: van Benthem R (1999) WO 99/16810 Proc. of the 25th Int. Conf. in Org. Coatings, Athens 25:345; van Benthem R, Muscat D, Stanssens D (1999) ACS Polym Mat Sci Eng Preprint 80:72
17. Hölter D, Burgath A, Frey H (1997) Acta Polym 48:30; Hölter D, Frey H (1997) Acta Polym 48:298. "Degree of branching" is often used as a descriptor for hyperbranched structures; see, e.g., Malmström E, Hult A (1997) JMS Rev Macromol Chem Phys 37:555; Dusek K (1997) TRIP 8:268
18. Bosman AW, Janssen HM, Meijer EW (1999) Chem Rev 99:1665
19. Jikei M, Chon SH, Kakimoto M, Kawauchi S, Imase T, Watanebe J (1999) Macromolecules 32:2061
20. Aharoni SM, Edwards SF (1989) Macromolecules 22:3361; Aharoni SM, Murthy NS, Zero K, Edwards SF (1990) Macromolecules 23:2533
21. DSM Pat, EP 99, 200, 919
22. DSM Pat, EP 99, 200, 929
23. Schmitt-Willich H, Platzek J, Radbüchel B, Ebert W, Frenzel T, Misselwitz B, Weinmann HJ (1999) Abstract book of the 1st International Dendrimer Symposium, p 25
24. Tiemersma-Thoone GPJM, Scholtens BJR, Dusek K, Gordon M (1991) J Polym Sci Polym Phys 29:463
25. Misev T (1991) Powder coatings, chemistry and technology. Wiley, New York
26. Lindeboom J (1997) Proceedings of the 23rd International Athens Conference on Organic Coatings, p 295
27. Petterson B (1994) Proceedings New Orleans Waterborne, Higher Solids and Powder Coatings Symposium, p 753
28. Saito H, Ishihara K (1997) Compare diethanolamine as anti-oxidant for sardine oil. J Am Oil Chem 74:1531
29. Malmström E, Johansson M, Hult A (1996) Macromol Chem Phys 197:3199
30. Jansen JFGA, de Brabander EMM, Meijer EW (1994) Science 266:1229
31. Baars MPWL, Froehling PE, Meijer EW (1997) Chem Commun, p 1959
32. Liu MJ, Kono K, Frechet JMJ (1999) J Polym Sci A – Polym Chem 37:3492
33. Froehling PE, Linssen HAJ (1998) Macromol Chem Phys 199:1691
34. Hawker CJ, Wooley KL, Fréchet JMJ (1993) J Chem Soc Perkin Trans Part I:1287

Dendrimer-Encapsulated Metals and Semiconductors: Synthesis, Characterization, and Applications

Richard M. Crooks, Buford I. Lemon III, Li Sun, Lee K. Yeung, Mingqi Zhao

Texas A&M University, Department of Chemistry, P.O. Box 30012, College Station, TX 77842-3012 USA, *E-mail: crooks@tamu.edu*

This chapter describes composite materials composed of dendrimers and metals or semiconductors. Three types of dendrimer/metal-ion composites are discussed: dendrimers containing structural metal ions, nonstructural exterior metal ions, and nonstructural interior metal ions. Nonstructural interior metal ions can be reduced to yield dendrimer-encapsulated metal and semiconductor nanoparticles. These materials are the principal focus of this chapter. Poly(amidoamine) (PAMAM) and poly(propylene imine) dendrimers, which are the two commercially available families of dendrimers, are in many cases monodisperse in size. Accordingly, they have a generation-dependent number of interior tertiary amines. These are able to complex a range of metal ions including Cu^{2+}, Pd^{2+}, and Pt^{2+}. The maximum number of metal ions that can be sorbed within the dendrimer interior depends on the metal ion, the dendrimer type, and the dendrimer generation. For example, a generation six PAMAM dendrimer can contain up to 64 Cu^{2+} ions. Nonstructural interior ions can be chemically reduced to yield dendrimer-encapsulated metal nanoparticles. Because each dendrimer contains a specific number of ions, the resulting metal nanoparticles are in many cases of nearly monodisperse size. Nanoparticles within dendrimers are stabilized by the dendrimer framework; that is, the dendrimer first acts as a molecular template to prepare the metal nanoparticles and then as a stabilizer to prevent agglomeration. These composites are useful for a range of catalytic applications including hydrogenations and Heck chemistry. The unique properties of the interior dendrimer microenvironment can result in formation of products not observed in the absence of the dendrimer. Moreover the exterior dendrimer branches act as a selective gate that controls access to the interior nanoparticle, which results in selective catalysis. In addition to single-metal nanoparticles, it is also possible to prepare bimetallic nanoclusters and dendrimer-encapsulated semiconductor nanoparticles, such as CdS, using this same general approach.

Keywords. Dendrimer, Nanocomposite, Nanoparticle, Catalysis, Polymer

Topics in Current Chemistry, Vol. 212

1 Introduction

Since the first report of the synthesis of dendrimers twenty years ago [1], there has been a remarkable increase in interest in these fascinating materials. For example, the number of publications relating to dendrimers was about 15 in 1990, but this number increased to 150 in 1995, and 420 in 1997. Until very recently emphasis in this field was placed on the synthesis of new families of dendrimers having novel architectures, but more recently there has been interest in finding technological applications for these materials [2–5]. The pursuit of applications has been greatly accelerated by the recent commercial availability of dendrimers through Dendritech, Inc. (Midland, MI), Dutch State Mines (DSM, The Netherlands), and the Aldrich Chemical Co. (Milwaukee, WI).

In this chapter we discuss an aspect of dendrimers that has yielded a rich body of fundamental information about the properties of dendrimers as well as

some clues to possible technological applications. Specifically, we address the synthesis, characterization, and applications of dendrimer hosts that contain metal-ion, metal, or semiconductor guests. These interesting composite materials have proven applications for homogeneous and heterogeneous catalysis, and they are likely to have a significant impact in the fields of chemical sensing, biosensing, and gene therapy in the future. There are two means for introducing metal ions into dendrimers: either as structural elements or as nonstructural components. An example of the former is dendrimers that contain a metalloporphyrin core. This class of metal-containing dendrimers was reviewed in the first book in this series [6] in 1998, so only a few illustrative examples are described here. The focus of this chapter is on nonstructural metal ions, as well as metal and semiconductor particles, sequestered within the interior of high-generation dendrimers.

1.1 Dendrimer Synthesis

Dendrimers are outstanding candidates for addressing a vast range of chemical, biological, and medical technological needs because of their regular structure and chemical versatility. Dendrimers have three basic anatomical features: a core, repetitive branch units, and terminal functional groups [2–5]. The physical and chemical properties of dendrimers depend strongly on the chemical structure of all three components as well as on the overall size and dimensionality of the dendrimer. For example, larger dendrimers are generally spherical in shape and contain interior void spaces, whereas lower generation materials are flat and open. Also, terminal groups largely, but not solely, determine the solubility and adsorption properties of dendrimers.

Dendrimers are usually synthesized by either the divergent method or convergent approach. An excellent introduction to the basic principles of dendrimer synthesis is given in [3] and therefore only the briefest of introductions is provided here. In the divergent method, growth is outward from the core to the dendrimer surface. This method of synthesis generally involves serial repetition of two chemical reactions and appropriate purification steps. For example, the generation 0 dendrimer (G0) is formed after the first cycle of reactions on the dendritic core. The generation, and thus the diameter of a dendrimer, increases more-or-less linearly with the number of the cycles. The number of surface functional groups increases exponentially with each ensuing cycle and, because 2 or 3 monomers are usually added to each branch point in the reaction cycle, the maximum size or generation of a dendrimer is governed by steric crowding at the end groups.

Like the divergent approach, the convergent method also involves repetition of several basic chemical reactions. However, the reaction cycles are used to synthesize individual dendrons (dendrimer branches) instead of complete dendrimers. The dendrons have a protected "focal point" which can be activated in the last synthetic step and linked to two or more attachment points of a core molecule. Dendrimers synthesized by either method contain defects, but the problem is less pronounced for materials prepared by the convergent method,

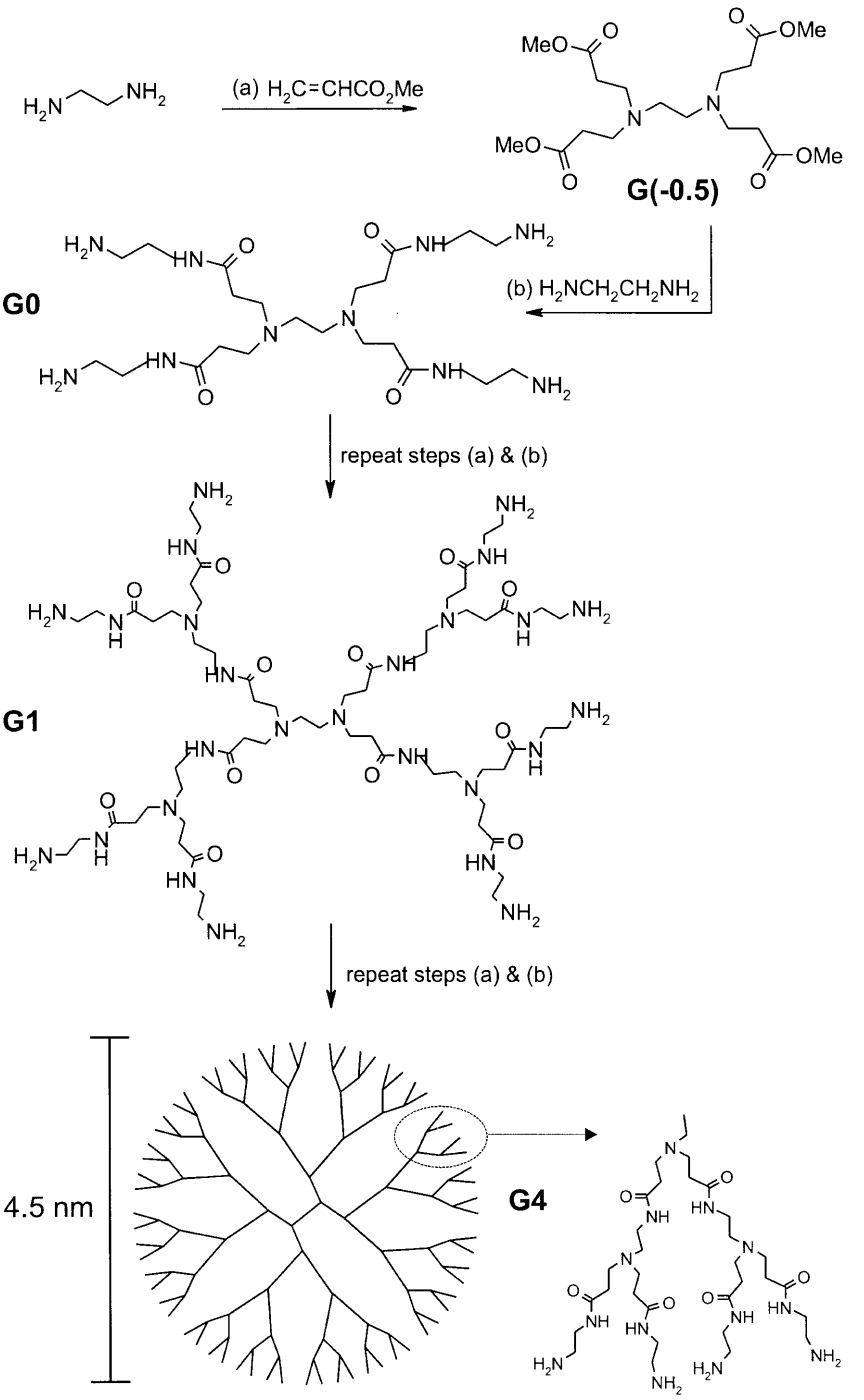

Fig. 1. Synthesis and structure of PAMAM dendrimers

because impurities (imperfect dendrons or other smaller molecules produced during synthesis) are very different in size from the fully assembled dendrimers and can therefore be removed easily by chromatography. However, very high generation dendrimers cannot be prepared efficiently by the convergent approach because the reaction yield between high generation dendrons and the core is usually low. Accordingly, the convergent approach is typically limited to the synthesis of generation 8 (G8) and lower dendrimers, while up to G10 dendrimers can be prepared by a divergent method. The divergent approach is perhaps more amenable to scale-up and, indeed, it has been used to synthesize kilogram quantities of the two commercially available materials poly(amidoamine) (PAMAM) and poly(iminopropane-1,3-diyl) (PPI) dendrimers through G4. Because these two materials figure prominently in this chapter, a brief introduction to their synthesis is given next.

Figure 1 shows the synthesis of amine-terminated PAMAM dendrimers having an ethylenediamine core. Preparation of PAMAM dendrimers consists of a reiterative sequence of two basic reactions: a Michael addition reaction of amino groups to the double bond of methyl acrylate (MA), followed by amidation of the resulting methyl ester with ethylene diamine (EDA). The ester-terminated, half-generation dendrimers are denoted as Gn.5 and the full-generation amine-terminated dendrimers are denoted Gn. By using different monomers for the last step of the dendrimer synthesis, or by modifying the terminal groups of primary amine-terminated dendrimers, different terminal groups can be introduced onto the dendrimer periphery. For example, if ethanolamine (NH_2-$(CH_2)_2$-OH) is used in the last amidation reaction instead of ethylene diamine (NH_2-$(CH_2)_2$-NH_2), hydroxyl-terminated dendrimers result. If the synthesis is stopped at the half-generation stage, carboxylate- or methyl ester-terminated dendrimer can be prepared.

PPI dendrimers are synthesized via the reaction sequence as shown in Fig. 2. This repetitive reaction sequence involves a Michael addition of two equivalents of acrylonitrile to a primary amine, followed by hydrogenation of the nitrile groups to primary amines. Commercially available PPI dendrimers are usually terminated with amine groups.

1.2 Chemical and Physical Properties of Dendrimers

Table 1 provides some general information about the evolution of size and molecular conformation as a function of generation for PAMAM and PPI dendrimers [7]. It is important to recognize that the data in this table are for ideal-structure dendrimers, while in practice both PAMAM and PPI dendrimers contain a statistical distribution of defects [3]. The diameter of PAMAM dendrimers increases by roughly 1 nm per generation, while the molecular weight and number of functional groups increase exponentially. The surface density of dendrimer terminal groups, normalized to the expanding surface area, also increases nonlinearly. Simulation results [8] show that up to G2, PAMAM dendrimers have an expanded or 'open' configuration, but as the dendrimer grows in size, crowding of the surface functional groups causes the dendrimer to adopt

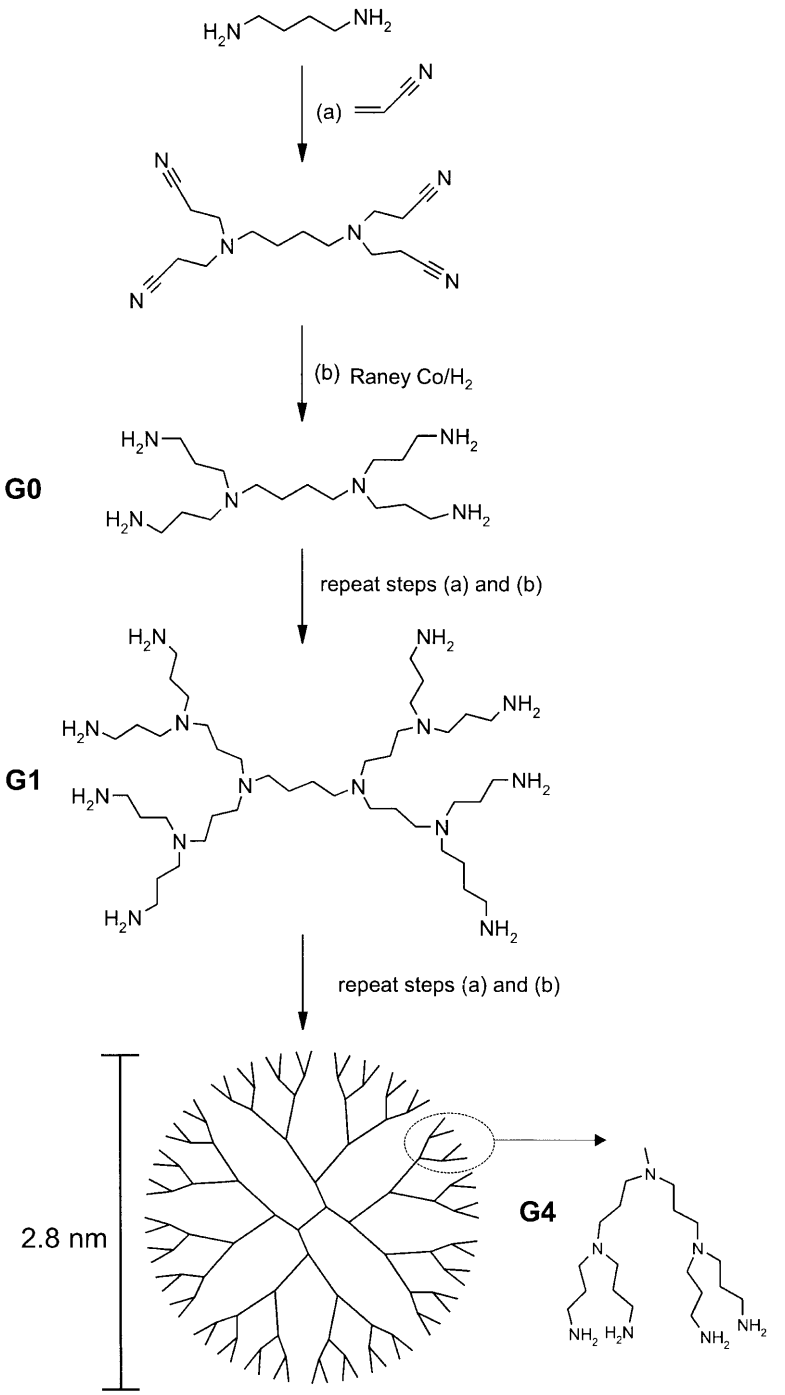

Fig. 2. Synthesis and structure of PPI dendrimers

Table 1. Physical characteristics of PAMAM and PPI dendrimers

Generation	Surface Groups	Tertiary Amines	Molecular Weight[a]		Diameter[b], nm	
			PAMAM	PPI[c]	PAMAM	PPI[c]
0	4	2	517	317	1.5	0.9
1	8	6	1,430	773	2.2	1.4
2	16	14	3,256	1,687	2.9	1.9
3	32	30	6,909	3,514	3.6	2.4
4	64	62	14,215	7,168	4.5	2.8
5	128	126	28,826	14,476	5.4	–
6	256	254	58,048	29,093	6.7	–
7	512	510	116,493	58,326	8.1	–
8	1024	1022	233.383	116,792	9.7	–
9	2048	2046	467,162	235,494	11.4	–
10	4096	4094	934,720	469,359	13.5	–

[a] Molecular weight is based on defect-free, ideal structure dendrimers.
[b] For PAMAM dendrimers, the molecular dimensions were determined by size-exclusion chromatography and the dimensions of PPI dendrimers were determined by SANs; data for the high-generation PPI dendrimers are not available.
[c] We have used the generational nomenclature typical for PAMAM dendrimers throughout this chapter. In the scientific literature the PPI family of dendrimers is incremented by one. That is, what we call a G4 PPI dendrimer (having 64 endgroups) is often referred to as G5.

a spherical or globular structure. Perhaps it is helpful to think of G4 PAMAM as a wet sponge and of G8 as having a somewhat hard surface like that of a beach ball. That is, the interior of high-generation dendrimers are rather hollow, while their exteriors are far more crowded. Both of these factors figure prominently in the work described later in this chapter.

As a consequence of their three-dimensional structure and multiple internal and external functional groups, higher generation dendrimers are able to act as hosts for a range of ions and molecules. Endoreception occurs when analyte molecules penetrate interstices present between densely packed surface groups and are incorporated into the interior cavities. Exoreception occurs when molecular species interact strongly with functional groups on the dendrimer surface. To prepare dendrimer-encapsulated metal and semiconductor nanoparticles, which are the main focus of this chapter, we rely on endoreception to bind the metal ions of choice to the dendrimer interior prior to chemical reduction. The exoreceptors are useful for attaching dendrimers to surfaces and other polymers, and they can be manipulated to control access to the dendrimer interior and the contents thereof (see below).

PAMAM dendrimers are large (G4 is 4.5 nm in diameter) and have a hydrophilic interior and exterior; accordingly, they are soluble in many convenient solvents (water, alcohols, and some polar organic solvents). Importantly, the interior void spaces are large enough to accommodate nanoscopic guests, such as metal clusters, and are sufficiently monodispersed in size so as to ensure fairly uniform particle size and shape. As we will show later, the space between the ter-

minal groups can act as size-dependent gates between the exterior and interior of dendrimers. As shown in the two-dimensional projections of PAMAM and PPI dendrimers in Figs. 1 and 2, higher generations have more closely spaced terminal groups and therefore only admit small molecules such as metal ions and O_2. For example, the exterior of G8 can distinguish linear and branched hydrocarbons (see below).

As shown in Table 1, the diameter of the amine-terminated, G4 PPI dendrimers, determined by small-angle neutron scattering (SANS), is 2.8 nm, so it is considerably smaller than the equivalent G4 PAMAM (4.5 nm) [7]. Like the PAMAM dendrimers, the PPI dendrimers have interior tertiary amine groups that may interact with guest molecules and ions, but in contrast they do not contain amide groups. As a consequence, PPI dendrimers are stable at very high temperatures (the onset of weight loss for G4 PPI is 470 °C) [9], which is a critical factor for some applications, including catalysis. In contrast, PAMAM dendrimers undergo retro-Michael addition at temperatures higher than about 100 °C [10]. Commercially available PPI dendrimers are terminated in primary amines, and they are soluble at synthetically useful concentrations in water, short-chain alcohols, DMF, and dichloromethane. Of course, simple amidation chemistry can be used to functionalize the endgroups, and thereby control solubility.

1.3 Dendrimers as Host Molecules

Dendrimer interior functional groups and cavities contain guest molecules selectively depending on the nature of the guest and the dendritic endoreceptors, the cavity size, and the structure and chemical composition of the terminal groups. The driving force for guest encapsulation within dendrimers can be based on electrostatic interactions, complexation reactions, steric confinement, various types of weaker forces (van der Waals, hydrogen bonding, the hydrophobic force, etc.), and combinations thereof. Many examples of dendrimer-based host-guest chemistry have been reported [3–5].

Meijer and co-workers were the first to demonstrate physical encapsulation and release of guest molecules from a "dendritic box" [11, 12]. In their early experiments, they encapsulated guest molecules such as the dye Bengal Rose or the EPR probe 2,2,3,4,5,5-hexamethyl-3-imidazolinium-1-yloxy methyl sulfate by allowing PPI dendrimers and guest molecules to equilibrate with one another and then adding bulky substituents to the dendrimer exterior. Guest molecules could subsequently be released by removing the protecting groups using any of several chemical approaches. Such encapsulation and controlled release of small molecules from macromolecular hosts has obvious applications to drug delivery, fluorescent markers, catalysis, and fundamental studies of chemical and physical properties of isolated molecules.

By manipulating the chemical properties of dendrimer functional groups, hydrophilic guest molecules can be dissolved in nonpolar solvents and hydrophobic molecules can be dissolved in polar solution. This is possible because, independent of an encapsulated guest, dendrimers terminated in hydropho-

bic groups are generally soluble in nonpolar solvents, while those having hydrophilic terminal groups are generally soluble in polar solvents such as water and low-molecular-weight alcohols [13–15]. Accordingly, it has been shown that hydrophobic molecules can be dissolved in water using water-soluble PAMAM dendrimers [16] and hydrophilic molecules can be dissolved in nonpolar solvents using dendrimers terminated with hydrophobic groups [13, 15, 17, 18]. Recently we showed that hydrophilic molecules can be transferred to low polarity solvents by extraction of guest-containing dendrimers having hydrophilic terminal groups. This is accomplished by complexation of the dendrim er's amine terminal groups with the acid groups of fatty acids [19]. This finding provides a very simple (non-covalent) means for using dendrimer-encapsulated guests (especially for catalysis) in organic, fluorous, and perhaps supercritical solvents.

In addition to molecules, dendrimer endoreceptors can also be used to sequester metal ions within dendrimers. In a later section we will describe how it is possible to take advantage of this property to prepare nanocomposite materials consisting of a dendritic shell (the host) and a metal or semiconductor particle encapsulant (the guest). Small clusters of metals [20] and semiconductors [21] are interesting because of their unique mechanical, electronic, optical, magnetic, and chemical properties. Of particular interest are transition-metal nanoclusters, which are useful for applications in catalysis and electrocatalysis [22–26]. There are two main challenges in this area of catalysis. The first is the development of methods for stabilizing the nanoclusters by eliminating aggregation without blocking most of the active sites on the cluster surfaces or otherwise reducing catalytic efficiency. The second key challenge involves controlling cluster size, size distribution, and perhaps even particle shape. Because dendrimers can act as both "nanoreactors" for preparing nanoparticles and nanoporous stabilizers for preventing aggregation, we reasoned that they would be useful for addressing these two issues. As discussed in Sect. 2, this turns out to be the case. Specifically, this section includes a discussion of the synthesis and characterization of dendrimer-encapsulated Cu, Ag, Au, Ni, Pd, Pt, and Ru clusters, and the application of some of these materials to heterogeneous O_2-reduction electrocatalysis, homogeneous hydrogenation catalysis of alkenes in water, organic, and fluorous solvents, as well as Heck chemistry in biphasic fluorous and supercritical solvents.

The terminal groups of dendrimers can function as exoreceptors to host suitable guests. A simple example involves complexation between metal ions and terminal functional groups. For example, by using the native acid or amine terminal groups of PAMAM dendrimers [27], or dendrimers modified with imine-, phosphino-, crown-containing, and other ligands [28–32], alkali- and transition-metal ions can be bound to dendrimer surfaces. For example, in an early example of this approach, a chelator for Gd^{3+} was attached to the periphery of amine-terminated PAMAM dendrimers. The composite showed superior properties as a contrast agent for molecular imaging [33]. The exoreceptive properties of dendrimers can also be used to bind organic molecules. For example, a variety of polyelectrolytes [34], dyes [35], and electroactive molecules [36] have been attached to dendrimer surfaces by electrostatic binding.

1.4
Dendrimers as Building Blocks for Surface Modification

Thus far, most of this discussion has been focused on the properties of dendrimers in bulk-phase solutions. However, the same physical and chemical properties that impart unique functions to these materials in solution could also lead to interesting properties of surface-immobilized dendrimers. For example, self-assembled monolayers (SAMs) prepared from small molecules are of widespread interest because of their potential applications to corrosion passivation [37, 38], lithography [39, 40], biochemical and chemical sensing [41, 42], and adhesion [43, 44]. However, for some applications SAMs prepared from molecules dominated by simple alkyl chains have significant disadvantages; for example, strictly two-dimensional surfaces and limited stability [45–50] arising from monopodal surface attachment. Clearly, SAMs prepared from dendrimers, which have a well-developed three-dimensional structure and a large number of potential surface attachment points per molecule, should exhibit improved substrate adhesion, stability, and other properties associated with their three-dimensional structure. For example, we have shown that surface-confined dendrimers are suitable as permselective membranes and as a component of corrosion passivation coatings [51, 52]. A vast range of other applications for surface-confined dendrimers have been reported or can be imagined. Many are summarized in recent review papers [3–5, 53].

The first report of surface-immobilized dendrimers was in 1994 [54]. Subsequently, our research group showed that the amine-terminated PAMAM and PPI dendrimers could be attached to an activated mercaptoundecanoic acid (MUA) self-assembled monolayer (SAM) via covalent amide linkages [55, 56]. Others developed alternative surface immobilization strategies involving metal complexation [10] and electrostatic binding [57]. These surface-confined dendrimer monolayers and multilayers have found use as chemical sensors, stationary phases in chromatography, and catalytic interfaces [41, 56, 58, 59]. Additional applications for surface-confined dendrimers are inevitable, and are dependent only on the synthesis of new materials and the development of clever, new immobilization strategies.

2
Dendrimer-Encapsulated Metal Ions, Metals, and Semiconductors

As discussed in the first section of this chapter, interest in dendrimers has increased rapidly since the successful synthesis of the first cascade molecules two decades ago. Much of this interest has been driven by the expectation that dendrimers will exhibit unique properties [2–5, 60]. Because dendrimers in many cases interact strongly with metal ions, it seems reasonable to expect that such composite materials might provide additional heretofore unknown or biomimetic functions. This is particularly true in light of the high number of metal ions that can be complexed to a single dendrimer and (in some cases) their well-defined position in the dendrimer. For example, there has been much recent speculation that these materials will be useful for catalysis [3, 4, 53,

59–62]. Other applications that take advantage of the photonic, electronic, and magnetic properties of these interesting materials are also envisioned [53, 61, 62].

Two main classes of metal-containing dendrimers will be discussed in this section: metal-ion/dendrimer composites and metal (or semiconductor)-cluster/dendrimer composites. For metal-ion/dendrimer composites, metal ions are electrostatically or covalently linked to endo- or exoreceptors of the dendrimer. One might expect that such composite materials would have properties that are not a simple linear combination of the properties of the individual components. For example, the close proximity of metal ions in such materials might result in cooperative catalytic properties, such as is observed frequently in natural enzymatic materials. Metal-nanoparticle-containing dendrimers are prepared by reduction of metal-ion-containing dendrimers. The metal clusters are contained within the dendritic cavity by both steric and chemical interactions, and like the previously described metal-ion-containing composites, the properties of dendrimer-encapsulated metal particles are not a linear combination of the starting materials. Finally, we have recently shown that semiconductor nanoclusters (quantum dots) may also be trapped within dendrimers, and these interesting new photonic materials will also be described in this section.

2.1
Introduction to Dendrimers Containing Metal Ions

There are three general categories of metal-ion-containing dendrimers. The first is composed of dendrimers that use metal ions as an integral part of their chemical structure. This includes, for example, dendrimers having an organometallic core and dendrimers that use metal ligation to assemble the dendrimer branches into the complete dendrimer. The second consists of dendrimers that have peripheral groups that are good ligands for metal ions. The surface functional groups of such dendrimers are usually distinct from the rest of the molecule; that is, they are added after the dendrimer is synthesized. The third group of metal-ion-containing dendrimers contains internal ligands that result in the partitioning of metal ions into the dendritic interior. Most of the metal-ion-containing dendrimers reported so far belong to the first and second classes. Such dendrimers are usually referred as organometallic dendrimers. Several review articles addressing all three types of dendrimers have appeared in recent years [3, 5, 53, 62–65].

2.1.1
Dendrimers Containing Metal Ions that are an Integral Part of their Structure

Metal ions within organometallic dendrimers can be incorporated at the core, in the branches, or at branch points. Examples of dendrimers having metal-ion-containing cores included the dendritic metalloporphyrins [66, 67] and related materials reported by Aida and Enomoto [68], Diederich et al. [69], Moore et al. [70], and Fréchet et al. [71], dendritic terpyridine-ruthenium complexes report-

ed by Newkome et al. [72], dendritic terpyridine-iron(II) complexes reported by Chow et al. [73], and metal-sulfur clusters reported by Gorman et al. [74]. These dendrimers have been synthesized by either connecting a metal ligand to the focal point of a dendron, and then connecting multiple dendrons to a suitable metal ion, or by synthetically linking dendrons to a preformed metal complex. Both of these are examples of the convergent synthetic approach first described by Hawker and Fréchet [75].

By employing coordination complexes as branch points, dendrimers can be synthesized that contain metal ions throughout their structure. The repetitive unit of such dendrimers contains M-C, M-N, M-P, or M-S bonds [53, 62]. The metal ions act as "supramolecular glue" [63], in which the complexation chemistry directs the assembly and structure of the dendrimer [53]. One of the synthetic procedures used to prepare organometallic dendrimers with coordination centers in every layer is based on a protection/deprotection procedure in which two complexes are used as dendritic building blocks wherein one acts as a metal and the other as a ligand [64, 76].

2.1.2
Metal Ions Bound to Ligands on the Surface of Dendrimers

To prepare dendrimers having metal ions on their periphery, the dendrimer is usually synthesized by the divergent approach and then the synthesis is completed by addition of a suitable ligand. The coordinating surface ligands are usually derived from pyridine, phosphine, sulfur, or amines [3, 65]. One of the first examples of metal-terminated dendrimers came from Newkome's group [77]. They prepared polyether dendrimers terminated with terpyridine ligands, and then reacted these with terpyridinyl ruthenium chloride to yield dodecaruthenium macromolecules.

Silicon chemistry also provides a means for preparing dendrimers capped with metal ions [3, 65]. For example, ferrocene [78, 79], Co^{2+}, [80], Ru^{+} [81], and Ni^{2+} [9] have been linked to the periphery of silicon-based dendrimers. These materials are prepared by displacing reactive Si-Cl functional groups with any of a variety of nucleophiles, such as amines, alcohols, or Grignard reagents, containing the metal complexes or ligands.

Amine-terminated, full-generation PAMAM and PPI dendrimers, as well as carboxylate-terminated half-generation PAMAM dendrimers, can directly bind metal ions to their surfaces via coordination to the amine or acid functionality. A partial list of metal ions that have been bound to these dendrimers in this way includes Na^{+}, K^{+}, Cs^{+}, Rb^{+}, Fe^{2+}, Fe^{3+}, Gd^{3+}, Cu^{+}, Cu^{2+}, Ag^{+}, Mn^{2+}, Pd^{2+}, Zn^{2+}, Co^{3+}, Rh^{+}, Ru^{2+}, and Pt^{2+} [18, 19, 27, 36, 54, 82–96]. Turro et al. have also shown that the metal ion complexes, such as tris(2,2′-bipyridine)ruthenium ($Ru(bpy)_3$), can be attached to PAMAM dendrimer surfaces by electrostatic attraction [97]. A wide variety of other families of dendrimers have also been prepared that bind metal ions to their periphery. These have recently been reviewed [3]. Such surface-bound metal ions can be used to probe dendrimer structure using optical spectroscopy, mass spectrometry, and electron paramagnetic resonance (EPR) [86–88, 90, 97–99].

2.1.3
Dendrimers Containing Nonstructural Metal Ions Within their Interior

Because PAMAM and PPI dendrimers are commercially available and can directly bind metal ions to their surface, they are perhaps best suited for technological applications at the present time. However, composites prepared from metal ion-terminated dendrimers may precipitate from solution because of metal-ion-induced dendrimer crosslinking. Moreover, dendrimers functionalized with exterior metal ions cannot be further functionalized (to modulate solubility, for example). Although such composite materials contain a high density of metal ions per macromolecule, they do not take full advantage of the many unique structural features of dendrimers, such as the hollow interior, the unique chemical properties of the interior nanoenvironment, the terminal-group-tunable solubility, or the nanofiltering capability of the dendrimer branches (see below). Accordingly, dendrimers containing non-structural metal ions within their interiors are attractive for certain applications, including catalysts and chemical sensing, because such composites retain the desirable structural properties of the uncomplexed dendrimers and leave free their terminal groups for subsequent modification.

Importantly, unmodified PAMAM and PPI dendrimers have functional groups within their interior as well as on their exterior. Specifically, PAMAM dendrimer interiors contain both tertiary and secondary (amide) amines, and both of these are ligands for many metals [19, 82, 83, 87, 89]. For example, Turro et al. [87, 89] investigated the binding of Cu^{2+} ions to integer and half-integer PAMAM dendrimers. Their EPR results indicated that Cu^{2+} can bind to both exterior acid and amine groups, as well as to interior tertiary amines and amides. Similarly, PPI dendrimers have interior tertiary amines and are also able to bind metal ions, such as Cu^{2+}, Zn^{2+}, and Ni^{2+} within their interior [90, 100].

We are especially interested in trapping metal ions *exclusively* within the interiors of unmodified, commercially available PAMAM dendrimers, because such composites are easy to prepare and retain the desirable structural properties of the uncomplexed dendrimers. It is possible to prevent metal-ion complexation to amine-terminated PAMAM dendrimers by either selective protonation of the primary amines or by functionalization with non-complexing terminal groups. The latter approach eliminates the restrictive pH window necessitated by selective protonation and generally results in more easily interpretable results [2, 101, 102]. Accordingly, most of our work has focused on hydroxyl-terminated PAMAM dendrimers (Gn-OH), although the amine-terminated PAMAM dendrimers (Gn-NH_2) are useful for control experiments, certain model studies, and perhaps catalysis. We have shown that many metal ions, including Cu^{2+}, Pd^{2+}, Pt^{2+}, Ni^{2+}, and Ru^{3+}, sorb into Gn-OH interiors via complexation with interior tertiary amines [59, 82, 83, 103]. Binding of metal ions to Gn-NH_2 is highly pH-dependent, but it is possible to find conditions under which metals only bind to the interior tertiary amines [19, 82].

2.2
Introduction to Dendrimers Containing Zero-Valent Metal Clusters

This section briefly describes dendrimer-encapsulated metal particles, a new family of composite materials, and their applications to catalysis.

2.2.1
Dendrimer-Encapsulated Metal Nanoparticles

A significant aspect of our recent work involves the first description of a general template-based method for preparing transition-metal nanoparticles suitable for fundamental studies and for use in electrocatalysis and homogeneous catalysis. Our approach involves the use of higher generation (Gn, n > 3) PAMAM dendrimers as both template and stabilizer. As discussed in the first section of this chapter, higher generation dendrimers are nearly monodisperse, hyperbranched polymers, which are roughly spherical in shape, highly functionalized, sterically crowded on the exterior, and somewhat hollow on the interior. Dendrimers that are sufficiently large to have evolved a three-dimensional structure contain cavities that have the ability to trap guest molecules [11, 12, 17]. As described in the first part of this section, transition-metal ions, including Cu^{2+}, Pt^{2+}, Pd^{2+}, Ru^{3+}, and Ni^{2+}, partition into the interior of PAMAM dendrimers where they are strongly complexed by interior functional groups. The number of complexed metal ions per dendrimer can be nearly monodisperse [82]. Thus, by preloading a dendrimer "nanotemplate" with suitable metal ions and then chemically reducing this composite in situ, a dendrimer-encapsulated metal nanocluster results (Fig. 3). The dendrimer stabilizes the metal cluster by preventing agglomeration; however, it does not fully passivate the metal surface and therefore the sequestered clusters can be used as electrocatalysts for the reduction of O_2 [59], and homogeneous catalysts for Heck chemistry [100] and the hydrogenation of alkenes (Fig. 3) [83, 103].

2.2.2
Catalysis Using Transition-Metal Nanoparticles

Transition-metal nanoparticles are of fundamental interest and technological importance because of their applications to catalysis [22, 104–107]. Synthetic routes to metal nanoparticles include evaporation and condensation, and chemical or electrochemical reduction of metal salts in the presence of stabilizers [104, 105, 108–110]. The purpose of the stabilizers, which include polymers, ligands, and surfactants, is to control particle size and prevent agglomeration. However, stabilizers also passivate cluster surfaces. For some applications, such as catalysis, it is desirable to prepare small, stable, but not-fully-passivated, particles so that substrates can access the encapsulated clusters. Another promising method for preparing clusters and colloids involves the use of templates, such as reverse micelles [111, 112] and porous membranes [106, 113, 114]. However, even this approach results in at least partial passivation and mass transfer limitations unless the template is removed. Unfortunately, removal of the template may re-

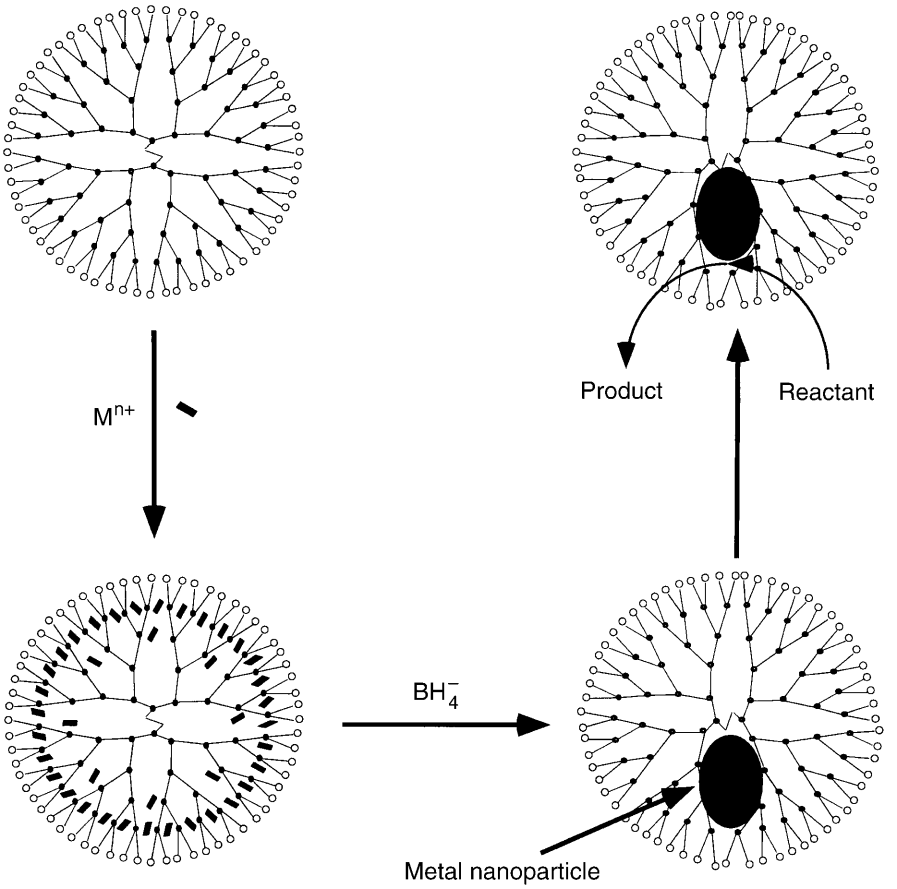

Fig. 3. Schematic illustration of the synthesis of metal nanoparticles within dendrimer templates. The composites are prepared by mixing of the dendrimer and metal ion, and subsequent chemical reduction. These materials can be immobilized on electrode surfaces where they serve as electrocatalysts or dissolved in essentially any solvent (after appropriate end-group functionalization) as homogeneous catalysts for hydrogenation and other reactions

sult in slow agglomeration of the naked particles. By using dendrimers as both monodisperse templates and stabilizers, we achieve particle stability and control over particle size, while simultaneously allowing substrates to penetrate the dendrimer interior and access the cluster surface. To the best of our knowledge this advantageous set of properties is unique.

2.3
Intradendrimer Complexes Between PAMAM Dendrimers and Metal Ions

The first step in the preparation of dendrimer-encapsulated metal and semiconductor particles involves complexation of metal ions with the dendrimer in-

terior (Fig. 3). Because the size and composition of the sequestered nanoparticles depends on this step, it is worth considering it in more detail than was presented in the introduction to this chapter.

2.3.1 *Intradendrimer Complexes Between PAMAM Dendrimers and Cu^{2+}*

The first studies of dendrimer-encapsulated metal nanoparticles focused on Cu [82]. This is because Cu^{2+} complexes with PAMAM and PPI dendrimers are very well behaved and have easily interpretable UV-vis and EPR spectra. For example, Fig. 4a shows absorption spectra for Cu^{2+} coordinated to different ligands. In the absence of dendrimer and in aqueous solutions Cu^{2+} exists primarily as $[Cu(H_2O)_6]^{2+}$, which gives rise to a broad, weak absorption band centered at 810 nm. This corresponds to the well-known d-d transition for Cu^{2+} in a tetragonally distorted octahedral or square-planar ligand field.

In the presence of G4-OH, λ_{max} for the d-d transition shifts to 605 nm ($\varepsilon \sim 100\ M^{-1}\ cm^{-1}$, based on the equivalents of Cu^{2+} present). In addition, a strong band centered at 300 nm ($\varepsilon \sim 4000\ M^{-1}\ cm^{-1}$) emerges, which can be assigned to a ligand-to-metal-charge-transfer (LMCT) transition. The complexation interaction between dendrimers and Cu^{2+} is strong: the d-d transition band and the LMCT transition do not decrease significantly even after 36 h of dialysis against pure water. These data show that Cu^{2+} partitions into the dendrimer from the aqueous phase and remains there.

To learn more about the Cu^{2+} ligand field, we quantitatively assessed the number of Cu^{2+} ions extracted into each dendrimer by spectrophotometric titration. Spectra of a 0.05 mmol/l G4-OH solution containing different amounts of Cu^{2+} are given in Fig. 4b. The absorbance at 605 nm increases with the ratio of $[Cu^{2+}]/[G4\text{-}OH]$, but only slowly when the ratio is larger than 16. The titration results are given in the inset of Fig. 4b, where absorbance at the peak maximum of 605 nm is plotted against the number of Cu^{2+} ions per dendrimer. We estimated the titration endpoint by extrapolating the two linear regions of the curve, and this treatment indicates that each G4-OH dendrimer can strongly sorb up to 16 Cu^{2+} ions. Because a G4-OH dendrimer contains 62 interior tertiary amines and Cu^{2+} is tetravalent, it is tempting to conclude that each Cu^{2+} is coordinated to about 4 amine groups. However, EPR and ENDOR data [99] indicate that most of the ions bind to the outermost 16 pairs of tertiary amine groups, and CPK models indicate that the dendrimer structure is not well configured for complexation between the innermost amines and Cu^{2+}. Thus, on average, each Cu^{2+} is coordinated to two amine groups, and the remaining positions of the ligand field are likely to be occupied by more weakly binding ligands such as amide groups or water (Fig. 5).

We also investigated the effect of dendrimer generation on the maximum number of Cu^{2+} ions that can bind within dendrimers. Figure 6a shows absorption spectra of 0.05 mmol/l Gn-OH (n = 2, 4, and 6) + 3.0 mmol/l $CuSO_4$ in the Cu^{2+} d-d transition region.

For G2-OH, there is an absorption shoulder at 605 nm and a band centered at 810 nm, which indicates only partial complexation of Cu^{2+}. For G4-OH, the band

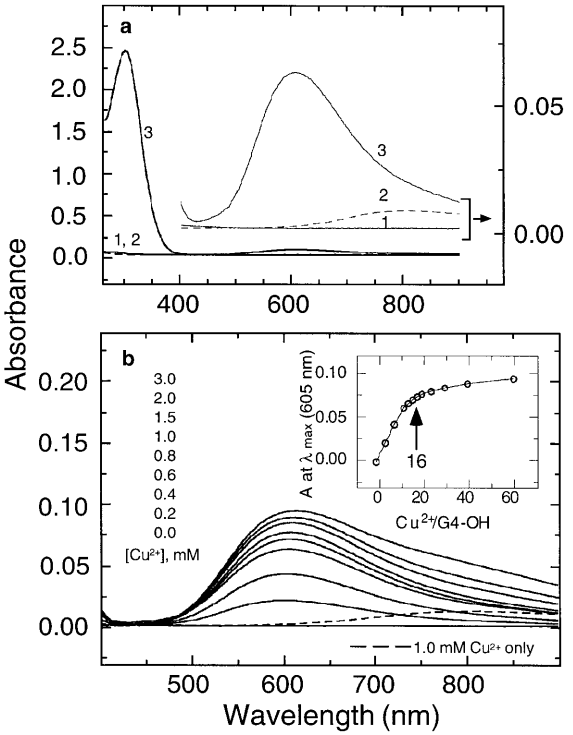

Fig. 4 a, b. **a** Absorption spectra of 0.6 mmol/l $CuSO_4$ in the presence (spectrum 3) and in the absence (spectrum 2) of 0.05 mmol/l G4-OH. The absorption spectrum of 0.05 mmol/l G4-OH vs water is also shown (spectrum 1). **b** Absorption spectra as a function of the Cu^{2+}/G4-OH ratio. The *inset* is a spectrophotometric titration plot showing absorbance at the peak maximum of 605 nm as a function of number of Cu^{2+} ions per G4-OH

at 605 nm becomes more pronounced, and it is the only absorption feature for G6-OH. This result is due to an increase in the concentration of tertiary amine groups as the dendrimer generation increases, which is due in turn to the fact that the number of interior amines increases geometrically as the dendrimer generation increases (Table 1). The end points of the spectrophotometric titration curves for G2-OH and G6-OH (Fig. 6b, c) indicate strong binding of 4 and 64 Cu^{2+} ions, respectively. A similar titration was carried out for G3-OH and it was found to bind tightly up to 8 Cu^{2+} ions. Interestingly, G2-OH, G3-OH, and G6-OH contain 4, 8, and 64 pairs of tertiary amines, respectively, in their outermost generational shell, and therefore these titration results are fully consistent with the one-Cu^{2+}-per-two-outermost-tertiary-amines model proposed for G4-OH (Fig. 5). Indeed, Fig. 6d shows that there is a linear relationship between the number of Cu^{2+} ions complexed within Gn-OH and the number of tertiary amine groups within Gn-OH.

In addition to hydroxyl-terminated PAMAM dendrimers, we also investigated the binding ability of amine-terminated G4-NH_2. Figure 7a shows the d-d

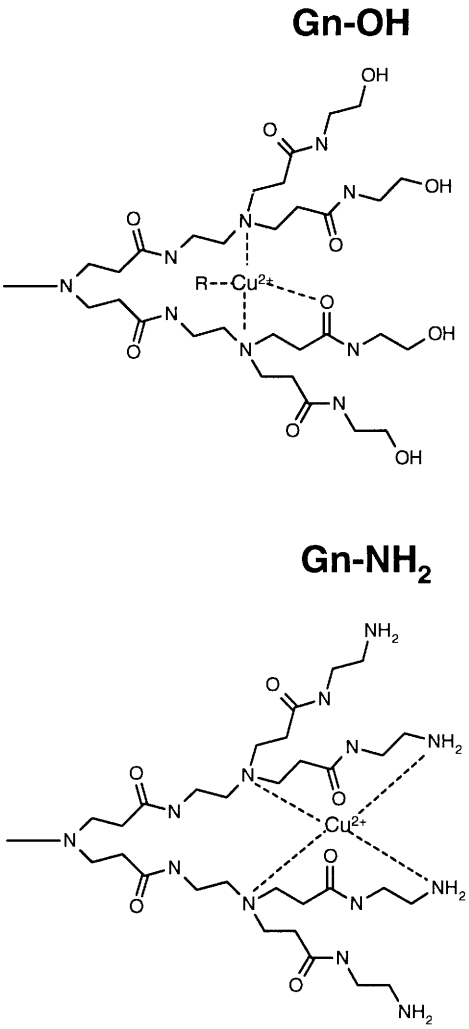

Fig. 5. Schematic illustration of the Cu^{2+} binding sites in G4-OH and G4-NH_2. The models are based on UV-vis, EPR, and ENDOR data

transition region of 0.05 mmol/l G4-R (R = NH_2 or OH) + 0.3 mmol/l $CuSO_4$. Compared to the optical absorbance of G4-OH/Cu^{2+}, the d-d transition of Cu^{2+} in G4-NH_2 shifts from 605 nm to 575 nm ($\varepsilon \sim 100\ M^{-1}\ cm^{-1}$) and the LMCT transition shifts to 270 nm from 300 nm. These wavelengths, which are somewhat pH dependent, are very similar to those found in the absorption spectra of complexes of ethylenediamine/Cu^{2+}, which suggests that Cu^{2+} at least partially binds to the primary-amine ligands on the G4-NH_2 exterior (Fig. 5). The pH dependence discussed later, and our recent EPR and ENDOR results, also confirm this assignment [99]. Additional evidence showing that G4-NH_2 is a stronger ligand than

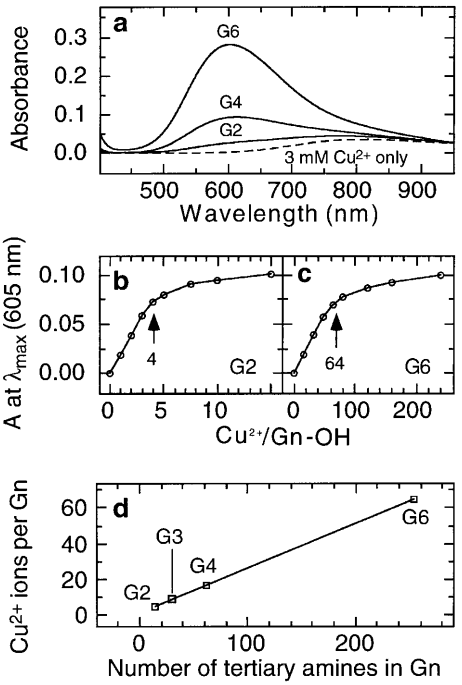

Fig. 6a–d. **a** The effect of dendrimer size on the absorbance of 3.0 mmol/l Cu^{2+} + 0.05 mmol/l Gn-OH solutions. **b, c** Spectrophotometric titration plots of the absorbance at the peak maximum of 605 nm as a function of the number of Cu^{2+} ions per G2-OH or G6-OH. The initial concentration of G2-OH and G6-OH was 0.2 or 0.0125 m^3, respectively. **d** The relationship between the number of Cu^{2+} ions complexed within Gn-OH and the number of tertiary amine groups within Gn-OH

G4-OH for Cu^{2+} is that G4-NH_2 can extract Cu^{2+} ions from G4-OH/Cu^{2+} complexes.

We titrated G4-NH_2 with Cu^{2+} by monitoring the increase of band intensity at λ_{max} = 575 nm, which results from the increasing Cu^{2+}/G4-NH_2 ratio (Fig. 7b). The titration results show that G4-NH_2 can complex up to 36 Cu^{2+} ions, which we believe bind primarily to the terminal primary amines. This result is consistent with a literature report that G4 PPI dendrimers bind 32 Cu^{2+} ions to the 32 dipropylenetriamine units on the outer-most layer of these dendrimers [90].

As mentioned above, binding between Cu^{2+} and PAMAM dendrimers is pH dependent. Figure 8 shows absorption spectra that illustrate the pH dependence of 0.025 mmol/l G4-OH+4 mmol/l $CuSO_4$ and 0.025 mmol/l G4-NH_2 + 8 mmol/l $CuSO_4$. The bands arising from complexation between G4-OH and Cu^{2+} at 300 nm and 605 nm decrease with decreasing pH. When the pH of the solution is adjusted to 3.0, these two bands essentially disappear and a broad, weak band, corresponding to free Cu^{2+}, appears at around 810 nm. Because the interior tertiary amines are protonated below pH 3.5 [115], we interpret this result in terms of the dendrimer releasing Cu^{2+} at low pH. The same type of behavior is ob-

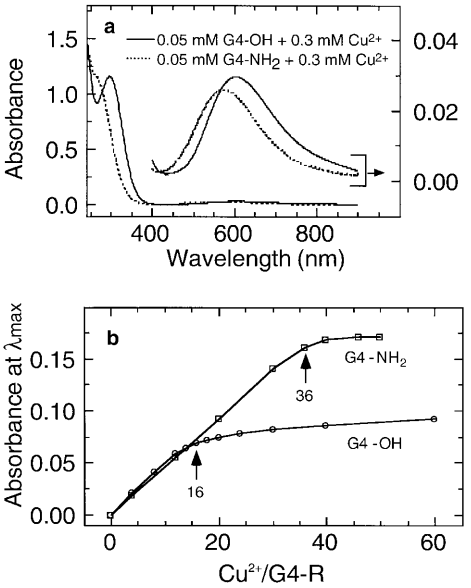

Fig. 7a, b. **a** The effect of the dendrimer terminal groups on the absorbance of 0.05 mmol/l G4-R (R = NH_2 or OH) + 0.3 mmol/l Cu^{2+} solutions. **b** Spectrophotometric titration plots of the absorbance at the peak maximum (G4-NH_2: 575 nm, G4-OH: 605 nm) as a function of the number of Cu^{2+} ions per G4-R. The pH was between 6 and 9

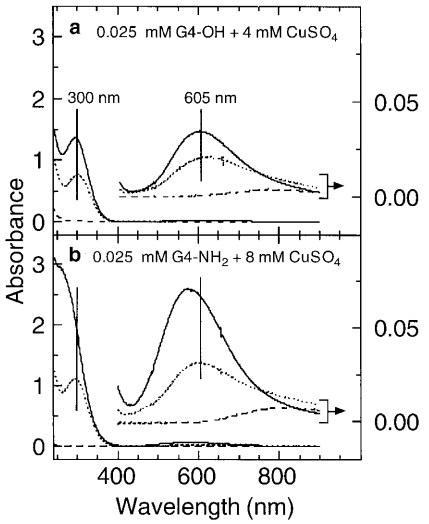

Fig. 8a, b. Absorption spectra of: **a** 0.025 mmol/l G4-OH + 4 mmol/l $CuSO_4$; **b** 0.025 mmol/l G4-NH_2 + 8 mmol/l $CuSO_4$ at pH 9.0 (*solid line*), 5.5 (*short dash*), and 3.0 (*long dash*)

served for G4-NH_2 + Cu^{2+}. For example, when the pH of a solution containing 0.025 mmol/l G4-NH_2+8 mmol/l $CuSO_4$ is adjusted from 9.0 to 5.5, there is a dramatic decrease in the absorbance arising from both the LMCT and d-d transition (Fig. 8b). This change corresponds to a fraction of the Cu^{2+} ions originally bound to the amines being released to the solution as $[Cu(H_2O)_6]^{2+}$ (as evidenced by the increase in the intensity of 810 nm band at pH 5.5). When the pH is reduced to 3.0, no Cu^{2+} ions can bind to G4-NH_2, and just the broad peak at 810 nm corresponding to free Cu^{2+} is apparent.

MALDI-TOF mass spectrometry (MS) has also been used to characterize PAMAM dendrimer composition with and without added Cu^{2+} [98]. Linear-mode MALDI-TOF mass spectra of G2 and G3, and their complexes with Cu^{2+} ions, are shown in Fig. 9.

Spectra of G2-OH and G3-OH indicate the presence of dendrimers corresponding to the molecular weight of the ideal dendrimer structure (M_{IS}): 3273.05 for G2-OH (Fig. 9a) and 6941.8 for G3-OH (Fig. 9c). Some lower masses corresponding to the loss of one or several 115 mass units ($M_{IS} - (n \times 115)$) are also evident; these are due to "missing arm" (-$CH_2CH_2CONHCH_2CH_2OH$) defects. The observation of an $M_{IS} - (4 \times 115) - 60$ peak in G2-OH is due to four missing arms and the formation of an intramolecular loop (M_{IS} – 4 arms + 1 loop). These defects have also been observed by electrospray (ES)-MS measurements [116]. The mass spectrum of G4-OH with or without Cu^{2+} is much more complicated than for the lower generations but a complete discussion is available in the primary literature [98].

When G2-OH is mixed with a fourfold molar excess of Cu^{2+} ions the spectrum in Fig. 9b results. These data indicate that each G2-OH can sorb at least four Cu^{2+} ions. Moreover, the separation between adjacent copper adducts is ~ 62.5, which indicates that the oxidation state of Cu inside dendrimer during the MALDI-MS experiments is +1. Reflectron-mode MS also confirms this assignment: the mass differences between the monoisotopic peaks of protonated dendrimers, single-copper adducts, and double-copper adducts are 61.96 and 61.93, respectively, which is consistent with the assignment of the adduct ions as $[M_{IS} + Cu(I)]^+$ and $[M_{IS} + 2Cu(I)\text{-}H]^+$. We speculate that the presence of Cu^+ is a consequence of the photochemical reduction of Cu^{2+} during ionization. Such photoreduction in MALDI MS measurements has been observed previously when polymers or peptides are used as ligands for Cu^{2+} [117, 118].

The relative intensities of the four copper adducts for G2-OH are not necessarily reflective of the actual concentrations of those four species in the sample. Because addition of each Cu ion to the dendrimer has to be accompanied by the loss of one proton to form a singly charged ion, composites containing higher Cu^{2+} loading are less favored than lower Cu^{2+} loadings in the MALDI process.

When G3-OH is loaded with an eightfold molar excess of Cu^{2+}, the corresponding spectrum (Fig. 9d) shows adducts containing up to eight ions. The signal-to-noise ratio of this spectrum is worse than that for G2-OH (compare with Fig. 9b). This may be because both structurally perfect and defect-containing G3-OH dendrimers sorb Cu^{2+} and the defect density increases with generation. It is also likely that the intrinsic efficiency of the MALDI process is lower for the heavier, higher generation materials.

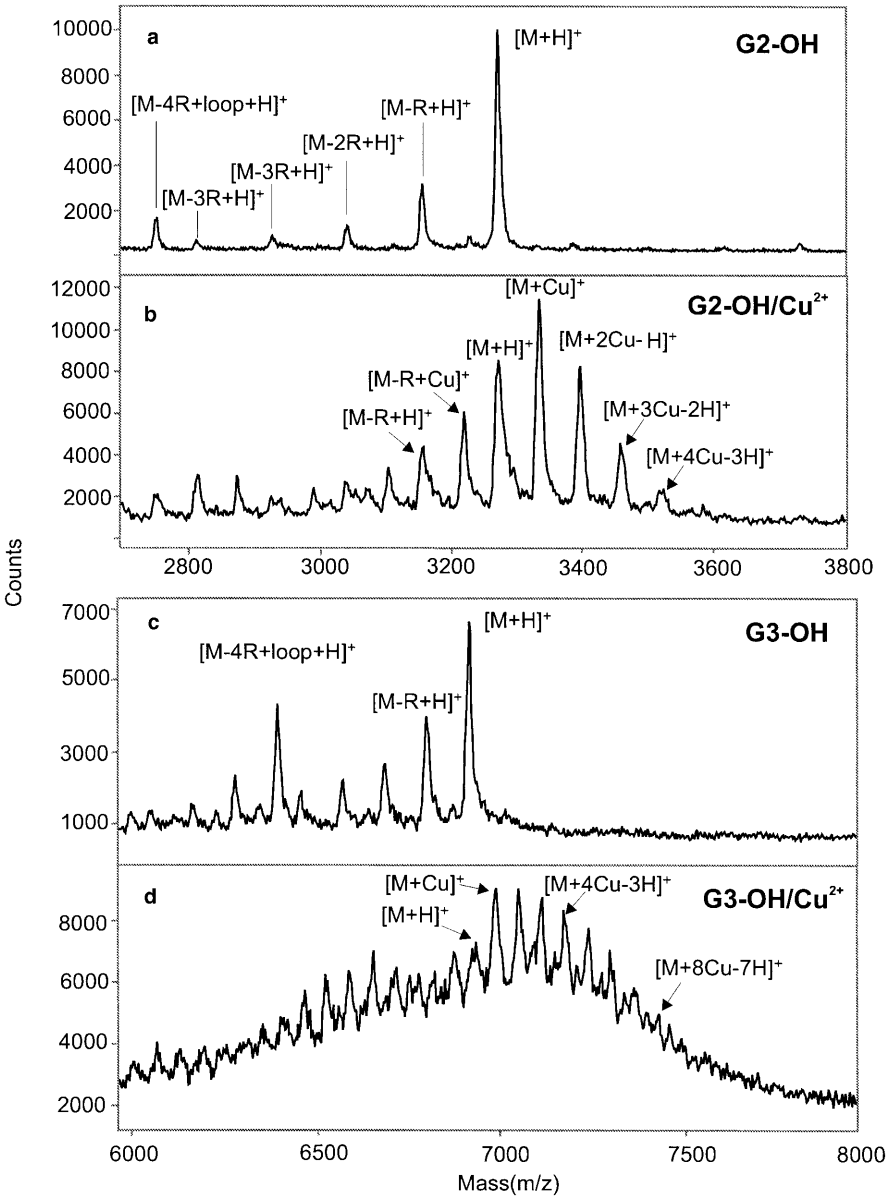

Fig. 9a–d. MALDI mass spectra of G2-OH, G3-OH, and their complexes with Cu^{2+} (Cu^{2+}/G2-OH = 4 and Cu^{2+}/G3-OH = 8)

2.3.2
Intradendrimer Complexes Between PAMAM Dendrimers and Metal Ions other than Cu^{2+}

Using chemistry similar to that just discussed for Cu^{2+}, we have shown that many other transition metal ions, including Pd^{2+}, Pt^{2+}, Ni^{2+}, and Ru^{3+}, can be extracted into the dendrimer interiors [59, 83, 84]. For example, a strong absorption peak at 250 nm ($\varepsilon = 8000\ M^{-1}\ cm^{-1}$) arising from a ligand-to-metal-charge-transfer (LMCT) transition indicates that $PtCl_4^{2-}$ is sorbed within Gn-OH dendrimers. The spectroscopic data also indicate that the nature of the interaction between the dendrimer and Cu or Pt ions is quite different. As discussed earlier, Cu^{2+} interacts with particular tertiary amine groups by complexation, but $PtCl_4^{2-}$ undergoes a slow ligand-exchange reaction, which is consistent with previous observations for other Pt^{2+} complexes [119]. The absorbance at 250 nm is proportional to the number of $PtCl_4^{2-}$ ions in the dendrimer over the range 0–60 ($G4\text{-}OH(Pt^{2+})_n$, n = 0–60), which indicates that it is possible to control the G4-OH/Pt^{2+} ratio.

Control experiments confirm that the Pt^{2+} ions are inside the dendrimer rather than complexed to the exterior hydroxyl groups. For example, when $G4\text{-}NH_2$ is added to a $PtCl_4^{2-}$ solution an emulsion, and then precipitation, results. This is a consequence of Pt^{2+}-induced crosslinking of the NH_2-functionalized dendrimers, which does not occur with the noncomplexing OH-terminated materials. Additionally, when a pH = 1 G4-OH solution is added to a $PtCl_4^{2-}$ solution no spectral changes occur, indicating that protonated interior tertiary amines do not complex Pt^{2+}. Finally, X-ray photoelectron spectroscopy (XPS) of $G4\text{-}OH(Pt^{2+})_{60}$ indicates that the ratio of Pt/Cl is 1/3, which strongly suggests that complexation of $PtCl_4^{2-}$ to the dendrimer occurs by ligand exchange. Specifically, loss of one chlorine ligand from the Pt complex is compensated by addition of the tertiary amine from the dendrimer. Taken together these three results suggest that up to 60 Pt^{2+} ions are complexed within G4-OH via Pt^{2+}-tertiary amine interactions. Very similar results are obtained upon mixing Gn-OH with $PdCl_4^{2-}$.

Figure 10 shows that Ru^{3+} and Ni^{2+} can also be extracted into G4-OH dendrimers. For example, a $[Ru(NH_3)_5Cl]^{2+}$ solution has an LMCT band at 327 nm ($\varepsilon \sim 1200\ M^{-1}\ cm^{-1}$). However, after addition of G4-OH to this solution the LMCT band blue shifts to 297 nm ($\varepsilon \sim 1300\ M^{-1}\ cm^{-1}$), which is close to λ_{max} value of 277 nm measured for $Ru(NH_3)_6^{3+}$. This suggests trapping of Ru^{3+} within the dendrimers via ligand exchange. In the case of Ni^{2+}, several absorbance peaks characteristic of $[Ni(H_2O)_6]^{2+}$ are evident in the absence of G4-OH [120]. In the presence of G4-OH, a shift in the wavelength of these bands, which is consistent with replacement of some H_2O ligands by tertiary amines or other functional groups within the dendrimers, is observed, suggesting dendrimer encapsulation of Ni^{2+}.

2.4
Synthesis and Characterization of Dendrimer-Encapsulated Metal Nanoparticles

In this section, two methods used to prepare dendrimer-encapsulated metal nanoclusters are discussed: direct reduction of dendrimer-encapsulated metal ions and displacement of less noble metal clusters with more noble elements.

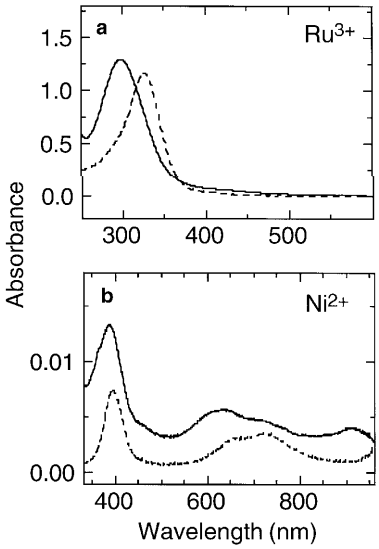

Fig. 10a,b. UV-vis spectroscopic data demonstrating sorption of Ru^{3+} and Ni^{2+} ions into G4-OH dendrimers: **a** absorption spectra of solutions containing 1.0 mmol/l $[Ru(NH_2)_5Cl]Cl_2$ (*dashed line*) and 1.0 mmol/l $[Ru(NH_2)_5Cl]Cl_2$ + 0.05 mmol/l G4-OH (*solid line*); **b** absorption spectra of solutions containing 4.0 mmol/l $Ni(ClO_4)_2$ (*dashed line*) and 4.0 mmol/l $Ni(ClO_4)_2$ + 0.2 mmol/l G4-OH (*solid line*)

2.4.1
Direct Reduction of Dendrimer/Metal Ion Composites

Chemical reduction of Cu^{2+}-loaded G4-OH dendrimers (G4-OH/Cu^{2+}) with excess $NaBH_4$ results in intradendrimer Cu clusters (Fig. 3). Evidence for this comes from the immediate change in solution color from blue to golden brown: the absorbance bands originally present at 605 nm and 300 nm disappear and are replaced with a monotonically increasing spectrum of nearly exponential slope towards shorter wavelengths (Fig. 11).

This behavior results from the appearance of a new interband transition corresponding to formation of intradendrimer Cu clusters. The measured onset of this transitions at 590 nm agrees with the reported value [121], and the nearly exponential shape is characteristic of a band-like electronic structure, strongly suggesting that the reduced Cu does not exist as isolated atoms, but rather as clusters [122]. The presence of metal clusters is also supported by loss of signal in the EPR spectrum [123] following reduction of the dendrimer Cu^{2+} composite.

The absence of an absorption peak arising from Mie plasmon resonance (around 570 nm) [124] indicates that the Cu clusters are smaller than the Mie-onset particle diameter of about 4 nm [124–126]. Plasmon resonance cannot be detected for very small metal clusters because the peak is flattened due to the large imaginary dielectric constant of such materials [122].

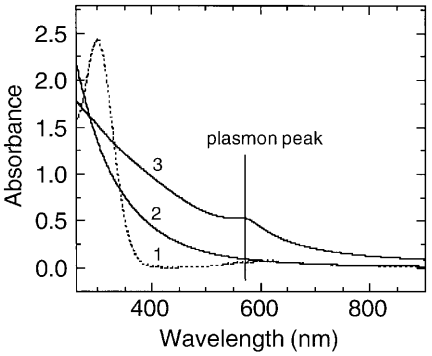

Fig. 11. Absorption spectra of a solution containing 0.6 mmol/l $CuSO_4$ and 0.05 mmol/l G4-OH before (*dashed line*, spectrum 1) and after (*solid line*, spectrum 2) reduction with a fivefold molar excess of $NaBH_4$. Spectrum 3 was obtained under the same conditions as those for spectrum 2 except 0.05 mmol/l G4-NH_2 was used in place of G4-OH. Reprinted with permission from Ref. 82 Copyright 1998 American Chemical Society

Transmission electron microscopy (TEM) results also indicate the presence of intradendrimer Cu clusters after reduction. Micrographs of Cu clusters within G4-OH reveal particles having a diameter less than 1.8 nm [127], much smaller than the 4.5 nm diameter of G4-OH [115, 128].

Finally, intradendrimer Cu clusters are extremely stable despite their small size, which provides additional strong evidence that the clusters reside within the dendrimer interior. Clusters formed in the presence of G4-OH or G6-OH dendrimers, and with a Cu^{2+} loading less than the maximum threshold values, were found to be stable (no observable agglomeration or precipitation) for at least one week in an oxygen-free solution. However, in air-saturated solutions the clusters revert to intradendrimer Cu^{2+} ions overnight. In contrast, when excess Cu^{2+} is added to a dendrimer solution, Cu^{2+} is present both inside the dendrimer and as hydrated ions in solution. After reduction, the excess Cu^{2+} forms a dark precipitate within a few hours, but the remaining transparent solution yields the same absorption spectrum as one prepared with a stoichiometric amount of Cu^{2+}. TEM images of the particles in these solutions reveal two size regimes: the first is 9 ± 4 nm average diameter and is responsible for the dark precipitate; the second, which is estimated to have an upper limit of 1.8 nm diameter [127], corresponds to intradendrimer clusters.

The ability to prepare well-defined intradendrimer metal nanoclusters depends strongly on the chemical composition of the dendrimer. Spectroscopic results, such as those shown in Fig. 7, indicate that when G4-NH_2, rather than the hydroxyl-terminated dendrimers just described, is used as the template a maximum of 36 Cu^{2+} ions are sorbed; most of these bind to the terminal primary amine groups. Reduction of a solution containing 0.6 mmol/l $CuSO_4$ and 0.05 mmol/l G4-NH_2 results in a clearly observable plasmon resonance band at 570 nm (Fig. 11) [122, 124, 125] which indicates that the Cu clusters prepared in this way are larger than 4 nm in diameter. This larger size is a consequence of ag-

glomeration of Cu particles adsorbed to the unprotected dendrimer exterior [89, 90].

The approach for preparing dendrimer-encapsulated Pt metal particles is similar to that used for preparation of the Cu composites: chemical reduction of an aqueous solution of G4-OH$(Pt^{2+})_n$ yields dendrimer-encapsulated Pt nanoparticles (G4-OH(Pt_n)). A spectrum of G4-OH(Pt_{60}) is shown in Fig. 12a; it displays a much higher absorbance than G4-OH$(Pt^{2+})_{60}$ throughout the wavelength range displayed. This change results from the interband transition of the encapsulated zero-valent Pt metal particles.

Spectra of G4-OH$(Pt)_n$, n = 12, 40, and 60, obtained between 280 nm and 700 nm and normalized to A = 1 at λ = 450 nm, are shown in Fig. 12b; all of these spectra display the interband transition of Pt nanoparticles. Control experiments clearly demonstrate that the Pt clusters are sequestered within the G4-OH dendrimer. For example, BH_4^- reduction of the previously described G4-$NH_2(Pt^{2+})_n$ emulsions results in immediate precipitation of large Pt clusters. Importantly, the dendrimer-encapsulated particles do not agglomerate for up to 150 days and they redissolve in solvent after repeated solvation/drying cycles.

The absorbance intensity of the encapsulated Pt nanoparticles is related to the particle size. A plot of log A vs log λ provides qualitative information about particle size: the negative slopes are known to decrease with increasing particle size. For aqueous solutions of G4-OH(Pt_{12}), G4-OH(Pt_{40}), and G4-OH(Pt_{60}), the

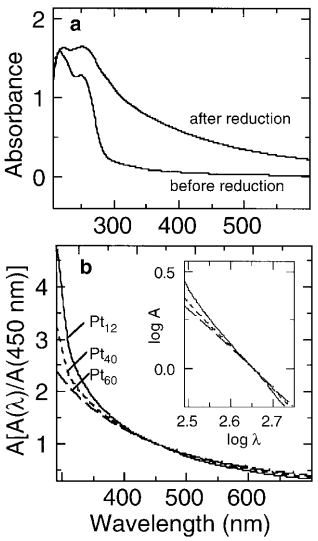

Fig. 12a, b. Spectral characterization of dendrimer-encapsulated clusters containing different numbers and types of atoms; **a** absorption spectra of solutions containing 0.05 mmol/l G4-OH$(Pt^{2+})_{60}$ before and after reduction; **b** UV-vis spectra of solutions containing G4-OH(Pt_{12}) (*solid line*), G4-OH(Pt_{40}) (*short dashes*), and G4-OH(Pt_{60}) (*long dashes*) normalized to A = 1 at λ = 450 nm. Logarithmic plots of these data, shown in the *inset*, demonstrate that larger particles result in less negative slopes

slopes are –2.7, –2.2, and –1.9, respectively (Fig. 12b inset). These results confirm that the size of the intradendrimer particles increases with increasing Pt^{2+} loading.

Dendrimers containing Pt^{2+} or Pt-metal nanoparticles are easily attached to Au and other surfaces by immersion in a dilute aqueous solution of the composite for 20 h, followed by careful rinsing and drying [59, 129]. Therefore it is possible to use X-ray photoelectron spectroscopy (XPS) to determine the elemental composition and the oxidation states of Pt within dendrimers. For example, Pt($4f_{7/2}$) and Pt($4f_{5/2}$) peaks are present at 72.8 eV and 75.7 eV, respectively, prior to reduction, but after reduction they shift to 71.3 eV and 74.4 eV, respectively, which is consistent with the change in oxidation state from +2 to 0 (Fig. 13a].

Importantly, XPS data also indicate the presence of Cl prior to reduction, but it is not detectable from the spectrum of G4-OH(Pt_{60})-modified surfaces (Fig. 13b).

High-resolution transmission electron microscopy (HRTEM) images (Fig. 14) clearly show that dendrimer-encapsulated particles are nearly monodisperse and that their shape is roughly spherical.

For G4-OH(Pt_{40}) and G4-OH(Pt_{60}) particles, the metal-particle diameters are 1.4 ± 0.2 nm and 1.6 ± 0.2 nm, which are slightly larger than the theoretical values of 1.1 nm and 1.2 nm, respectively, calculated by assuming that particles are contained within the smallest sphere circumscribing an fcc Pt crystal. When prepared in aqueous solution, Pt nanoparticles usually have irregular shapes and a large size distribution. The observation of very small, predominantly spherical particles in this study may be a consequence of the dendrimer cavity; i.e., the template in which they are prepared. X-ray energy dispersive spectroscopy (EDS) was also carried out, and it unambiguously identifies the particle composition as platinum.

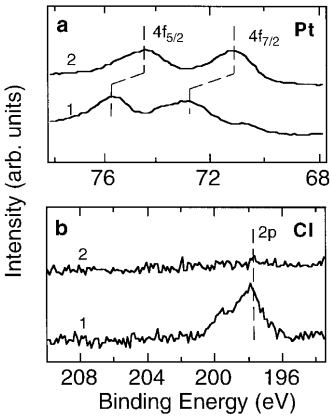

Fig. 13a,b. **a** XPS spectra of G4-OH(Pt^{2+})$_{60}$ before (1) and after (2) reduction. **b** The shifts in the peaks, and the disappearance of the Cl signals indicate reduction of Pt^{2+} within the dendrimer

Results similar to those discussed for dendrimer-encapsulated Cu and Pt are also obtained for Pd, Ru, and Ni nanoclusters. An example of 40-atom Pd nanoclusters confined within G4-OH is shown in the bottom micrograph of Fig. 14.

2.4.2 Displacement Reaction Method

In the previous section, it was shown that dendrimer-encapsulated metal nanoclusters can be prepared by direct reduction if the corresponding metal ions can

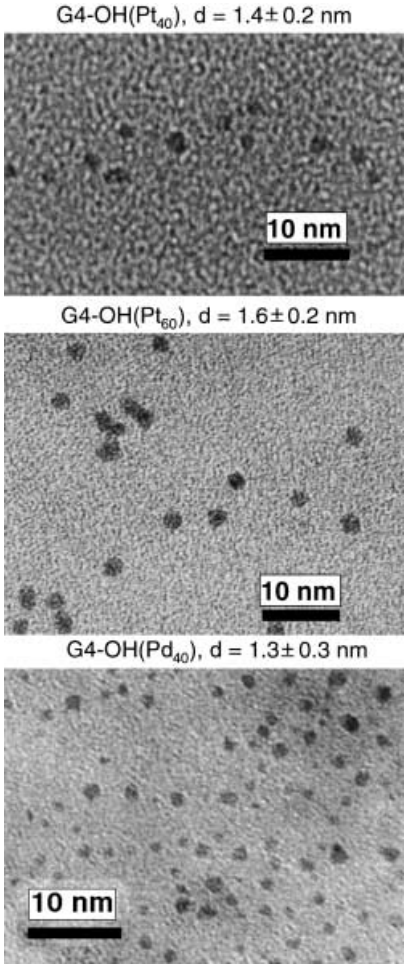

Fig. 14. HRTEM images of G4-OH(Pt_{40}), G4-OH(Pt_{60}), and G4-OH(Pd_{40}), which demonstrate the nearly monodisperse size and shape distribution of the encapsulated metal nanoparticles, especially in the case of G4-OH (Pt_{60}). Reprinted with permission from Ref. 83 Copyright 1999 Wiley-VCH

be extracted into the dendrimer interior. The preparation of Cu and Pt nanoparticles prepared by this technique was discussed in detail. However, this approach is not suitable for encapsulation of Ag particles because the equilibrium between PAMAM dendrimers and Ag^+ ions does not strongly favor the intradendrimer complex.

Although it is not possible to prepare Ag particles inside Gn-OH by direct reduction of interior ions, stable, dendrimer-encapsulated Ag particles can be prepared by a metal exchange reaction. In this approach, dendrimer-encapsulated Cu nanoclusters are prepared as described in a previous section [82], and then upon exposure to Ag^+ the Cu particles oxidize to Cu^{2+} ions, which stay entrapped within the dendrimer at pH values higher than 5.5, and Ag^+ is reduced to yield a dendrimer-encapsulated Ag nanoparticle (Fig. 15).

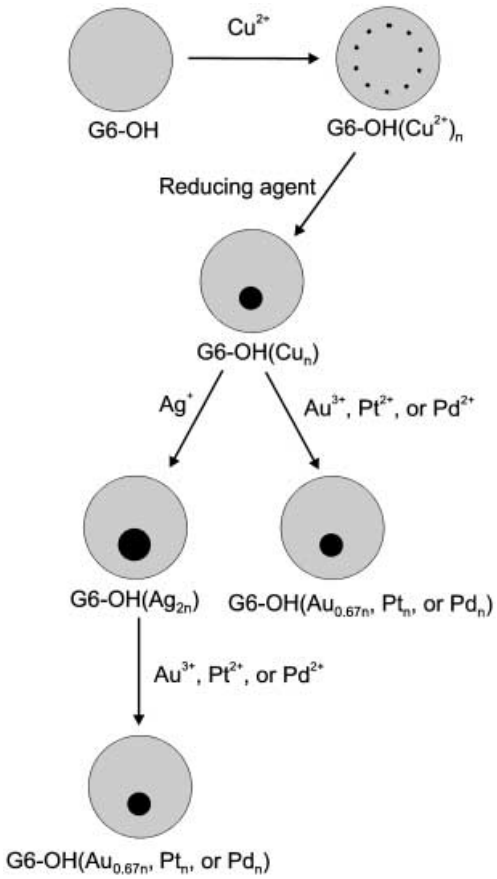

Fig. 15. Schematic illustration of the method used to prepare dendrimer-encapsulated Ag, Au, Pd, and Pt nanoclusters by primary and secondary displacement reactions using G6-OH(Cu_n) or G6-OH(Ag_{2n}) as starting materials

Figure 16a shows UV-vis spectra of an aqueous Cu^{2+}/G6-OH solution before and after reduction. At pH 7.5 a strong LMCT band is evident at 300 nm ($\varepsilon \sim 4000\ M^{-1}\ cm^{-1}$), which (as discussed earlier) is not present in the absence of the dendrimer or Cu^{2+} [130]. Spectrophotometric titrations indicate that each G6-OH can bind as many as 64 Cu^{2+} ions. Because the Cu^{2+}/G6-OH ratio is equal to 55 in the experiments discussed here, we expect that all Cu^{2+} is sorbed into the G6-OH interiors. This species is denoted as G6-OH$(Cu^{2+})_{55}$.

As signaled by the loss of the band at 300 nm, chemical reduction of a pH 7.5, G6-OH$(Cu^{2+})_{55}$ solution with a threefold excess of BH_4^- results in formation of intradendrimer Cu nanoclusters. The postreduction spectrum is dominated by a monotonic and nearly exponential increase towards shorter wavelengths, which results from the interband transition of intradendrimer Cu clusters [82]. The absorption spectrum of aqueous G6-OH(Cu_{55}) solutions is independent of pH in the range 3–7.5.

Ag^+ is a stronger oxidizing agent than Cu^{2+}, and therefore Eq. (1) leads to conversion of a dendrimer-encapsulated Cu nanoparticle to Ag [131]:

$$Cu + 2\,Ag^+ = 2\,Ag + Cu^{2+} \tag{1}$$

Figure 16b shows the spectroscopic evolution of such a reaction. Spectrum 1 is the UV-vis spectrum of G6-OH(Cu_{55}), which is the same as spectrum 2 in Fig. 16a. When Ag^+ is added to a G6-OH(Cu_{55}) solution at pH 3.0, a new absorb-

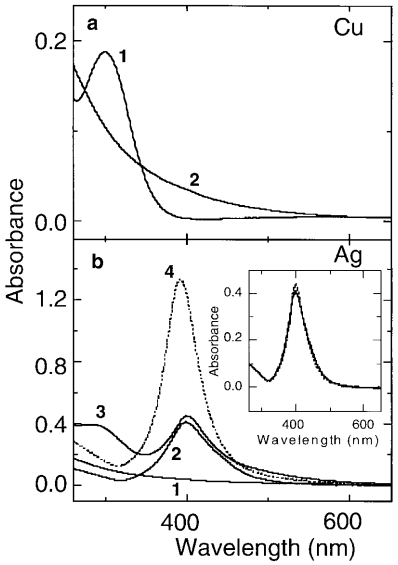

Fig. 16a,b. **a** Absorption spectra of aqueous 0.55 mmol/l $Cu(NO_3)_2$ + 0.01 mmol/l G6-OH before (spectrum 1) and after (spectrum 2) reduction. **b** Absorption spectra of 0.01 mmol/l G6-OH(Cu_{55}) + 1.1 mmol/l Ag^+ (spectrum 2, pH 3.0 and spectrum 3, pH 7.5). Spectrum 1 is the same as spectrum 2 in a. Spectrum 4 corresponds to the direct reduction of 1.1 mmol/l Ag^+ + 0.01 mmol/l G6-OH 1 h after the addition of BH_4^-. The *inset* shows spectra 10 min (*solid line*) and 18 h (*dashed line*) after displacement

ance band centered at 400 nm appears (spectrum 2), which corresponds to the plasmon resonance of Ag particles [122]. When the pH of the solution is adjusted to 7.5 (spectrum 3), the Ag plasmon peak does not change much, but a new peak at 300 nm ($\varepsilon \sim 4000\ M^{-1}\ cm^{-1}$) appears. This is the G6-OH$(Cu^{2+})_{55}$ LMCT band discussed earlier, and it indicates that when the interior tertiary amines are deprotonated Cu^{2+} resides within the dendrimer after intradendrimer oxidation of Cu. Thus, both the metallic Ag nanoparticles and the Cu^{2+} ions generated by the displacement reaction are present within the dendrimers simultaneously. Such versatile and well-defined nanoenvironments are unique and should find a variety of fundamental and applied applications, especially in the area of catalysis. The Ag particles synthesized by this displacement reaction are very stable; for example, spectra taken 10 min and 18 h after reduction are nearly identical (Fig. 16b, inset) and no precipitation is observed even after storage in air for > 2 months. XPS and TEM analysis confirm the presence of dendrimer-encapsulated Ag metal particles formed by exchange. Of course, this displacement method can be used to prepare other types of noble metal particles (Fig. 15), such as Au, Pt, and Pd, because the standard potentials (E°) of the corresponding half reactions are more positive than for Cu^{2+}/Cu. Finally, Ag nanoparticles synthesized by primary displacement of dendrimer-encapsulated Cu nanoparticles can themselves be displaced to yield Au, Pt, or Pd nanoparticles by secondary displacement reactions (Fig. 15).

2.4.3
Dendrimer-Encapsulated Bimetallic Nanoclusters

Bimetallic metal particles are important materials because their characteristics, especially their catalytic properties, are often quite different from those of pure metal particles. Dendrimer-encapsulated bimetallic clusters can be synthesized by any of three methods (Fig. 17): (1) partial displacement of the dendrimer-encapsulated cluster, (2) simultaneous co-complexation of two different metal ions followed by reduction, or (3) sequential loading and reduction of two different metal ions.

Preparation of mixed-metal intradendrimer clusters by partial displacement is a straightforward extension of the complete displacement approach for forming single-metal clusters described in the previous section. If less than a stoichiometric amount of Ag^{+}, Au^{3+}, Pd^{2+}, or Pt^{2+} is added to a G6-OH(Cu_{55}) solution, or if less than a stoichiometric amount of Au^{3+}, Pd^{2+}, or Pt^{2+} is added to G6-OH(Ag_{110}) solution, it is possible to form Ag/Cu, Au/Cu (Au/Ag), Pd/Cu (Pd/Ag), and Pt/Cu (Pt/Ag) bimetallic clusters inside dendrimers.

Dendrimer-encapsulated bimetallic clusters can also be prepared by simultaneous co-complexation of two different metal ions, followed by a single reduction step. For example, the absorption spectrum of a solution containing G6-OH, $PtCl_4^{2-}$, and $PdCl_4^{2-}$ is essentially the sum of the spectra of a solution containing G6-OH + $PtCl_4^{2-}$ and a second solution containing G6-OH + $PdCl_4^{2-}$, which strongly suggests co-complexation of Pt^{2+} and Pd^{2+} within individual dendrimers. After reduction of these co-complexed materials, a new interband transition, which has an intensity different from that of either a pure Pt or Pd cluster, is observed.

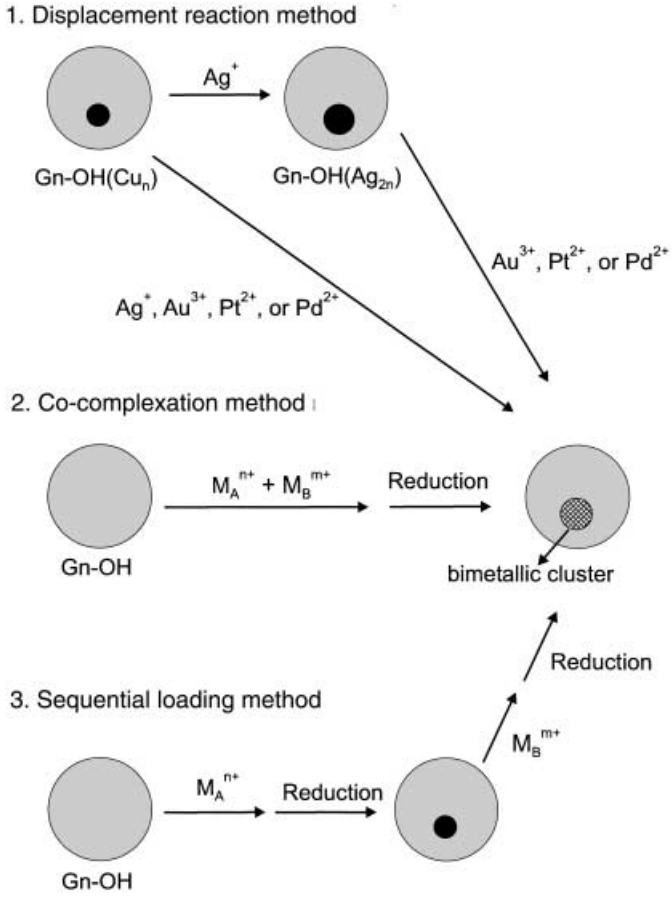

Fig. 17. Schematic illustration of the preparation of dendrimer-encapsulated bimetallic clusters by three different methods. Displacement reaction, co-complexation, and sequential loading

The sequential loading method is also effective for preparing bimetallic clusters. For example, dendrimer-encapsulated Pt/Pd clusters are synthesized as follows. First, a solution containing G6-OH(Pt_{55}) is prepared using the direct reduction approach already described. Next, K_2PdCl_4 is added to this solution to form a mixed metal/ion intradendrimer composite: G6-OH[(Pt_{55}) + (Pd^{2+})$_{55}$]. That is, Pd^{2+} partitions into the dendrimer and complexes with tertiary amine sites vacated by Pt^{2+} after the first reduction step. The existence of the mixed valent composite can be confirmed by the UV-vis spectrum, which is nearly the sum of the two individual components. However, after reduction of G6-OH[(Pt_{55}) + (Pd^{2+})$_{55}$] the intense LMCT band arising from Pd^{2+} complexed to interior tertiary amines essentially disappears and the interband transition due to the formation of the bimetallic clusters appears. After the first reduction step, HRTEM indicates that the Pt nanoclusters in G6-OH(Pt_{55}) are 1.4 ± 0.2 nm in

diameter. However, after addition of Pd^{2+} and subsequent reduction the particles grow to 3.0 ± 1.0 nm. The relatively wide distribution in particle size may be due to interdendrimer transfer of Pd atoms during the second reduction process.

Presumably these three methods for preparing bimetallic, dendrimer-encapsulated nanoparticles can be extended to trimetallics, bi- and trimetallics having unique structures (such as core/shell materials), and interesting combinations of two (or more) zero-valent metals plus intradendrimer ions. However, analysis of such materials await more sophisticated analytical methods than are currently at our disposal.

2.5 Dendrimer-Encapsulated Metal Nanoclusters as Catalysts

Two classes of catalysts account for most contemporary research. The first class includes transition-metal nanoparticles (e.g., Pd, Pt), their oxides (e.g., RuO_2), and bimetallic materials (e.g., Pt/Ni, Pt/Ru) [104, 132–134]. The second class, usually referred to as molecular catalysts, includes all transition-metal complexes, such as metalloporphyrins, in which the metal centers can assume multiple oxidation states [135–137]. Previous studies have not only yielded a wealth of information about the preparation and catalytic properties of these materials, but they have also revealed shortcomings where further research is needed. Here we summarize the main barriers to progress in the field of metal-particle-based catalysis and discuss how dendrimer-encapsulated metal nanoparticles might provide a means for addressing some of the problems.

The active sites of particulate catalysts are on the surface. The activity per unit mass of such catalysts usually increases dramatically as the particle size decreases, because a higher fraction of the total metal atoms reside on the particle surface. Additionally, very small particles (< 1 nm) sometimes exhibit quantum effects that influence their properties in ways that are just beginning to be understood [104, 138]. Unfortunately, the high total surface energy of small particles is a strong driving force for aggregation. Aggregation can be avoided by lowering the surface energy of the particles with surface-confined stabilizers [134, 139–141]. However, complete (i.e., monolayer coverage) and irreversible adsorption of stabilizers or other molecules on the particle surface is generally undesirable because they block active sites which results in loss of catalytic activity (poisoning of the catalyst). Thus, a strong adsorbate really behaves as a deactivator. Clearly, synthesis of highly efficient nanoparticle catalysts requires optimization of both the particle size and the surface protective chemistry. Moreover, the optimal characteristics of each appear to be orthogonal: maximum passivation (desirable to reduce agglomeration) results in catalyst passivation, while high catalytic activity implies a naked surface which in turn leads to agglomeration. Ideally, particulate catalysts should be surrounded by a nonadherent coating, or nanoporous filter, that prevents agglomeration but permits passage of the catalyst's substrate and product, but does not adversely affect catalytic properties. It would be highly desirable to have some control over the mesh of the filter, and also its chemical characteristics, in order to control selectivity. This is precisely the role

played by the dendrimer in catalytic applications of the dendrimer-encapsulated metal particle nanocomposites we recently discovered.

Dendrimers have previously been recognized as attractive building blocks for constructing highly efficient catalysts. The reasons for this are largely due to the unique structural and chemical properties of dendrimers described earlier [3, 74, 142]. For example, dendrimer-related catalysts may involve placement of a catalyst at or near the dendritic core [3, 67, 143–145]. The goal of such studies is to enhance the catalytic rate or selectivity. Additionally, the interior and exterior dendrimer functional groups of these materials can be used to advantage in many ways. For example, dendrimers can be used to stabilize catalysts. That is, appropriate functionalization of dendrimer terminal groups can lead to prevention of agglomeration. Dendrimer functional groups also facilitate manipulation of catalysts by expanding avenues for structure stabilization (via crosslinking) [51, 52], surface immobilization [55–57, 59, 129, 146, 147] and solubility modulation (via the polarity of the surface functional groups) [19, 103]. Finally, surface functional groups form a porous barrier with a defined porosity that allows size-selective entry into the dendrimer's endocavity, which is the usual location of the catalyst [11, 12].

Molecular catalysts, often in the form of metal ions complexed to a suitable ligand, can also be attached to dendrimer surfaces [3, 9, 10, 93, 94, 96, 148, 149]. Such materials are generally structurally better defined than catalysts bounded to linear polymers, but like random-polymer catalysts they can be easily separated from reaction products. Note, however, that this approach results in a synthetic dead-end as far as further manipulation of the terminal groups is concerned, and thus some of the advantages of using dendrimers, such as solubility modulation, are lost.

The endocavity of dendrimers offer many new possibilities for the design of catalysts based on metal clusters. First, as has already been shown, the dendrimer can be used to control the size of the encapsulated metal particle. The endocavity is also an ideal matrix for hosting a highly active catalyst and for maintaining its activity, because it is more or less hollow and stabilization occurs primarily by confinement rather than molecular adsorption or ligation. Accordingly, critical surface active sites are not blocked. Additionally, the polarity or the hydrophobicity of the cavity can be engineered to be different from that of the external environment. This difference may be used to enrich desired substrate molecules inside the cavity or to speed up mass transport of product molecules out of the cavity. Finally, as described later in this section, the dendrimer terminal groups can be used to control solubility of the composite and enhance catalytic selectivity.

2.5.1 *Dendrimer-Encapsulated Pt Nanoclusters as Heterogeneous Electrocatalysts for O_2 Reduction*

Pt is the most effective practical catalyst known for O_2 reduction, which is an important electrode reaction in fuel cells [24]. To achieve efficient utilization of Pt in such applications, a large amount of work has been devoted to developing methods for fabricating very small, stable, O_2-accessible clusters. Because the den-

drimer-encapsulated metal nanoparticles seemed likely to exhibit these properties, we thought it reasonable to test them as heterogeneous O_2 reduction catalysts. Such applications require immobilization of the dendrimer composites on a conducting substrate in such a way that electrons can transfer from the substrate to the metal nanoparticle [59]. Methodologies for attaching dendrimers to surfaces by electrostatic, covalent, and coordination means have been discussed in the literature [55–57, 59, 129, 146, 147]. We have generally found it most convenient to prepare surface-confined, dendrimer-encapsulated catalysts by first depositing the nanoclusters within the dendrimer, and then affixing the dendrimers to a gold electrode by dipping it into the dendrimer solution [59, 129, 147]. Even dendrimers terminated in hydroxyl groups adhere to gold, presumably via interactions with internal tertiary amine groups that are able to configure themselves in a way that puts them in intimate contact with the gold surface [59, 129].

Figure 18a shows cyclic voltammograms (CVs) obtained from Au electrodes coated with a monolayer of 60-atom Pt clusters entrapped within G4-OH (Au/G4-OH(Pt_{60})) in the presence and absence of O_2. For comparison, data in the presence of O_2 were also obtained from an Au electrode modified only with G4-OH (no Pt nanoparticle). In the presence of O_2, the Au/G4-OH-modified electrode yields a relatively small current. However, when an Au/G4-OH(Pt_{60})-modified electrode is used in the same solution, a much larger current is observed and the peak potential shifts positive, indicating a substantial catalytic effect. In the absence of O_2, only a small background current is observed, confirming that the process giving rise to the peak is O_2 reduction. Importantly, these results con-

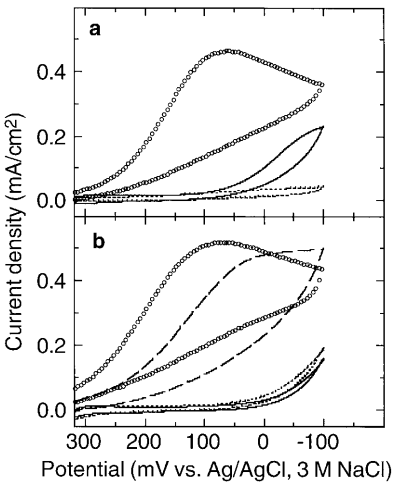

Fig. 18a,b. Electrocatalytic O_2 reduction by Pt or Pd clusters: **a** cyclic voltammograms of Au electrodes coated with G4-OH in O_2-saturated 1 mol/l H_2SO_4 (*solid line*) or coated with G4-OH (Pt_{60}) prepared by direct reduction in N_2- (*dashed line*) or O_2- (*open circles*) saturated 1 mol/l H_2SO_4; **b** cyclic voltammograms of Au electrodes coated with G6-OH(Cu_{55}) (*solid line*) and their primary displacement reaction products with stoichiometric Ag^+ (*short dash*), Pd^{2+} (*long dash*), and Pt^{2+} (*open circle*). Electrode area. 0.09 cm^2, scan rate 50 mV/s

clusively demonstrate that the surface of at least some of the dendrimer-encapsulated Pt nanoparticles are accessible to reactants in the solution and can exchange electrons with the underlying electrode surface.

Intradendrimer Pt and Pd nanoparticles synthesized using displacement reactions also show electrocatalytic activity for O_2 reduction. Figure 18b shows cyclic voltammograms obtained in 1 mol/l H_2SO_4 saturated with O_2 using Au electrodes coated with G6-OH$(Pt)_{55}$ and G6-OH$(Pd)_{55}$ catalysts prepared by Cu displacement (Sect. 2.4.2). For comparison, analogous results for electrodes coated with G6-OH(Cu_{55}) (prepared by direct reduction) or G6-OH(Ag_{110}) (prepared by primary displacement of a Cu-containing dendrimer) are also shown. It is known that Pt and Pd are highly efficient electrocatalysts for O_2 reduction in acid electrolytes, while Ag and Cu show no significant catalytic effect under the same conditions [150, 151]. In accordance with this precedent, the Au/G6-OH(Cu_{55})- and G6-OH(Ag_{110})-modified electrodes yield relatively small currents. However, when the Cu particles in G6-OH(Cu_{55}) were displaced by Pt or Pd and then immobilized to the Au surface, a much larger current was observed and the peak potential for O_2 reduction shifted positive to 80 mV for Pt and to about 0 mV for Pd, indicating a substantial catalytic effect. Note especially the similarity of the two Pt-based catalysts shown in Fig. 18.

2.5.2
Homogeneous Catalysis in Water Using Dendrimer-Encapsulated Metal Particles

Ligand- or polymer-stabilized colloidal noble metals have been used for many years as catalysts for the hydrogenation of unsaturated organic molecules [152–155]. Additionally, there is a special interest in developing methodologies for catalyzing organic reactions in aqueous solutions [152]. Accordingly, we investigated the homogeneous catalytic hydrogenation of alkenes in aqueous solutions using dendrimer-encapsulated nanoparticles. The hydrogenation activities for dendrimer-encapsulated Pd nanoparticles for a simple, unbranched alkene (allyl alcohol) and an electron-deficient, branched alkene (*N*-isopropyl acrylamide) in water are given in Fig. 19. Similar data have been obtained for dendrimer-encapsulated Pt nanoparticles and the results are analogous. The product of these hydrogenation reactions was confirmed by GC and NMR. G4-OH(Pd_{40}) shows a high catalytic activity for the hydrogenation of both alkenes. For example, the turnover frequencies (TOFs, mol of H_2/mol of metal atoms/h) for G4-OH(Pd_{40}) for hydrogenation of *N*-isopropyl acrylamide and for allyl alcohol hydrogenation compare favorably to water-soluble polymer-bound Rh(I) catalysts [153, 154] and are comparable to PVP-stabilized colloidal Pd dispersions in water [155]. The key result is that substrates (the alkenes and hydrogen in this case) can permeate dendrimers, encounter the nanoparticle therein, and undergo intradendrimer chemical transformation. Moreover, the yields and TOFs, which have by no means been optimized for the dendrimer systems, are comparable to others reported in the literature for similar reactions.

Importantly, the hydrogenation reaction rate can be controlled using dendrimers of different generations. This key finding is a consequence of the fact that dendrimer porosity is a function of generation: higher generation materials

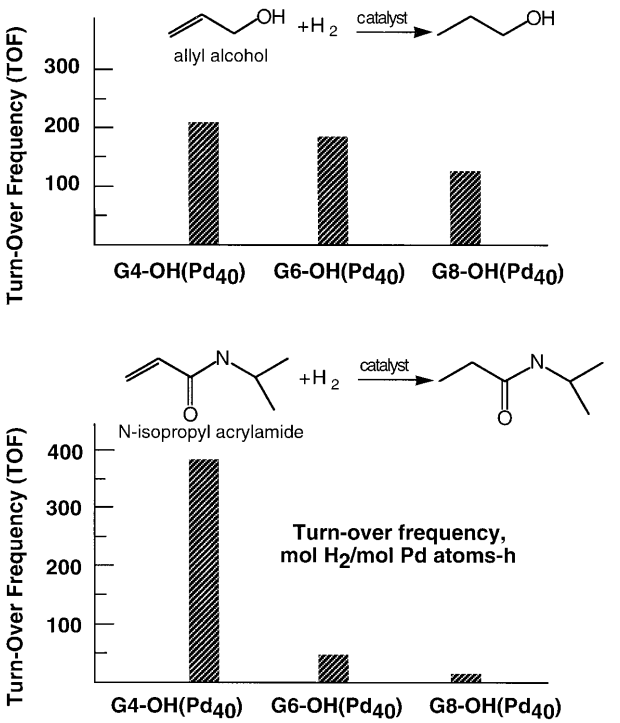

Fig. 19. Turn-over frequencies for hydrogenation of allyl alcohol and *N*-isopropyl acrylamide obtained in water using dendrimer-encapsulated Pd nanoparticles of constant average size. The hydroxyl-terminated PAMAM dendrimer generation varies from G4 to G8

are more sterically crowded on their exterior and thus less porous and less likely to admit substrates to interior metal nanoparticles than the lower generations [55, 83]. That is, the dendrimer acts as a selective nanoscopic filter that controls the catalytic activity of the composite (Fig. 20).

For example, the TOFs for G6-OH(Pd_{40}) and G8-OH(Pd_{40}) are only 10% and 5%, respectively, that of G4-OH(Pd_{40}) for *N*-isopropyl acrylamide. However, when the same materials are used to hydrogenate the linear alkene a much smaller decrease in activity is noted. This key finding shows that it is possible to control reaction rates and do selective catalysis by adjusting the "mesh" of the dendrimer "nanofilter." In this case the high-generation dendrimers selectively excluded the branched alkene, but the linear molecule was able to reptate through the dense G6 and G8 exteriors and encounter the catalyst. Finally, solutions of dendrimer-encapsulated Pt and Pd nanoparticles are stable before, during, and after hydrogenation reactions. For example, they do not aggregate after up to four months in water. Additionally they can be isolated as a black powder and redissolved in water to yield a stable, dark-brown solution identical to that present before drying. Finally, there are no spectroscopically detectable differences before and after hydrogenation reactions are carried out for up to 3 h.

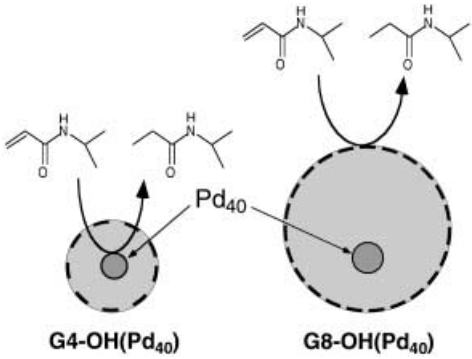

Fig. 20. The catalytic rate can be controlled using dendrimers of different generation. Pd or Pt clusters present within dendrimers of lower generation exhibit the highest catalytic activity. The sterically crowded terminal groups of higher generation dendrimers hinder substrate penetration. Reprinted with permission from Ref. 83 Copyright 1999 Wiley-VCH

2.5.3 Homogeneous Catalysis in Organic Solvents Using Dendrimer-Encapsulated Metal Particles

From an environmental and economic perspective it would be highly desirable to carry out all catalytic reactions in water. Unfortunately, many substrates and products are water insoluble, and therefore many important catalytic reactions in industry are run in organic solvents. Accordingly, we also tested the activity of dendrimer-encapsulated Pd nanoparticles for their hydrogenation activity in organic phases. As mentioned previously, the solubility of dendrimers can be controlled by functionalization of the terminal groups. For example, alkyl functionalization renders the otherwise water-soluble PAMAM dendrimers soluble in organic solvents. Importantly, functional groups need not be added to the dendrimer by covalent grafting, although this is certainly a viable strategy. A simpler and more versatile approach that is suitable for many applications takes advantage of the acid-base interaction between fatty acids and dendrimer terminal amine groups.

Using an approach similar to that discussed previously, Pd nanoparticles were prepared within amine-terminated PAMAM dendrimers. To prevent coordination of Pd^{2+} to the primary amine groups of the dendrimers, the solution pH was adjusted to around 2, which preferentially protonates the exterior amines to a greater extent than the interior tertiary amines. Accordingly, Pd^{2+} binds preferentially to the interior tertiary amines and upon reduction Pd particles form only within the dendrimer interior. G4-NH_2 dendrimer-encapsulated nanoparticles can then be quantitatively transported from an aqueous phase into toluene by addition of 10–20% of dodecanoic acid to the organic phase (Fig. 21) [19]. This transition is readily visualized by the color change: the brown aqueous solution of Pd nanoparticles becomes clear after addition of the acid, while the toluene layer turns brown. Our studies have shown that this is a consequence of

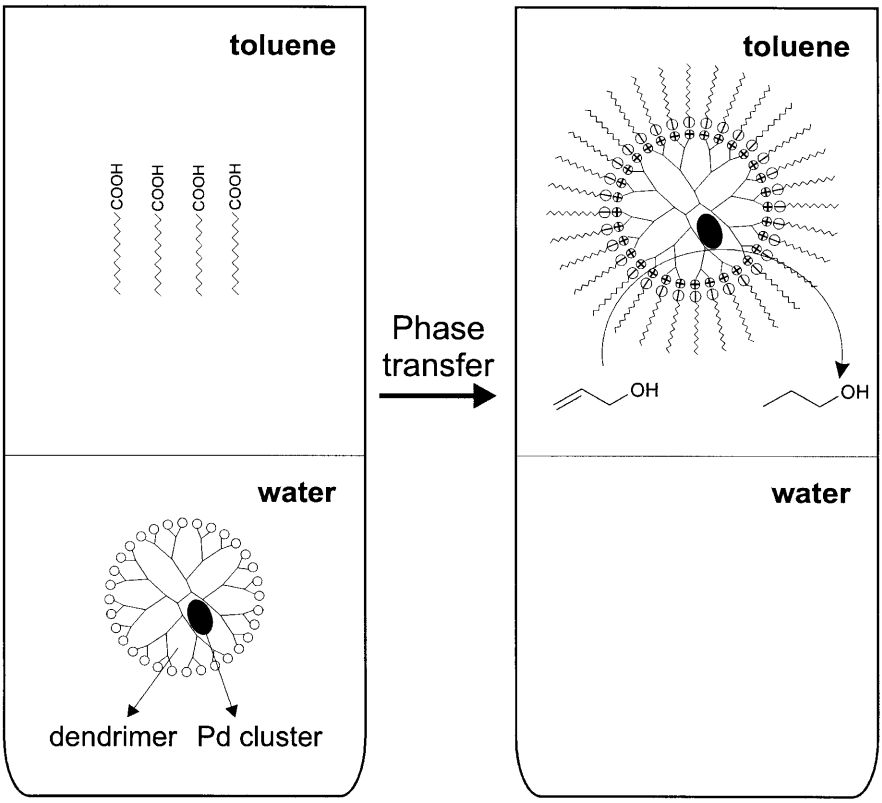

Fig. 21. Schematic illustration of phase-transfer catalysis using an amine-terminated dendrimer-encapsulated nanoparticle complexed with a fatty acid (present in the organic phase). The fatty acid surrounds the dendrimer, yielding a monodisperse inverted micelle which is soluble in the organic phase. After catalysis, the catalyst can be reclaimed by changing the pH of the aqueous phase

the formation of monodisperse inverted micelles of the type depicted on the right side of Fig. 21.

Toluene solutions of Pd encapsulated within dendrimer-templated inverted micelles have been tested for catalytic activity by examining their effectiveness towards hydrogenation of allyl alcohol in organic solvents [19]. The reaction product was confirmed to be *n*-propanol by ^{1}H NMR spectroscopy, and the turnover frequency, calculated from the rate of hydrogen uptake, was ~760 mol H_2 (mol Pd)$^{-1}$ h^{-1} at 20 °C. This value compares favorably with the value of 218 mol H_2 (mol Pd)$^{-1}$ h^{-1} obtained for the same reaction carried out in water using Pd nanoparticles encapsulated in hydroxy-terminated dendrimers.

2.5.4
Homogeneous Catalysis in Fluorous Solvents Using Dendrimer-Encapsulated Metal Particles

Reactions in biphasic fluorous/organic systems were suggested by Horvath and co-workers in 1994 [156] to facilitate recovery and recycling of soluble catalysts. The general approach to biphasic catalysis is illustrated in Fig. 22 [157].

The system consists of organic and fluorous layers. The catalyst is selectively soluble in the fluorous phase, while the reactants are preferentially soluble in the organic solvent. Stirring and/or heating of the mixture leads to formation of a fine emulsion and partial homogenization (with some solvents complete homogenization is obtained at elevated temperatures) and the catalytic reaction proceeds at the interface between the two liquids. When the reaction is over the liquid phases are allowed to settle, the product is isolated from the organic phase, and the catalyst-containing fluorous layer is recycled. Such easy separation and recycling are particularly attractive in terms of "green chemistry," and a number of fluorous phase-soluble catalysts have been reported in the literature, including some based on metal complexes [158, 159]. However, only dendrimers have thus far been used to solubilize metal nanoparticles in fluorous phases [100, 103].

In this section we describe two approaches for using dendrimer-encapsulated metal particles to perform biphasic catalysis. The first is hydrogenation catalysis using dendrimers rendered soluble in the fluorous phase by electrostatic attachment of perfluoroether groups [103]. The second demonstrates the use of perfluoroether groups covalently linked to the dendrimer exterior to carry out a Heck reaction [100].

Figure 23 shows a biphasic toluene/perfluoro-2-butyltetrahydrofuran (Fluoroinert FC-75) mixture containing dendrimer-encapsulated Pd nanoparticles complexed with poly(hexafluoropropylene oxide-*co*-difluoromethylene oxide) monocarboxylic acid prepared via the type of electrostatic modification de-

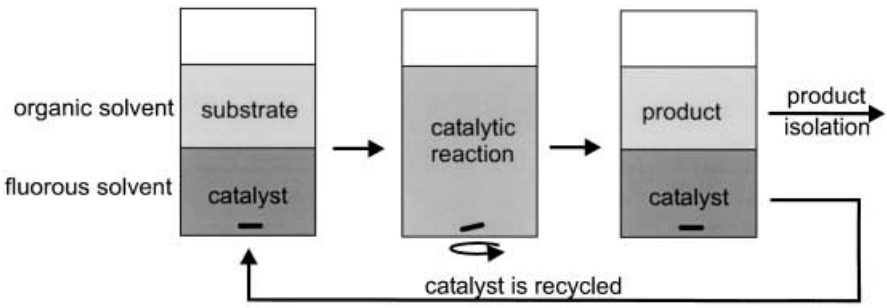

Fig. 22. Schematic illustration of the approach used to carry out fluorous biphasic catalysis using dendrimer-encapsulated metal nanoparticles modified on their exterior with perfluoroether "ponytails." Note that the ponytails can be attached by either electrostatic or covalent means. Reprinted with permission from Ref. 103 Copyright 2000 American Chemical Society

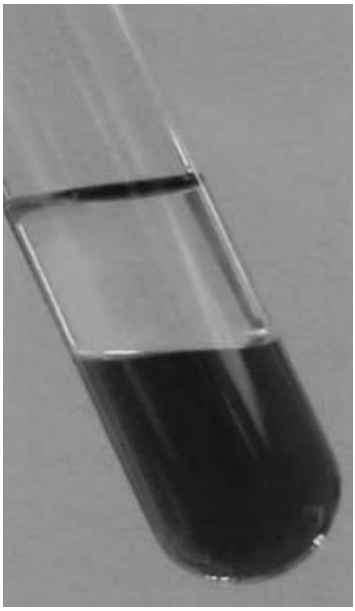

Fig. 23. This photograph shows a two-phase system consisting of (*top phase*) toluene and (*bottom phase*) perfluoro-2-butyltetrahydrofuran (Fluoroinert FC-75). The dark color (brown) in the bottom phase indicates that the dendrimer-encapsulated Pd nanoparticles, complexed with poly (hexafluoropropylene oxide-*co*-difluoromethylene oxide) monocarboxylic acid, are selectively extracted into the fluorous phase. No detectable color was observed in the organic phase. Reprinted with permission from Ref. 103 Copyright 2000 American Chemical Society

scribed in the previous section and shown in Fig. 21. The important result from this photograph is that the dark (brown) Pd/dendrimer catalyst resides exclusively in the fluorous phase. To the best of our knowledge, this is the first example of a stable solution of metal nanoparticles in fluorous solvents.

To probe the catalytic properties of this biphasic system, we performed hydrogenation of alkenes. In this example, tetrahydrofuran and FC-75 were used as the organic and fluorous solvents, respectively. The structures of the substrates used in these experiments and the corresponding TOFs are shown in Table 2. The identity of the reaction products was confirmed by NMR after isolation, and the TOFs were calculated from the rate of hydrogen uptake or the accumulation of product assessed by NMR. In some cases the TOF was calculated using both methods and found to be nearly identical. Interestingly, we found that addition of polar organic substrates to the reaction mixture often caused precipitation of the catalyst. This is likely due to competition between the substrate and perfluorinated acid for the amine groups of the dendrimer. This problem was circumvented by using large excesses of the perfluorinated acid, but note that it is possible to carry out the same sort of chemistry using dendrimers that are covalently attached to a stoichiometric number of perfluoroethers (see below).

The key result from this study is that the Pd/dendrimer nanocomposites are catalytically active under fluorous biphasic conditions. Indeed, one catalyst was

Table 2. Substrate, structures, and turn-over frequencies obtained for hydrogenation reactions in fluorous biphasic systems employing dendrimer-encapsulated Pd nanoparticles

Substrate	TOF in biphasic mixture, [mol H_2 (mol Pd)$^{-1}$ h^{-1}]	TOF with polymer-bound Pd(0) particles [mol H_2 (mol Pd)$^{-1}$ h^{-1}][d]
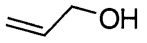	400	565
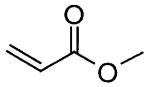	50	820[a]
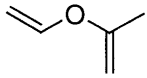	10	–
	3	122
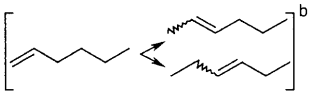	20	165
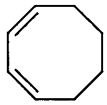	40[c]	884

[a] Butyl acrylate. [b] 1-hexene was used as the starting material. After 15 h the reaction mixture contained *n*-hexyane and 1-hexene:2-hexenes:3-hexenes in a 1:10:1 ratio. [c] Product is a mixture of cyclooctene (*ca.* 99%) and cyclooctane. [d] From [161].

recycled 12 times without appreciable loss of catalytic activity [103]. Moreover, despite significant mutual solubility of THF and FC-75, leaking of the catalyst into the organic phase has not been observed. These new catalysts can be used for hydrogenation of a range of unsaturated compounds, and also for isomerization of terminal alkenes. The reaction selectivity (Table 2) resembles that of colloidal, rather than bulk, Pd catalysts. For instance, Hirai and co-workers found that colloidal Pd can selectively hydrogenate 1,3-cyclooctadiene to cyclooctene (yield 99.9%), while conventional Pd/C catalysts are only moderately selective (ca. 83%) [160]. The unoptimized dendrimer-encapsulated catalysts yield a 99% conversion of 1,3-cyclooctadiene to cyclooctene.

Some conclusions can be drawn from comparison of the TOF values obtained using biphasic catalysis with literature data for the same reactions catalyzed by a polymer-supported Pd(0) catalyst (Table 2) [161]. First, although the TOFs for the dendrimer-encapsulated catalysts are consistently lower than for the polymer-supported catalysts, the values are in some cases comparable. Second, the selectivity pattern exhibited by the two types of catalysts is somewhat different. Specifically, the range of TOF numbers for biphasic catalysis is far greater than for conventional polymer catalysis, which suggests the possibility of the type of

selective hydrogenation discussed in Sect. 2.5.2. This added selectivity may arise from the unique polar nanoenvironment within the dendrimer interior in which the catalytic reactions occur. For example, the data in Table 2 indicate that more polar substrates undergo catalytic conversion faster in the biphasic system. Taking into account that the dendrimer interior is hydrophilic, one could reason that polar substrates would partition in the dendrimer interior more easily. As we have previously shown, selectivity can also be influenced by the size of the substrate: for a given polarity, smaller substrates more easily penetrate the sterically crowded dendrimer surface [83]. Solubility of the substrate in the fluorous phase might also affect catalytic selectivity.

To demonstrate further the powerful utility of the fluorous/organic biphasic approach to catalyst recycling, a dendrimer-encapsulated catalyst (DEC) with covalently attached perfluorinated polyether chains was synthesized [17] and metallic nanoparticles were introduced into the interior.

These composites were prepared by mixing a fluorocarbon solution of the perfluorinated PPI dendrimers with an aqueous ethanolic solution of Pd^{2+}, thereby forming an emulsion. After phase separation, the fluorous phase, which contains the dendrimer-encapsulated Pd^{2+}, was treated with a reducing agent yielding zero-valent Pd nanoclusters trapped within the dendrimer (Fig. 24).

Pd nanoparticles have only recently been shown to be effective in the very useful carbon-carbon bond-forming Heck reaction [162–165]. These colloidal Pd particles eliminate the need for toxic phosphine ligands, which are necessary for standard molecular Heck catalysts [176]. However, as presently implemented for Heck chemistry, colloidal Pd particles are not recoverable and require reaction conditions involving high temperatures and harsh organic solvents such as dimethylacetamide (DMA). The fluorous phase soluble DECs may help to solve one or more of these issues. Under a variety of conditions, the novel dendrimer-encapsulated nanoparticles were shown to be effective in the Heck heterocoupling reaction [100]. For example, DEC-catalyzed Heck reactions generally occurred homogeneously at 90 °C compared to >120 °C for colloidal Heck catalysts [162–167], and phase separation occurred at room temperature facilitating the recovery of the fluorous soluble catalyst from the organic-soluble product. Moreover, DEC-catalyzed coupling of phenyl halides with *n*-butyl acrylate

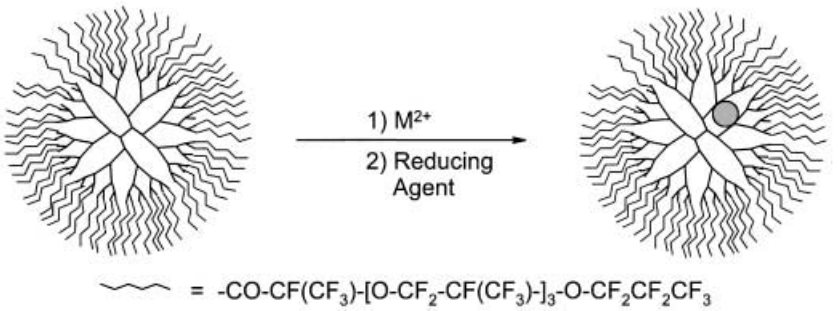

Fig. 24. Synthetic scheme for the introduction of metallic nanoparticles into perfluorinated polyether chain derivatized poly (propylene imine) PPI dendrimers. Reprinted with permission from Ref. 100 Copyright 2000 Wiley-VCH

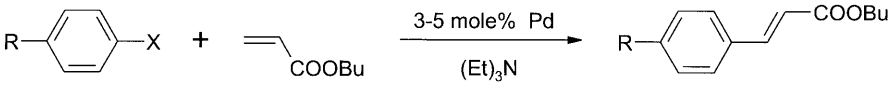

Fig. 25. Heterocoupling between an arylhalide and olefin is achieved using dendrimer-encapsulated catalysts with 100% selectivity for the *trans* isomer product (R = -H, -NO_2 and X = -I,-Br)

in the presence of triethylamine [100] yielded exclusively the *trans* isomer of *n*-butyl-formylcinnamate (Fig. 25).

For comparison, fluorous-phase-soluble Pd complexes are only 74–98% selective towards the *trans* product [168–170]. The isolated yields of the product approached 70% when a threefold excess of olefin to iodobenzene was used (Table 3); however, the percent yield decreased with the use of bromobenzene as expected since activation of bromine-carbon bonds is less favorable than iodocarbon bonds. It was also possible to catalyze the reaction in the absence of additional triethylamine base (Table 3). In this case, the tertiary amines of the dendrimer most likely act as the base. The catalysts, in general, were fully recover-

Table 3. Results obtained from Heck coupling of *n*-butylacrylate (BA) with aryl halides (X = halide, and R = para substituent) under various conditions using 3–5 mol % Pd

G4 PPI/Pd^0 BA (mmol)	-R	-X (mmol)	Base (mmol)	% yield
1.89	H	I (0.63)	Et_3 N (1.89)	70
0.63	H	I (0.63)	Et_3 N (1.89)	34
0.63	H	I (0.63)	Et_3 N (1.89)	19[a]
0.63	H	Br(0.63)	Et_3 N (1.89)	26
1.89	H	Br(0.63)	Et_3 N (1.89)	7[a]
1.89	H	Br(0.63)	none	19
0.63	H	Br(0.63)	none	0[a]
0.63	NO_2	Br(0.63)	Et_3 N (0.63)	≈ 10[b]
G3 PPI/Pd^0 BA	-R	-X	Base	% yield
1.89	H	I (0.63)	Et_3 N (1.89)	38
1.89	H	I (0.63)	Et_3 N (1.89)	28[c]
1.89	H	I (0.63)	Et_3 N (1.89)	37[d]
1.89	H	I (0.63)	None	59
0.63	H	Br(0.63)	Et_3 N (1.89)	10
1.89	NO_2	Br(0.63)	Et_3 N (1.89)	≈ 11[b]

[a] These reactions were performed with recovered catalysts.
[b] The yields were estimated by NMR.
[c] Hydrogen gas was used to reduce the palladium.
[d] The DEC was refluxed for 24 h in the solvent mixture before the reactants were added.
We have used the generational nomenclature typical for PAMAM dendrimers throughout this chapter. In the scientific literature the PPI family of dendrimers is incremented by one. That is, what we call a G4 PPI dendrimer (having 64 endgroups) is often referred to as G5.

able and showed no visible signs of agglomeration or precipitation, however catalytic activity decreased dramatically upon reuse.

Table 3 also shows that dendrimer size has an effect on the activity of the DECs. As mentioned earlier, metal particles of roughly the same size can be prepared within dendrimers of different generation [83]. This is accomplished by using a constant metal ion/dendrimer ratio, but dendrimers of different generation. As long as this ratio does not exceed the saturation threshold for the interior ligands, dendrimer-encapsulated nanoparticles of the same average size will result. Note, however, that as this ratio becomes smaller, the polydispersity of the metal particles increases. Figure 26 shows Pd particles containing an average of 31 Pd atoms prepared within G3 PPI dendrimers functionalized with the perfluoropolyether shown in Fig. 24. The average size of the Pd nanoparticles is 2.3 ± 0.3 nm. Similar data were obtained for the functionalized G4 PPI den-

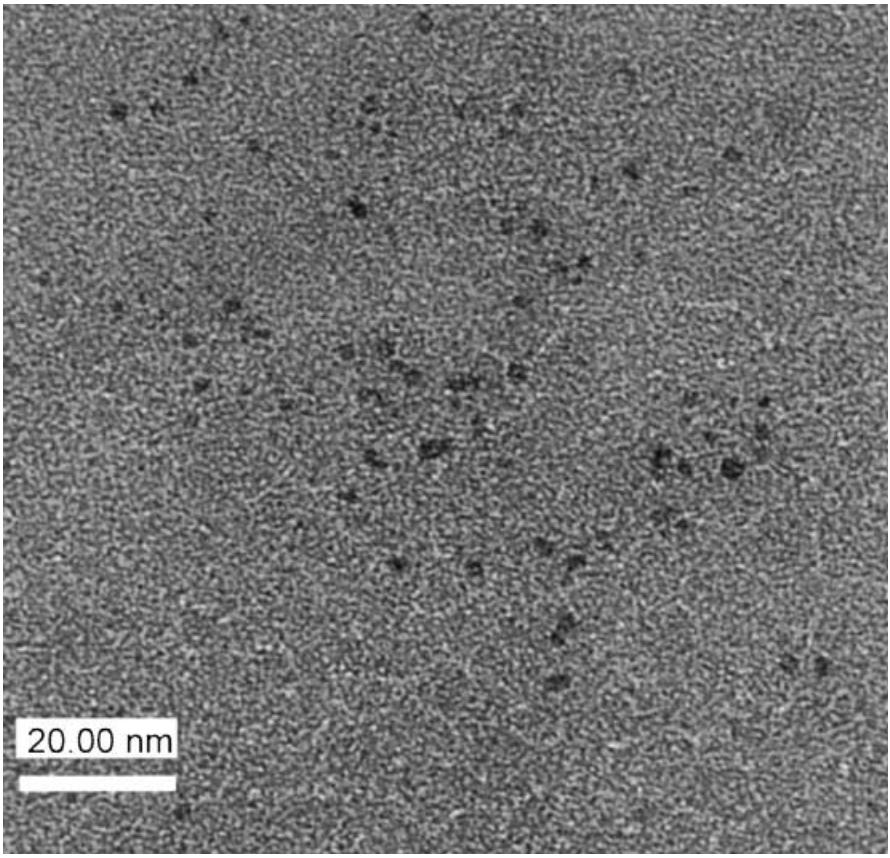

Fig. 26. High-resolution transmission electron microscopy (HRTEM) image of perfluoropolyether-modified G3 PPI dendrimers containing Pd metal nanoclusters prepared on a holey carbon copper grid by evaporation of a dilute solution of the dendrimer composite. Reprinted with permission from Ref. 100 Copyright 2000 Wiley-VCH

drimers. The data in Table 3 indicate that smaller dendrimer hosts are less active, probably because the interior nanoenvironment is more confining than it would be in a larger dendrimer. Note that this is the opposite of the behavior described in Sect. 2.5.2 for PAMAM-based dendrimers, and it likely reflects the more compact size of the PPI materials.

Taken together, these initial findings may eventually lead to other recyclable DECs having either modulated activities or selectivities arising from steric effects. Moreover, other catalytic processes requiring a co-catalyst, such as the Wacker process, may be particularly amenable to dendrimer-based catalytic systems because (as discussed in Sect. 2.4.2) the dendrimer interior can accommodate two or more catalytic moieties: for example, a metal particle (e.g., Pd) and a metal ion (e.g., Cu^{2+}), two different metal ions, or two different zero-valent metal.

2.5.5
Homogeneous Catalysis in Supercritical CO_2 Using Dendrimer-Encapsulated Metal Particles: Heck Chemistry

As mentioned in the previous section, there are good reasons to search for new reaction conditions for Heck and related reactions, which permit catalyst recovery, the use of less toxic solvents, and simpler product recovery. The use of liquid or supercritical (SC) CO_2 addresses all of these issues [171]. Until recently, however, the use of supercritical CO_2 had been limited to organometallic Pd complexes functionalized with perfluorinated ligands [172–174], due to the limited solubility of metal colloids in CO_2, and often required the use of water as a co-solvent [175]. The work described here shows that dendrimers can be used to solubilize Pd nanoclusters in liquid and SC CO_2. This new finding opens the door to the combined benefits of a catalyst that promotes Heck couplings, but without the need for toxic ligands or solvents.

As discussed in the previous section, perfluorinated polyether "pony-tails" can be covalently grafted onto PPI dendrimers, and it has previously been shown that such materials are soluble in liquid CO_2 [17]. HRTEM confirms that particles prepared within such dendrimer templates are nearly monodisperse and are of a size that is consistent with the dendrimer template (Sect. 2.5.4). Such dendrimer-encapsulated metal particles are quite soluble in liquid and SC CO_2.

Preliminary results from a study of catalytic activation of the heterocoupling between arylhalides and alkenes using pony-tail-functionalized dendrimer-encapsulated Pd nanoparticles have shown promise. For example, the classic Pd-catalyzed Heck coupling between arylhalides and methacrylate yields predominately (>97%) the *trans*-cinnimaldehyde product [176]. On the other hand, the CO_2-soluble dendrimer nanocomposite exclusively catalyzes the production of the highly unfavored 2-phenyl-acrylic acid methyl ester isomer at 5000 psi and 75 °C (Fig. 27] [177].

This important result conclusively proves that it is possible to catalyze synthetically useful carbon-carbon bond-forming reactions between two reactants, which have significant size and mass, within a dendrimer interior using CO_2 as

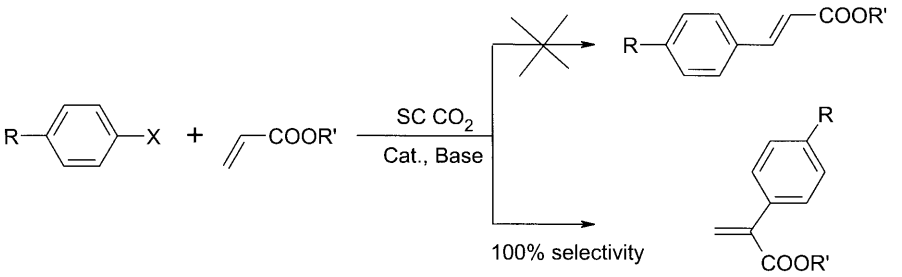

Fig. 27. Heck coupling of substituted arylhalides to acrylates in the presence of sc(CO_2) soluble PPI dendrimers containing palladium nanoparticles is highly selective for the non-standard 1,1-substituted product

the solvent. Perhaps even more significantly, it suggests the dendrimer architecture may be involved in enantioselective behavior. Such behavior has previously been observed in colloidal metal systems [178], as well as within dendritic molecules [179–181], and so is not entirely unexpected in the system described here. Future work may be directed towards the rational design of the pony-tails, the dendrimer structure, and the inorganic clusters (and possibly dendrimer-encapsulated co-catalysts) to tune the selectivity of such catalytic nanocomposites.

2.6 Dendrimer-Encapsulated Semiconductor Nanoparticles

In principle, any type of particle can be prepared inside a dendrimer template if a means can be found first to sequester the components and then to transform them chemically into the desired product. As discussed earlier, the simplest way to accomplish this goal is to take advantage of strong interactions between functional groups within the dendrimer and ions in solution, and then chemically reduce the ions to the zero-valent metal. In certain cases, Ag for example, this approach does not work (at least not with dendrimers having interiors dominated with tertiary amines) because the partition coefficient is too small. However, in that case it was possible first to prepare a less noble metal nanoparticle, and then to displace it with Ag.

Another family of nanoclusters that are important from both a fundamental and technological perspective are semiconductors [182]. Such materials have important electronic properties that make them useful in certain microelectronic applications. Additionally, because of their high photostability, tunable luminescence, and high quantum yield, semiconductor nanoparticles (quantum dots, QDs), especially modified CdS or CdSe QDs, have found use as ultrasensitive biological probes [183, 184]. This has further increased the need for simple, environmentally friendly, high-yield synthetic approaches for preparing stable, monodisperse QDs. Extrapolating from the previous discussion of metal nanoparticles, it seems likely that dendrimers could play a significant role in addressing some of these needs. In particular, we envisioned that dendrimer templates could be used to control the size, and thus the photoluminescent pro-

perties, of encapsulated CdS, CdSe, and other QD nanoparticles [185, 186]. Additionally, dendrimers have, in some cases, a high degree of biological selectivity [187], their solubility can be controlled via endgroup manipulation, and they act as protective hosts for encapsulated guests. Finally, the large number of functional groups on the dendrimer exterior may be biofunctionalized to target particular receptors. Taken together, these factors suggest that the development of methods aimed at the preparation of dendrimer-encapsulated CdS and CdSe is a worthy goal.

Efforts to prepare composites of dendrimers and technologically important QDs [188–191] have so far yielded primarily *inter*dendrimer composites. Such materials have been shown to be agglomerates in which multiple dendrimers stabilize relatively large CdS QDs. Results from these important studies suggested to us that it might be feasible to prepare *intra*dendrimer QD nanocomposites equivalent to the dendrimer-encapsulated metals described early in this chapter.

Indeed, recent results from our laboratory indicate that dendrimer-encapsulated CdS QDs can be prepared by either of two methods [192]. The first approach is analogous to the methodology described earlier for preparing dendrimer-encapsulated metal particles. First, Cd^{2+} and S^{2-} salts are added to an aqueous or methanolic PAMAM dendrimer solution. This yields a mixture of intradendrimer (templated) and interdendrimer particles. The smaller, dendrimer-encapsulated nanoparticles may then be separated via size-selective photoetching [193], dendrimer modification and extraction into a nonpolar phase [19], or by washing with solvent in which the dendrimer-encapsulated particles are preferentially soluble. An alternative, higher-yield method relies on sequential addition of very small aliquots of Cd^{2+} and S^{2-} to alcoholic dendrimer solutions.

Figure 28 shows absorption and luminescence spectra of an alcoholic solution of G4 PAMAM dendrimers in which ultrasmall (< 2 nm) CdS QDs have been grown. The extreme blue shift of both the absorbance and emission spectra (from that of bulk CdS), as well as the narrow linewidths, point to the existence of intradendrimer CdS [185]. Further evidence for intradendrimer templating comes from generation-dependent studies in which CdS QDs prepared in the presence of the higher generation dendrimers G6 (spectrum b) and G8 (spectrum c) yield larger particles that have red-shifted absorbance and emission spectra. HRTEM data confirm these generation-dependent increases in size of the QDs. Moreover, dynamic light scattering (DLS) measurements show no evidence of large, interdendrimer aggregates [192].

As mentioned above, QDs show desirable properties for use as luminescent biological probes: high quantum yields, resistance to photobleaching, high chemical photostability, and color tunability. Moreover, dendritic templates can be electrostatically or covalently modified with a host of highly selective biological components, e.g., DNA, proteins, and antibodies [194–196]. The most promising aspect of these QD nanocomposites lies in the ability of the dendrimer template to act as a bioselective agent that chaperones DNA through cell membranes [196] (PAMAM dendrimers are commercially available as DNA transfection hosts [197]). Accordingly, these nanocomposite probes may permit a detailed in vitro or in vivo look at the uptake mechanism of genetic material in cells.

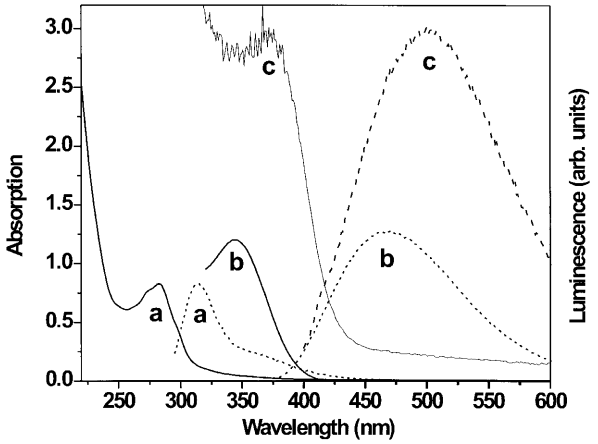

Fig. 28. Absorption (*solid lines*) and luminescence (*dotted lines*) spectra of dendrimer-encapsulated CdS nanoparticles. (a) G4-OH; (b) G6-OH; (c) G8-OH

3 Perspectives

In this chapter we have described two general families of metal-containing dendrimers. The first are dendrimers in which an organometallic complex, such as a porphyrin or iron-sulfur complex, is an integral part of the dendritic structure (usually the core). This important class of materials, and their applications to catalysis, energy transfer, photonics, and the like, have been extensively reviewed very recently and were only briefly touched upon here [2, 3, 198]. This chapter has primarily emphasized the synthesis, characterization, and applications of dendrimers hosting metal ions, metal particles, and semiconductor quantum dots that are not structural components of the dendrimer. Although metal-ion-containing dendrimers have shown promise as catalysts, we believe that metal and semiconductor particles sequestered within dendrimers are also of fundamental and technological interest. This is because the dendrimer can act as a template for preparing the particles, as a host for the particle that prevents agglomeration, as a nanofilter that selectively allows particular substrates to encounter the encapsulated particle, and as a unique chemical environment in which to carry out chemical synthesis. Additionally, the dendrimer terminal groups can be used to control solubility, as a synthetic handle for stabilization of the nanocomposite in polymer coatings, and as a means for enabling direct surface immobilization of dendrimers on metal, semiconducting, and insulating surfaces. Thus, the approach described here for preparing dendrimer-encapsulated nanoparticles takes advantage of each of the unique aspects of dendrimer structure: the chemistry of the terminal groups, the generation-dependent size, the three-dimensional structure, the low-density core, and endoreceptors present within the dendrimer interior.

These materials are likely to find three major uses in the years ahead. First, interactions between metalated dendrimers, particularly those containing semiconductor quantum dots, and biologically relevant materials, will be important. In this application, the dendrimer can act as a site-specific shuttle for any number of guests (DNA, drugs, contrast agents, and the like), while an encapsulated semiconductor is a highly stable, biocompatible luminescent tag for the composite. Second, the application of dendrimers to catalysis is likely to be of great importance for a number of reasons. For example, the unique nanoenvironment of the dendrimer interior can be used to house one or more catalysts and co-catalysts, while the exterior functional groups can be used to control solubility (even in supercritical fluids), enhance catalyst recovery, and selectively gate access of substrates into the interior. Moreover, intriguing recent results suggest that it may be possible to control the dendrimer interior to selectively favor particular isomeric products, perhaps even particular enantiomers. Finally, the ability to precisely control the size (and perhaps shape) of metal and semiconductor particles opens the door to a vast range of fundamental studies relevant to the fields of electronics, photonics, and magnetism.

The work described in the second section of this chapter is generally rather simple from an experimental viewpoint. For example, the dendrimers are all commercially available from either Dendritech or DSM, end-group modifications normally involve a single synthetic step, and separations are generally straightforward. Such simplicity should be a strong enticement to workers in the fields of catalysis, biotechnology, medicine, electronics, photonics, physics, materials science, and engineering to (1) begin to use the types of materials described herein for technological applications and fundamental discoveries, (2) invent new, related materials, and (3) begin to use these dendrimer composites as components in the next generation of molecular machines and devices.

Acknowledgements. We acknowledge our coworkers past and present who contributed to the results described in this chapter. We are particularly grateful to Dr Victor Chechik (presently at the University of York, UK), who performed many of the catalysis experiments in nonaqueous solvents. Thanks are also due to Ms. Yanhui Niu (Texas A&M) for clarifying some aspects of pH-dependent behavior of PAMAM dendrimers. We are also indebted to our colleagues Prof. Victoria J. DeRose and Dr Tomasz Wasowicz, who designed and executed the EPR and ENDOR experiments, Prof. David H. Russell and Mr Li Zhou, with whom we collaborated on the MALDI-TOF MS experiments, and Prof. Keith P. Johnston and C. Ted Lee at the University of Texas in Austin, with whom we collaborated on the catalysis experiments in CO_2. Mr Mark Kaiser (Dendritech, Inc.), with whom we have collaborated for many years, has provided invaluable technical advice and most of the PAMAM dendrimers used in our studies at Texas A&M. Finally, we would also like to express our gratitude to the Office of Naval Research, the National Science Foundation, and the Robert A. Welch Foundation for providing financial support for our work. Additional support was provided via subcontract from Sandia National Laboratories, which is supported by the U.S. Department of Energy (Contract DE-AC04–94AL8500). Sandia is a multiprogram laboratory operated by the Sandia Corporation, a Lockheed-Martin company, for the U.S. Department of Energy. M.Z. acknowledges fellowship support from The Electrochemical Society, Inc., the Eastman Chemical Company, and Phillips Petroleum. We are also indebted to Ms. Mary Sacquety for her careful and diligent editing and formatting of this manuscript.

4 References

1. Buhleier E, Wehner W, Vögtle F (1978) Synthesis 155
2. Vögtle F (ed) (1998) Topics in current chemistry. Springer, Berlin Heidelberg New York
3. Zeng F, Zimmerman SC (1997) Chem Rev 97:1681
4. Matthews OA, Shipway AN, Stoddart JF (1998) Prog Polym Sci 23:1
5. Fischer M, Vögtle F (1999) Angew Chem Int Ed 38:884
6. Venture M, Serroni S, Juris A, Campagna S, Balzani V (1998) Topics Curr Chem 197:193
7. Technical data from DSM Fine Chemicals (The Netherlands) and Dendritech, Inc (Midland, MI, USA)
8. Naylor AM, Goddard WA, Kiefer GE, Tomalia DA (1989) J Am Chem Soc 11:2339
9. De Brabander-van den Berg EMM, Mijenhuis A, Mure M, Keulen J, Reintjens R, Vandenbooren F, Bosman B, de Raat D, Frijins T, van den Wal S, Castelijns M, Put J, Meijer EW (1994) Macromol Symp 77:51
10. Miedaner A, Curtis CJ, Barkley RM, DuBois DL (1994) Inorg Chem 33:5482
11. Jansen JFGA, Meijer EW, de Brabander-van den Berg EMM (1995) J Am Chem Soc 117:4417
12. Jansen JFGA, de Brabander-van den Berg EMM, Meijer EW (1994) Science 266:1226
13. Sayed-Sweet Y, Hedstrand DM, Spinder R, Tomalia DA (1997) J Mater Chem 7:1199
14. Schenning APHJ, Elissen-Roman C, Weener J-W, Baars MWPL, van der Gaast SJ, Meijer EW (1998) J Am Chem Soc 120:8199
15. Jansen JFGA, Meijer EW, de Brabander-van den Berg EMM (1996) Macromol Symp 102:27
16. Caminati G, Turro NJ, Tomalia DA (1990) J Am Chem Soc 112:8515
17. Cooper AI, Londono JD, Wignall G, McClain JB, Samulski ET, Lin JS, Dobrynin A, Rubinstein M, Burke ALC, Fréchet JMJ, DeSimone JM (1997) Nature 389:368
18. Ottaviani MF, Cossu E, Turro NJ, Tomalia DA (1995) J Am Chem Soc 117:4387
19. Chechik V, Zhao M, Crooks RM (1999) J Am Chem Soc 121:4910
20. Schmid G (ed) (1994) Clusters and colloids. VCH, Weinheim
21. Kamat PV (1997) Prog Inorg Chem 44:273
22. Acres GJK, Hards GA (1996) Phil Trans R Soc Lond A 354:1671
23. Stonehart P (1994) In: Drake JAG (ed) Electrochemistry and clean energy. The Royal Society of Chemistry, Cambridge
24. Hamnett A (1996) Phil Trans R Soc Lond A 354:1653
25. Fonseca ITE (1991) In: Sequeira CAC (ed) Chemistry and energy I. Elsevier, New York
26. McEvoy AJ, Grätzel M (1991) In: Sequeira CAC (ed) Chemistry and energy I. Elsevier, New York
27. Tomalia DA, Durst HD (1993) Top Curr Chem 165:193
28. Moors R, Vögtle F (1993) Chem Ber -Recl 126:2133
29. Nagasaki T, Ukon M, Arimori S, Shinkai S (1992) J Chem Soc Chem Commun 608
30. Nagasaki T, Kimura O, Ukon M, Arimori S, Hamachi I, Shinkai S (1994) J Chem Soc Perkin Trans 1:75
31. Slany M, Bardaji M, Casanove M-J, Caminade A-M, Majoral J-P, Chaudret B (1995) J Am Chem Soc 117:9764
32. Gebbink RJMK, Bosman AW, Feiters MC, Meijer EW, Nolte RJM (1999) Chem Eur J 5:65
33. Wiener EC, Brechbiel MW, Brothers H, Magin RL, Gansow OA, Tomalia DA, Lauterbur PC (1994) Mag Res Med 31:1
34. Li Y, Dubin PL, Spindler R, Tomalia DA (1995) Macromolecules 28:8426
35. Jockusch S, Turro NJ, Tomalia DA (1995) Macromolecules 28:7416
36. Ottaviani MF, Turro C, Turro NJ, Bossmann SH, Tomalia DA (1996) J Phys Chem 100:13, 667
37. Laibinis PE, Whitesides GM (1992) J Am Chem Soc 114:9022

38. Zamborini FP, Crooks RM (1997) Langmuir 13:122
39. Chan KC, Kim T, Schoer JK, Crooks RM (1995) J Am Chem Soc 117:5875
40. Kumar A, Whitesides GM (1993) Appl Phys Lett 63:2002
41. Crooks RM, Ricco AJ (1998) Acc Chem Res 31:219
42. Ricco AJ, Crooks RM, Osbourn GO (1998) Acc Chem Res 31:289
43. Thomas RC, Kim T, Crooks RM, Houston JE, Michalske TA (1995) J Am Chem Soc 117:3830
44. Bain CD, Whitesides GM (1988) J Am Chem Soc 110:5897
45. Finklea HO, Snider DA, Fedyk J, Sabatani E, Gafni Y, Rubinstein I (1993) Langmuir 9: 3660
46. Widrig CA, Chung C, Porter MD (1991) J Electroanal Chem 310:335
47. Walczak MM, Popenoe DD, Deinhammer RS, Lamp BD, Chung C, Porter MD (1991) Langmuir 7:2687
48. Weisshaar DE, Walczak MM, Porter MD (1993) Langmuir 9:323
49. Tarlov MJ, Newman JG (1992) Langmuir 8:1398
50. Scott JR, Baker LS, Everett WR, Wilkins CL, Fritsch I (1997) Anal Chem 69:2636
51. Liu Y, Zhao M, Bergbreiter DE, Crooks RM (1997) J Am Chem Soc 119:8720
52. Zhao M, Liu Y, Crooks RM, Bergbreiter DE (1999) J Am Chem Soc 121:923
53. Frey H, Lach C, Lorenz K (1998) Adv Mater 10:279
54. Watanabe S, Regen SL (1994) J Am Chem Soc 116:8855
55. Wells M, Crooks RM (1996) J Am Chem Soc 118:3988
56. Tokuhisa H, Crooks RM (1997) Langmuir 13:5608
57. Tsukruk VV, Rinderspacher F, Bliznyuk VN (1997) Langmuir 13:2171
58. Castagnola M, Cassiano L, Lupi A, Messana I, Patamia M, Rabino R, Rossetti DV, Giardina B (1995) J Chromatogr 694:463
59. Zhao M, Crooks RM (1999) Adv Mater 11:217
60. Newkome GR, Moorefield CN, Vögtle F (1996) Dendritic molecules. VCH, Weinheim
61. Puddephatt RJ (1998) J Chem Soc Chem Commun 1055
62. Hearshaw MA, Moss JR (1999) J Chem Soc Chem Commun 1
63. Constable EC (1997) J Chem Soc Chem Commun 1073
64. Balzani V, Campagna S, Denti G, Juris A, Serroni S, Venturi M (1998) Acc Chem Res 31:26
65. Rietveld MHP, Grove DM, van Koten G (1997) New J Chem 21x:751
66. Jin R-H, Aida T, Inoue SJ (1993) J Chem Soc Chem Commun 1260
67. Jian DL, Aida T (1996) J Chem Soc Chem Commun 13:1523
68. Enomoto M, Aida T (1999) J Am Chem Soc 121:874
69. Dandliker PJ, Diederich F, Gross M, Knobler M, Louati A, Sanford EM (1994) Angew Chem Int Ed Engl 33:1739
70. Bhyrappa P, Young JK, Moore JS, Suslick KS (1996) J Am Chem Soc 118:5708
71. Pollak KW, Leon JW, Fréchet JMJ, Maskus M, Abruña HD (1998) Chem Mater 10:30
72. Newkome GR, Guther R, Moorefield CN, Cardullo F, Echegoyen L, Perezcordero E, Luftmann H (1995) Angew Chem Int Ed Engl 34:2023
73. Chow HF, Chan IYK, Chan DTW, Kwok RWM (1996) Chem Eur J 2:1085
74. Gorman CB, Smith JC, Hager MW, Parkhurst BL, Sierzputowska-Gracz H, Haney CA (1999) J Am Chem Soc 121:9958
75. Hawker CJ, Fréchet JMJ (1990) J Am Chem Soc 112:7638
76. Serroni S, Denti G, Campagna S, Juris A, Ciano M, Balzani V (1992) Angew Chem Int Ed 31:1493
77. Newkome GR, Cardullo F, Constable EC, Moorefield CN, Thompson AMWC (1993) J Chem Soc, Chem Commun 925
78. Alonso B, Cuadrado I, Morán M, Losada J (1994) J Chem Soc Chem Commun 2575
79. Takada K, Dïaz DJ, Abruña HD, Cuadrado I, Casado C, Alonso B, Morán M, Losada J (1997) J Am Chem Soc 119:10, 763
80. Seyferth D, Kugita T, Rheingold AL, Yap GPA (1995) Organometallics 14:5362
81. Kriesel JW, König S, Freitas MA, Marshall AG, Leary JA, Tilley TD (1998) J Am Chem Soc 120:12, 207

82. Zhao M, Sun L, Crooks RM (1998) J Am Chem Soc 120:4877
83. Zhao M, Crooks RM (1999) Angew Chem Int Ed Engl 38:364
84. Zhao M, Crooks RM (1999) Chem Mater 11:3379
85. Balogh L, Tomalia DA (1998) J Am Chem Soc 120:7355
86. Ottaviani MF, Ghatlia ND, Bossmann SH, Barton JK, Durr H, Turro NJ (1992) J Am Chem Soc 114:8946
87. Ottaviani MF, Bossmann S, Turro NJ, Tomalia DA (1994) J Am Chem Soc 116:661
88. Ottaviani MF, Montalti F, Romanelli M, Turro NJ, Tomalia DA (1996) J Phys Chem 100: 11, 033
89. Ottaviani MF, Montalti F, Turro NJ, Tomalia DA (1997) J Phys Chem B 101:158
90. Bosman AW, Schenning APHJ, Janssen RAJ, Meijer EW (1997) Chem Ber/Recueil 130: 725
91. Takada K, Storrier GD, Morán M, Abruña HD (1999) Langmuir 15:7333
92. Díaz DJ, Storrier GD, Bernhard S, Takada K, Abruña HD (1999) Langmuir 15:7351
93. Vassilev K, Fored WT (1999) J Polym Sci A37:2727
94. Bourque SC, Maltais F, Xiao WJ, Tardiff O, Alper H, Arya P, Manzer LE (1999) J Am Chem Soc 121:3035
95. Muto T, Hanabusa, K, Shirai H (1999) Macromolecular Rapid Comm 20:98
96. Gebbink RJMK, Bosman AW, Feiters MC, Meijer EW, Nolte RJM (1999) Chem Eur J 5:65
97. Moreno-Bondi MC, Orellana G, Turro NJ, Tomalia DA (1990) Macromolecules 23:910
98. Zhou L, Russel DH, Zhao M, Crooks RM (2000) Anal Chem (submitted)
99. Wascowicz T, Zhao M, Crooks RM, DeRose VJ (2000) (in preparation)
100. Yeung LK, Crooks RM (2000) Adv Mater (submitted)
101. Skoog DA, West DM, Holler FJ (1994) Analytical Chemistry, 6th edn. Harcourt Brace College Publishers, Philadephia
102. Niu Y, Sun L, Crooks RM (unpublished results)
103. Chechik V, Crooks RM (2000) J Am Chem Soc 122:1243
104. Lewis LN (1993) Chem Rev 93:2693
105. Bradley JS (1994) In: Schmid G (ed) Clusters and colloids. VCH, Weinheim
106. Che GL, Lakshmi BB, Fisher ER, Martin CR (1998) Nature 393:346
107. Reddington E, Sapienza A, Gurau B, Viswanathan R, Sarangapani S, Smotkin ES, Mallouk TE (1998) Science 280:1735
108. Schmid G (1992) Chem Rev 92:1709
109. Aiken JD III, Lin Y, Finke RGA (1996) J Mol Catal A Chem 114:29
110. Reetz MT, Helbig W (1994) J Am Chem Soc 116:7401
111. Petit C, Lixon P, Pileni M (1993) 97:12, 974
112. Murray CB, Norris DJ, Bawendi MG (1993) J Am Chem Soc 115:8706
113. Martin CR (1994) Science 266:1961
114. Zhang Y, Raman N, Bailey JK, Brinker CJ, Crooks RM (1992) J Phys Chem 96:9098
115. Dendritech (1995) Technology Review
116. Kallos GJ, Tomalia DA, Hedstrand DM, Lewis S, Zhou J (1991) Rapid Comm Mass Spec 5:383
117. Bouchonnet S, Hoppilliard Y, Ohanessian G (1995) J Mass Spec 30:172
118. Llenes CF, Omalley RM (1992) Rapid Comm Mass Spec 6:564
119. Fanizzi F, Intini FP, Maresca L, Natile G (1990) J Chem Soc Dalton Trans 199
120. Cotton FA, Wilkinson G (1988) Advanced inorganic chemistry, 5th edn. Wiley, New York
121. Fong CY, Cohen ML, Zucca RRL, Stokes J, Shen YR (1970) Phys Rev Lett 25:1486
122. Kreibig U, Vollmer M (1995) Optical properties of metal clusters. Springer, Berlin Heidelberg New York
123. Klabunde KJ (1994) Free atoms, clusters, and nanoscale particles. Academic Press, San Diego
124. Abe H, Charle K-P, Tesche B, Schulze W (1982) Chem Phys 68:137
125. Curtis AC, Duff DG, Edwards PP, Jefferson DA, Johnson BFG, Firkland AI, Wallace ASA (1988) Angew Chem Int Ed 27:1530

126. Lisiecki I, Pileni MP (1993) J Am Chem Soc 115:3887
127. The value of 1.8 nm represents an upper limit on the cluster size. The actual particles certainly have a critical dimension of less than 1 nm (based on CPK models), which is below our TEM resolution
128. Jackson CL, Chanzy HD, Booy FP, Tomalia DA, Amis EJ (1997) Proc Am Chem Soc 77: 222
129. Tokuhisa H, Zhao M, Baker LA, Phan VT, Dermody DL, Garcia ME, Peez RF, Crooks RM, Mayer TM (1998) J Am Chem Soc 120:4492
130. Gerloch M, Constable EC (1994) Transition metal chemistry: the valence shell in d-block chemistry. VCH, Weinheim
131. Because the dendrimer-encapsulated nanoparticles are so small, they do not have the properties of bulk metals. Therefore, it is not possible to calculate the reduction potential for the exchange reactions from tabulated literature data
132. Sullivan BP (1989) Platinum Metals Rev 33:2
133. Liu R, Her W, Fedkiw PS (1992) J Electrochem Soc 139:15
134. Kiwi J, Gratzel M (1979) J Am Chem Soc 101:7214
135. Zagal JH (1992) Coord Chem Rev 119:89
136. Bedioui F, Devynck J, Bied-Charreton CJ (1996) Mol Catal A 113:3
137. Deronzier A, Moutet J-C (1989) Acc Chem Res 22:249
138. Nashner MS, Somerville DM, Lane PD, Adler DL, Shapley JR, Nuzzo RG (1996) J Am Chem Soc 118:12, 964
139. Hirai H (1979) J Macromol Sci-Chem A13:633
140. Toshima N, Takahashi T (1992) Bull Chem Soc Jpn 65:400
141. Boutonnet M, Kizling J, Touroude R, Maire G, Stenius P (1986) Appl Catal 20:163
142. Tomalia DA (1990) Macromol Symp 101:245
143. Jiang DL, Aida T (1997) J Macromolecular Sci Pure Appl Chem A34:2047
144. Bhyrappa P, Young JK, Moore JS, Suslick KS (1996) J Am Chem Soc 118:5708
145. Brunner H (1995) Organomet Chem 500:39
146. Tsukruk VV (1998) Adv Mater 10:253
147. Zhao M, Tokuhisa H, Crooks RM (1997) Angew Chem Int Ed 36:2596
148. Lee J-J, Ford WT, Moore JA, Li Y (1994) Macromolecules 27:4632
149. Fréchet JM, Hawker CJ, Wooley KL (1994) JMS-Pure Appl Chem 11:1627
150. Bard AJ (ed) (1976) Electroanalytical chemistry: a series of advances. Marcel Dekker, New York
151. Bard AJ (ed) (1967) Electroanalytical chemistry: a series of advances. Marcel Dekker, New York
152. Herrmann WA, Kohlpaintner CW (1993) Angew Chem Int Ed 32:1524
153. Joó F, Somsák L, Beck MT (1984) J Mol Catal 24:71
154. Bergbreiter DE, Liu Y-S (1997) Tetrahedron Lett 38:7843
155. Nádasdi L, Joó F, Horváth I, Vígh L (1997) Appl Catal A 162:57
156. Horvath IT, Rabai J (1994) Science 266:72
157. de Wolf E, van Koten G, Deelman B-J (1999) Chem Soc Rev 28:37
158. Cornils B (1997) Angew Chem Int Ed Engl 36:2057
159. Curran DP (1998) Angew Chem Int Ed 37:1174
160. Hirai H, Chawanya H, Toshima N (1981) Makromol Chem Rapid Commun 2:99
161. Selvaraj PC, Mahadevan VJ (1997) Polymer Sci A 35:105
162. Beller M, Fischer H, Kuhlein K, Reisinger CP, Herrmann WA (1996) J Organomet Chem 520:257
163. Le Bars J, Specht U, Bradley JS, Blackmond DG (1999) Langmuir 15:7621
164. Klingelhofer S, Heitz W, Greiner A, Oestreich S, Forster S, Antonietti M (1997) J Am Chem Soc 119:10, 116
165. Reetz MT, Lohmer G (1996) J Chem Soc Chem Comm 16:1921
166. Reetz MT, Breinbauer K, Wanninger K (1996) Tetrahedron Lett: 4499
167. Dhas NA, Gedanken A (1998) J Mat Chem: 445
168. Moineau J, Pozzi G, Quici S, Sinou D (1999) Tetrahedron Lett: 7683

169. Kling R, Sinou D, Pozzi G, Choplin A, Quignard F, Busch S, Kainz S, Koch D, Leitner W (1998) Tetrahedron Lett: 9439
170. Cabri W, Candani I (1995) Acc Chem Res 28:2
171. Kaupp G (1994) Angew Chem Int Ed Engl 33:1452
172. Morita DK, Pesiri DR, David SA, Glaze WH, Tumas W (1998) Chem Commun 13:1397
173. Carroll MA, Holmes AB (1998) Chem Commun 13:1395
174. Bhanage BM, Ikushima Y, Shirai M, Arai M (1999) Tetrahedron Lett 40:6427
175. Ji M, Chen XY, Wai CM, Fulton JL (1999) J Am Chem Soc 121:2631
176. Heck RF (1979) Acc Chem Res 12:146
177. Yeung LK, Lee CT, Johnston KP, Crooks RM (2000) J Am Chem Soc (submitted)
178. Bonnemann H, Braun GA (1997) Chem Eur J 3:1200
179. Bhyrappa P, Vaijayanthimala G, Suslick KS (1999) J Am Chem Soc 121:262
180. Bhyrappa P, Young JK, Moore JS, Suslick KS (1996) J Am Soc 118:5708
181. Chow HF, Mak CC (1997) J Org Chem 62:5116
182. Kamat PV (1993) Chem Rev 93:267
183. Bruchez M, Moronne M, Gin P, Weiss S, Alivisatos AP (1998) Science 281:2013
184. Chan WCW, Nie S (1998) Science 281:2016
185. Vossmeyer T, Katsikas L, Giersig M, Popovic IG, Diesner K, Chemseddine A, Eychmuller A, Weller H (1994) J Phys Chem 98:7665
186. Dabbousi BO, Rodriguez-Viejo J, Mikulec FV, Heine JR, Mattoussi H, Ober R, Jensen KF, Bawendi MG (1997) J Phys Chem B 101:9463
187. Kukowska-Latallo JF, Bielinska AU, Johnson J, Spindler R, Tomalia DA, Baker JR (1996) Proc Natl Acad Sci USA 93:4897
188. Sooklal K, Hanus LH, Ploehn HJ, Murphy CJ (1998) Adv Mater 10:1083
189. Lackowicz JR, Gryczynski I, Gryczynski Z, Murphy CJ (1999) J Phys Chem B 103:7613
190. Hanus LH, Sooklal K, Murphy CJ, Ploehn HJ (2000) Langmuir 16:2621
191. Huang J, Sooklal K, Murphy CJ, Ploehn HJ (1999) Chem Mater 11:3595
192. Lemon BI, Crooks RM (unpublished results)
193. Matsumoto H, Sakata T, Mori H, Yoneyama H (1996) J Phys Chem 100:13781
194. Anzai J, Kobayashi Y, Nakamura N, Nishimura M, Hoshi T (1999) Langmuir 15:221
195. Kobayashi H, Wu C, Kim MK, Paik CH, Carrasquillo JA, Brechbiel MW (1999) Bioconjugate Chem 10:103
196. Kukowska-Latallo JF, Chen C, Eichman J, Bielinska A, Baker JR (1999) Biochem Biophys Res Commun 264:253
197. QIAGEN Inc, 28159 Avenue Stanford, Valencia, CA 91355
198. Newkome GR, He E, Moorefield CN (1999) Chem Rev 99:1689

Hyperbranched Macromolecules: Soft Particles with Adjustable Shape and Persistent Motion Capability

Sergei S. Sheiko[1], Martin Möller[2]

Laboratory of Organic and Macromolecular Chemistry, University of Ulm, 89069 Ulm, Germany
[1] *E-mail: sergei.sheiko@chemie.uni-ulm.de*
[2] *E-mail: martin.moeller@chemie.uni-ulm.de*

The conformational constraints resulting from dense and regular branching lead to three-dimensional macromolecules which do not interpenetrate and overlap like polymer coils, retaining flexibility of the chain segments and molecular shape. Examples of branched macromolecules with a defined primary structure are dendrimers and comb polymers (molecular brushes). Such highly branched macromolecules can be regarded as *soft particles*. Their shape is variable and sensitive to intramolecular interactions and perturbations in the surrounding medium. At an interface, the molecular conformation is governed by interplay between intramolecular interactions of the branches and interaction of the branches with the surface. Within this context, the organization of dendrimers, arborescent graft polymers, and comb polymers on surfaces is discussed with emphasis placed on conformational transitions and motion. Scanning force microscopy is used as a powerful tool for investigation of single molecules and the examination of structural parameters and driving forces that control the shape and the position of molecules on the substrate.

Keywords. Hyperbranched macromolecules, Polymer films, Scanning force microscopy, Conformational transitions and interfacial ordering of single molecules

Topics in Current Chemistry, Vol. 212

List of Abbreviations

AGP	arborescent graft polymer
DP	degree of polymerization
GPC	gel permeation chromatography
HOPG	highly oriented pyrolytic graphite
PBA	poly(*n*-butyl acrylate)
PS	polystyrene
PVP	polyvinylpyridine
SAM	self-assembled monolayer
SFM	scanning force microscopy
SLS	static light scattering

1 Introduction

Hyperbranched macromolecules such as dendrimers and cylindrical brushes (Fig. 1) are peculiar nanoobjects which combine properties of particles and polymer molecules [1–34]. An increasing degree of branching changes the spatial distribution of the chain segments from that of a statistical coil to a more dense packing of the monomers with an outward orientation of the chain ends and a gradient in the segmental distribution. The increasing steric interaction and excluded volume impedes interpenetration and overlapping of highly branched molecules and they become more like colloidal particles which interact via surfaces across an intervening medium [35–48]. Depending on their density, the forces between macroscopic bodies are effectively of much longer range and exhibit strong variations due to the medium [49–53].

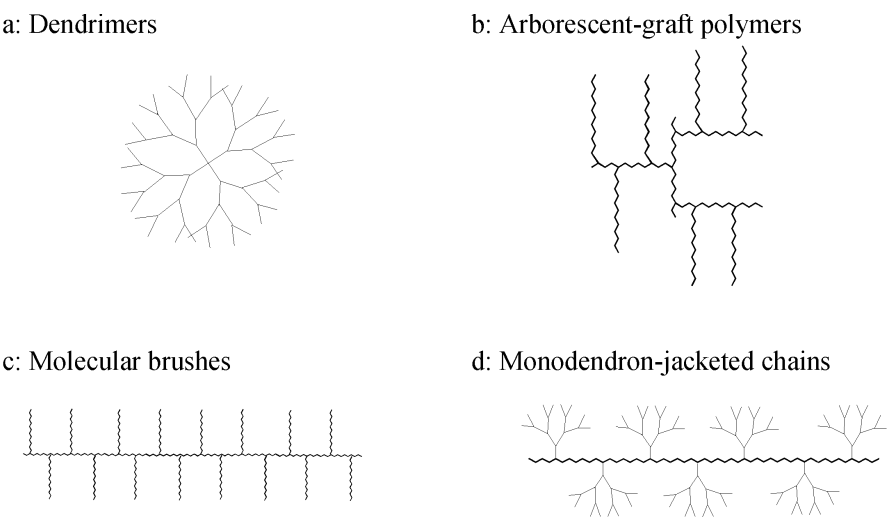

Fig. 1. Hyperbranched molecular architectures

At the same time, hyperbranched structures retain typical molecular features, such as covalent connectivity, rotational isomeric flexibility of the chain segments, and a great number of the branch arms and end groups which can cause entanglements and undergo specific interactions. Thus, hyperbranched macromolecules can be regarded as *soft molecular particles*, which are distinguished from solid particles by their inhomogeneous density distribution and variable shape.

The variability in the primary molecular structure and molecular conformation makes hyperbranched polymers intriguing objects as building units for nanotechnology [54–70]. Here we focus on the most regular structures such as dendrimers [1–9], arborescent graft polymers [10–14], comb polymers/molecular brushes [15–21], and monodendron jacketed macromolecules [22–26] (Fig. 1). We have been particularly interested in the interfacial behavior of the hyperbranched molecules [71–89]. The hyperbranched molecules can be employed for the preparation of nanostructured films and self-organized surface patterns that can respond specifically to external fields [90–105]. Chemical modification via reactive, photoactive, or conductive groups provides unique perspectives for functional application in molecular and cell biology, information technology, and tailoring of surface properties [54–70]. Variation of the segmental flexibility, branching density, and surface groups allows one to tailor the molecular shape, the compliance, and the interaction with the substrate [90–105]. Figure 2 gives a schematic view of three types of self-assembled monofilms, i.e., SAMs of small molecules controlled by specific surface interaction and lateral ordering [106–110]; a colloidal film whose formation is promoted by rather long range surface forces [111–144], and a cartoon of a monofilm from hyperbranched molecules combining elements of both molecules and colloids.

Molecular and surface forces are sensitive to the same variables, e.g., temperature, electrostatic susceptibility, ionic strength, and pH control different events on different length scales [49]. The surface forces can be tuned over a broad range by changing the shape, size, and density of the particles as well as the physical properties and chemical composition of the surrounding medium [49–53]. If a film is prepared by solution casting, evaporation of the solvent results in capillary forces which can be repulsive and attractive depending on the wetting properties of the particle surface [128–131]. In addition, attractive forces of entropic origin can take place when electrostatic interactions are completely screened [132–144]. Using such effects in combination with surface forces, it is possible to obtain dense [111–120] or sparse [80, 121–137] coatings of nanoparticles with long range order (Fig. 3).

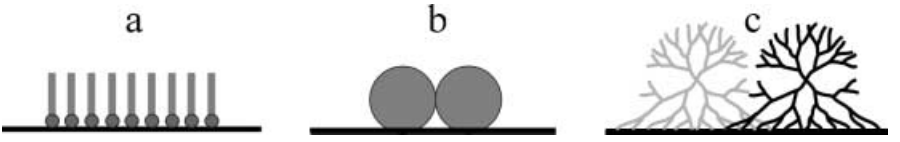

Fig. 2a–c. Monolayer structure of: **a** small molecules; **b** solid particles; **c** hyperbranched macromolecules

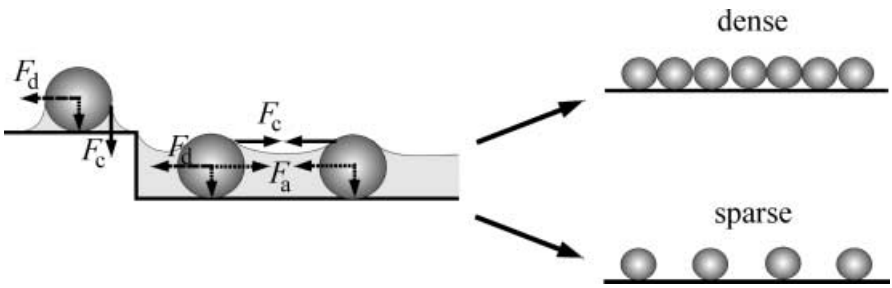

Fig. 3. Adhesion F_a, capillary F_c, and depletion F_d forces, acting between colloidal particles and the substrate in the presence of liquid

Thus, film formation and self-organization of hyperbranched molecules are particularly sensitive to the interplay of short range molecular interactions and long range surface forces. Understanding these correlations will give us a key to functional nanoparticles with controllable shape and motion. Following this objective, organization of molecular particles on surfaces will be discussed with emphasis placed on conformational transitions and motion of individual molecules. We will demonstrate the use of scanning force microscopy for investigation of single molecules along with examination of structural parameters and driving forces controlling the shape and the position of molecules on the substrate. Although we focus on hyperbranched synthetic polymers, it must be noted that these macromolecules are a subclass of soft polymer particles including lattices, micelles, proteins, DNA, and vesicles.

2
Dendritic Molecules

Cascade-type branching results in globular molecules in which one can distinguish a central core, the interior, and the branch ends [1–14]. Convergent and divergent synthetic schemes or a combination thereof allows one to tailor these structures and to obtain well defined dendritic macromolecules with controllable physical properties. Depending on the junction points and the molecular weight of the subunits, one can distinguish dendrimers [1–9] and arborescent graft polymers [10–14] (Fig. 1a, b). Randomly branched structures are usually denoted as hyperbranched macromolecules where branch points may have different functionalities and chain segments between branch points are of different length [27–34].

2.1
Persistent Shape Molecules

If the branching density is sufficiently high to hinder segmental flexibility and impose strong excluded volume and even steric interactions, molecular dimensions become rigid. Measurements of solution and melt viscosity showed that the properties of dendritic molecules approached that of solid spheres as the

branching density increased [35–48]. However, synthetic difficulties arise as the size and branching density of molecules increase and defects in the molecular structure are inevitable.

Complementary to using repulsive interactions in order to achieve shape control, attractive interactions of relatively large building blocks, which are rationally designed regarding their shape, polarity, and functional groups, can be employed for intramolecular self-assembly [23]. In this case, the molecular structure optimizes itself to realize specific interactions between the blocks and minimize the interfacial energy.

Regarding shape control by extensive branching, monodispersity can be neglected if the branching density is high and the branches are of rather uniform length. This is demonstrated by cascade-branched or arborescent graft polymers that were obtained by using the so-called "graft on graft" strategy [10–14]. Starting from a linear polymer, the branching functionality was progressively increased by repeated functionalization and anionic grafting steps. Each functionalization step led to random distribution of grafting functionalities within the molecule. A high degree of branching and narrowing of the polydispersity due to coupling resulted in rather uniform molecules. In addition, the spherical shape resulted from minimization of the interfacial area provided that branches are sufficiently flexible.

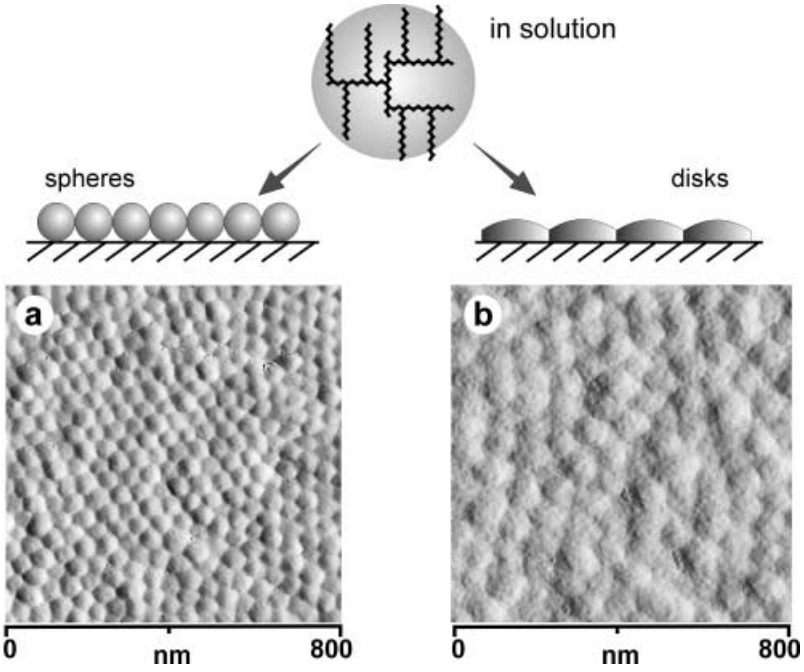

Fig. 4a,b. Monolayer structure of arborescent graft polystyrenes of different branching densities adsorbed on mica [71]: **a** spherical particles correspond to individual molecules of $M_w = 2.8 \times 10^7$ g/mol and N = 5; **b** disk-like structures correspond to AGP with $M_w = 5.5 \times 10^7$ g/mol and N = 20

Using this approach, one can obtain molecular particles whose size and softness can be varied widely. SFM was used to investigate the effect of the branching density on the shape of adsorbed molecules [71]. Figure 4 compares two arborescent graft polystyrenes of similar molecular mass, but different branching density. In both cases, the molecules formed spontaneously a closed monolayer primarily driven by the capillary forces acting during evaporation of the solvent. Figure 4a shows a monolayer structure of a strongly branched polymer (3rd generation, $M_w = 2.8 \times 10^7$ g/mol) with N = 5 monomers between neighboring grafts. The monolayer exhibited a fairly ordered structure of densely packed spheres. A few defects are explained by the polydispersity $M_w/M_n = 1.13$. The lateral diameter of the individual spheres was about the same as the film thickness. Thus, owing to the high branching density, the molecules also retained their spherical shape in contact with the substrate. In contrast, the less densely branched polystyrene molecules in Fig. 4b (2nd generation, $M_w = 5.5510^7$ g/mol, N = 20) were flattened by adsorption forces. The example clearly demonstrates how dendritic molecules can form monolayers of hexagonally ordered spherical particles, which interpenetrate each other only a little but are able to adjust their shape depending on the branching density and interaction with the substrate.

Shape persistence due to high branching can also be achieved by linking low molecular weight monomers in cascade reactions to well defined dendrimers, either via the divergent or convergent synthesis [1–9]. Maximum molecular weights to be achieved are considerably smaller than in the case of the arborescent polymers and the configurational entropy contribution is less important. As a consequence, a large number of generations (n > 5) is required to achieve a persistent globular conformation. As mentioned above, shape control can be improved by designing the branches in such a way that their mutual interaction favors assembly to a particular shape [1]. This approach has been studied intensively by V. Percec who developed a library of monodendrons, i. e., taper shaped building units that can be linked to a common core [22, 23]. The high branching density in combination with favorable specific interactions of the subunits re-

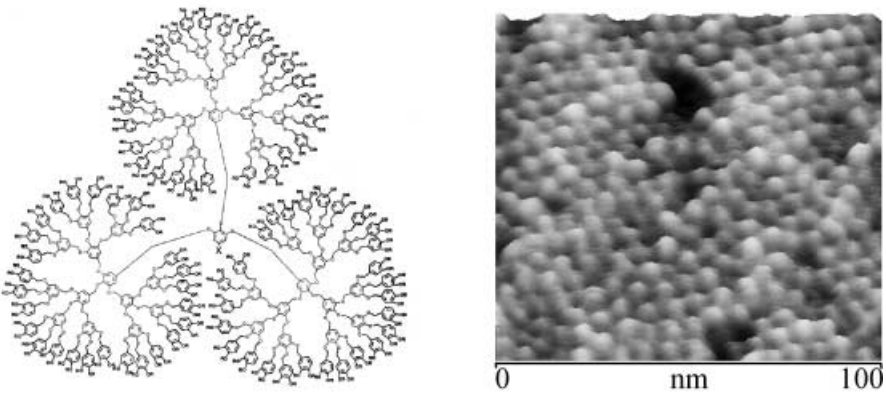

Fig. 5. Shape-persistent dendrimer and height micrograph of the monolayer structure on mica obtained by tapping mode SFM [88]

sults in a remarkable shape control [35–37]. Figure 5a shows such a dendrimer prepared by convergent linkage of benzyl ether monodendrons to a focal unit [88]. The image in Fig. 5b was recorded from a solution cast monofilm. Also in this case, the globular shape of the molecules was not evidently affected by the interaction with the highly polar substrate, i.e., mica. With the accuracy of the tapping mode experiment, nearly identical values were determined for the lateral diameter and the height of the particles, i.e., 5.5 nm and 4.5 nm, respectively. The values are consistent with the diameter d = 5 nm calculated for a hypothetical sphere of molar mass M = 42731.19 g/mol and with a density of 1 g/cm^3.

2.2
Shape Adjustment on Surfaces

So far we have focused on rather persistent and invariant structures. Molecules with a persistent shape are of value for applications where size, diffusion, and permeation of the particles need to sustain variations in the surrounding medium (e.g., carriers and standards) [62–66]. Eventually, more interesting will be molecules that can adopt different geometrically defined shapes. A concept for such switchable shapes results when similar monodendrons like those in the example of Fig. 5 are linked to a flexible linear backbone. Polymerization of monodendrons with a monomer unit in the focal position results in such monodendron jacketed macromolecules [22]. Also in this case, shape persistence is achieved by the steric demand of the dendritic side groups in combination with their ability to undergo self-assembly to columnar or spherical structures [23]. If the dendron structure, however, is such that they tend to form globuli but the degree of polymerization (DP) is larger than the number of units that fit into the equivalent sphere, the dendrons have to adjust their conformation and interaction to an alternative geometry [84]. This is outlined in Fig. 6. At low DPs, the conical monodendrons assemble to a globule with random-coil backbone. On increasing the DPs, the self-assembly pattern of the monodendritic units changes to give cylindrical polymers with extended backbone.

The disordered arrangement of the globuli and worm-like species in combination with their uniform shape and diameter of 50 Å demonstrates that the intramolecular self-assembly did not depend on intermolecular ordering. For both types of particles, the monolayer thickness was similar to the lateral diameter of the particles d = 50 ± 5 Å. The topographic contrast of the images in Fig. 6 was enabled by strong molecular segregation and weak interpenetration of the particles.

The transformation from spheres to cylinders is a peculiar example for the self-adjustment of the molecular conformation. The switching shape can be regarded as an example for the principle of quasi equivalency established by A. Klug for the self-assembly of biomolecules and viruses [145]: for the sake of an improved intermolecular packing, the molecules adopt a conformation different from the minimum energy one. This also demonstrates that shape control does not mean a fully constrained structure. Similar to biomolecules, the combination of flexible macromolecules and self-assembly principles is a powerful strategy for preparation of molecules with well-defined but *switchable shape* [23].

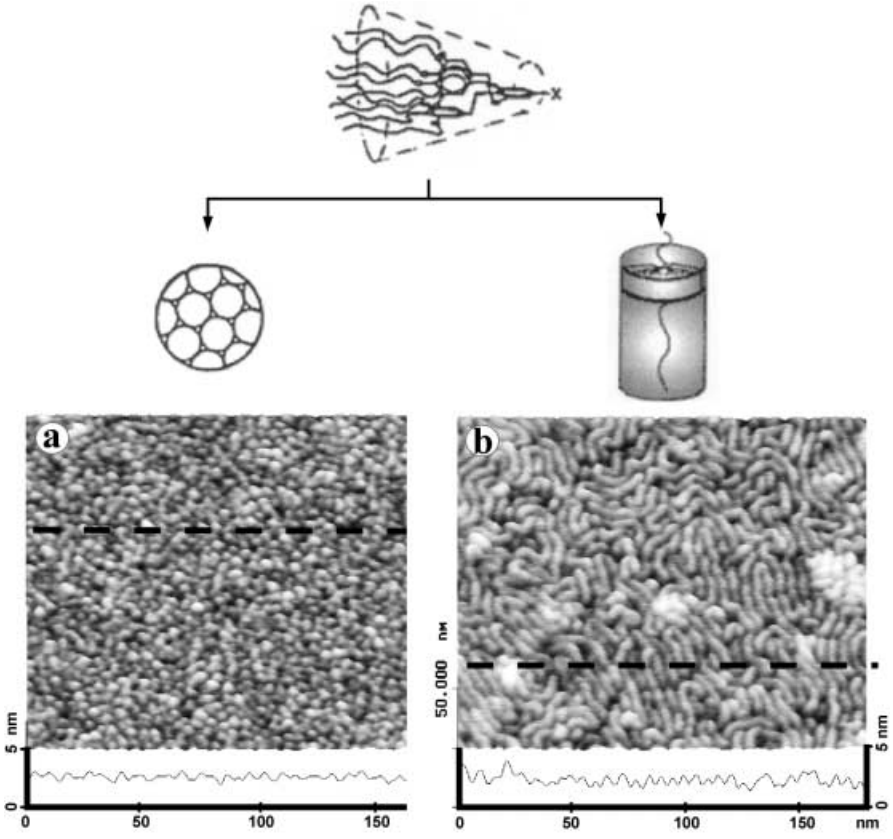

Fig. 6a,b. Height micrographs obtained by tapping mode SFM from monolayers of: **a** spherical; **b** cylindrical molecules adsorbed on mica [84]. Top: self-assembly of monodendron side groups into spherical and cylindrical supramolecular dendrimers. The process depends on the degree of polymerization of the polystyrene main chain

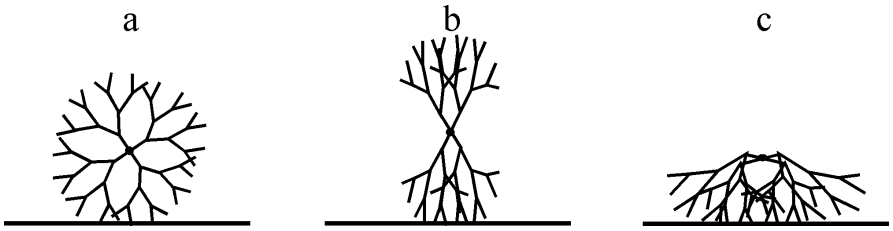

Fig. 7a–c. Different conformations of a dendrimer molecule depending on the interaction of the branches with the substrate: **a** strong repulsion between branches + weak attraction to the substrate; **b** strong attraction between branches + weak attraction to the substrate; **c** strong repulsion between branches + strong attraction to the substrate

In the following we focus on molecules that can adopt their shape in response to intermolecular and surface forces. In the case of a centrosymmetric dendrimer that is in contact with a flat substrate, a few plausible conformations can be envisaged depending on the interplay between the intramolecular and surface forces (Fig. 7).

Such structural variations have been observed experimentally for carbosilane dendrimers differing in branching density and chemical structure of the end groups [72–77]. Figure 8 depicts the chemical structure of three carbosilane dendrimers with different terminal groups – CH_3, OH, and CF_3. At room temperature all three dendrimers are well above the glass transition temperature and exhibit liquid behavior ($\eta \sim 1$ Pa·s). In spite of the lack of hardness and the rather weak adsorption of the carbosilane dendrimers, it became possible to visualize single molecules and even monitor the spreading of the dendrimer fluids on solid surfaces by tapping mode SFM. The intermittent scanning allows one to minimize lateral forces and reduce normal forces and liquid droplets could also be scanned, retaining their equilibrium shape [72–74, 146, 147].

Figure 9 shows an SFM image of the carbosilane dendrimer 1 in Fig. 8 with CH_3 end groups. Black spots represent small holes in the glass substrate, light spots represent the single dendrimers. In agreement with a similar study on hyperbranched macromolecules [95] and other studies on well defined dendrimers [96–103], the height of the adsorbed particles was more than two times smaller than the lateral dimensions. This confirms flattening of the dendrimer conformation due to interaction with the substrate [90].

In contrast to solid dendrimers [71, 84, 88], molecular resolution was not achieved for a closed film of the carbosilane dendrimers. However, one could extract structural information about the molecular conformation from the film thickness and wetting edges on a solid substrate and from surface pressure/area

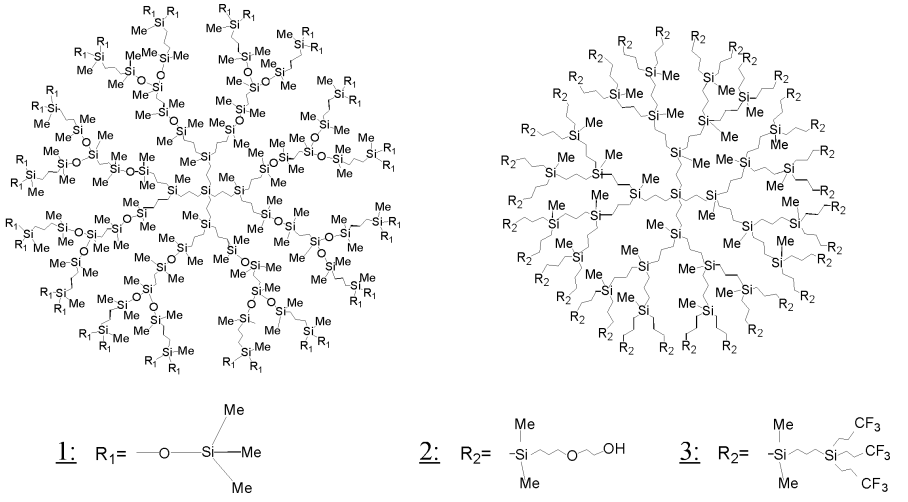

Fig. 8. Carbosilane dendrimers with different branch ends prepared by A. Muzafarov et al. [7]

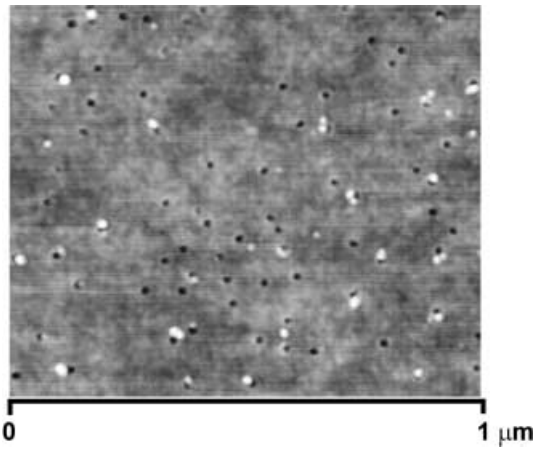

Fig. 9. SFM micrograph of single carbosilane dendrimers on glass [72]

isotherms on water. In the first case, the liquid dendrimer was cast onto either mica or highly oriented pyrolytic graphite (HOPG) and allowed to equilibrate [72, 73]. The spreading process was monitored by SFM at different stages starting from liquid droplets to a solid-like adhering film. The Langmuir experiment was focused on the reversed process, i. e., lateral compression of a monolayer to a thick film [74]. Both experiments demonstrate how the molecular structure responds to variation of the terminal groups and reduction of the surface area available for each molecule.

Owing to their liquid nature, dendrimers spread slowly on a flat surface of mica, glass, or pyrolytic graphite to yield either monolayer or double layer films. The film structure exhibited strong dependence on the branch ends. Carbosilane dendrimers with CH_3 end groups resulted in thin films with a uniform thickness of 4.5 nm consisting of two monolayers (Fig. 10). Molecular layering indicates strong segregation and little interpenetration of the dendritic molecules. The fact that the thickness corresponds fairly well to the diameter calculated for the undisturbed globular conformation demonstrates that within the closed film the dendritic carbosilanes tend to retain their globular conformation (Fig. 7 a). The same behavior was observed for carbosilane dendrimers with CF_3 end groups [75].

When the end groups of the dendrimer carried a primary alcohol group, monolayers were formed more quickly over large areas. In spite of the similar molecular weight, the layer thickness was however reduced to about 1 nm compared to 2.4 nm for the trimethylsilyl terminated dendrimers. Thicker films of dendrimer 2 in Fig. 8 demonstrated autophobic dewetting of the monolayer surface (Fig. 11). Apparently the specific interaction of the terminal groups promoted adsorption of the molecules on the mica substrate and enforced a transition of the molecular conformation. By this means, the more hydrophobic inner segments get exposed to the air interface, causing the autophobicity.

The experimental observation is confirmed by molecular dynamics simulation of carbosilane dendrimers [77] on a polar substrate (Fig. 12). The interac-

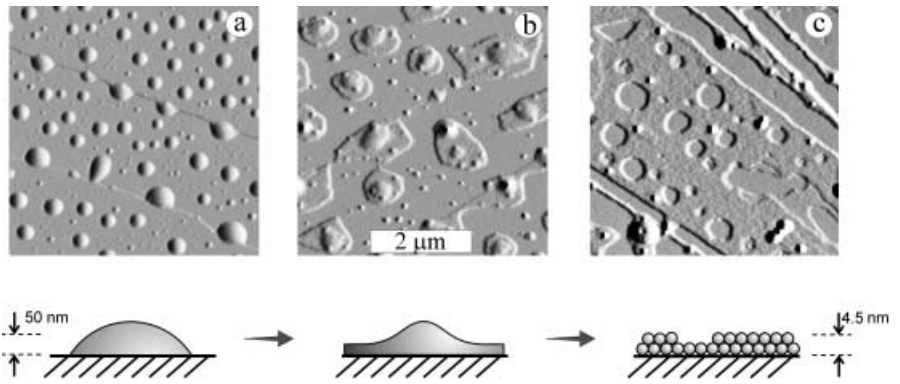

Fig. 10 a–c. SFM micrographs demonstrate wetting of HOPG by carbosilane dendrimers [72]: **a** initially, droplets with a contact angle of 8° were observed; **b** after 1 month at 23 °C, the droplets spread and formed islands with a spherical cap providing a reservoir for spreading; **c** after 20 min at 150 °C, lamellae, mostly bilayers with a thickness of about 4.5 nm, were formed. Within small areas single layer films are also observed with a thickness of 2.4 nm

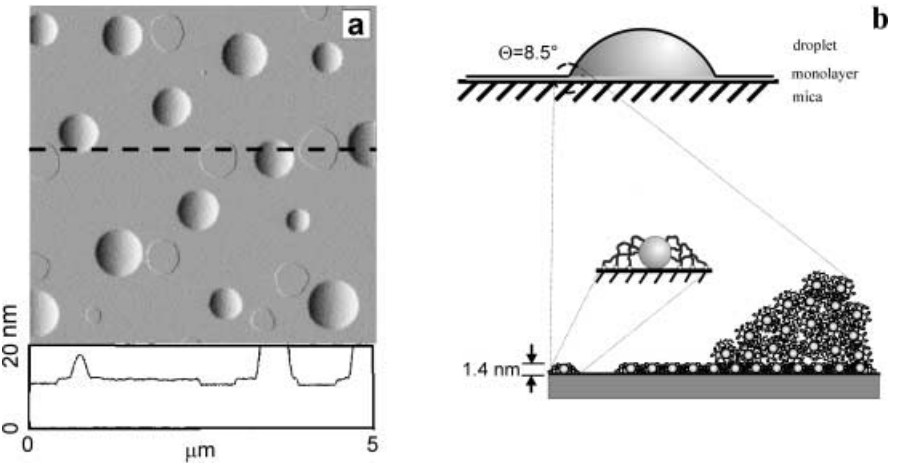

Fig. 11 a, b. Autophobic wetting of mica by carbosilane dendrimer with OH end groups [73]

tion of the terminal groups reoriented the branches towards to the surface and caused flattening of the molecules [148].

Complementary information about the interfacial conformation of the carbosilane dendrimers was obtained from π-A isotherms measured during compression of molecular films at the air/water interface [74]. The full reversibility of the isotherm in Fig. 13 a indicated that the experiment was done under equilibrium conditions, and that the data give direct evidence on the phase behavior. Two transitions, marked by I and II in Fig. 13 a, were observed for the OH terminated carbosilane dendrimer (dendrimer 2 in Fig. 8). The first transition (I) was

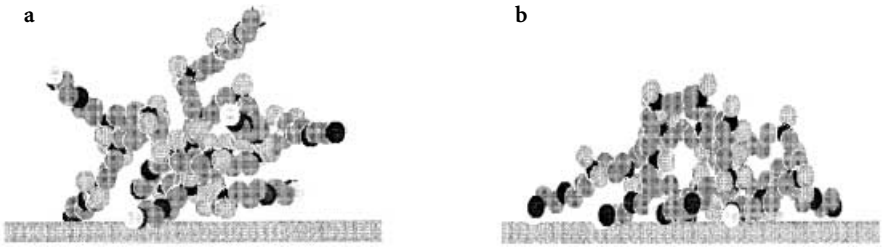

Fig. 12a,b. Molecular dynamic simulation of carbosilane dendrimer with polar OH branch ends on: **a** neutral; **b** polar substrates [148]

assigned to formation of a closed monolayer of the molecules in the spider-like conformation. The second transition (II) in the range between 650 Å^2 and 350 Å^2 is explained by a conformational change within the monolayer from the spider to a more globular and ultimately dumbbell shape (Fig. 13b). This conformational change is caused by partial desorption of the OH-end groups from the water surface. Compression beyond 350 Å^2 occurred at a constant pressure, as it is typical for an isotropic liquid film.

In contrast to the uniform dendrimer, a polydisperse hyperbranched polymer with OH-terminal groups showed only one transition corresponding to the collapse from the monolayer of flatly spread molecules to a disordered liquid. Dendrimer 1 is similar to dendrimer 2 in Fig. 8, except the difference in branch ends (CH_3 vs OH), did not spread and exhibited no structural transitions upon compression.

The interpretation of the Langmuir experiments with the carbosilane dendrimers is supported by the results of molecular dynamics simulation. Figure 14 shows snapshots of a dumbbell-like conformation of carbosilane dendrimers observed during lateral compression of a dendrimer monolayer on a polar sub-

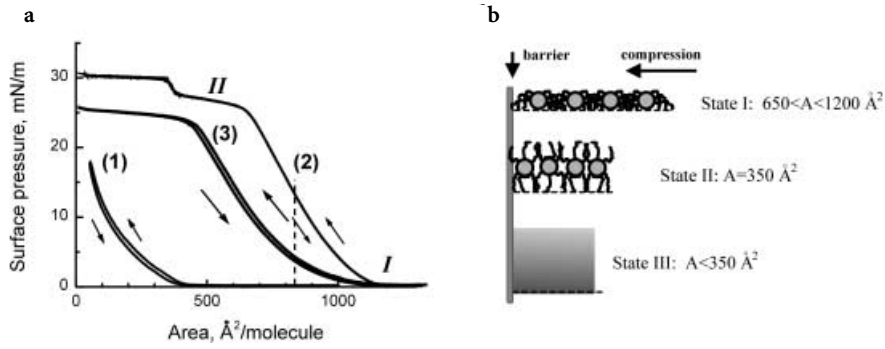

Fig. 13a,b. **a** Surface pressure – film area isotherms of (1) dendrimer 1, (2) dendrimer 2, and (3) hyperbranched polymer with OH end groups [74]. **b** Schematic interpretation of the phase transitions from a dense monolayer (I) via a reoriented monolayer (II) to a thick liquid film (III)

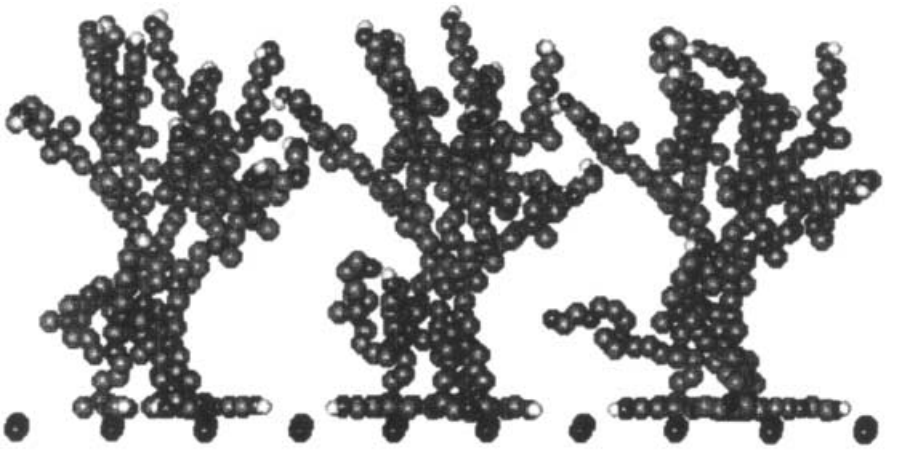

Fig. 14. Snapshot of MD computer simulation of a monolayer of carbosilane dendrimers with OH end groups upon lateral compression on a polar surface [148]

strate. The original spider conformation at low surface pressure was shown in Fig. 12b.

In line with the results described so far is a report on the shape transformation of dendrimers that were adsorbed on gold [98]. A transformation from an oblate to a prolate configuration was affected by competitive adsorption of alkanetiols that reduced the surface area available per dendrimer (Fig. 15).

Switching between two distinct conformations can also be observed for other types of soft, branched particles. For example, (poly)styrene-*b*-(poly)-4-(*N*-vinylpyridinium iodide) diblock copolymers were shown to form a regular monofilm of micelles when spread on water from a solution in $CHCl_3$ [149] (Fig. 16b). The block copolymers aggregate to micelles with a polystyrene core and a poly(*N*-alkylpyridinium iodide) corona. Due to the interaction of the pyridinium ions with the water phase, the polypyridinium gets adsorbed in a two-dimensional conformation with the *n*-alkyl groups pointing to the air. In this case a distinct phase transition was also observed upon lateral compression as the corona chains get desorbed from the water/air interface (Fig. 16a). The transition was particularly pronounced in the case of longer chains, i.e., *n*-octyl pyridinium groups. The cooperative desorption/collapse is consistent with recent X-ray reflectivity data [150].

Fig. 15a,b. a Oblate configuration of adsorbed dendrimers in a dense monolayer. **b** The prolate configuration of dendrimers was obtained by adsorption from solution containing alkanetiols molecules. Redrawn after [98]

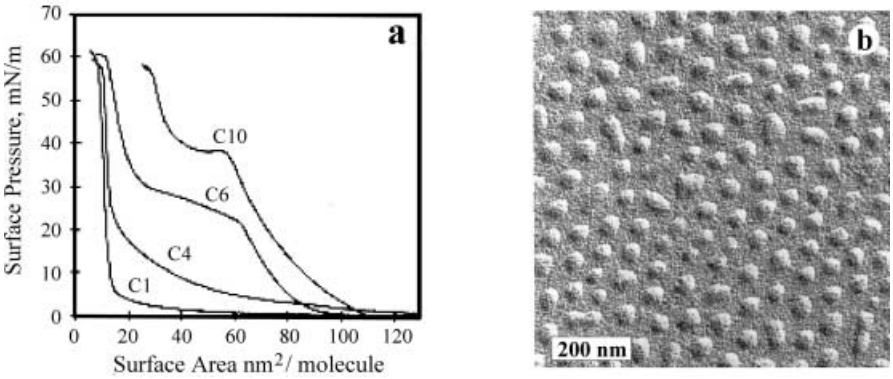

Fig. 16a,b. **a** Surface pressure – area/molecule isotherms of Langmuir films of $(PS)_{260}$ $(RPVP^{+}I^{-})_{240}$, where the P4VP block was quaternized with different *n*-alkyliodides R = C_1, C_4, C_6, C_{10}. **b** Metal shadowed TEM micrographs of the LB films of $P(S_{260}$-b-VP_{71}/C10I) deposited on a carbon-coated surface at 2 mN/m from a pure water surface [149]

All these observations indicate that these conformational transformations depend strongly on the branching structure (regular vs irregular) and the nature of the end groups. The transformation observed in the Langmuir experiment can occur smoothly, or through a conformational order-disorder transition. A critical behavior as observed in the experiment can occur due to the fact that the adsorption of the end groups is counterbalanced by an entropy penalty due to the extension of the branches. Visualization of the conformational transition of individual molecules would allow one to confirm the interpretation given so far. This has not been possible with the small dendrimers. However, corresponding studies on worm-like brush molecules allowed one to observe a conformational transition directly (Sect. 3.3).

2.3
Microphase Segregation and Crystallization

The fact that hyperbranched macromolecules can flatten and at the same time remain strongly segregated without noticeable interpenetration can be exploited to switch surface properties and to create lateral nanopatterns when core-shell molecules are employed, i. e., consisting of different monomers in the core and shell. Preferential adsorption of the shell branches can result in monolayers with a patterned structure. Preparation of arborescent graft co-polymers consisting of a polystyrene core and poly(2-vinyl pyridine) shell was described by M. Gauthier [13, 151]. Adsorption of these molecules from a non-selective solvent onto a polar substrate like SiO_2 or GaAs resulted in a microphase separated structure where protruding globuli of PS are surrounded by a thin film of PVP [89] (Fig. 17). Due to their rather uniform molecular size, the molecules were ordered in a distorted hexagonal lattice. The phase separated structure is covalently fixed and thus less dependent on the substrate type.

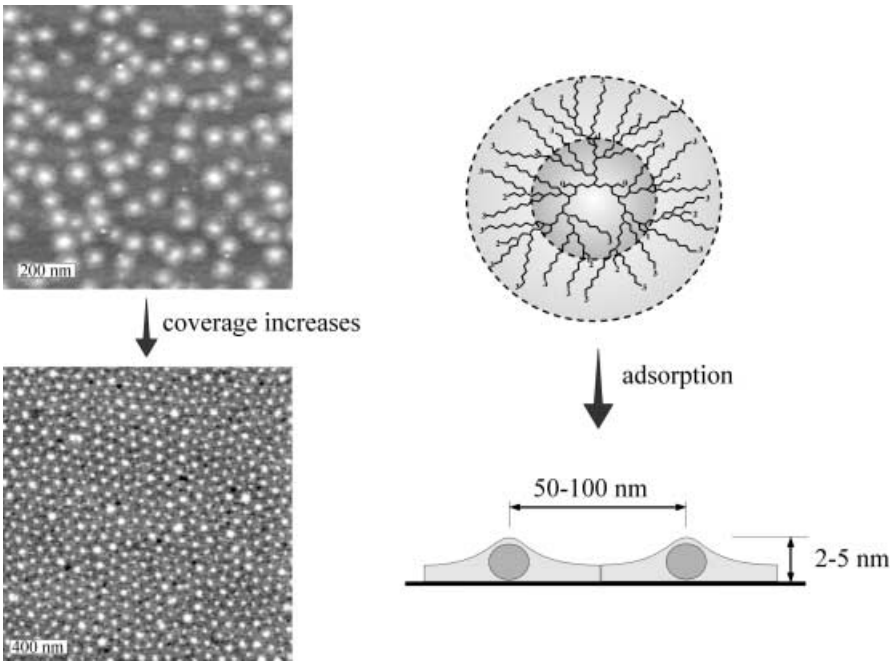

Fig. 17. Monolayer of arborescent graft macromolecules consisting of a polystyrene core and poly(2-vinylpiridine) shell. Microphase separation between the blocks and strong interaction of the PVP block with mica resulted in lateral arrangement of the PS and PVP domains [89]

Another peculiar aspect of the flexibility of dendritic molecules is the intermolecular ordering upon crystallization. Dendritic polyethylenes can be prepared by hydrogenation of arborescent graft polybutadienes [152]. Figure 18a shows an SFM micrograph of arborescent graft polyethylene molecules of 2nd generation adsorbed from a dilute solution in hot xylene on mica. The micrograph depicts a grainy structure of a thin film, which is uneven in thickness and coverage. Irrespective of the macroscopic appearance of the film, the grains were uniform in size of about 50 nm, which is consistent with the diameter of a single molecule. After annealing at 150°C, the film structure changed dramatically (Fig. 18b). The spherical molecules of polyethylene recrystallized into fibers with a defined thickness of ca. 50 nm. From the fact that this value is consistent with the molecular diameter in Fig. 18a, the fibers in Fig. 18b may be assigned to linearly aligned molecules.

This reorganization process is schematically shown in Fig. 19. Similar to other arborescent graft polymers [71], adsorption of the polyethylene molecules gives thin films in which each molecule segregates into individual particle of a spherical shape (Fig. 19a). The spheres do not overlap and interpenetrate only partially. Apparently the evaporation process was too fast to allow ordering of the molecules via crystallization of the polyethylene branches. Annealing at temperatures above the melting point of linear polyethylene enabled significant reorganization of the molecules in such a way that, upon subsequent cooling, the

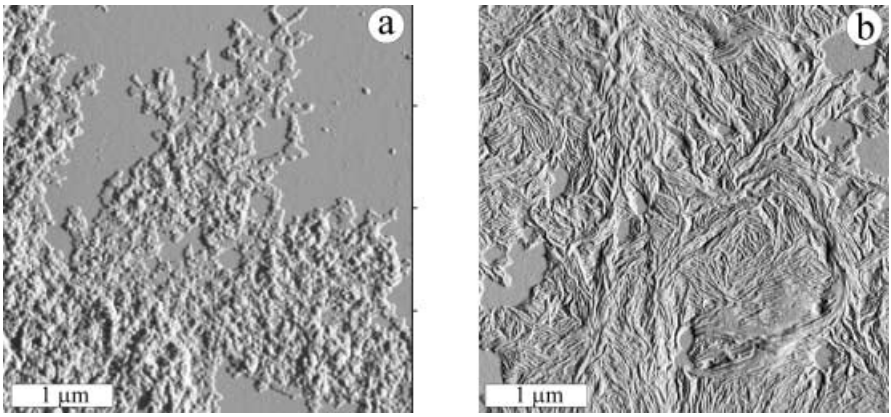

Fig. 18a,b. Amplitude micrographs of arborescent graft polyethylene on mica obtained by tapping mode SFM after: **a** adsorption from a dilute solution in hot xylene; **b** annealing for 24 h at 150°C

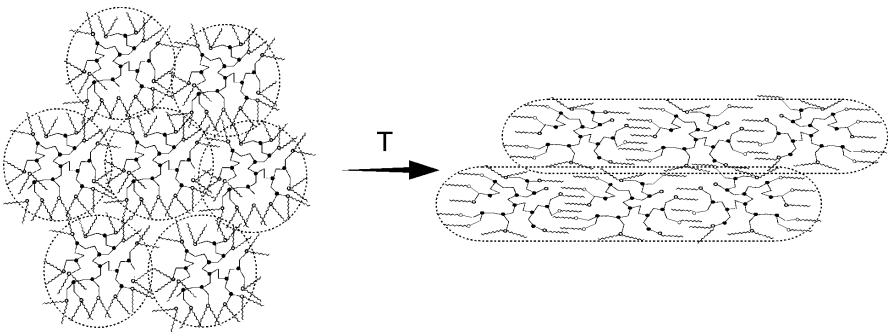

Fig. 19. Recrystallization of arborescent graft polyethylenes from dense packing of spheres to fibers of linearly aligned molecules upon annealing

branches were able to crystallize. Such crystallization is rather constrained because the center-symmetric distribution of the branches impedes uniaxial crystallization of the PE chain segments. This is similar to the situation of dendrimers containing liquid crystalline moieties as terminal groups [104].

3
Brush Molecules

3.1
Brush Molecules With a Flexible Backbone

Dense substitution of side chains along a main chain gives brush-like macromolecules such as "hairy rods" [15], worm-like brushes [16–21] or, in the case of the side chains, further branching and monodendron jacketed chains [22–26].

Brushes with long side chains can be synthesized by polymerization of macromonomers [117–119] or by grafting of the side chains to [16–20] or from [21] a main chain. In contrast to globular dendrimers, these molecules have an anisotropic primary structure and experience bending or coiling of the molecular contour. Depending on the relative stiffness of the main and side chains, one may distinguish four types of molecular cylinders (Fig. 20).

If the backbone as well as the side chains consist of flexible units, the molecular conformation arises out of the competition of the entropic elasticity of the confined side chains and the backbone [153–155]. In this case, coiling of the side chains can occur only at the expense of the stretching of the backbone. In addition to the excluded volume effects, short range enthalpic interactions may become important. This is particularly the case for densely substituted monodendron jacketed polymers, where the molecular conformation can be controlled by the optimum assembly of the dendrons [22–26, 156]. If the brush contains ionizable groups, the conformation and flexibility may be additionally affected by Coulomb forces depending on the ionic strength of the solvent [79, 80].

In a bad solvent collapse of the expanded conformation can occur in two principally different ways (Fig. 21):

1. Axial contraction leads to cylinders with a length shorter than the contour length of the fully stretched main chain [81].
2. At the same moment, microsegregation of the pinned chains may result in a density modulation along the cylinder axis [82].

Figure 22 represents a theoretical phase diagram obtained from a scaling analysis for a stiff backbone with flexible side chains taking into account elastic and surface contributions to the free energy [82]. The diagram considers the states of a molecular brush under poor solvent conditions ($x \equiv N^{1/2} h^{-1}$, $z \equiv N^{1/2} |\tau|$) as a

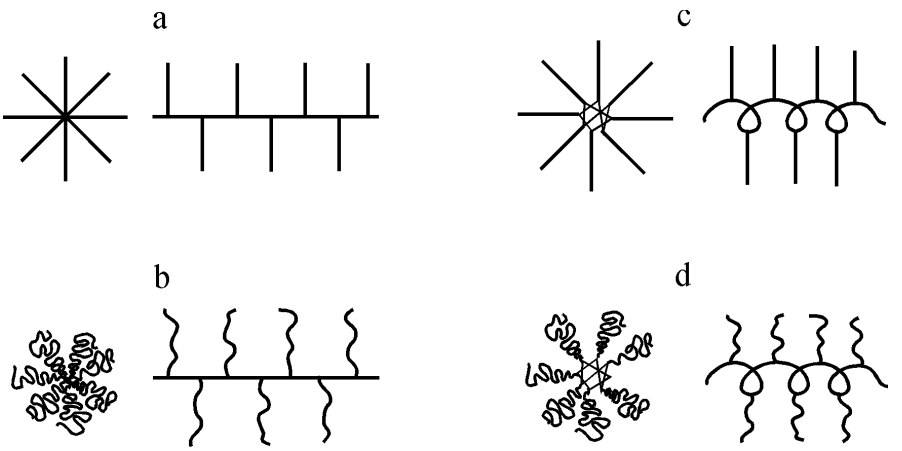

Fig. 20a–d. Four types of cylindrical brushes with different flexibility of the side chain and the main chain: **a** stiff backbone – stiff side chains; **b** stiff backbone – flexible side chains; **c** flexible backbone – stiff side chains; **d** flexible backbone – flexible side chains

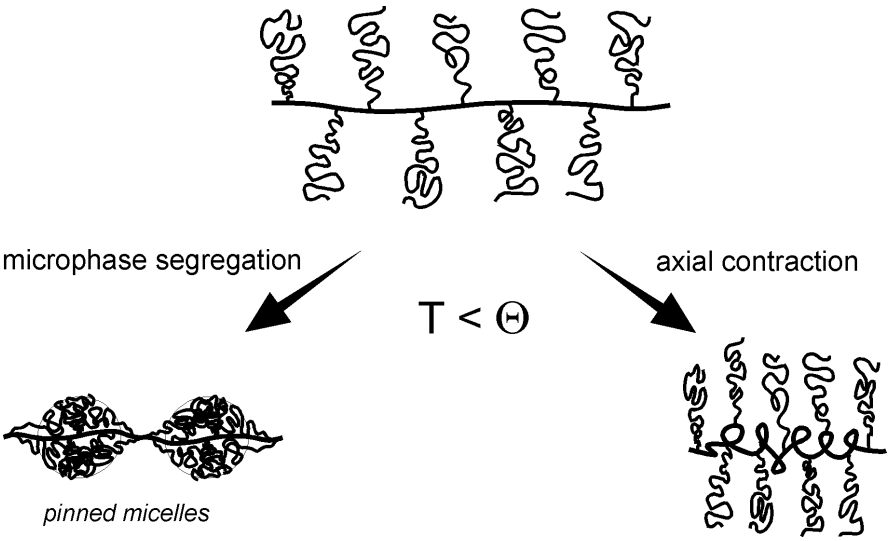

Fig. 21. Microphase segregation and axial contraction of molecular brushes [82]

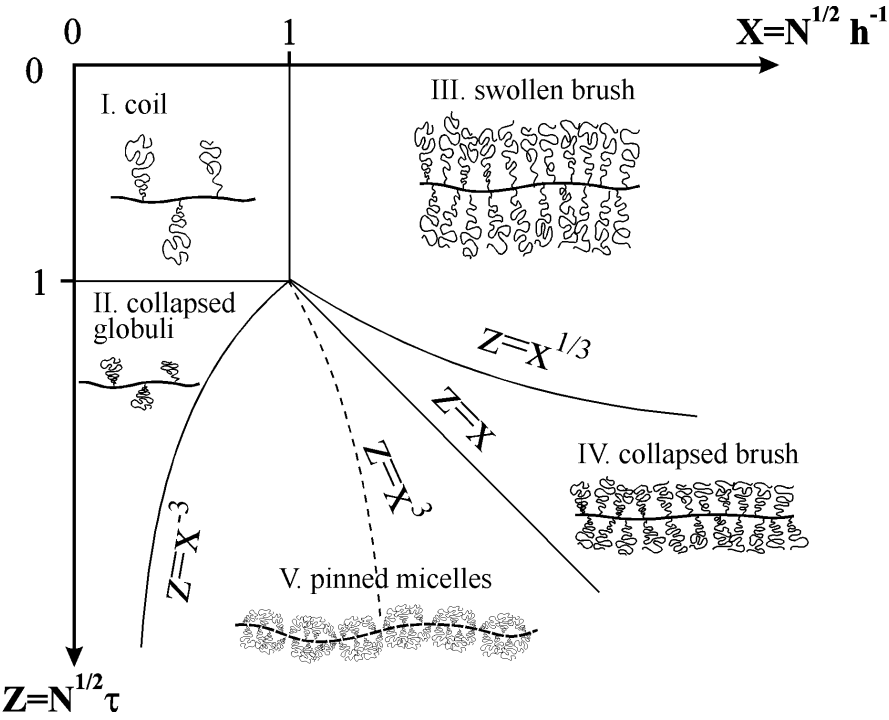

Fig. 22. Diagram of states of a molecular brush as function of solvent quality $z = N^{1/2}|\tau|$ and the grafting density $x = N^{1/2}\, h^{-1}$ under poor solvent conditions [82]

function of the grafting density h^{-1} (h is the axial distance between neighboring chain), the length of the side chains N, and the temperature below the Θ-point $\tau = (T - \Theta)/\Theta$. At low grafting density, the side chains have a Gaussian coil conformation (region I) or collapse to globuli pinned to the stiff backbone (region II). At high grafting density, homogeneous and uniformly collapsed brushes are observed in regions III and IV, respectively. In order to minimize the free energy for intermediate grafting densities, the side chains segregate into globular clusters thread on the backbone (region V). The free energy of a cluster formed by ν chains grafted within a distance $L = \nu h$ can be presented as

$$\Delta F(\nu)/kT = (\nu N \tau^2)^{2/3} - \nu(N\tau^2)^{2/3} + \nu L|\tau| \quad (1)$$

where the first and second terms describe the difference in the excess interfacial energy of a cluster core and that of ν individual globules, while the third term describes the entropy changes caused by the extra extension of the side chains required for the cluster formation. Minimization of the free energy per chain, $\partial(\nu^{-1}\Delta F(\nu))/\partial\nu = 0$, gives the equilibrium aggregation number $\nu \cong N^{1/2}|\tau|^{1/4} h^{-3/4}$ and the period of the thickness modulations $L \cong N^{1/2}|\tau|^{1/4} h^{1/4}$. The thus formed undulated cylinders correspond to the "pinned micelles" in planar brushes [157–162].

Stretching of the side chains with respect to their Gaussian dimensions leads to conformational entropy losses for region III of the diagram. As a consequence, the cylindrical brush experiences an extensional axial force of entropic origin. In region IV, a negative contribution to the axial force has to be taken into account due to the interfacial energy of the collapsed brush. Thus, the free energy per side chain in a collapsed brush comprises the elastic penalty for extension of a side chain, excess free energy of the interface, and the free energy of excluded volume interaction, respectively:

$$\frac{F}{k_b T} = \frac{R^2}{N} + |\tau| R^2 h - r^2 N \quad (2)$$

The brush thickness and the axial distance per side chain are interrelated due to the condition of fixed monomer density $\sim|\tau|$ in the collapsed brush as $R \cong \sqrt{N/|t|h}$. The axial tension is given by

$$\frac{f}{k_b T} = \frac{dF/k_B T}{dh} \cong (|\tau| h^2) - |\tau|^{\frac{3}{2}} (N/h)^{\frac{1}{2}} \quad (3)$$

The degree of stretching of side chains and the extensional force on the backbone decrease with decreasing grafting density and decreasing solvent quality. In the range $x^{1/3} < z < x^{3/5}$ the axial tension is positive, i.e., the entropy losses in the extended side chains predominate over surface tension, while in the range $z > x^{3/5}$ the axial tension becomes negative. An additional negative tension in the backbone occurs in region V of the diagram due to the extended "legs" of the clusters.

In the case where the macromolecular backbone is flexible, the axial tension may affect the molecular conformation. Flexibility of the main chain can be realized by bond rotational isomerism and minimizes the entropic penalty caused by the stretching of the main chain. As depicted in Fig. 21 on the right:

1. Backbone flexibility enables axial shrinkage of the worm-like macromolecule compared to the contour length of the main chain.
2. The undulations can vanish as the distance between the grafting points will decrease.
3. On large scales, the whole brush can collapse into a globule.

Tapping mode SFM was employed to visualize cylindrical brushes of polymethyl-methacrylate as single species laying flat on a solid substrate (Fig. 23a). Light scattering studies in solution allowed a complementary characterization of the size and conformation of the molecules in the diluted state. Two important observations have been made, that corroborate the theoretical predictions:

1. The length of the worm-like macromolecules in solution as well as in the dry state, is significantly shorter than the contour length of the backbone.
2. The dry molecular brushes adsorbed on mica appear to exhibit undulations along the molecular contour (Fig. 23b).

Table 1 summarizes the experimental data obtained for PMMA brushes [81, 82]. A length per repeat unit of the backbone $l_{SFM} = 0.076$ nm was measured directly by SFM. The value is three times shorter than the monomer length of a completely stretched backbone in an all-*trans* planar conformation ($l_{max} = 0.25$ nm). Static light scattering in solution also yielded a length per monomer $l_{sol} = 0.081$ nm that was considerably shorter than in the all-*trans* conformation [81]. The axial contraction is indicative of a significant flexibility on the short length scale, while the molecules are relatively stiff on the long length scale characterized by a persistence length of 60 nm. Two characteristic length scales were also observed by Monte Carlo simulation studies [155].

Although the observed undulations are consistent with the scaling picture, it is somewhat in contradiction to the axial contraction. On the other hand, axial contraction in molecular brushes can be limited, first because the backbone segments have limited flexibility and second because of hard core repulsion near the backbone or cylinder axis. In contrast to loose comb-like polymers [153], an

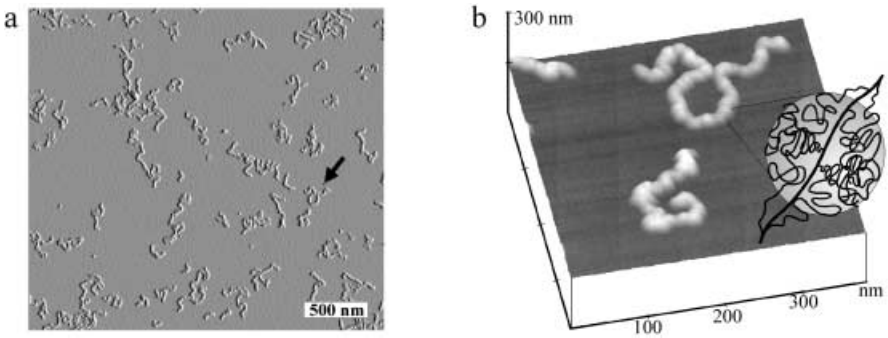

Fig. 23 a, b. **a** An amplitude micrograph of PMMA brushes adsorbed on mica from a dilute solution in chloroform measured by tapping mode SFM. **b** Three-dimensional SFM micrograph of single brush-molecules indicated by the arrow in (**a**). The axial modulations have been explained by phase segregation of the side chains into nodules (insert) [82]

Table 1. Molecular properties of cylindrical brushes of polymethylmethacrylate

Property	Value	Method
$\langle M_0 \rangle$ (side chain)	2410 g/mol	MALDI-TOF
$\langle M_w \rangle$ (brush)	1.4×10^7 g/mol	SEC-MALLS
M_w/M_n (brush)	1.25	SEC
λ (persistence length)	60 nm	SEC-MALLS
$\langle DP_w \rangle$ (main chain)	5809	$\langle DP_w \rangle = M_w/M_0$
$\langle L_w \rangle = \frac{\sum_i N, L_i^2}{\sum_i N, L_i}$	443 nm	SFM
$\langle L_w \rangle / \langle L_n \rangle$	1,38	SFM
$l_{SFM} = \frac{\langle L_w \rangle}{\langle M_w \rangle} m$	0.076 nm	SFM (in dry state)
l_{sol}	0.081 nm	SEC-MALLS (in solution)

axial tension of the order of kT per monomer length is sufficient to reach the limiting extension of the densely grafted backbone. Rather independently of solvent strength, the extended conformation is weakly perturbed by small fluctuations around the extended contour. Indeed, the experimental observation on the PMMA brush demonstrated small difference in the axial length in the dry state and in solution (Table 1).

It must be noted that the end-to-end distance of the brushes is also affected by adsorbing them flatly on a hard wall. In monolayers ($d = 2$) the molecules are constrained to two dimensions which favors extension and parallel alignment [163]. This is particularly pronounced if the side chains get tightly adsorbed and will be discussed in detail below. Yet even in the case of a weak interaction with a substrate, the chains are extended. In contrast, in thick films the individual chain can adopt a less straight conformation by transition between "layers" in the z-direction. Figure 24 clearly demonstrates the difference in the ordering of cylindrical brushes of polystyrene depending on the film thickness [78].

3.2
Monodendron Jacketed Linear Chains

It has been noted already that monodendron jacketed polymers are distinguished from brush molecules with flexible side chains by the even higher steric demand of the side chains and their ability to assemble to defined superstructures [22–26]. Scheme 1 depicts two examples of a monodendron jacketed macromolecule: 14-ABG-PS carries three monoalkoxybenzylether groups per monomer unit, whereas the stronger branched 3,4,5-t-3,4,5-PS monomer is substituted by three trisalkoxybenzylether groups and has a two times larger molecular mass of 2140 g/mol. The tapered shape and a certain amphiphilicity of the monodendrons provide additional factors favoring the extension of the main chain due to their self-assembly into columns [156]. Depending on the degree of polymerization and the degree of branching of the side groups, the monoden-

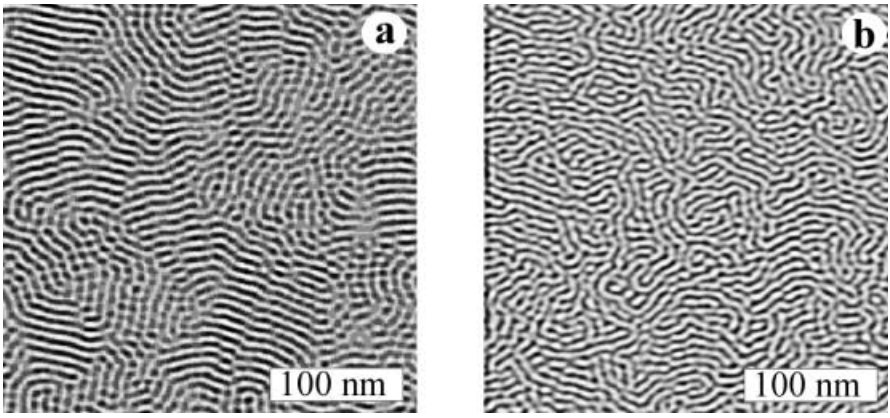

Fig. 24 a, b. Micrographs of: **a** a monolayer; **b** thick film of cylindrical brushes of polystyrene on mica. The order is significantly higher in the monolayer film [78]

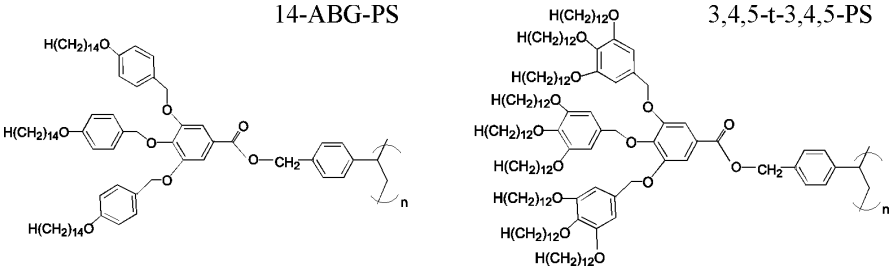

Scheme 1

dron jacketed polymers were shown to undergo ordering into a hexagonal columnar or cubic mesophase [23, 84].

When deposited on a surface of highly oriented pyrolytic graphite (HOPG), these molecules are depicted by SFM as 5 nm thick threads aligned parallel to the substrate plane (Fig. 25 a). Because of the regular adsorption of the alkyl tails on graphite, the segments of 14-ABG-PS get aligned along the main axis of the HOPG-surface [87]. This was not the case for the sterically crowded 3,4,5-t-3,4,5-PS. The attained resolution of the chain ends enabled direct measurement of the molecular length [85, 86]. In combination with the independently determined molecular weight (GPC and SLS), the chain length per repeat unit was evaluated as $l_{SFM} = L_n/DP_n$, where DP_n is the number average degree of polymerization. In agreement with the X-ray periodicity of the columnar packing in the hexagonal mesophase and the density of this compound, the monomer length of 14-ABG-PS $l_{SFM} = 1.2$ Å turned out to be almost two times less than the length $l_c = 2.5$ Å expected for a fully extended main chain in an all-*trans* planar zigzag conformation. In contrast, 3,4,5-t-3,4,5-PS with the sterically more demanding side groups demonstrated almost complete stretching of the carbon backbone approaching the all-*trans* planar conformation (Table 2).

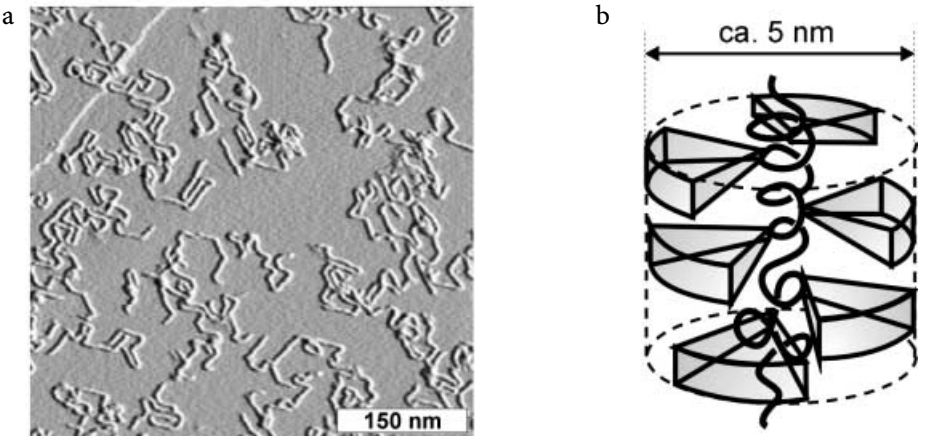

Fig. 25 a, b. **a** SFM-micrograph of single 14-ABG-PS molecules on HOPG. **b** Suggested conformation of monodendron jacketed linear chains [85]

Table 2. Molecular dimensions and length per monomer unit of 14-ABG-PS, 3,4,5-t-3,4-PS, and 3,4,5-t-3,4,5-PS determined from SFM micrographs and SEC- and SLS data [86]

Polymers	14-ABG-PS	3,4,5-t-3,4-PS	3,4,5-t-3,4,5-PS
M[a], g/mol	1194	1612	2140
M_w[b], 10^6 g/mol	1.1	1.2	2.0
M_w/M_n	2.6	2.6	2.2
a[c], Å	52.1	41.4	47.7
l_{XDR}[d], Å	0.8	1.8	2.0
l_{SFM}[e], Å	1.2	1.9	2.3

[a] Molecular weight of the monomer unit.
[b] Molecular weight of the polymers determined by size exclusion chromatography in tetrahydrofuran using a light scattering detector.
[c] Column diameter determined by X-ray diffraction measurement in the columnar mesophase.
[d] X-ray spacing along the column axis per repeat unit of the main chain as determined for the columnar mesophase in bulk.
[e] SFM length of the cylindrical molecules per repeat unit of the main chain determined from the SFM micrographs as $L_{SFM} = M \times L_n/M_n$.

The axial contraction compared to the contour length can occur via local disordering or coiling or twisting (Fig. 25b). Regular helix formation may not be expected because of the stereo irregularity of the backbone and was also not observed by X-ray diffraction upon cooling the mesophase [164]. Indirect evidence for a twisted backbone conformation was found when the monodendron jacketed polystyrenes were imaged on mica [86]. In this case, the molecules were adsorbed randomly without interfacial ordering effects. Some molecules in Fig. 26a were twisted to supercoils called plectoneme (from the Greek meaning "braided string"). Plectoneme formation represents a way of releasing torsional stress [165, 166]. Due to the intramolecular crossings, the dense monolayer in

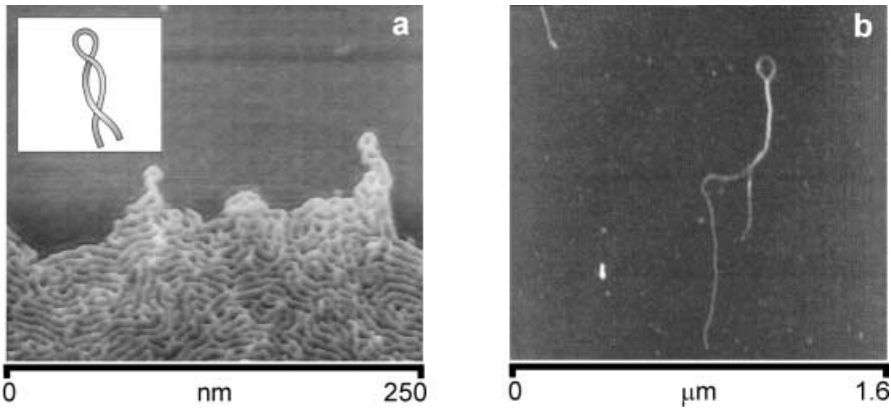

Fig. 26a,b. High resolution height SFM-micrographs of: **a** 14-ABG-PS on mica [86]; **b** Twisted ribbon structure of polypeptide β-sheets [167]. The plectoneme conformation is caused by the backward folding of the torsionally stressed molecules [86]. Insert in (a) depicts a plectoneme supercoil

Fig. 26a resembles a network or felt-like structure. Figure 26b shows a similar conformation observed for a polypeptide [167].

To the best of our knowledge, the supercoil conformation of the monodendron jacketed polystyrene is one of the first observations of a defined tertiary structure in synthetic polymers. The plectoneme conformation could be caused by underwinding or overwinding of a backbone from its equilibrium state [168]. Quick evaporation of the solvent certainly can cause a residual torsion in the molecule as it contracted in itself. Unlike macroconformations of biomolecules, where the tertiary structures are often stabilized by specific interactions between side groups, the supercoil of the monodendron jacketed polymers is metastable. Eventually, annealing offered a path for the stress relaxation and allowed the structural defects to heal [86].

3.3
Interfacial Ordering and Conformational Transitions

It has been mentioned in Sect. 3.1 that the molecular conformation can be altered strongly compared to that in solution if the side chains of a brush molecule are specifically adsorbed on the substrate or tend to spread on the surface to minimize the interfacial energy (Fig. 27). Moreover, the substrate changes the dimensionality of the system and breaks its symmetry [169, 170]. Depending on the interfacial interactions and distribution of the side chains we can discuss a number of distinct conformations: (a) stretched brush, (b) two-dimensional helix [170], and (c) globule state.

The structures depicted in Fig. 27 represent states where the free energy is minimized regarding different contributions. The fully stretched backbone in Fig. 27a corresponds to a maximum in interaction or surface contacts of the mo-

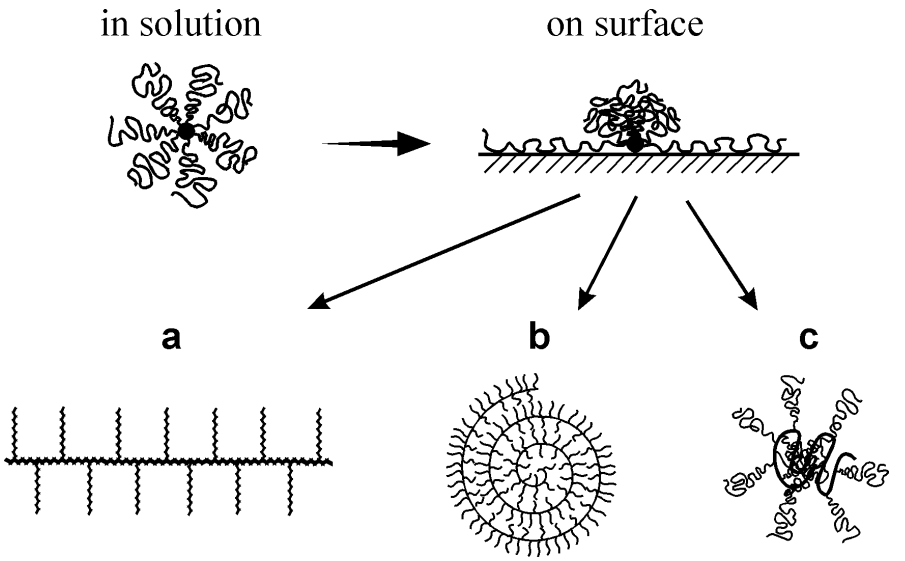

Fig. 27 a–c. Conformations of cylindrical brushes upon adsorption on a surface: **a** extended coil; **b** two-dimensional helix; **c** globule

nomer units, in particular the side chains. The spiral conformation in Fig. 27 b is characterized by a reduced contact line at the expense of the uneven distribution of the side chains to either side of the backbone. The conformation in Fig. 27 c is favored by a disordered or coiled backbone and coiling of a fraction of desorbed side chains on expense of the number of interfacial contacts.

The qualitative picture demonstrates that the interplay of intramolecular and surface forces can lead to pronounced conformational changes. In particular, this concerns the fully stretched backbone and the globular conformation. Since the free energies of these two conformations vary in different manners with the interaction strength, the brushes can undergo a transition of the critical surface pressure π_c at which the free energies become identical. The surface pressure corresponds to the gain in energy due to spreading $\pi = \gamma_1 - \gamma_{12} - \gamma_2$, which is a combination of water/air (γ_1) water/polymer (γ_{12}) and polymer/air (γ_2) interfacial energies. Such a transition may also occur upon changing of others properties of the surrounding medium, e.g., solvent quality and temperature, or under the effect of an external field. Thus, instead of variation of the interfacial energies, the number of surface contacts available per molecule or side chain can be altered by reducing or expanding the surface area per molecule as it can be done experimentally on a Langmuir trough.

This way it has been possible to observe the anticipated conformational transition by experiment. Cylindrical brushes of polybutylacrylate-graft polymethacrylate were adsorbed on the surface of water from a $CHCl_3$ solution on a Langmuir trough and studied by recording the π-A (surface pressure vs molecular area) isotherm. At different stages of compression, the monolayer was

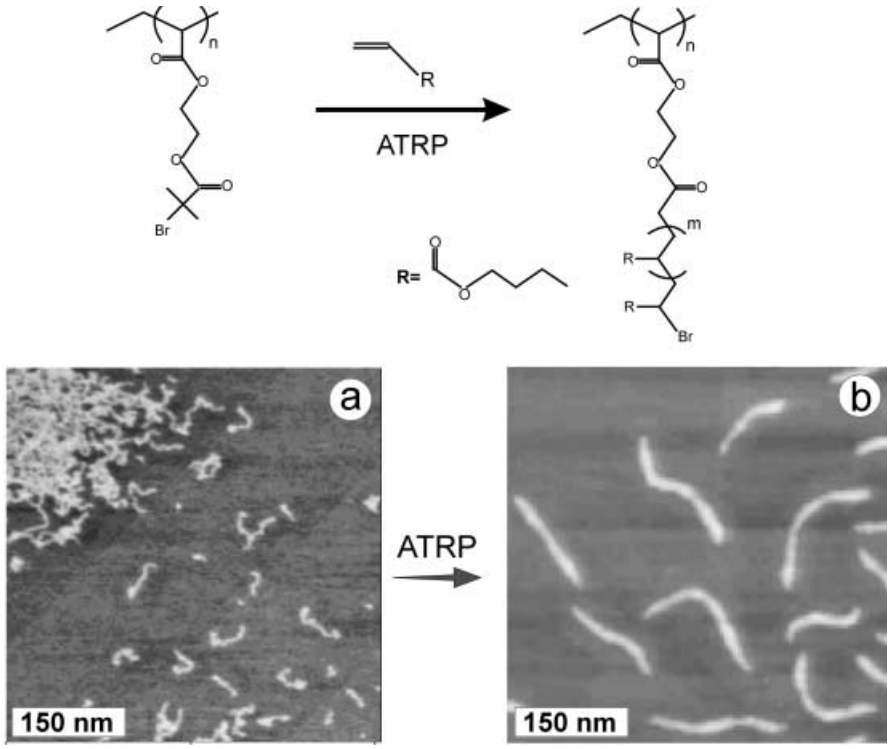

Fig. 28a,b. The synthetic scheme depicts preparation of PBA brushes by grafting from the macroinitiator using ATRP [187]. Single molecules of: **a** the macroinitiator; **b** PBA brushes adsorbed on mica were visualized by taping mode SFM. Clearly, the grafting of long side chains led to almost full extension of the backbone approaching the contour length $L = N \times 0.25$ nm

transferred onto a solid substrate (mica) for microscopic studies [83]. This experiment allowed one to monitor changes in molecular conformation at different fractions of the adsorbed monomers.

The PBA brush was chosen because of its low glass transition temperature ($T_g = -60\,°C$), which was in favor of prompt equilibration. Furthermore, *n*-butylacrylate is known to spread on the water surface [172, 173] and to adhere strongly to mica [83]. The brush molecules were presented by living radical polymerization by grafting from a multifunctional macromolecular initiator [171]. As shown in Fig. 28b, brushes in the uncompressed state are fully extended approaching a *trans* zig-zag conformation of the main chain. In contrast, macroinitiators, i.e., backbones without side chains, demonstrate a twofold contraction relatively to the contour length (Fig. 28a). Furthermore, a detailed resolution of the molecular arrangement has been possible by phase contrast SFM, which enabled clear visualization of both the backbone and side chains. The phase micrograph in Fig. 29 shows an island of several brush molecules adsorbed flatly on mica. White contours correspond to the backbone, while grayish areas in between the white threads show the hairy structure of the side chains.

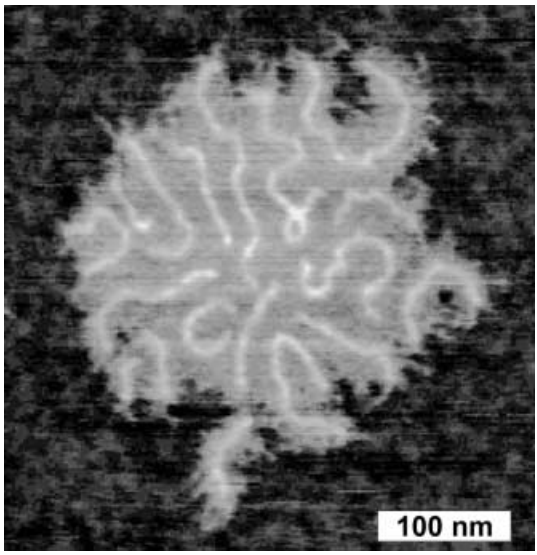

Fig. 29. The island of PBA brushes on mica was observed by tapping mode SFM. The phase image enabled clear resolution of the backbones (*white threads*) and the side chains (*gray hairs*) on the mica substrate (*black background*)

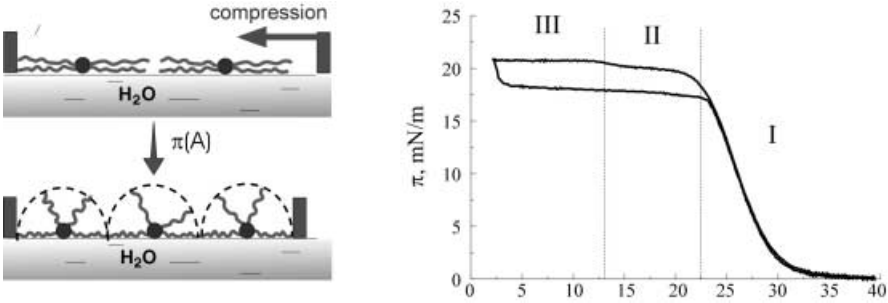

Fig. 30. *Left*: Lateral compression of a monolayer of PBA brushes on water. *Right*: Corresponding surface pressure-area isotherm measured during compression

Figure 30 presents the π-*A* isotherms for the PBA brushes spread on water. Compression of the PBA brushes was fully reversible as expected for equilibrium spreading. The isotherms can be divided onto three characteristic regions. In region I the pressure onset occurred at a surface area of about 35 Å^2/BA-monomer. Linear extrapolation of the isotherm to zero pressure gave the area $A_0 = 28 \pm 1$ Å^2, consistent to a monomer area of 27 Å^2 measured for linear PBA [172]. The pressure in the plateau region III $\pi = 21$ mN/m was similar to that of linear PBA (22 mN/m). The values indicate that practically all BA monomer units are in contact with the water surface, whereby the butyl tails are oriented towards air perpendicular to the surface. In between the expanded and the

collapsed film, the pressure increased within a broad range until a critical monomer area of 22 Å^2, at which the pressure leveled off at 19.5 mN/m. Region II corresponds to the plateau confined between 22 Å^2/BA-monomer and another inflexion point at 13 Å^2/BA-monomer.

Transfer of the surface films at distinct areas per monomer onto a mica substrate was achieved while the pressure was kept constant automatically. Figure 31 shows such a series of SFM micrographs obtained at different compression. In each micrograph the brush molecules were clearly resolved individually. At areas above 22 Å^2 the molecular cylinders retained their conformation but became packed increasingly densely until a closed film was formed. The light worm-like stripes in Fig. 31 a, b represent the brush molecules in a conformation corresponding to the cartoon in Fig. 27 a. The bright stripes mark the contour of the backbone. The space in between is occupied by the fraction of the side chains which are tightly adsorbed. The fundamental collapse of the worm-like structure predicted was observed in the transition zone between 22 Å^2 and 13 Å^2. The SFM images in Fig. 31 c – e demonstrate a significant decrease in length while at the same time the molecules appeared to become more flexible and coiled up. The round spots in Fig. 31 c – e are assigned to single molecules which collapsed to a pancake-like or nearly globular state as illustrated in Fig. 27 c. The number of chains in Fig. 31 a and number of globuli in Fig. 31 e are fairly equal. We conclude that the molecular collapse is accompanied by desorption of the side chains from the water surface and occurs in the first instance as an intramolecular collapse and only later by intermolecular aggregation as the collapsed molecules get piled up.

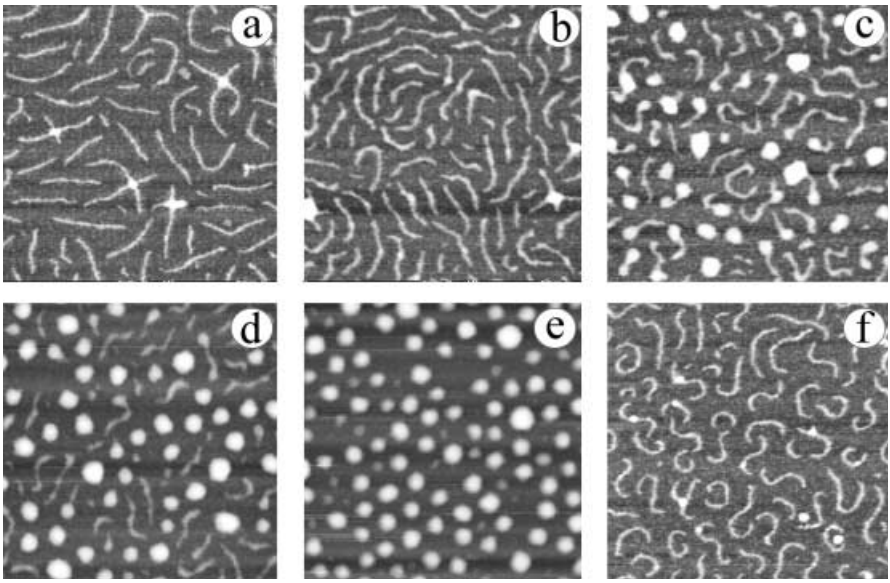

Fig. 31 a–f. SFM micrographs of monolayers of PBA brushes transferred on mica at different degree of compression: **a** 30 Å^2; **b** 23 Å^2; **c** 21 Å^2; **d** 17 Å^2; **e** 13 Å^2; **f** 30 Å^2 (after expansion)

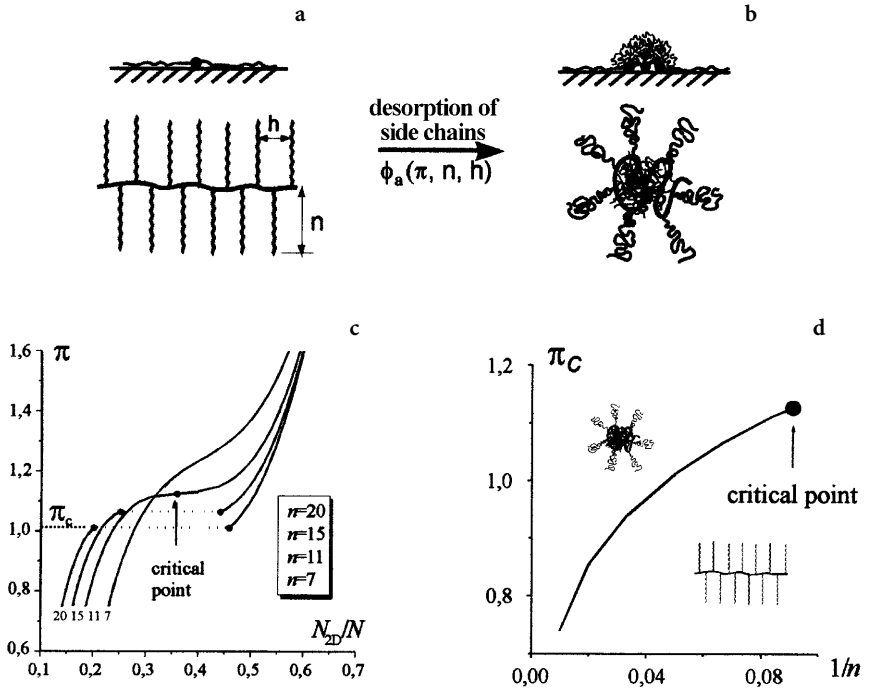

Fig. 32a–d. Phase transition: **a** from the extended coil; **b** to a globule state as found by scaling analysis [83]; **c** the transition is caused by lowering the surface pressure below a certain critical value π_c at which the fraction of adsorbed monomers $\phi_a = N_{2D}/N$ undergo discrete changes; **d** hereby, the π_c depends critically on the side chain length

The observed conformational transition is schematically summarized in Fig. 32 a, b. It has been explained by a scaling analysis considering the liquid state for the brush layer and assuming that air is a poor solvent for the side chains. An equilibrium value of the total free energy $F = F_{el}^{2D} + F_{el}^{3D} + F_s + F_{mix}$ (F_{el} = elastic contribution to the free energy, F_s = surface energy of the brush, F_{mix} = mixing entropy of the side chains) can be found by minimization with respect to two independent variables: the fraction of adsorbed 2D chains, ϕ_a, and the relative contour length of the brush, L/aN. For long enough side chains the free energy has two minima, i.e., (i) the extended brush with a large fraction of adsorbed side chains and (ii) the collapsed globuli with a smaller fraction of adsorbed side chains. Variation of either the area available per molecule or the surface pressure can cause a discontinuous transition from one state to the other. The transition is of first order and exhibits a critical dependence on the side chain length [83].

The data demonstrate clearly the importance of the interaction of the subunits of brush like molecules with the substrate. In the case shown in Fig. 31, the structure was formed on a liquid substrate. Detailed studies of the molecular conformation affected by adsorption on a solid substrate have been possible with the monodendron jacketed polymers discussed before [87]. It has been

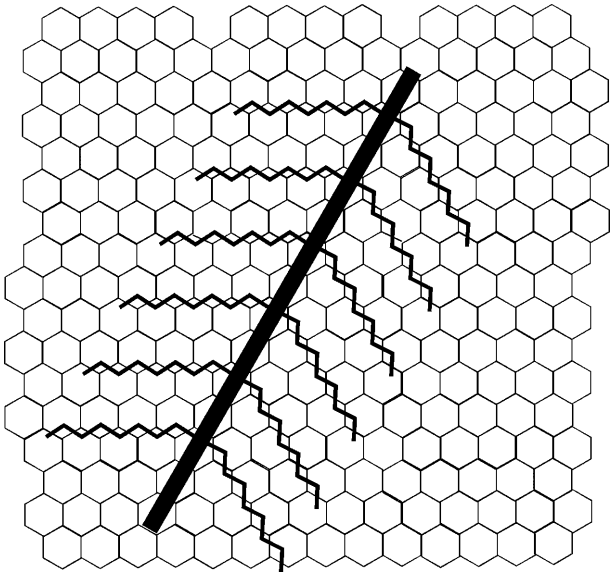

Fig. 33. Monodendron jacketed linear chains adsorbed epitaxially on a HOPG substrate. The *solid bar* depicts the backbone including benzyl groups, whereas the *zig-zag lines* correspond to the alkyl side chains

mentioned that the height of 14ABG-PS molecules adsorbed on graphite was considerably smaller than their lateral diameter. Also in this case, flattening indicates strong interaction of the side chains to the substrate. Besides changes in the molecular cross section, the adsorption can cause ordered macroconformations (Fig. 33).

Figure 34a represents another SFM-micrograph of 14ABG-PS (Scheme 1 in Sect. 3.2) on graphite. The macromolecules are arranged in straight segments with bends of a characteristic angle of 60° and 120°. On mica, the same polymer did not show any particular order (Fig. 34b). Only a short range orientational order of densely packed cylinders was observed. The ordering of the macromolecules was explained by an epitaxial adsorption of the alkyl tails of the monodendron side groups on HOPG. Formation of highly ordered monolayers due to preferential orientation of the hydrocarbon chains with respect to the graphite lattice was reported for linear alkanes and cycloalkanes [174, 175] as well as for comb-like molecules with alkyl substituents such as oligothiophenes [176]. The repeat length $l_e = 2.54$ Å of a $-(CH_2-CH_2)-$ sequence in all-*trans* planar zig-zag conformation matches the crystallographic spacing $a = 2.46$ Å of the graphite surface.

The hypothesis of the epitaxial adsorption of the side chains has been verified by STM studies on monolayers of the monodendrons. Figure 35 depicts high resolution images of a monolayer of tris-3,4,5-(*p*-dodecyloxybenzyloxy) benzoic acid, which shows parallel aligned stripes with a mean periodicity of 3.9 ± 0.1 nm. Within the stripes in Fig. 35b, the three benzyl groups and the gallic acid core were depicted as bright spots forming the threefold structure. The

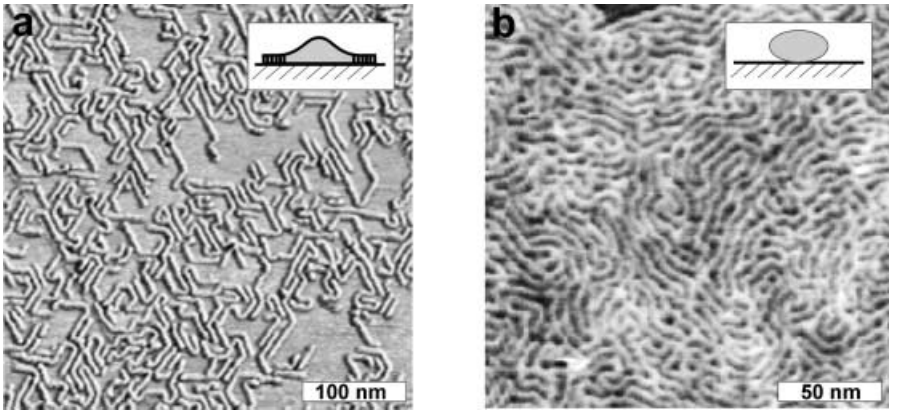

Fig. 34a, b. SFM-micrographs of the monolayers on; **a** HOPG; **b** mica prepared by spincasting of 14-ABG-PS solutions in cyclopentane (c = 0.1 mg/ml). Individual molecules in (**a**) aligned parallel to the substrate and bent at characteristic angles of 60° and 120° to follow the three-fold symmetry of graphite. The worm-like molecules in (**b**) wound around each other and resulted in a felt-like structure [86]

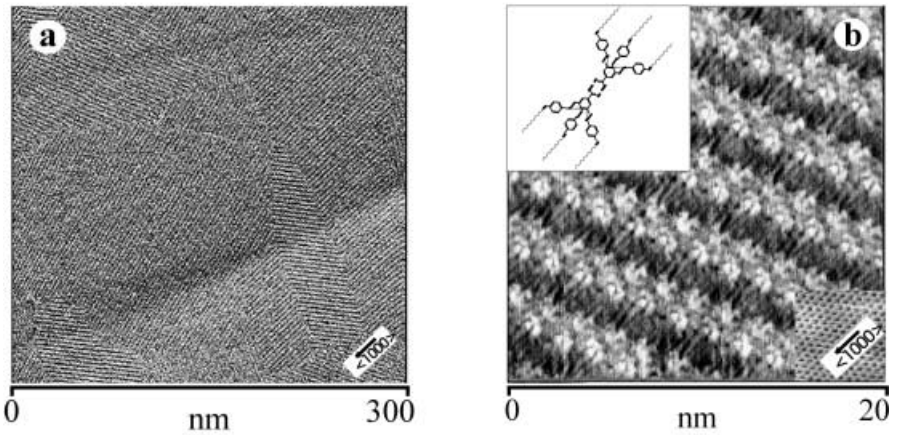

Fig. 35a, b. STM micrographs at: **a** low; **b** high resolution of a monolayer of monodendrons obtained by adsorption from a saturated solution in trichlorobenzene. The inserts in (**b**) show orientation of the molecules relative to the crystalline lattice of HOPG [87]

alkyl chains could be identified as straight lines between the benzyl rows aligned at an angle of 65° with respect to the stripes. The STM image indicates that the alkyl chains are arranged in an interdigitated comb structure. The length of the alkyl chains was measured to be 1.5 nm, which is consistent with the length of a dodecane molecule $H(CH_2)_{12}H$ in its all-*trans* conformation.

3.4
Persistent Motion by Partial Desorption and Reptating Relaxation

The two examples of adsorbed side chain substituted macromolecules, i.e., the poly(*n*-butyl acrylate) brush and the tris(*p*-undecyloxybenzyloxo) benzoate jacketed polystyrene, demonstrate two rather complementary aspects of the interaction of such molecules with a planar surface. In the first case the two-dimension to three-dimension transition results in a cooperative collapse of an extended coil conformation to a globule. The second case shows a rather high degree ordering with a distinct orientation of the backbone in the substrate plane. Combination of both effects and partial desorption can lead to a reptation-like directed motion as depicted schematically in Fig. 36.

As the desorption is combined with a contraction while the subsequent adsorption involves stretching, the molecule should move in the direction favored by the adsorption pattern. Such a motion was indeed observed in preliminary experiments for monodendron jacketed polymethacrylates with ethylene oxide

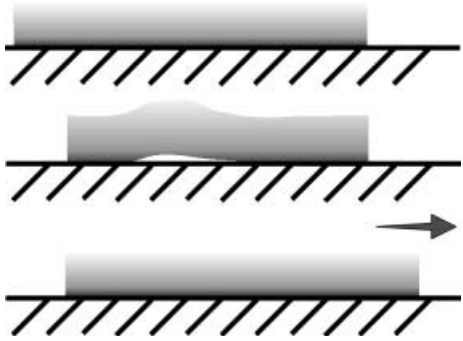

Fig. 36. Directed motion of cylinders with broken symmetry on a solid surface

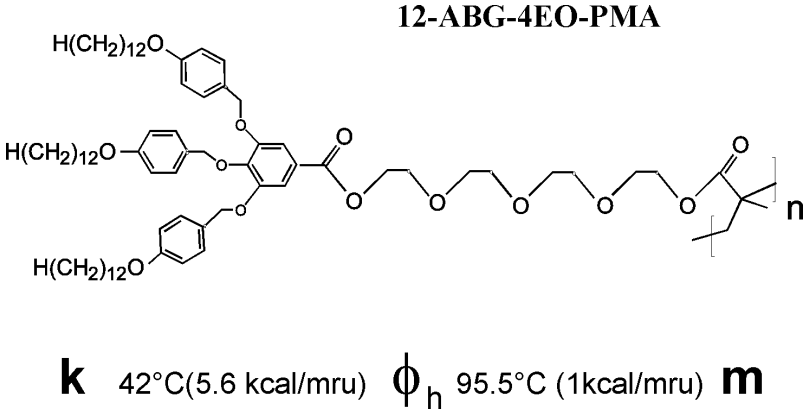

Fig. 37. Chemical structure and phase transitions of 12-ABG-4EO-PMA [164]

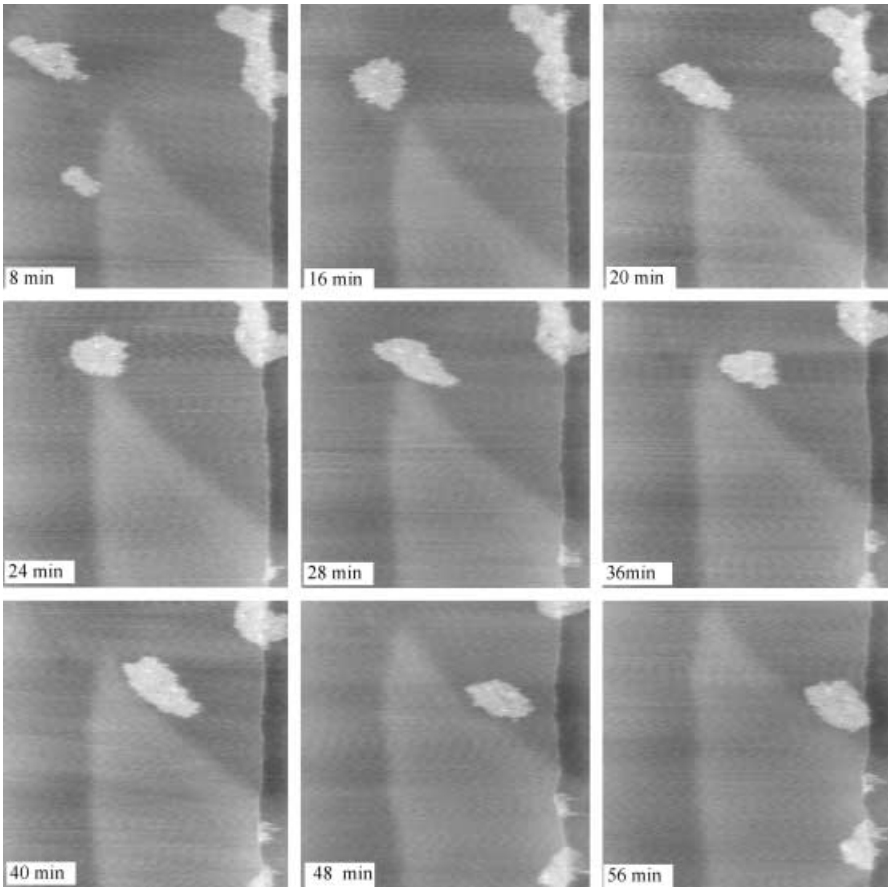

Fig. 38. Persistent and directed motion of a small cluster of five 14ABG-4EO-PMA molecules along the terrace of HOPG

spacers between the monodendron and the main chain (Fig. 37) [164]. Thus, the molecule combines the structural features of a relatively short side chain that can disorder upon desorption and the monodendron that is adsorbed in a pattern as depicted in Fig. 35.

A scanning force microscope equipped with a temperature cell enabled in-situ monitoring of both single molecules and their clusters at elevated temperature on highly oriented pyrolytic graphite (HOPG). Figure 38 shows a series of six micrographs captured during a time period of 1 h at a temperature of 46 °C, just after the phase transition from the crystalline phase (k) to the columnar mesophase (ϕ_h). One can clearly see that a small cluster consisting of ca. five molecules moves steadily along the terrace of the HOPG substrate. The motion started at 46 °C and continued within 60 min until the cluster reached the topographic obstacle, a terrace on the HOPG surface.

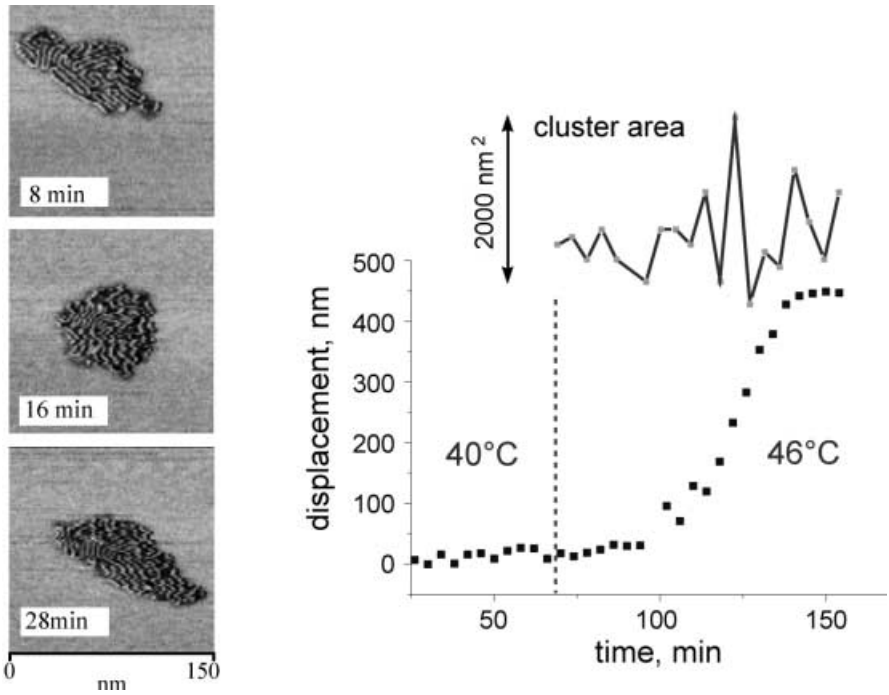

Fig. 39. Time variation of the displacement and cluster size during its motion on HOPG at 46 °C. The in-situ measured SFM micrographs depict momentary shape and inner structure of the cluster including packing of the molecules at different intervals after the motion started – 8 min, 16 min, and 28 min

Besides the remarkable directionality of the motion, the images also demonstrate a periodic variation of the cluster from an elongated to a circular shape (Fig. 39). The diagrams in Fig. 39 depict the time dependence of the displacement and the cluster size. Until the cluster was finally trapped, the speed remained fairly constant as can be seen from the constant slope in Fig. 39a. The oscillatory variation of the cluster shape is shown in Fig. 39b. Although a coarse model for the motion has been presented in Fig. 39, the actual cause of the motion remains unknown. The ratchet model proposed by J. Prost requires a non-equilibrium variation in the energetic potential to bias the Brownian motion of a molecule or particle under anisotropic boundary conditions [177]. Such local perturbations of the molecular structure are believed to be caused by the mechanical contact with the scanning tip. A detailed and systematic study of this question is still in progress.

4 Synopsis

The examples discussed above demonstrate that the complex architecture of hyperbranched and brush-like macromolecules can lead to properties and charac-

teristics in the molecular conformation that are not known for linear macromolecules. Competing effects at different length scales result in very peculiar ordering and transformations. The admittedly not yet proven model of a molecular motion demonstrates how the interplay of the different interactions and elastic forces can result in a directed action. All the examples discussed here showed the molecules adsorbed on a flat surface. This has its origin in the analytical method applied to study the molecules, i. e., scanning force microscopy. Yet the surface interaction is just one possible perturbation of the free molecule. Other ways to affect the molecular structure may result from photo-chemical transformations or varying electrical or magnetic fields. We are convinced that the hyperbranched molecules provide a great challenge to the synthetic chemist to design molecules that are capable of undergoing specific actions.

Acknowledgements. The authors are indebted to Mario Gauthier, Krzysztof Matyjaszewski, Aziz Muzafarov, Virgil Percec, and Manfred Schmidt for providing well characterized samples of dendrimers, arborescent graft polymers, molecular brushes, and monodendron-jacketed linear chains. We are also grateful to our colleagues at the University of Ulm, A. Mourran and S. Prokhorova, for skillful measurements with scanning probe techniques. This work was financially supported by the Deutsche Forschungsgemeinschaft (SH 46/2-1), Graduiertenkolleg-328 "Molecular organization and dynamics on surfaces and interfaces".

5 References

1. Dvornic PR, Tomalia DA (1996) Curr Opin Colloid Interf Sci 1:221
2. Fréchet JMJ, Hawker CJ, Gitsov I, Leon JW (1996) JMS – Pure Appl Chem A33:1399
3. Newkome GR, Moorefield CN, Vögtle F (eds) (1996) Dendritic molecules. concept, synthesis, perspectives. VCH, Weinheim
4. Newkome GR, He E, Moorefield CN (1999) Chem Rev 99:1689
5. Fischer M, Vögtle F (1999) Angew Chem Int Ed 38:884
6. Zeng F, Zimmerman SC (1997) Chem Rev 97:1681
7. Muzafarov AM, Rebrov EA, Papkov VS (1991) Russian Chemical Reviews 60:807; Ignat'eva GM, Rebrov EA, Myakushev VD, Chenskaya TB, Muzafarov AM (1997) Polymer Sci A 39:843
8. Majoral JP, Caminade AM (1998) Topics in Current Chemistry 197:79
9. Bosman AW, Jansen HM, Meijer EW (1999) Chem Rev 99:1665
10. Gauthier M, Möller M (1991) Macromolecules 24:4548
11. Tomaila DA, Hedstrand DH, Ferrito MS (1991) Macromolecules 24:1435
12. Jean-Luc S, Gnanou Y (1995) Macromol Symp 95:137
13. Gauthier M, Tichagwa L, Downey JS, Gao S (1996) Macromolecules 29:519
14. Taton D, Cloutet E, Gnanou Y (1998) Macromol Chem Phys 199:2501
15. Wu J, Lieser G, Wegner G (1996) Adv Materials 8:151
16. Cao Y, Smith P (1993) Polymer 34:3139
17. Ito K, Kawaguchi S (1999) Adv Polym Sci 142:129
18. Tsukahara Y, Tsutsumi K, Yamashita Y, Shimada S (1990) Macromolecules 23:5201
19. Wintermantel M, Gerle M, Fischer K, Schmidt M, Wataoka I, Urakawa H, Kajiwara K, Tsukahara Y (1996) Macromolecules 29:978; Wintermantel M, Fischer K, Gerle M, Ries R, Schmidt M, Kajiwara K, Urakawa H, Wataoka I (1995) Angew Chem Int Ed Engl 34:1472
20. Ruokolainen J, Torkkeli M, Serimaa R, Vahvaselkä S, Saariaho M, ten Brinke G (1996) Macromolecules 29:6621
21. Beers KL, Gaynor SG, Matyjaszewski K, Sheiko SS, Möller M (1998) Macromolecules 31:9413

22. Percec V, Ahn C-H, Cho W-D, Jamieson AM, Kim J, Leman T, Schmidt M, Gerle M, Möller M, Prokhorova SA, Sheiko SS, Cheng SZT, Zhang A, Ungar G, Yeardley DJP (1998) J Am Chem Soc 120:8619
23. Percec V, Holerca MN (2000) Biomacromolecules 1:6
24. Karakaya B, Claussen W, Gessier K, Säanger W, Schlüter A-D (1997) J Am Chem Soc 119: 3296; Bo Z, Zhang C, Severin N, Rabe JP, Schlüter AD (2000) Macromolecules (in press)
25. Yin R, Zhu Y, Tomalia DA (1998) J Am Chem Soc 120:2678
26. Jahromi S, Coussens B, Meijerink N, Braam AWM (1998) J Am Chem Soc 120:9753
27. Kim YH, Webster OW (1988) Polym Prepr (Am Chem Soc Div Polym Chem) 29:310; Kim YH (1998) J Polym Sci Polym Chem 36:1685
28. Fréchet JMJ, Henmi M, Gitsov I, Aoshima S, Leduc MR, Grubbs RB (1995) Science 269:1080
29. Voit B (1995) Acta Polym 46:87; Turner SR, Voit BI (1997) Polymer News 22:197
30. Hawker CJ (1999) Adv Polym Sci 147:113
31. Hult A, Johansson M, Malmström E (1999) Adv Polym Sci 143:1
32. Frey H, Lach C, Lorenz K (1998) Adv Mater 10:279; Sunder A, Hanselmann R, Frey H, Mülhaupt R (1999) Macromolecules 32:4240
33. Yan D, Müller AHE, Matyjaszewski K (1997) Macromolecules 30:7042
34. Gates DP, Svejda SA, Onate E, Killian CM, Johnson LK, White PS, Brookhart M (2000) Macromolecules 33:2320
35. Mourey TH, Turner SR, Rubinstein M, Fréchet JMJ, Hawker CJ, Wooley KL (1992) Macromolecules 25:2401
36. Gauthier M, Möller M, Burchard W (1994) Macromol Symp 77:43
37. Hawker CJ, Farrington PJ, Mackay ME, Wooley KL, Fréchet JMJ (1995) J Am Chem Soc 117:4409
38. Hempenius MA, Zoetelief WF, Gauthier M, Möller M (1998) Macromolecules 31:2299
39. Burchard W (1999) Adv Polym Sci 143:113
40. Choi S, Briber RM, Bauer BJ, Topp A, Gauthier M, Tichagwa L (1999) Macromolecules 32:7879
41. Pötschke D, Ballauff M, Linder P, Fischer M, Vögtle F (2000) Macromol Chem Phys 201:330
42. Bosman AW, Bruining M, Kooijmans H, Spek AL, Janssen RAJ, Meijer EW (1998) J Am Chem Soc:8547
43. Lescanec RL, Muthukumar M (1990) Macromolecules 23:2280
44. Mansfield ML, Klushin LI (1993) Macromolecules 26:4262
45. Murat M, Grest GS (1996) Macromolecules 29:1278
46. Boris D, Rubinstein M (1996) Macromolecules 29:7251
47. Borrega R, Cloitre M, Betremieux I, Ernst B, Leibler L (1999) Europhys Lett 47:729
48. Gujrati PD (1995) Phys Rev Lett 74:1367
49. Israelachvili J (1992) Intermolecular & Surface Forces. 2nd edn. Academic Press, San Diego
50. Parsegian VA, Evans EA (1996) Curr Opin Colloid Interface Sci 1:53
51. Löwen H (1994) Phys Rep 237:249
52. Löwen H, Schmidt M (1997) In: Kremer F, Lagaly G (eds) Progress in colloid and interface sciences. Steinkopf Verlag, Darmstadt
53. Zhulina EB, Borisov OV, Priamitsyn VA (1990) J Coll Interf Sci 137:495
54. Wang PW, Liu YJ, Devadoss C, Bharathi P, Moore JS (1996) Adv Mater 8:237
55. Dandliker J, Diederich F, Gisselbrecht J-P, Louati A, Gross M (1995) Angew Chem Int Ed Engl 34:2725
56. Zhao M, Crooks RM (1999) Adv Mater 11:217
57. Albrecht M, van Koten G (1999) Adv Mater 11:171
58. Vasilenko NG, Rebrov EA, Muzafarov AM, Eßwein B, Striegel B, Möller M (1998) Macromol Chem Phys 199:889
59. Leduc MR, Hawker CJ, Dao J, Frechet JMJ (1996) J Am Chem Soc 118:11,111
60. Zimmerman SC (1997) Curr Opin Coll Interf Sci 2:89

61. Cooper AJ, Londono JD, Wignall G, McClain JB, Samulski ET, Lin JS, Dobrynin A, Rubinstein M, Burke ALC, Frechet JMJ (1997) Nature 389:368
62. Jansen JFGA, de Brabander-van der Berg EMM, Meijer EW (1994) Science 266:1226; Jansen JFGA, de Brabander-van der Berg EMM, Meijer EW (1995) J Am Chem Soc 117:4417; Jansen JFGA, de Brabander-van der Berg EMM, Meijer EW (1996) J Am Chem Soc 118:7398
63. Archut A, Vögtle F, Decola L, Azzellini GC, Balzani V, Ramanujam PS, Berg RH (1998) Chemistry Europ J 4:699
64. Goino M, Esumi K (1998) J Coll Interf Sci 203:214
65. Esumi K, Suzuki A, Aihara N, Usui K, Torigoe K (1998) Langmuir 14:3157
66. Larre C, Donnadieu B, Caminade AM, Majoral JP (1998) Chemistry Europ J 4:2031
67. Lorenz K, Hölter D, Stühn B, Mülhaupt R, Frey H (1996) Adv Mater 8:414
68. Richardson RM, Ponomarenko SA, Boiko NI, Shibaev VP (1999) Liquid Crystals 26:101
69. Peerlings HWI, Meijer EW (1997) Chem Eur J 3:1563
70. van Hest JCM, Delnoye DAP, Baars MWPL, van Genderen MHP, Meijer EW (1995) Science 268:1592
71. Sheiko SS, Gauthier M, Möller M (1997) Macromolecules 30:2343
72. Sheiko SS, Eckert G, Ignat'eva G, Muzafarov AM, Spickermann J, Räder HJ, Möller M (1996) Macromol Rapid Comm 17:283
73. Sheiko SS, Muzafarov AM, Winkler RG, Getmanova EV, Eckert G, Reineker P (1997) Langmuir 13:4172
74. Sheiko SS, Buzin AI, Muzafarov AM, Rebrov EA, Getmanova EV (1998) Langmuir 14:7468
75. Sheiko SS, Muzafarov AM (1999) Communication at ACS meeting in New Orleans
76. Zhang X-Y, Klein J, Sheiko SS, Muzafarov A (2000) Langmuir 16:3893
77. Mazo MA, Zhilin PA, Gusarova EB, Sheiko SS, Balabaev NK (1999) J Molec Liquids 82:105
78. Sheiko SS, Gerle M, Fischer K, Schmidt M, Möller M (1997) Langmuir 20:5368
79. Dziezok P, Sheiko SS, Fischer K, Schmidt M, Möller M (1997) Angew Chemie Int Ed Engl 109:2812
80. Sheiko SS, Prokhorova SA, Schmidt U, Dziezok P, Schmidt M, Möller M (1999) In: Tsukruk VV, Wahl K (eds) ACS Symposium Series 741:346, ACS Washington
81. Gerle M, Fischer K, Schmidt M, Roos S, Müller AHE, Sheiko SS, Prokhorova SA, Möller M (1999) Macromolecules 32:2629
82. Sheiko SS, Borisov OV, Prokhorova SA, Schmidt U, Gerle M, Schmidt M, Möller M (2000) Europ Phys J (to be submitted)
83. Sheiko SS, Prokhorova SA, Beers K, Matyjaszewski K, Potemkin II, Khokhlov AR, Möller, M. (2000) Phys Rev Lett (submitted)
84. Percec V, Ahn C-H, Ungar G, Yeardley DSP, Möller M, Sheiko SS (1998) Nature 391:161
85. Prokhorova SA, Sheiko SS, Möller M, Ahn C-H, Percec V (1998) Macromol Rapid Comm 19:359
86. Prokhorova SA, Sheiko SS, Möller M, Ahn C-H, Percec V (1999) Macromolecules 32:2653
87. Prokhorova SA, Sheiko SS, Mourran A, Azumi R, Zipp G, Beginn U, Möller M, Ahn C-H, Holerca MA, Percec V (2000) Langmuir (in press)
88. Percec V, Cho W-D, Möller M, Prokhorova SA, Ungar G, Yeardley DJP (2000) J Am Chem Soc 122:4249
89. Sheiko SS, Gauthier M, Möller M (in preparation)
90. Mansfield ML (1996) Polymer 37:3835
91. Tsukruk VV (1998) Adv Mater 10:253; Tsukruk VV, Rinderspacher F, Bliznyuk VN (1997) Langmuir 13:2171
92. Takada K, Diaz DJ, Abruna HD, Cuadrado I, Casado C, Alonso B, Moran M, Losada J (1997) J Am Chem Soc 119:10, 763
93. Watanabo S, Regen SL (1994) J Am Chem Soc 116:8855
94. Hierleman A, Campbell JK, Baker LA, Crooks RM, Ricco AJ (1998) J Am Chem Soc 120:5323
95. Huck WTS, van Veggel FCJM, Sheiko SS, Möller M, Reinhoudt DN (1998) J Phys Org Chem 11:540

96. Saville PM, White JW, Hawker CJ, Wooley KL, Fréchet JMJ (1993) J Phys Chem 97:293; Kirton GF, Brown AS, Hawker CJ, Reynolds PA, White JW (1998) Physica B 248:184
97. De Leuze-Jallouli AM, Swanson D, Dvornic PR, Perz SV, Owen MJ (1997) PMSE Proceedings 77:93
98. Tokuhisa H, Zhao M, Baker LA, Phan VT, Dermody DL, Garcoa ME, Peez RF, Crooks RM, Mayer TM (1998) J Am Chem Soc 120:4492
99. Schenning APHJ, Elissen-Román C, Weener J-W, Baars MWPL, van der Gaast SJ, Meijer EW (1998) J Am Chem Soc 120:8299
100. Iyer J, Hamond PT (1999) Langmuir 15:1299
101. Imae T, Funayama K, Aoi K, Tsutsumiuchi K, Okada M, Furusaka M (1999) Langmuir 15:4076
102. Cui G, Xu Y, Liu M, Fang F, Ji T, Chen Y, Li Y (1999) Macromol Rapid Comm 20:71
103. Coen MC, Lorenz K, Kressler J, Frey H, Mülhaupt R (1996) Macromolecules 29:8069
104. Ponomarenko SA, Boiko NI, Shibaev VP, Magonov SN (2000) Langmuir 64:5487
105. Hellmann J, Hamano M, Karthaus O, Ijiro K, Shimomura M, Irie M (1998) Jpn J Appl Phys 37:L816
106. Landau EM, Levanon M, Leiserowitz L, Lehav M, Sagiv J (1985) Nature 318:353
107. Singhi R, Kumar A, Lopez GP, Stephanopoulos GN, Wang DIC, Whitesides GM, Ingber DE (1994) Science 264:696
108. Kumar A, Whitesides GM (1993) Appl Phys Lett 14:63
109. Weissbuch I, Baxter PNW, Cohen S, Shubert US, Lehn J-M, Leiserowitz L (1998) J Am Chem Soc 120:4850
110. Jackman RJ, Brittain ST, Adams A, Prentiss MG, Whitesides GM (1998) Science 280:2089
111. Deckman HW, Dunsmuir JH (1988) J Vac Sci Technol B 6:333
112. Dinsmore AD, Crocker JC, Yodh AG (1998) Curr Opin Coll Interf Sci 3:5
113. Padberg T (1997) Curr Opin Coll Interf Sci 2:607
114. Burmeister F, Schaefle C, Mattes T, Boehmisch M, Boneberg J, Leiderer P (1997) Langmuir 13:2983
115. Pieranski P (1980) Phys Rev Lett 45:569
116. Pusey PN, van Megen W (1986) Nature 320:340
117. Grier DG (1998) MRS Bull 23:21
118. Adachi E, Nagayama K (1996) Langmuir 12:836
119. Joannopoulos JD, Villeneuve PR, Fan S (1997) Nature 386:143
120. Holtz JH, Asher SA (1997) Nature 389:829
121. Johnson CA, Lenhoff AM (1996) J Coll Interface Sci 179:587
122. Stamou D, Liley M, Vogel H, Duschl C (1998) Polymer Prepr Am Chem Soc Polym Div 39(2):1161
123. Semmler M, Mann EK, Ricka J, Borkovec M (1998) Langmuir 14:5127
124. Adamczyk Z, Warszynski P (1996) Adv Coll Interf Sci 63:41
125. Pan G, Kesavamoorthy R, Asher SA (1997) Phys Rev Lett 78:3860
126. van Blaaderen A, Ruel R, Wiltzius P (1997) Nature 385:321
127. Bubeck R, Bechinger C, Neser S, Leiderer P (1999) Phys Rev Lett 82:3364
128. Kralchevsky PA, Nagayama K (1994) Langmuir 10:23
129. Akiba T, Yoshimura H, Namba N (1991) Science 252:1544
130. Ishii N, Yoshimura H, Nagayama K, Kagawa Y, Yoshida M (1993) J Biochem 113:245
131. Ribi HO, Ludwig DS, Mercer KL, Schoolnik GK, Kornberg RD (1988) Science 239:1272
132. Asakura S, Oosawa F (1958) J Pol Sci 33:183
133. Flory PJ (1978) Macromolecules 11:1138
134. Dinsmore AD, Yodth AG, Pine DJ (1996) Nature 383:239
135. Bolhuis P, Stroobants A, Frenkel D (1997) J Chem Phys 107:1551
136. Herzfeld J (1996) Acc Chem Rec 29:31
137. ten Wolde PR, Frenkel D (1997) Science 277:1975
138. Dinsmore AD, Wong DT, Nelson O, Yodh AG (1998) Phys Rev Lett 80:409
139. Adams M, Dogic Z, Keller SL, Fraden S (1998) Nature 393:349
140. Dogic Z, Fraden S (1997) Phys Rev Lett 78:2417

141. Rosenfeld Y (1994) Phys Rev Lett 72:3831
142. Sato T, Teramoto A (1996) Adv Polym Sci 126:85
143. Poulin P, Stark H, Lubensky TC, Weitz DA (1997) Science 275:1770
144. Bechinger C, Rudhardt D, Leiderer P, Roth R (1999) Phys Rev Lett 83:3960
145. Klug A (1983) Angew Chem 95:579
146. Pompe T, Fery A, Herminghaus S (1998) Langmuir 14:2585
147. Tamayo J, García R (1996) Langmuir 12:4430
148. Mazo M, Balabaev NK, Sheiko SS (private communication)
149. Zhu J, Lennox RB, Eisenberg A (1992) J Phys Chem 96:4727
150. Li Z, Zhao W, Rafailovich MH, Sokolov J, Lennox RB, Eiseberg A, Wu XZ, Kim MW, SK Sinha, Tolan M (1995) Langmuir 11:4785
151. Kee RA, Gauthier M (1999) Macromolecules 32:6478
152. Hempenius MA, Michelberger W, Möller M (1997) Macromolecules 30:5602
153. Birshtein TM, Borisov OV, Zhulina EB, Khokhlov AR, Yurasova TA (1987) Polymer Science USSR 29:1293
154. G. Fredrickson (1993) Macromolecules 26:2825
155. Saariaho M, Ikkala O, Szleifer I, Erukhimovich I, ten Brinke G (1997) J Chem Phys 107:3267
156. Balagurusamy VSK, Ungar G, Percec V, Johansson G (1997) J Am Chem Soc 119:1539
157. Williams DRM (1993) J Phys II (France) 3:1313
158. Rouault Y, Borisov OV (1996) Macromolecules 29:2605
159. Soga KG, Guo H, Zuckermann MJ (1995) Europhys Lett 29:531
160. Zhulina E, Singh C, Balazs AC (1996) Macromolecules 29:6338
161. Siqueira DF, Kohler K, Stamm M (1995) Langmuir 11:3092
162. Stamouli A, Pelletier E, Koutsos V, van der Vegte E, Hadziionaou G (1996) Langmuir 3221
163. Carmesin I, Kremer K (1990) J Phys France 51:915
164. Kwon YK, Chvalun SN, Schneider AI, Blackwell J, Percec V, Heck JA (1994) Macromolecules 27:6129
165. Marko JF, Siggia ED (1994) Science 265:506
166. Marko JF, Siggia ED (1995) Physical Review E 52:2912
167. McLeish T (1997) Science 278:1577
168. Strick TR, Allemand J-F, Bensimon D, Croquette V (1998) Biophys J 74:2016
169. Saariaho M, Ikkala O, ten Brinke G (1999) J Chem Phys 110:1180
170. Khalatur PG, Khokhlov AR, Prokhorova SA, Sheiko SS, Möller M, Reineker P, Shirvanyanz DG, Starovoitova N (2000) Europ Phys J 1:99
171. Beers K, Matyjaszewski K, Sheiko SS, Prokhorova SA, Möller M (1999) Polymer Preprint (Am Chem Soc, Div Polym Chem) 40(2):446
172. Crisp DJ (1946) J Coll Sci 1:49
173. Li S, Hanley S, Khan I, Varshney SK, Eisenberg A, Lennox RB (1997) Langmuir 9:2243
174. Rabe JP, Buchholz S (1991) Phys Rev Lett 66:2096
175. Wavkuschewskij A, Cantow H-J, Magonov SN, Möller M, Liany W, Whanbo M-H (1995) Adv Mater 5:821
176. Bauerle P, Fischer T, Bidlingmeier B, Stabel A, Rabe JP (1995) Angew Chem Int. Ed Engl 34:303
177. Ajdari A, Prost J (1993) C R Acad Sci Paris II 315:1635

Structure of Dendrimers in Dilute Solution

Matthias Ballauff

Polymer-Institut, Universität Karlsruhe, Kaiserstrasse 12, 76128 Karlsruhe,
E-mail: Matthias.Ballauff@chemie.uni-karlsruhe.de

The equilibrium structure of dendrimers in dilute solution is reviewed. It is shown that small-angle neutron scattering (SANS) is suitable to determine the radial density distribution inside of the dendritic structure. For low generations (4,5) available data indicate a density distribution that has its maximum in the center of the molecule. Higher generations studied by small-angle X-ray scattering (SAXS) exhibit a more and more compact conformation which is due to the increase back-folding of the peripheral groups. In general, SANS is shown to be a highly suitable tool for the investigation of dendrimers and related supramolecular structures in solution.

Keywords. Dendrimers, SANS, SAXS, Contrast variation

1 Introduction

The chemical synthesis of dendrimers has been the subject of intense research and the number of publications on this subject has undergone an exponential increase in recent years. For a survey of current work in this field the reader is

Topics in Current Chemistry, Vol. 212

referred to recent reviews [1 – 3]. Fewer studies are available on the spatial structure in solution, in bulk, or at surfaces. The structure of dendrimers in different states of aggregation present an interesting problem, however, since dendritic structures are intermediates between macromolecules and colloids. The mass of the molecule increases exponentially with the number of generations and grows more rapidly than the available volume. The spatial structure hence must saturate at a given number of generations. The consequences of this spatial architecture are immediately obvious; at low generation number, on the one hand, the structure will be related to the one of star polymers having a great number of available conformations. At high generation number, on the other hand, a densely packed radial structure will result that has much less internal degrees of

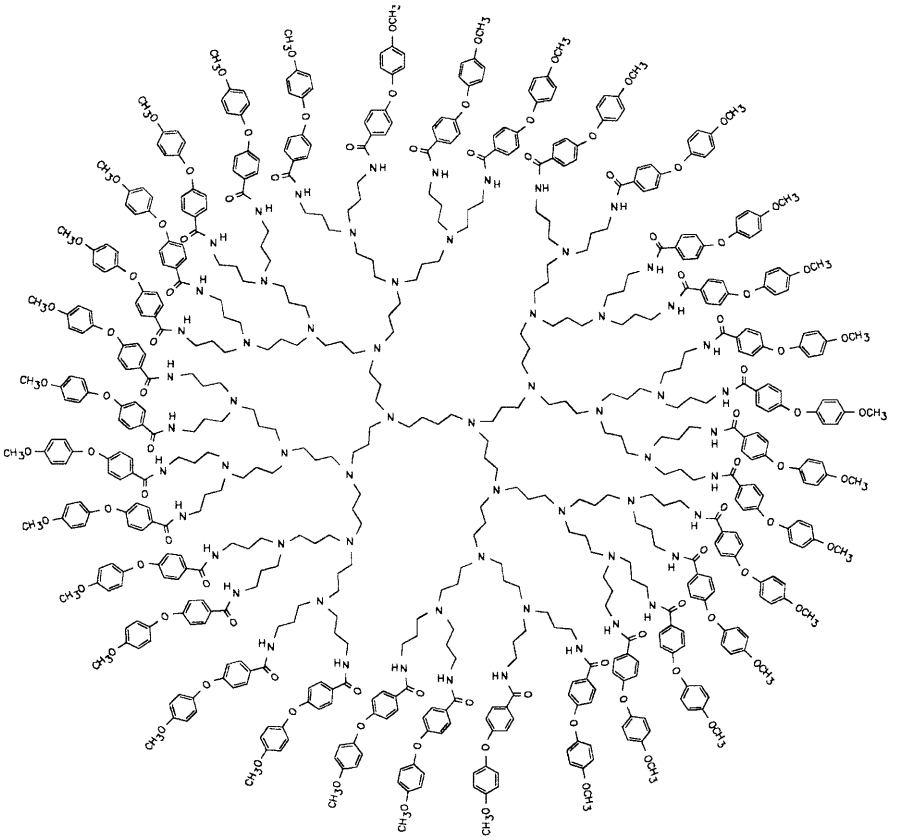

Fig. 1. Chemical structure of a dendrimer of fourth generation (G4). Starting with a focal group in the center of the molecule, a fractal-like structure is built up by branches which emanate from three-functional groups. The outer ends of the branches are terminated by endgroups [3]. The molecule may be divided into „dendrons" designating the substructures originating from a branch point. Hence, the dendrimer shown here may be viewed upon as composed of four dendrons emanating from a central ethylenediamine group

freedom. In this respect dendrimers bridge the gap between strongly fluctuating polymeric structures and solid colloidal particles.

The understanding of the conformation of dendrimers of different generation as function of concentration, temperature, solvent power, etc., is necessary for further work directed towards the dynamics of these structures as well as to the energy transfer within these molecules. A precise tuning of the conformational freedom is also a prerequisite for all applications discussed so far for dendritic structures [1–3].

In this chapter we shall review recent investigations devoted to the equilibrium structure of defined dendritic molecules. It is to be understood that the present review deals solely with recent work on flexible dendrimers. Figure 1 shows a typical examples of such a dendritic structure with defined endgroups [3]. It is obvious that this structure has a great number of conformational degrees of freedom. This is opposed to dendritic structures composed of stiff building blocks. Figure 2 displays the first example of such a structure which is set up entirely from phenyl groups. These fully aromatic dendrimers that have been synthesized recently by Müllen and coworkers [4] exhibit a virtually stiff skeleton since rotations about the bond angle between different phenyl groups do not lead to a totally different shape of the molecule. No systematic study of the solution properties of these structures is available yet, however, and the present review will hence be restricted to the discussion of flexible dendrimers having a flexible skeleton (cf. Fig. 1).

The central question to be addressed in this context is the conformation of isolated flexible dendrimers in solution. Here a considerable number of computer simulations are available by now that have come to unambiguous results regarding the equilibrium structure of flexible dendrimers in solution. The main conclusions of these studies will be presented in a first section of this chapter.

Scattering methods such as small-angle neutron scattering (SANS) or small-angle X-ray scattering (SAXS) are highly suitable for determining the structure of dendrimers in dilute solution and for comparing the results to recent simulations. Hence, a discussion of recent studies employing these methods will be given here. A more detailed review of scattering methods as applied to dissolved dendrimers has been given recently [5]. The overall shape of dissolved dendrimers may also be determined by their hydrodynamic volume as determined through measurements of the intrinsic viscosity $[\eta]$. Therefore a brief survey of studies devoted to precise measurements of $[\eta]$ will be presented as well.

Many applications of dendrimers discussed so far in the literature [1–3] such as, e. g., for diagnostic or medical purposes will take place in semi-dilute or concentrated solutions. Hence, possible changes of conformation in this regime that may be induced by mutual interaction of the solute molecules requires special attention. Here again SAXS and SANS furnish valuable information on how the conformation may change upon increase of the mutual interaction between the dendrimers. Detailed knowledge of the conformation of dendrimers may also furnish valuable insight when trying to understand the structure of these molecules in bulk.

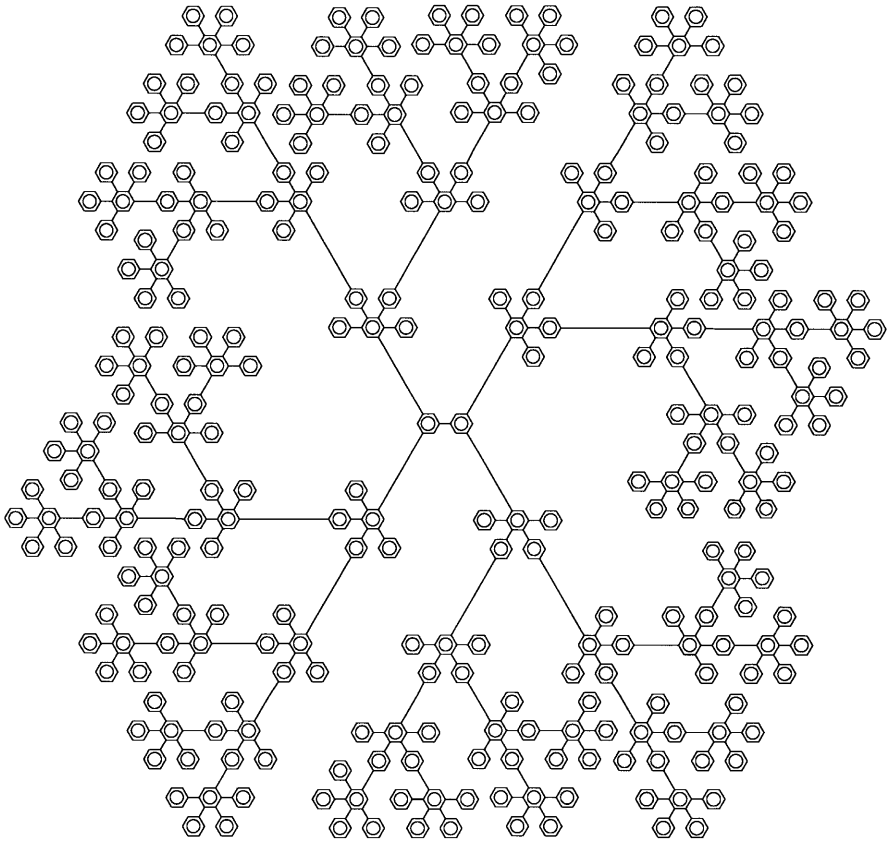

Fig. 2. Chemical structure of a stiff dendrimer [4]

2 Theory and Simulations

Up to now, the equilibrium structure of flexible dendrimers in solution has been treated in several exhaustive theoretical studies [6 – 13]. Shortly after the first experimental reports on the synthesis of dendrimers their spatial structure was considered by de Gennes and Hervet [6]. These authors derived a density profile which has a minimum at the center of the starburst and increased monotonically to the outer edge. It must be noted that de Gennes and Hervet assumed that all subsequent bonds point to the periphery of the molecule. A structure complying with this assumption may be given by the fully aromatic dendrimers as displayed in Fig. 2. In consequence, the „dense-shell picture" deriving from this theory is built into the model. It should not be regarded as its result.

All subsequent theoretical studies devoted to flexible dendrimers came to the conclusion that the segment density has its maximum in the center of the molecule. Lescanec and Muthukumar [7] were the first to present this conclusion

which they derived from simulations of a random growth process. The results thus obtained may also reflect non-equilibrium structures. Manfield and Klushin performed a series of MD-simulation studies of dendrimers which solved this problem [8]. Their study which comprises dendrimers up to the ninth generation corroborated qualitatively the results presented by Lescanec and Muthukumar [7]. In addition to this, these authors made the first detailed predictions of the scattering function of dendrimers. Murat and Grest presented a molecular dynamics study which included the effect of solvent quality on the internal structure of dendrimers [9]. The relaxation times of the fluctuations of the structures were determined in order to prove adequate sampling of equilibrium configurations.

These authors [9] also presented a study of a highly interesting phenomenon which is due to the dendritic architecture, namely dendron segregation. The dendrimer may be subdivided into dendrons emanating from a central unit (see Fig. 1). These dendrons are predicted to demix despite the fact that they are of identical chemical composition. This problem was first discussed by Mansfield [10]. Dendron segregation opens the possibility of making supramolecular structures with different functionalities sitting on different dendrons. Dendron segregation in such particles may result in asymmetric nano-objects such as, e. g., "Janus-grains".

A detailed MD-study of the dendrimers functionalized by endgroups was recently presented by Cavallo and Fraternali [11]. A most important contribution to the theoretical understanding of dendrimers was advanced by Boris and Rubinstein [12]. An analytical Flory-type model of the starburst structure was developed by these authors. The results of theory was subsequently corroborated by a self-consistent mean-field model. The theory of Boris and Rubinstein [12] allows one to understand the basic factors controlling the size of dendritic structures as a function of solvent power. The calculation have been performed using reasonable parameters deriving from experimental data. These authors also made detailed prediction regarding the scattering function of dendrimers. They demonstrated that small-angle scattering is capable of distinguishing between different models of the radial structure.

As stated above, the theory of Boris and Rubinstein [12] comes to the unambiguous conclusion that the density has its maximum at the center of the molecule. As an example, Fig. 3 displays the density profile of dendritic structures calculated for generations 2 – 7. Here the volume fraction of segments (properly normalized to unity at the center of the molecule) is plotted as function of the radial distance to the center. There is significant back-folding of the outer groups into the center of the molecule. This is demonstrated in Fig. 4 which shows the probability distribution of the endgroups calculated for dendrimers of different generation [12]. It is obvious that the endgroups will be located preferentially in the periphery of the dendrimer where the distribution has its maximum. But there is a finite probability, however, to find an endgroup near the center of the molecule. All results demonstrate that dendritic structure of lower generation present strongly fluctuating objects as expected from their chemical structure.

Recent Monte Carlo- and Molecular Dynamics-simulations [8, 9, 11] seem to suggest a slight local decrease of the density directly at the center of the mole-

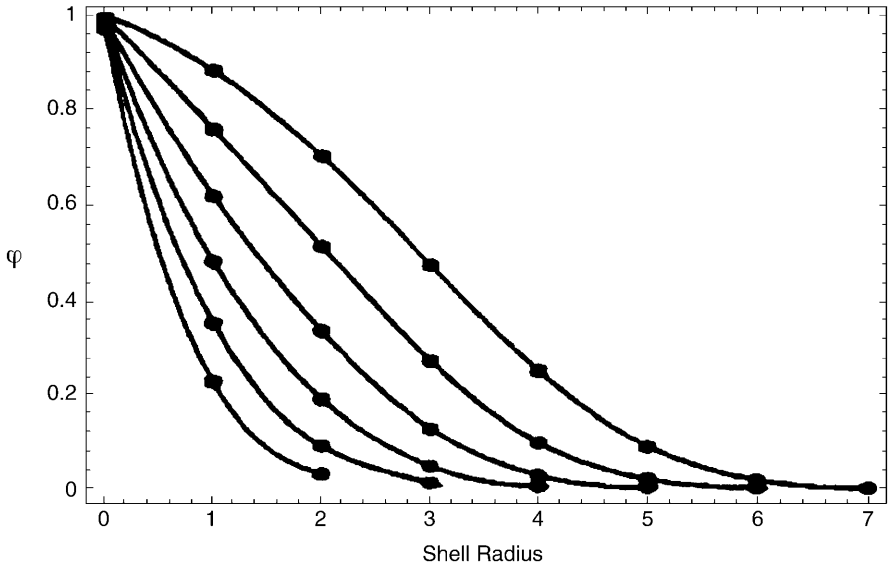

Fig. 3. Theoretical density profile of dendritic structures of generations 2–7 [12]. The radial volume fraction properly normalized to unity at the center of the molecule is plotted against the radial distance to the origin. All data has been calculated assuming a realistic excluded volume parameter of the segments of the dendrimer. Reproduced with permission from [12]

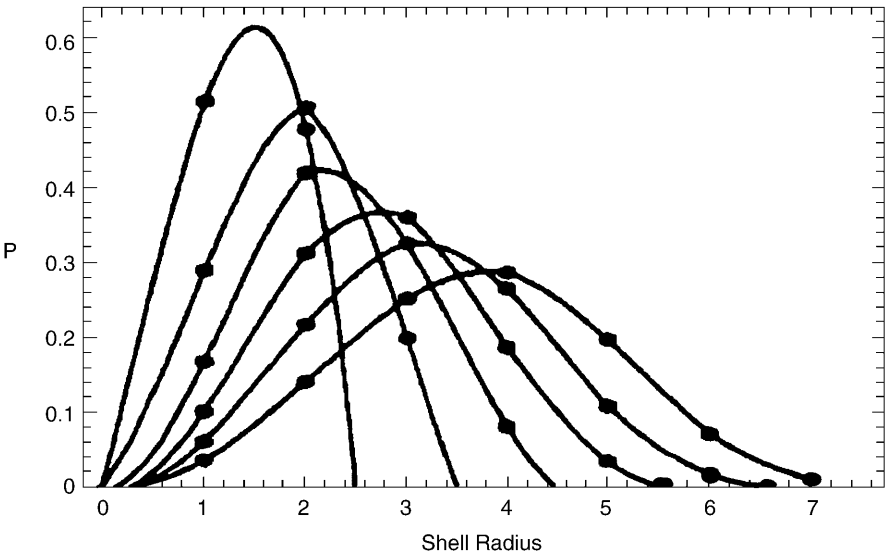

Fig. 4. Backfolding in dendrimers as predicted by analytical theory [12]. Free end probability distribution function of the radial distance for generations 2–7. All data has been calculated assuming a realistic excluded volume parameter of the segments of the dendrimer (see [12] for further details). Reproduced with permission from [12]

cule. This feature is not consistent with the findings of Boris and Rubinstein [12] who doubt the accuracy of the simulation with respect to this particular result. For greater radial distances, however, analytical theory [12] as well as simulations [7–9, 11] agree on a smooth decay of the density of the segments. Very recently, this point has been further pursued by a simulation of Welch and Muthukumar [13]. These workers demonstrated that charges within the dendrimer may lead to a transition between a dense core and a dense shell structure. A transition between a dense-core and a dense-shell structure may be induced by tuning the electrostatic repulsion through adjustment of the Debye-length in the system.

This section may be concluded by the statement that flexible dendrimers are predicted to exhibit a strongly fluctuating structure in solution. According to these studies the endgroups are not strictly located at the surface of the molecules but may also fold back into the interior of the dendrimer. It must be noted that this conclusion originates from models which idealize the dendritic architecture in terms of model parameter common in polymer theory [14, 15]. In this respect theory may not lead to fully quantitative predictions. Theory, however, certainly arrives at correct qualitative conclusions which are largely backed by available experimental evidence as shown further below.

3
Experimental Studies

3.1
Investigations in Solution by Small-Angle Scattering

By now, a considerable number of studies of dendrimers in solution by SANS and SAXS has been presented [16–31]. An early study conducted by Prosa et al. [18] using SAXS showed the transition of a polymer-like scattering behavior to the scattering pattern of a colloidal structure with increasing number of generations (see Sect. 1). For low generations a virtually structureless scattering curve resulted whereas the dendrimer of generation 10 exhibited two side maxima in the measured SAXS-intensity $I(q)$ as function of the magnitude of the scattering vector q ($q = (4\pi/\lambda)\sin(\theta/2)$ where λ is wavelength of radiation and θ the scattering angle). These side maxima are to be expected for a dense spherical structure predicted for dendritic structures of high generation. A SANS-study by Scherrenberg et al. [19] showed a similar trend. Here a maximum showed up in Kratky plots $I(q)\,q^2$ vs q with increasing generation number. The resulting scattering function agrees qualitatively with the theory of Boris and Rubinstein (see Fig. 11 of [12]).

We have presented a new method of using SANS to elucidate the radial structure of dissolved dendrimers [23, 24]. It has been demonstrated that SANS in conjunction with contrast variation [32–37] is a valid tool to determine the internal structure of dendrimers. The main result of [23, 24] is the clear proof that the density distribution has its maximum at the center of the molecule. Hence this corroborates the general deductions of theory as discussed in the preceding section.

Moreover, SANS-data measured at different contrast allow one to determine the molecular weight. Imae et al. [25] also used contrast variation to determine the molecular weight of dendrimers. The problem of molecular weights and possible imperfections in dendrimer has been addressed very recently by Rietveld and Smit [26]. These workers employed static light scattering and vapor pressure osmometry which give the molecular weight of the dissolved objects but allow no further conclusion regarding their radial structure.

Very recently, Topp et al. [29] probed the location of the terminal groups of a dendrimer of seventh generation using SANS. These authors concluded that the terminal units as well as nearly half of its monomer units are located in the vicinity of the surface of the molecule. This is in contradiction to the results derived from simulations (see Sect. 2). In addition, it is difficult to reconcile this result with the findings of [23, 24] which showed that flexible dendrimers have the maximum density at the center of the molecule.

3.2
Small-Angle Scattering Experiments: Problems

The preceding section may be concluded by the statement that the experimental studies published hitherto did not come to a clear conclusion regarding the radial density distribution of dendrimers. It is therefore interesting to delineate the main problems of scattering studies as applied to small dissolved objects and enumerate possible sources of scattering intensity not related to the spatial structure of the particles [5, 23, 24]:

1. Dendrimers are small structures with diameters of a few nanometers only. Their radius of gyration [32, 33] R_g which may, to first approximation, be taken as a measure of overall spatial extensions is of the same order of magnitude. Reliable structural information can only be obtained from $I(q)$ if $q \times R_g$ is considerably larger than unity. The measured scattering data must therefore extend far beyond the Guinier region [32, 33]. On the other hand, the molecular weight of typical dendrimers is rather low and $I(q)$ is much lower than the scattering intensities measured from, e.g., high polymers in solution. Taking SANS-data at high $q \times R_g$ requires high scattering angles. This is followed by poor statistics of the data in the q-range where most of the information is to be gained.
2. Theory and simulations describe dendrimers as spatial objects of small or point-like scattering units of the same scattering power. Real dendrimers are composed of chemically different units, however, which may have a different scattering length. The spatial inhomogeneity resulting from this fact will give an additional contribution to the measured SANS- or SAXS-intensity.
3. A problem of SANS-measurements is given by the incoherent part I_{incoh} of the scattering intensity which is caused by the hydrogen atoms in the chemical structure of the dendrimers [33]. If n is the number of scattering units the coherent part scales with n^2 at small scattering angles while the incoherent part scales with n. For large objects such as, e.g., long polymeric chains in solution this part may usually be neglected. For small entities such as den-

drimers it may become a contribution of the measured intensity comparable to the coherent part of $I(q)$. At sufficiently high scattering angles, however, $I(q)$ probes only the local structure. In this region the coherent part of $I(q)$ scales therefore only with n and I_{incoh} cannot be neglected any more.

4. The solvent is usually treated as an incompressible continuum. However, it must be kept in mind that SAXS- or SANS-studies in solution only probe the difference between the scattering length density of the dissolved object and the solvent. Hence, the scattering intensity is determined by the contrast between solute and solvent. This contrast may fluctuate too because of the density fluctuations of the solvent and there is a small but non-zero contribution to $I(q)$, even at vanishing contrast.

SANS offers the unique ability to address this problem by change of the contrast between solute and solvent through use of mixtures of deuterated and protonated solvents [32, 33]. In the following section the method of contrast variation as applied to the analysis of dissolved dendrimers will be discussed.

3.3
Small-Angle Scattering Experiments: Contrast Variation

3.3.1
General Considerations

The central idea of contrast variation is shown in Fig. 5. The dissolved object is depicted as an assembly of scattering units with different scattering power. The entire object occupies a volume in the system depicted by the shaded area in Fig. 5, left-hand side. The local scattering length density $\varrho(\vec{r})$ is rendered as a product of the shape function $T(\vec{r})$ and the local scattering length density inside the object:

$$\varrho(\vec{r}) = T(\vec{r})\,\varrho_{\text{p}}(\vec{r}) + \varrho_{\text{m}}[1 - T(\vec{r})] \tag{1}$$

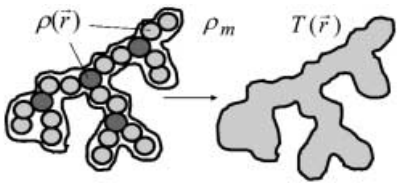

Fig. 5. Contrast applied to macromolecular structures in solution. The dissolved molecule is schematically shown as an assembly of connected spheres. The different units exhibit in scattering power expressed through the local scattering length density $\varrho(\vec{r})$. The scattering length density $\varrho(\vec{r})$ is rendered as a product of the shape function $T(\vec{r})$ and the local scattering length density inside the object. The shape function $T(\vec{r})$ defines the volume in the solution into which the solvent cannot penetrate. An additional contribution to the measured scattering intensity arises from the variation of scattering power inside of the particle as depicted by the differently shaded spheres. At high contrast, however, the scattering experiment "sees" only the shape of the dissolved molecule, i.e., the Fourier-transform of the shape function $T(\vec{r})$ (see text for further explanation). After [5]

where ϱ_m is the scattering length density of the solvent. Here $\varrho_p(\vec{r})$ is the scattering length density which is measured in a crystal structure of the object. The shape function $T(\vec{r})$ is related to the shape of the object in a given solvent. It is the description of the cavity in the system in which the solvent has been replaced by the solute. Therefore the shape function also depends on the solvent used for the SANS-analysis. It measures not only the shape of the dissolved object as embodied in $\varrho_p(\vec{r})$ but also the ability of the solvent to penetrate into the object itself. $T(\vec{r})$ is regarded as a continuous function varying between 0 and 1.

From this definition of the shape function the partial volume V_p of the solute is given by

$$V_p = \int T(\vec{r})\, d\vec{r} \tag{2}$$

By the definition of $T(\vec{r})$, V_p is the volume of the cavity in which the particular solvent is replaced by the solute. Therefore V_p depends on the particular solvent chosen for the SANS-experiment and also on concentration. For the dilute regime under consideration here the latter dependence can safely be dismissed.

For small number densities N of dissolved objects the volume fraction ϕ of the solute is $\phi = N \cdot V_p$ and its average scattering length density $\bar{\varrho}$ results as

$$\bar{\varrho} = \frac{1}{V_p} \int T(\vec{r})\, \varrho_p(\vec{r})\, d\vec{r} \tag{3}$$

The contrast of the dissolved molecule is therefore given by $\bar{\varrho} = \varrho_m$.

With these definitions the scattering intensity of a single particle may be split into three terms [23, 24, 34–37]:

$$I_0(q) = [\bar{\varrho} - \varrho_m]^2\, I_S(q) + 2 \cdot [\bar{\varrho} - \varrho_m]\, I_{SI}(q) + I_S(q) \tag{4}$$

The first term having a front factor which scales with the square of contrast is related to the shape function (see Fig. 5):

$$I_S(q) = \iint T(\vec{r}_1)\, T(\vec{r}_2)\, \frac{\sin(q|\vec{r}_1 - \vec{r}_2|)}{q|\vec{r}_1 - \vec{r}_2|}\, d\vec{r}_1\, d\vec{r}_2 \tag{5}$$

The discussion of the other two terms may be found in [5, 23, 24]. $I_S(q)$ is the scattering contribution referring to an object composed of structureless scattering units, the spatial arrangement of which is given by $T(\vec{r})$. This part may therefore be regarded as the scattering intensity extrapolated to infinite contrast. It is important to note that $I_S(q)$ is related to the Fourier-transform of the pure shape function of the molecule, i. e., of the cavity cut into the solvent by the solute. It must be kept in mind that static scattering methods measure the average structure of the dissolved objects. $I_S(q)$ therefore refers to the Fourier-transform of the average shape function $\langle T(\vec{r}) \rangle = T(r)$ which for centrosymmetric dendrimers is a centrosymmetric function because of the averaging over all conformations and orientations. Therefore $T(r)$ may directly be compared to radial density distributions suggested from model calculations and theory discussed in Sect. 2. Hence, $I_S(q)$ presents the main result of the SANS-analysis, i. e., the desired information about the spatial structure of the molecules in solution.

The self term $I_I(q)$ is related to inhomogeneities which result from the fact that not all atoms and groups constituting the dendritic structure have the same scattering length. (see Fig. 5). This term therefore takes care of problem 2. In practical determinations by SANS it also contains the incoherent contribution of the hydrogen atoms in the dendritic structure (problem 3 in Sect. 3.2; [5, 23, 24]). The cross term $I_{SI}(q)$ which can assume negative values as well was found to be zero within limits of error which can be explained by averaging over all conformations of the dendritic structure [23, 24].

From Eq. (4) it follows that all three terms may be extracted from experimental data if scattering intensities have been measured at at least three different contrasts. Hence, the dendrimer is dissolved in appropriate mixtures of the deuterated and protonated solvent and its scattering intensity is determined by SANS. The scattering length density ϱ_m strongly depends on the amount of deuterium in the solvent. Hence, the contrast as defined above may changed drastically by using these mixtures. If SANS-measurements are taken from at least three different mixtures all three terms in Eq. (4) can be determined experimentally [23, 24]. This method termed contrast variation requires that no preferential adsorption of either the deuterated or the protonated solvent onto the dissolved dendrimer takes place. In this case the local contrast would deviate considerably from the value calculated from the overall composition of the solvent mixture. The chemical difference of deuterated and protonated solvent molecules are so small, however, that preferential interaction of one component of the solvent mixture is not to be expected at all. Moreover, preferential adsorption would immediately show up because of the vastly different scattering length density of the deuterated and the protonated solvent. In this case the above decomposition (Eq. 4) would not work at all. In this respect the method of contrast variation also allows one to check the internal consistency of the treatment of data.

3.3.2
Radius of Gyration

For small scattering angles the scattering intensity of an isolated particle (Eq. 4) may be expanded to yield Guinier's law [32, 33]:

$$I_0(q) \cong N \cdot V_p^2 \cdot (\bar{\varrho} - \varrho_m)^2 \cdot \exp\left(-\frac{R_g^2}{3} \cdot q^2\right) \tag{6}$$

where R_g denotes the radius of gyration. Equation (6) thus serves for the extrapolation of the measured intensity to vanishing scattering angle and to determine the forward scattering $I_0(q=0)$. It must be noted that R_g is an explicit function of contrast as expressed through Eq. (7) [36, 37]:

$$R_g^2 = R_{g,\infty}^2 + \frac{\alpha}{(\bar{\varrho} - \varrho_m)} - \beta(\bar{\varrho} - \varrho_m)^{-2} \tag{7}$$

These expressions are due to Stuhrmann and Kirste [36] and to Luzzati et al. [37]. The term $R_{g,\infty}^2$ is a measure for the spatial dimensions of the shape function

$T(r)$. The coefficient α is a measure for the internal variation of the scattering length density discussed in Sect. 3.2, problem 2 [36]. The coefficient β differs from zero only in case of dendritic structures which are not centrosymmetric [37]. A comprehensive discussion of Eq. (7) and the three different terms including their derivation may be found in [5]. Here it suffices to note that R_g as determined by application of Eq. (6) may not be taken as a measure for the spatial extensions of the dissolved molecule. This is only the case when the contrast between solute and solvent is very high so that the 2. and 3. term in Eq. (7) may be disregarded.

3.4 Small-Angle Scattering Experiments: Influence of Concentration

The foregoing considerations have been devoted solely to the discussion of $I_o(q)$ of a single isolated molecule in solution. Experiments require finite concentrations, however, which may be of the order of a few percent. In dilute solutions of dendrimers the influence of concentration can be taken into account in terms of the structure factor $S(q)$:

$$I(q) = NI_o(q)\,S(q) \tag{8}$$

where N denotes the number of solute molecules per unit volume. The structure factor $S(q)$ is related to the pair correlation function of the solute objects [33] and may be evaluated to give valuable information on intermolecular interaction. In the limit of vanishing concentration $S(q) = 1$. Since dilute solutions of solute molecules interacting through a short-range potential do not exhibit long-range order, $S(q)$ will become unity if q is large enough [33]. Hence, the influence of concentration is restricted to the region of smallest scattering angles.

In general, it is more expedient to measure at volume fractions ϕ high enough in order to arrive at $S(q) \neq 1$ than going to exceedingly low volume fractions and disregard $S(q)$. If the dilution is high enough, extrapolation to $\phi = 0$ may be done by (see, e.g., the discussion in [5])

$$\frac{1}{S(q)} = 1 + 2 \cdot B_{app} \cdot \phi + O(\phi^2) \tag{9}$$

with the apparent virial coefficient B_{app} given by [5]

$$B_{app} = B_2\left(1 - \frac{1}{6} d^2 q^2 + \ldots\right) \tag{10}$$

Here B_2 denotes the thermodynamic limit of B_{app}. Equations (8) and (9) possess complete generality and the effective diameter d of interaction is determined by the balance of repulsive and attractive forces between the particles. Plots of $\phi/I(q)$ vs ϕ for given q-values can be used to extrapolate the scattering intensity to vanishing concentration. The slope of these lines may be evaluated to yield d. The description of the scattering data according to Eq. (7) requires, however, that the incoherent contribution due to the hydrogen atoms in the dendritic structure is small in the angular region used for this extrapolation. Moreover, the so-

lute molecules must be monodisperse or at least exhibit a very narrow distribution of sizes and/or chemical structures. Otherwise $S(q)$ will become an explicit function of contrast [38].

3.5 Small-Angle Scattering Experiments: Results

In this section a brief survey over the results achieved so far by small-angle scattering studies is given. The discussion is done in two parts. First data obtained at vanishing concentration are presented that allow one to assess the density distribution inside the dissolved dendrimers. Then data measured at finite concentration are shown which give highly interesting information on the mutual interaction of dendrimers in solution.

3.5.1 *Radial Density Distribution*

The discussion in Sect. 3.3 has suggested that the intensity measured in SANS-experiments contains an appreciable contribution not related to the structure of the dissolved dendrimers. Only the part $I_S(q)$ (see Eq. 4) is connected to the average spatial structure as expressed through the shape function $T(r)$. Figure 6

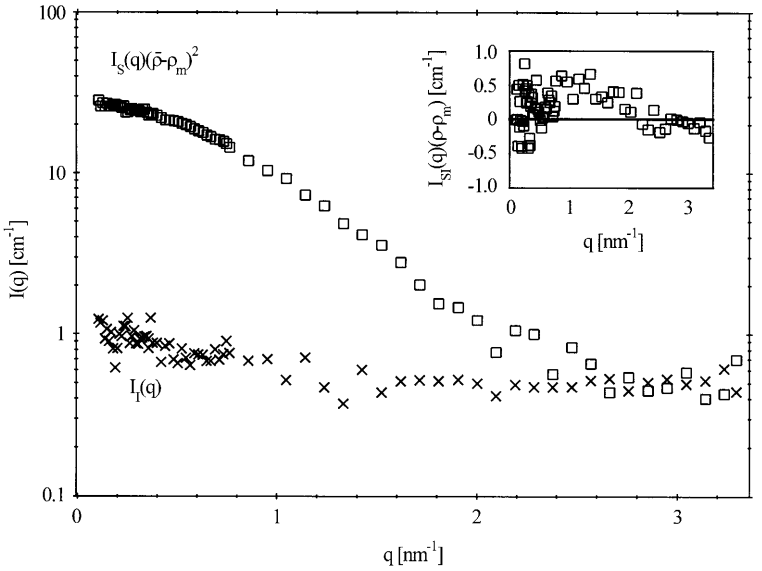

Fig. 6. Comparison of the three different contributions to the measured scattering intensity $I(q)$ according to Eq. (4) for a dendrimer of fourth generation (see Fig. 1). The squares give the intensity $I_S(q)\,(\bar{\varrho} - \varrho_m)^2$ with $\bar{\varrho} - \varrho_m$ being the highest contrast possible (see Eq. (4), in deuterated DMA). The *crosses* show the contribution $I_I(q)$ which is independent of contrast. The *inset* gives the contribution $I_{SI}(q)\,(\bar{\varrho} - \varrho_m)$ (cross term) which is virtually negligible for the present system

shows a comparison of all three terms determined by contrast variation for a flexible dendrimer of forth generation shown in Fig. 1 [24].

From this comparison is becomes obvious that the term independent of contrast becomes appreciable at higher scattering angles. This is due to the various contributions discussed in Sect. 3.2. In addition, the cross term is practically zero as expected (see Sect. 3.3).

Figure 7 demonstrates the necessity of separating the different contributions to the measured intensity according to Eq. (4) [23, 24]. The difference between the intensity measured at highest contrast (triangles; measured in deuterated dimethylacetamide) and the term $I_S(q)\,(\bar{\varrho} - \varrho_m)^2$ calculated for the highest contrast is appreciable. The solid line gives a fit of the latter data by a suitable empirical expression [5, 23, 24] which allows a Fourier-Inversion of Eq. (5) [23, 24]. The inset shows the radial density distribution which decays smoothly with increasing radial distance to the center of the dendrimer. This is in full accord with the theoretical deductions discussed in Sect. 2.

The dashed line give the scattering function calculated for a homogeneous sphere. The experimental data can only be described at small q by this model; at

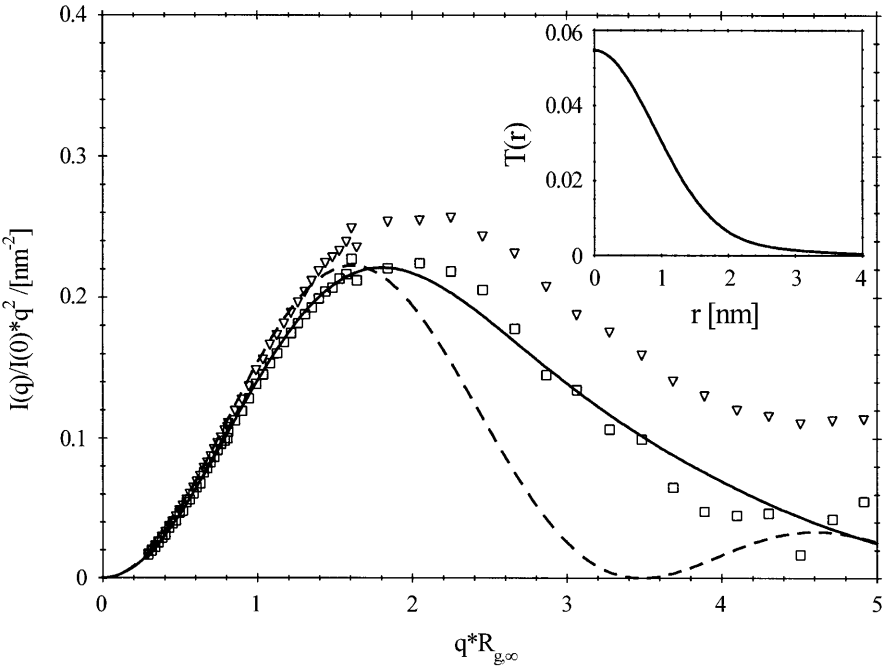

Fig. 7. Normalized scattering intensities $I(q)/I(0)$ of a dendrimer of fifth generation G5 [23] in a Kratky-plot vs $qR_{g,\infty}$. The *triangles* mark the data measured at highest contrast (in fully deuterated DMA) normalized to unity at $q = 0$. The squares give the term $I_S(q)\,(\bar{\varrho} - \varrho_m)^2$ of Eq. (4) calculated for the highest contrast possible. The *solid line* gives the best fit of the latter term by an empirical expression whereas the *inset* displays $T(r)$ obtained from $T(q)$ by Fourier-inversion. The *dashed line* in Fig. 7 is the scattering function of a homogeneous sphere of same $R_{g,\infty}$

higher q there are significant deviations which demonstrate that the dendrimer of fifth generation under consideration in [23] is a flexible, fluctuating structure in solution. The data obtained by Prosa et al. [18] demonstrate, however, that dendrimers of higher generation must have a much more compact internal structure. This can be argued directly from the fact that the scattering intensities of these dendrimers exhibit side maxima that are indicative of a rather densely packed arrangement of segments.

3.5.2
Interaction at Finite Volume Fraction

Figure 8 displays the structure factor $S(q)$ obtained from solutions of dendrimer G4 in deuterated dimethylacetamide by application of Eq. (8) [24]. In this solvent the high contrast between solute and solvent allows one to determine $S(q)$ conveniently. For low scattering angles $S(q)$ is considerably smaller than unity whereas at higher q the structure factor $S(q)$ is unity, as expected for dissolved molecules [32, 33]. There is no distinct maximum as in concentrated suspensions of rigid colloidal objects [32, 33]. One reason for this is the rather low volume fraction of the dendrimers. In addition, dendrimers are not expected to

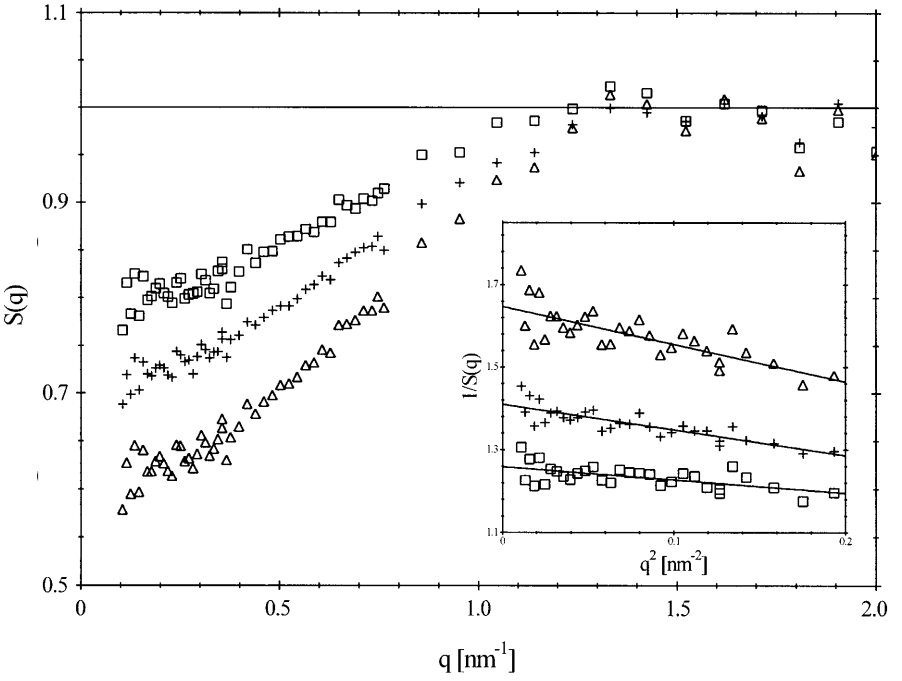

Fig. 8. Structure factor $S(q)$ (Eq. 8) of dendrimer G4 (see Fig. 1) as function of volume fraction and q according to Eqs. (12) and(13). $S(q)$ as function of q for different volume fractions ϕ: □: 0.017; +: 0.024; Δ: 0.04. The *inset* shows the dependence of $S(q)$ on q according to Eq. (13) by plotting $1/S(q)$ vs q^2 for different volume fractions: □: 0.017; +: 0.024; △: 0.04. Taken from [24]

interact via a steep repulsion but rather via a soft repulsion similar to the case of star polymers [39]. A quantitative investigation of this problem is still lacking, however. For small q-values and small volume fractions, however, Eq. (10) seems to provide a good fit of the data as seen from the inset of Fig. 8. The resulting diameter of interaction d compares favorably with the dimensions of the dissolved molecule [24].

4 Intrinsic Viscosity of Dendrimers

The preceding sections have demonstrated that dendrimers of lower generation are akin to branched polymeric structures. It is therefore to be expected that their flow behavior in dilute solution may be described in terms of the well-known concepts of dilute polymer solutions [14, 15]. Hence, dissolved dendrimers should behave like non-draining spheres. From an experimental comparison of R_g and R_h the immobilization of solvent inside the dendrimer can be compared directly since in this case the dendrimer may be approximated by a homogeneous sphere. Therefore $R_g^2 \approx 3/5\, R_h^2$ where R_h denotes the hydrodynamic radius of the dendrimer. This has been found experimentally [19].

From this the intrinsic viscosity is related to the hydrodynamic volume V_h and the molecular weight M by

$$[\eta] = 2.5\, N_L \frac{V_h}{M} \propto \frac{R_h^3}{M} \tag{11}$$

A number of experimental studies show that $[\eta]$ goes through a maximum as a function of the number of generations [15, 26, 40]. The first theoretical discussion of this problem is due to Lescanec and Muthukumar [7]. Some time ago Mourey et al. [40] presented a comprehensive experimental study of density-dependent properties of dendrimers including the intrinsic viscosity and the refractive index. A thorough discussion of the literature on this subject has recently be given by Rietveld and Smit [26] who also presented a systematic experimental investigation of $[\eta]$. The experimental data of R_h^3/M taken by these workers pass through a shallow maximum. From these investigations a shallow maximum of the intrinsic viscosity seems to be a well-established experimental fact by now.

The reasons for a maximum of the intrinsic viscosity is obvious from the fact that in first approximation R_h grows linear with the number g of generations. The molecular weight M, however, grows as 2^g. For low g the volume increases faster as function of generation up to the point where the growth of M will be the determining factor. This discussion demonstrates also that there is no simple scaling law $[\eta] \propto M$ as is the case for solution of high polymers. Dendrimers do not possess the self-similarity that is the prerequisite for the validity of such a scaling law. Hence, a description of dendritic structures in terms of fractals although being suggested by the chemical structure (see Fig. 1) are not admissible and lead to erroneous results.

Acknowledgement. Financial support by the Bundesministerium für Forschung und Technologie is gratefully acknowledged.

5 References

1. Newkome GR, Moorefield CN, Vögtle F (1996) Dendritic molecules. VCH, Weinheim
2. Tomalia DA, Naylor A, Goddard WA (1990) Angew Chem Intl Ed 29:138–175
3. Fischer M, Vögtle, F (1999) Angew Chem Intl Ed 38:884; Schlüter AD, Rabe JP (2000) Angew Chem 112:861
4. Morgenroth F, Kübel C, Müllen K (1997) J Mater Chem 7:1207
5. Pötschke D, Ballauff M (2000) Structure and dynamics of polymer and colloidal systems. In: Pecora R, Borsali R (eds) NATO ASI Studies (accepted)
6. de Gennes PG, Hervet H (1983) J Phys (Paris) 44:L351
7. Lescanec RL, Muthukumar M (1990) Macromolecules 23:2280
8. Mansfield ML, Klushin LL (1993) Macromolecules 26:4262
9. Murat M, Grest GS (1996) Macromolecules 29:1278
10. Mansfield ML (1994) Polymer 35:1827
11. Cavallo L, Fraternali F (1998) Chem Eur J 4:927
12. Boris D, Rubinstein M (1996) Macromolecules 29:7251
13. Welch P, Muthukumar M (1998) Macromolecules 31:5892
14. Flory P (1953) Principles of polymer chemistry. Ithaca
15. De Gennes PG (1988) Scaling concepts in polymer physics, 3rd edn. Ithaca
16. Bauer BJ, Briber RM, Hammouda B, Tomalia DA (1992) Polym Mater Sci Eng 66:704
17. Briber RM, Bauer BJ, Hammouda B, Tomalia DA (1992) Polym Mater Sci Eng 67:430
18. Prosa TJ, Bauer BJ, Amis EJ, Tomalia DA, Scherrenberg R (1997) J Polym Sci Part B Polym Phys 35:2913
19. Scherrenberg R, Coussens B, van Vliet P, Edouard G, Brackman J, de Brabander E, Mortensen K (1998) Macromolecules 31:456
20. Ramzi A, Scherrenberg R, Brackman J, Joosten J, Mortensen K (1998) Macromolecules 31:1621
21. Kleppinger R, Reynaers H, Desmedt K, Forier B, Dehaen W, Koch M, Verhaert P (1998) Macromol Chem Phys Rapid Comm 19:111
22. Micali N, Scolaro L, Romeo A, Lombardo D, Lesieur P, Mallamace F (1998) Phys Rev E 58:6229
23. Pötschke D, Ballauff M, Lindner P, Fischer M, Vögtle F (1999) Macromolecules 32:4079
24. Pötschke D, Ballauff M, Lindner P, Fischer M, Vögtle F (2000) Macromol Chem Phys 201:330
25. Imae T, Funayama K, Aoi K, Tsutsumiuchi K, Okada M, Furusaka M (1999) Langmuir 15:4076
26. Rietveld IB, Smit JAM (1999) Macromolecules 32:4608
27. Ramzi A, Bauer BJ, Scherrenberg R, Froehling P, Joosten J, Amis EJ (1999) Macromolecules 32:4983
28. Förster S, Neubert I, Schlüter AD, Lindner P (1999) Macromolecules 32:4013
29. Topp A, Bauer BJ, Klimash JW, Spindler R, Tomalia DA, Amis EJ (1999) Macromolecules 32:7226
30. Topp A, Bauer BJ, Tomalia DA, Amis EJ (1999) Macromolecules 32:7232
31. Topp A, Bauer BJ, Tomalia DA, Prosa TJ, Scherrenberg R, Amis EJ (1999) Macromolecules 32:8923
32. Feigin LA, Svergun DI (1987) Structure analysis by small-angle X-ray scattering and neutron scattering. Plenum, New York
33. Higgins JS, Benoit HC (1994) Polymers and neutron scattering. Clarendon Press, Oxford

34. Hickl P, Ballauff M (1997) Physica A 235:238
35. Hickl P, Ballauff M, Jada A (1996) Macromolecules 29:4006
36. Stuhrmann HB, Kirste RG (1967) Z Phys Chem NF 56:334
37. Luzatti V, Tardieu A, Mateu L, Stuhrmann HB (1976) J Mol Biol 101:115
38. Banchio AJ, Nägele G, Ferrante A, Klein R (1998) Progr Colloid Polym Sci 110:54
39. Jusufi A, Watzlawek M, Löwen H (1999) Macromolecules 32:4470
40. Mourey TH, Turner SR, Rubinstein M, Fréchet JMJ, Hawker CJ, Wooley KL (1992) Macromolecules 25:2401P

Author Index Volume 201–212

Author Index Vols. 26–50 see Vol. 50
Author Index Vols. 51–100 see Vol. 100
Author Index Vols. 101–150 see Vol. 150
Author Index Vols. 151–200 see Vol. 200

The volume numbers are printed in italics

Printing (Computer to Film): Saladruck, Berlin
Binding: Lüderitz & Bauer, Berlin